ELIANA SOUSA DA SILVA

NAPHTHALENE BASED PLANT REGULATING COMPOUNDS: PHOTOPHYSICS, DIRECT AND POLYOXOMETALATE CATALYSED DEGRADATION IN HOMOGENEOUS AND HETEROGENEOUS MEDIA BY LAYERED DOUBLE HYDROXIDES

Doctoral thesis in Chemistry submitted to Chemistry Department of FCTUC under the supervision of Profs Hugh D. Burrows and Mohamed Sarakha and co-supervision of Prof. Pascal Wong-Wah-Chung

2013

· U   C ·

UNIVERSIDADE DE COIMBRA

ELIANA SOUSA DA SILVA

· U C ·

NAPHTHALENE BASED PLANT REGULATING COMPOUNDS:

PHOTOPHYSICS, DIRECT AND POLYOXOMETALATE CATALYSED

DEGRADATION IN HOMOGENEOUS AND HETEROGENEOUS

MEDIA BY LAYERED DOUBLE HYDROXIDES

UNIVERSITE BLAISE PASCAL
CLERMONT-FERRAND
UBP

PhD thesis submitted to University of Coimbra in partial fulfillment of the requirements for the degree of Doctor of the Philosophy in Chemistry, specialty in Photochemistry, in co-tutelle with Université Blaise Pascal (France) under the supervision of Professor Hugh D. Burrows (University of Coimbra, Portugal) and Professor Mohamed Sarakha (Université Blaise Pascal, France) and co-supervision of Professor Pascal Wong-Wah-Chung (Université Blaise Pascal, France)

Coimbra

2013

To my father António

and to my brothers Sérgio and

Manoel for their love and support

To the memory of my mother Maria

ABSTRACT

Water pollution originating from pesticides is a global threat with its magnitude increasing day-by-day due to their large-scale use in intensive agriculture. This current extensive use of pesticides can induce hazardous effects on human health and contribute to a serious international problem of water contamination. Recognition of this issue has prompted increasing interest in the development of new technologies to eliminate/reduce the presence of these pollutants in aqueous media. Among the existing advanced oxidation processes, photocatalysis is accepted as an effective method for water purification, particularly the branch of heterogeneous photocatalysis.

The main aim of this thesis involves the study of the photophysics, direct and sensitized photochemical degradation of the naphthalene based plant regulators pesticides 2-(1-naphthyl) acetamide (NAD) and 2-naphthoxyacetic acid (2-NOA).

The first part of this thesis consists in study the photophysical properties of these pesticides in order to have a better insight into their photochemical behavior. The study was carried out in water and representative organic solvents using steady state (UV-vis, fluorescence and phosphorescence spectroscopy) and time resolved techniques (nanosecond laser flash photolysis and time correlated single photon counting). NAD and 2-NOA show fluorescence in aqueous solution (ϕ_{NAD}=0.066, τ_{NAD}=35 ns and $\phi_{2\text{-}NOA}$=0.13, $\tau_{2\text{-}NOA}$=10 ns) and phosphorescence at 77 K (ϕ_{NAD}=0.051 and $\phi_{2\text{-}NOA}$=0.022). In water, both compounds are degraded under direct irradiation with UV and simulated solar light. In aerated conditions occurs the photoionization of NAD and 2-NOA with formation of radical cation, hydrated electron and superoxide anion ($O_2^{\bullet-}$). $O_2^{\bullet-}$ is thought to be the primary species responsible for the degradation of these two pesticides leading to the formation of hydroxylation and oxidation products. Additionally, the mechanism of 2-NOA degradation also involves the participation of singlet oxygen ($^1O_2$), even though as a minor pathway, and Photo-Fries rearrangements. In contrast, $^1O_2$ did not induce NAD degradation. 2-Naphthol was identified as one of the major primary degradation products of 2-NOA. Toxicity tests on irradiated NAD show that the initial photoproducts are more toxic then the parent compound. Studies involving inclusion complexes of NAD with β-cyclodextrin (β-CD) indicates that this can act as stabilizer towards NAD photodegradation. This suggests that β-CD may be used as potential additive and stabilizer for NAD formulations.

Alternative methods to direct photolysis have to be considered for water treatment, as is the case of photocatalysis since it can take advantage of solar light and may also lead to mineralization of the pollutant. Among the existing catalysts, the polyoxometalate decatungstate anion $W_{10}O_{32}^{4-}$ has proved to be an excellent photocatalyst in both homogeneous and heterogeneous media since its absorption band partially overlaps the solar spectrum providing the possibility of photo-assisted applications. As a result, the second part of the thesis aimed to test the photocatalytic activity of $W_{10}O_{32}^{4-}$ towards NAD degradation upon 365 nm irradiation. In homogeneous aqueous solutions NAD is efficiently degraded and mineralized into CO_2 and nitrate anions. The high solubility of $W_{10}O_{32}^{4-}$ is a drawback for application in water remediation due to problems of catalyst recovery. Consequently, it was necessary to immobilize the catalyst in a solid matrix which was done by choosing layered double hydroxides (LDHs) materials as support. These materials present excellent anionic exchange properties, are easily synthesized, catalytically inert, and easily recovered from the reaction medium. The last part of this thesis consists in the synthesis of LDHs with different properties, intercalation of the $W_{10}O_{32}^{4-}$ on the *as*-prepared LDH and assessment of its photocatalytic activity towards NAD degradation under irradiation at 365 nm. $Mg_2Al-W_{10}O_{32}^{4-}$ LDHs materials were synthesized using three different methods: (1) classical co-precipitation at constant pH, $Mg_2Al-W_{10}O_{32}^{4-}$ LDH, (2) fast co-precipitation followed by supercritical CO_2 drying, $SC-Mg_2Al-W_{10}O_{32}^{4-}$ LDH and (3) use of sacrificial polystyrene colloidal crystal template impregnation-coprecipitation to form three dimensionally ordered macroporous LDH, 3-DOM-$Mg_2Al-W_{10}O_{32}^{4-}$ LDH. All the materials have been characterized by a variety of analytical techniques. The heterogeneous photocatalytic degradation of NAD in presence of the three catalysts at 365 nm was studied. Results show that NAD is efficiently degraded in the presence of the catalysts (2) and (3) with consequent mineralization and excellent recovery efficiency. The open structure and porosity presented by the catalyst (3) induces a more efficient light penetration in the LDH layers with consequent increase in the photocatalytic activity of $W_{10}O_{32}^{4-}$. Therefore, the macroporous and supercritical LDH materials intercalated with decatungstate anion can be considered as promising catalysts for pollutant water treatment.

RESUME

A cause des activités humaines la pollution des eaux par les pesticides engendre des problèmes environnementaux dont les préoccupations ne cessent de croître. Cette utilisation intensive et en grandes quantités, notamment dans les activités agricoles, peut conduire à des effets importants sur la santé humaine et contribue à de sérieux problèmes de contamination des eaux. De ce fait, de nombreuses études s'intéressent à l'élimination/réduction de ces polluants dans les milieux aqueux. Parmi ces différentes études, les processus d'oxydation avancée et notamment la photocatalyse s'avèrent des méthodes prometteuses pour la décontamination des eaux.

L'objectif principal de cette thèse concerne les études photophysiques et la dégradation directe et sensibilisée de deux pesticides dérivés du naphtalène: 1-naphthalèneacétamide (NAD) et acide naphtyloxy-acétique (2-NOA).

Dans un premier temps et dans le but d'avoir d'étudier le comportement photochimique de ces deux pesticides, nous avons examiné leurs propriétés photophysiques. Cette étude a été entreprise en utilisant principalement dans l'eau et dans certains solvants organiques en utilisant les spectroscopies UV-Visible, fluorescence et phosphorescence mais également des techniques résolues dans le temps (photolyse laser nanoseconde). NAD et NOA sont fluorescents en solutions aqueuses (ϕ_{NAD}=0.066; $\tau_{NAD} = 35$ ns et $\phi_{2\text{-}NOA}$=0.13, $\tau_{2\text{-}NOA} = 10$ ns) et phosphorescent à 77K ($\phi_{NAD} = 0.051$ and $\phi_{2\text{-}NOA} = 0.022$). Sous excitation directe dans le domaine UV et solaire (Simulateur solaire) les deux composés montrent une photodégradation non négligeable. Le processus prédominant pour les deux composés semblent être un processus de photoinionisation, mis en évidence par des mesures en photolyse laser nanoseconde et permettant la génération de radicaux superoxydes ($O_2^{\bullet-}$). Le mécanisme de photodégradation de 2-NOA semble également impliquer des réarrangements de type PhotoFries et aussi la participation minoritaire de l'oxygène singulet ($^1O_2$). Le 2-naphtol est formé comme l'un des principaux produits de 2-NOA photodégradation. Au cours de ce processus de photodégradation, des photoproduits (produits d'hydroxylation et d'oxydation) ont été générés et leur toxicité (étudiée dans le cadre de ce travail) a été clairement démontrée.

Des études de complexation de NAD par β-cyclodextrine (β-CD) a montré une stabilisation de NAD: la vitesse de photodégradation diminue fortement. β-CD peut donc être utilisé comme additif et stabilisateur pour les formulations de NAD.

Sachant que la photodégradation sous excitation directe génère des photoproduits dont la toxicité est avérée, des processus photocatalytiques ont été étudiés dans la cadre de cette thèse. Ce processus peut permettre l'élimination du pesticide mais également sa minéralisation en solution. Parmi les photocatalyseurs employés, nous avons choisi un polyoxométalate de type $W_{10}O_{32}^{4-}$ dont le spectre d'absorption montre un bon recouvrement avec le spectre d'émission solaire. Les études de photocatalyse ont pu être réalisées en phase homogène mais également en phase hétérogène. En phase homogène, l'excitation du mélange NAD/$W_{10}O_{32}^{4-}$ à 365 nm permettant l'excitation sélective du photocatalyseur et conduit à une disparition efficace du pesticide mais également à sa minéralisation en solution.

Cependant, la très grande solubilité du photocatalyseur limite son éventuelle utilisation pour la décontamination des eaux. Par conséquent, il s'est donc avéré de l'immobiliser sur un support solide. Nous avons opté, dans la dernière partie de la thèse, pour l'utilisation des hydroxydes doubles lamellaires (HDL) comme supports. Les supports ont été synthétisés en utilisant trois méthodes différentes: (1) Mg₂Al-$W_{10}O_{32}^{4-}$ LDH, par co-précipitation classique à pH constant, (2) SC-Mg₂Al-$W_{10}O_{32}^{4-}$ LDH, par co-précipitation suivie d'un séchage CO₂ supercritique, (3) 3-DOM-Mg₂Al-$W_{10}O_{32}^{4-}$LDH, par imprégnation/co-précipitation eu utilisant un réseau d'agent sacrificiel (polystyrène) permettant de former un réseau tridimensionnel. Toutes les études de caractérisation et de comportement photocatalytique de ces matériaux ont été effectuées. L'excitation à 365 nm a montré que tous les matériaux permettent l'élimination et la minéralisation des solutions. Cependant, une meilleure efficacité a été démontrée avec le matériau (3) grâce à la structure ouverte et de la porosité du support qui induit une meilleure pénétration de la lumière d'excitation dans le LDH couches et par conséquent une meilleure absorption de la lumière par $W_{10}O_{32}^{4-}$.

Cela signifie que les LDH préparés avec structure macroporeuse et par séchage supercritique intercalés avec decatungstate anions peuvent être considérés comme des catalyseurs prometteurs pour le traitement de l'eau des polluants.

__Mots Clés:__ Pesticides, régulateurs de croissance des plantes, naphthalèneacétamide, acide naphtyloxy-acétique, pollution de l´eau, photophysique, photocatalyse, polyoxométalates, décatungstate, photocatalyse, hydroxydes double lamellaire, macropores.

RESUMO

Os problemas ambientais associados à poluição da água são motivo de preocupação global. A crescente aplicação de pesticidas em atividades agrícolas por forma a promover e controlar a produtividade de alimentos pode induzir efeitos nocivos na saúde humana e contribuir para um grave problema de contaminação da água a nível internacional. O reconhecimento do problema fez com que surgisse um interesse crescente no desenvolvimento de novas tecnologias para eliminar/reduzir a presença destes contaminantes em meios aquosos. De entre as várias metodologias existentes, a fotocatálise é aceite como um método eficaz para a purificação de água, particularmente a área da fotocatálise heterogênea.

O objetivo principal desta tese envolveu o estudo fotofísico e a degradação fotoquímica direta e sensibilizada dos pesticidas derivados do naftaleno: 2-(1-naftil) acetamida (NAD) e ácido 2-naftoxi acético (2-NOA).

Numa primeira fase foram estudadas as propriedades fotofísicas destes pesticidas com o intuito de se obter uma melhor compreensão do seu comportamento fotoquímico. O estudo foi efetuado em água e em solventes orgânicos utilizando o estado estacionário (espectroscopia UV-vis, fluorescência e fosforescência) e técnicas resolvidas no tempo. NAD e 2-NOA apresentam fluorescência em solução aquosa (ϕ_{NAD}=0.066, τ_{NAD}=35 ns and $\phi_{2\text{-NOA}}$=0.13, $\tau_{2\text{-NOA}}$=10 ns) e fosforescência a 77K (ϕ_{NAD}=0.051 and $\phi_{2\text{-NOA}}$=0.022). Ambos são degradados em solução aquosa sob irradiação UV e luz solar simulada. Na presença de ar, os dois compostos sofrem fotoionização com consequente formação do radical catião, electrão hidratado e anião superóxido $O_2^{\bullet-}$. Este último é formado pela reação do electrão hidratado com oxigénio presente em solução e é considerado como a espécie primária responsável pelo processo de degradação, originando produtos hidroxilados e oxidados. Outra etapa na degradação do 2-NOA parece envolver o rearranjo de Photo-Fries, assim como a participação do oxigénio singuleto $^1O_2$ tendo em conta os estudos efetuados com Rose Bengal. Contudo, o $^1O_2$ contribui minoritariamente para o processo global de degradação. Adicionalmente, 2-naphthol foi identificado com um dos produtos primários maioritários da degradação de 2-NOA.

Estudos de toxicidade do NAD e dos produtos de degradação revelam a formação de fotoprodutos mais tóxicos que o próprio NAD, o que sugere que devem ser encontradas alternativas ao processo fotoquímico de degradação estudado. A fotodegradação do NAD quando complexado com β-ciclodextrinas (β-CD) revelou um

efeito protetor por parte da β-CD face a degradação. Isto sugere que a β-CD pode ser usada como potencial aditivo nas formulações de NAD, aumentado a eficiência do ingrediente ativo quando aplicado no tratamento de frutos e legumes.

A degradação fotocatalisada do NAD foi estudada neste trabalho como alternativa "verde" e mais eficaz no tratamento de águas contaminadas dado que a fotocatálise apresenta como vantagem relativamente à fotólise directa o uso da luz solar e a mineralização dos poluentes (pesticidas e não só). Para o efeito foi usado um polioxometalato, o anião decatungstato $W_{10}O_{32}^{4-}$, o qual absorve uma parte da luz solar. Os estudos de degradação e mineralização efetuados em meio homogéneo atestam a eficácia do catalisar. No entanto este apresenta como desvantagem a sua elevada solubilidade em água, a qual não permite a recuperação do meio. Daí surgiu o interesse e anecessidade em imobilizar este catalisador num suporte sólido por forma a favorecer a sua recuperação e reutilização. A escolha do suporte sólido recaiu sobre os hidróxidos duplos lamelares (LDH) tendo em conta a sua capacidade de troca iónica. LDH intercalados com $W_{10}O_{32}^{4-}$ foram sintetizados recorrendo a três métodos: i) co-precipitação clássica, Mg_2Al-$W_{10}O_{32}^{4-}$ LDH, ii) rápida co-precipitação seguida de secagem com CO_2 supercrítico, SC-Mg_2Al-$W_{10}O_{32}^{4-}$ LDH e iii) impregnação/co-precipitação de cristais coloidais de poliestireno para formar materiais macroporosos tridimensionalmente ordenados de LDH, 3-DOM-Mg_2Al-$W_{10}O_{32}^{4-}$. Estes materiais catalíticos apresentam diferenças na sua morfologia, a qual se verificou estar diretamente relacionada com a eficácia catalítica do anião decatungstato. A degradação do NAD foi mais eficaz na presença de 3-DOM-Mg_2Al-$W_{10}O_{32}^{4-}$ oriunda da estrutura aberta e da maior porosidade do material, o que permite uma penetração de luz mais eficiente para o interior do LDH por forma a fotoactivar o catalisador $W_{10}O_{32}^{4-}$. A mineralização do NAD na presença dos materiais 3-DOM-Mg_2Al-$W_{10}O_{32}^{4-}$ e SC-Mg_2Al-$W_{10}O_{32}^{4-}$ ocorreu de forma eficiente, assim como o processo de recuperação e reutilização dos mesmos. Estes dois materiais revelaram excelente actividade fotocatalítica e estabilidade, podendo ser considerados promissores catalisadores para aplicação no tratamento de águas.

Palavras chave: *pesticidas, reguladores do crescimento de plantas, poluição da água, polioxometalatos, 2-(1-naftil) acetamida, ácido 2-naftoxi acético, processos fotofísicos, fotocatálise , anião decatungstato, hidróxidos duplos lamelares, macroporos.*

ACKNOWLEDGEMENTS

Professor Sérgio Melo for his friendship, advices and for finding always a place for me to stay when I was "office homeless". I am very grateful to Sofia Fonseca (PhD) with whom I shared the office in Coimbra, for guide me with some of the equipment, for the pleasant and long conversations and for the friendship. I also acknowledge João Pina (PhD) for his kind and simple way of being, and for his willingness to help every time I request his assistance with equipments even without having the obligation to do so. I acknowledge Carlos Serpa (PhD) for giving me the first training with laser flash photolysis and for all the times that followed that moment. I acknowledge Catherine for helping me with the TCSPC measurements, for the company at breakfast and lunch time and for all the moments we shared. I thank Kamila and Ana Luísa for the good moments we spent in lab and outside. I thank Susy Lopes for her help and long friendship.

I would like to acknowledge all the personal from UBP, particularly the people of ICCF, for the kind way I was always received and treated. Each time I was in Clermont I felt at home. I leave a special word of gratitude to the persons of the Photochimie (Chimie 6) and Materials (Chimie 5) teams with whom I spent more time. I would like to acknowledge Claire Richard from Photochemistry group (Research Director at CNRS) for accepting me as a student in the LPPM while she was still the Director of the Photochemistry Laboratory. She was always very kind and available to help. I would like to acknowledge all the "permanent" persons from Chimie 6: Marcello Brigante, for the good environment he created in the lab (always teasing me), for being always available to help either on scientific or personal side; Giles Mailhot for his constant kindness and good mood; Gislan Guyot for all the help, including the precious help to find a dentist! and Guillaume Voyard for his assistance in lab, for being always available to help and for carrying out the ionic chromatography measurements. I would like to thank all the laboratory colleagues that I met during all my stays in Clermont. Marie, one of the kindest person I ever met, for her friendship, for opening the door of her home, for making me laugh with her daily greeting "hello miss sunshine" and for my "oh come on Marie, you are not shy" and for her help with bureaucratic papers. I am also very grateful to her parents for the kind and tender way they always treated me and for giving me accommodation when necessary; Natacha, for her friendship, for our French-English conversations and for giving me the honor to be godmother of her daughter; Shirin, just for being the way she is, for her friendship, support and help; Runsigma, for "taking care" of me when I was ill, for the encouragement and for her family company; Claudia, post doc at LMI, for always try to make me see the fun side of life, for the surprise gifts and

for the encouragement; Jeoffrey (fantastic person!), Edith (LMI, for the trips, for the lunch's at her home), Stefano (for the trips company), Aurelian (always in a good mood! and available to help), Cristiano (with whom I could speak portuguese!), Cyril (wonderful and funny moments we share while working in the lab), Claire (for her help), Maxime (always teasing), Boris (for his advices), Tiffany, Jing, Sarka (the company we did each other working in night), Anne, Aurélie, Bafai, Elisa, Wen Yu, Souad (LMI) and Assam (LMI). All of them contributed in some way for my welfare while I was in Clermont. The excellent environment in the laboratory, the great moments we shared and the surprise I received in my last day in lab before my departure will stay forever with me.

I would like to acknowledge all my friends (they know who they are) with whom I shared special moments and that always support my decisions even if sometimes they disagree with it. I want to acknowledge in particular Maria José Tapia for a wonderful and unlikely friendship that was born many years ago in Coimbra. I thank her for being the way she is, for being present through the encouragement and support that she transmits me despite the distance, for the daily life shared stories and for giving me accommodation in all my car trips between Coimbra⇔Clermont. A particular word to Sandra, Mariana, Elsa and Lúcia for the two decades of friendship and to the friends working at ex-CCDRC and FEUP. A special thanks to Luis for all the moments and trips we shared and for being my conscience when mine was not able to rationalize some situations.

I would like to acknowledge my family, most particularly my father Antonio, my brothers Sérgio and Manoel and my sister in law Marta. Through their love I found encouragement and strengths to keep on going when sometimes I did not know I had it. I am deeply grateful to them for helping me reach my goals and dreams.

Abbreviations and symbols

NAD	2-(1-Naphthyl) acetamide
2-NOA	2-Naphthoxyacetic acid
1-NAA	1-Naphthyl acetic acid
$^1NAD^*$	NAD singlet excited state
$^3NAD^*$	NAD triplet excited state
$NAD^{\bullet+}$	NAD radical cation
$NAD^{\bullet-}$	NAD radical anion
$2\text{-}NOA^{\bullet+}$	2-NOA radical cation
$^1 2\text{-}NOA^*$	2-NOA singlet excited state
$^3 2\text{-}NOA^*$	2-NOA triplet excited state
S_0	Ground singlet state
S_1	Lowest singlet excited state
T	Triplet state
T_1	Lowest triplet excited state
ic	Internal conversion
isc	Intersystem crossing
vr	Vibrational relaxation
nr	Non-radiative
r	Radiative
F.	Fluorescence
P.	Phosphorescence
ϕ	Quantum yield
k	Rate constant
ε	Molar absorption coefficient
τ	Lifetime
$t_{1/2}$ (or $\tau_{1/2}$)	Half-lifetime
λ	Wavelength
ϵ	Dielectric constant
η	Viscosity
n	Refractive index
EPA	Environmental Protection Agency
EFSA	European Food Safety Authority
WHO	World Health Organization
FAO	Food and Agriculture Organization
K_{OW}	n-octanol-water partition coefficient
K_{OC}	Adsorption coefficient
H	Henry´s Law constant
PGR	Plant growth regulators
BCF	Bio concentration factor
LD_{50}	Lethal dose at fifty percent
LC_{50}	Lethal concentration at fifty percent
CD	Cyclodextrin
β-CD	βeta-cyclodextrin
H_2O_2	Hydrogen peroxide
D_2O	Deuterated water
DSS	Sodium dodecylsulfate

Abbreviations and symbols (continuation)

TA	Terephthalate
H_2O_2	Hydrogen peroxide
D_2O	Deuterated water
K_{SV}	Stern-Volmer constant
KI	Potassium iodide
KSCN	Potassium thiocyanate
KCl	Potassium chloride
KBr	Potassium bromide
TEA	Triethylamine
NaN_3	Sodium azide
e^-	Hydrated electron
$^1O_2$	Singlet oxygen
$O_2^{\bullet-}$	Superoxide anion radical
$HO^\bullet$	Hydroxyl radical
Q	Quencher
P	Pesticide
% I	Intensity of luminescence (%)
AOPs	Advanced oxidation processes
POM	Polyoxometalate
$Na_4W_{10}O_{32}$	Sodium decatungstate
$W_{10}O_{32}^{4-}$	Decatungstate anion
SC	Semiconductor
VB	Valence band
CB	Conduction band
h^+	Hole
E_g	Band gap energy
TiO_2	Titanium dioxide
LDH	Layered double hydroxide
d	Basal spacing
l	Gallery height
A.E.C.	Anionic exchange capacity
S_{theo}	Theoretical surface area
UV-vis	Ultraviolet-visible
FTIR	Fourier transform Infrared spectroscopy
HPLC	High performance liquid chromatography
LC	Liquid chromatography
GC	Gas chromatography
DAD	Diode array detection
TCSPC	Time-correlated single photon counting
PXRD	Powder X-ray diffraction
SEM	Scan electron microscopy
TEM	Transmission electron microscopy
EDS	Energy dispersive X-ray spectroscopy
MS	Mass spectrometry
ESI	Electrospray ionization
TG	Thermogravimetry

Publications and communications related to the scientific topic of the thesis

Manuscripts published in international journals with peer view-process:

1. Photochemical degradation of the plant growth regulator 2-(1-naphthyl) acetamide in aqueous solution upon UV irradiation, **Eliana Sousa Da Silva**, Pascal Wong-Wah-Chung, Hugh Douglas Burrows, Mohamed Sarakha,[*] *Photochem. Photobiol.*, 2013, 89, 560-570.

2. Photophysical characterisation of the plant growth regulator 2-(1-naphthyl) acetamide, **Eliana Sousa Da Silva,** Pascal Wong-Wah-Chung, Mohamed Sarakha, Hugh Douglas Burrows,[*] *J. Photochem. Photobiol. Chem. A*, 2013, 265, 29-40.

3. β-Cyclodextrin as a photostabilizer of the plant growth regulator 2-(1-naphthyl) acetamide in aqueous solution, **Eliana Sousa Da Silva,**[*] Mohamed Sarakha, Pascal Wong-Wah-Chung, Hugh Douglas Burrows,[*] *J. Inclusion Phenom. Macrocyclic Chem.*, DOI 10.1007/s10847-013-0355-5, 2013.

4. Photocatalytic degradation of pesticides by $W_{10}O_{32}^{4-}$/Macroporous-Mg_2Al layered double hydroxides, **Eliana Sousa Da Silva**, Pascal Wong-Wah-Chung, Hugh Douglas Burrows, Mohamed Sarakha,[*] Claude Forano, Vanessa Prevot, Invited publication for the special issue of the journal "*Environmental Science and Pollution Research* (ESPR)" that is dedicated to "Photocatalysis: new highlights from JEP 2013".

Manuscripts in preparation:

1. Homogeneous photocatalytic degradation of the plant growth regulator 2-(1-naphthyl) acetamide by sodium decatungstate in aqueous solution, Eliana Sousa Da Silva, Mohamed Sarakha, Hugh Douglas Burrows, Pascal Wong-Wah-Chung.

2. Efficient photocatalytic degradation of 2-(1-naphthyl) acetamide by sodium decatungstate immobilized on aerogel of MgAl layered double hydroxide prepared by supercritical dry, Eliana Sousa Da Silva, Mohamed Sarakha, Pascal Wong-Wah-Chung, Hugh Douglas Burrows, Claude Forano, Vanessa Prevot.

3. Photochemical degradation of the plant growth regulator 2-naphthoxy acetic acid in aqueous solution upon UV irradiation, Eliana Sousa Da Silva, Pascal Wong-Wah-Chung, Hugh Douglas Burrows, Mohamed Sarakha.

4. Effect of solvents on the photophysical properties of the plant growth regulator 2-naphthoxyacetic acid, Eliana Sousa Da Silva, Mohamed Sarakha, Hugh Douglas Burrows, Pascal Wong-Wah-Chung.

Communications in national/international conferences

A. Oral presentations

1. Catalysed photodegradation of pesticides in aqueous solution using sensitizers, **Eliana S. Da Silva,**[*] Pascal Wong-Wah Chung, Mohamed Sarakha, Hugh D. Burrows, *International School on "Monitoring, fate and toxicity of toxic compounds in the terrestrial environment"*, 29 November-12 December 2010, Nova Gorica, Slovenia.

2. Solvent effects on photophysics of 2-(1-naphthyl) acetamide, **Eliana S. Da Silva,**[*] Pascal Wong-Wah Chung, Mohamed Sarakha, Hugh D. Burrows, *Photochemistry and Photochemical Techniques*, 16-18 May 2011, Dublin, Ireland.

3. Photocatalytic degradation of the plant growth regulator 2-naphthoxyacetic acid in aqueous solution by decatungstate anion, **Eliana S. Da Silva,**[*] Pascal Wong-Wah-Chung, Mohamed Sarakha, Hugh D. Burrows, *SPEA 7 - 7th European Meeting on Solar Chemistry and Photocatalysis: Environmental Applications (flash communication)*, 17-20 June 2012, Porto, Portugal.

4. Influence of solvents on the ground and excited states properties of 2-(1-Naphthyl) acetamide and 2-Naphthoxyacetic acid, **Eliana S. Da Silva,**[*] Pascal Wong-Wah Chung, Mohamed Sarakha, Hugh D. Burrows, *23rd Lecture Conference on Photochemistry*, 8-10 October 2012, Potsdam, Germany.

5. Photocatalytic degradation of pesticides by 3-DOM-$Mg_2Al/W_{10}O_{32}^{4-}$ layered double hydroxides, **Eliana S. Da Silva,**[*] Mohamed Sarakha, Claude Forano, Pascal Wong-Wah Chung, Hugh D. Burrows, Vanessa Prevot, *9º Encontro Nacional de Catálise e Materiais Porosos (IX ENCMP)*, 6-7 May 2013, Porto, Portugal.

6. Effect of substituent groups of naphthalene derivatives on excited states properties, **Eliana S. Da Silva,**[*] Pascal Wong-Wah Chung, Mohamed Sarakha, Hugh D. Burrows, *XXIII Encontro Nacional da Sociedade Portuguesa de Química*, 12-14 June 2013, Aveiro, Portugal.

7. Macro/mesoporus layered double hydroxide aerogels: preparation and applications, Eliana S. Da Silva, Hugh D. Burrows, Pascal Wong-Wah Chung, Mohamed Sarakha, Claude Forano, **Vanessa Prevot,**[*] *XV International Clay Conference*, 7-11 July 2013, Rio de Janeiro, Brazil. (keynote lecture).

8. Photocatalytic degradation of pesticides by 3-DOM-$Mg_2Al/W_{10}O_{32}^{4-}$ layered double hydroxides, **Mohamed Sarakha**,[*] Eliana S. Da Silva, Claude Forano, Pascal Wong-Wah Chung, Hugh D. Burrows, Vanessa Prevot, *3rd European Symposium in Photocatalysis*, 24-26 September 2013, Slovenia.

B. Poster presentations

1. Naphthaleneacetamide: direct and photocatalysed degradation by sodium decatungstate, **Eliana S. Da Silva,**[*] Pascal Wong-Wah Chung, Mohamed Sarakha, Hugh D. Burrows*, Solar Chemistry and Photocatalysis: *Environmental applications (SPEA 2010)*, 13-16 June 2010, Prague, Czech Republic.

2. Photophysical and photochemical characterisation of α-Naphthaleneacetamide in solution, **Eliana S. Da Silva,**[*] Pascal Wong-Wah Chung, Hugh D. Burrows, Mohamed Sarakha, *XXIII IUPAC Symposium in Photochemistry*, 11-16 July 2010, Ferrara, Italy.

3. Photodegradation of α-naphthaleneacetamide using sodium decatungstate as a photocatalyst, **Eliana S. Da Silva,**[*] Pascal Wong-Wah Chung, Mohamed Sarakha, Hugh D. Burrows, EMEC 11 - The 11th European Meeting on Environmental Chemistry, 8-11 December 2010, Portoroz, Slovenia.

4. Photophysical characterization of the plant growth regulator 2-naphthoxyacetic acid, **Eliana S. Da Silva,**[*] Pascal Wong-Wah Chung, Hugh D. Burrows, Mohamed Sarakha, *EMEC 12 - The 12th European Meeting on Environmental Chemistry*, 7-10 December 2011, Clermont-Ferrand, France.

5. Photocatalytic degradation of the growth regulator 2-Naphthoxyacetic acid in aqueous solution by decatungstate anion, **Eliana S. Da Silva,**[*] Pascal Wong-Wah Chung, Hugh D. Burrows, Mohamed Sarakha, *SPEA 7 - 7th European Meeting on Solar Chemistry and Photocatalysis: Environmental Applications*, 17-20 June 2012, Porto, Portugal.

6. Layered Double Hydroxides intercalated with polyoxometalate $W_{10}O_{32}^{4-}$: synthesis and visible light photocatalytic activity towards pesticide degradation, **Eliana S. Da Silva,**[*] Pascal Wong-Wah Chung, Vanessa Prevot, Claude Forano, Hugh D. Burrows, Mohamed Sarakha, *XXIV IUPAC Symposium on Photochemistry*, 15-20 July 2012, Coimbra, Portugal.

* (correspondent/presenting author)

Table of contents

Part 1. Photochemical behavior of plant growth regulators

Chapter 1. Photophysical and photochemical processes
of some pesticides water pollutants

Chapter 3. Photophysical and photochemical studies of

the plant growth regulator 2-naphthoxyacetic acid

Part 2. Photocatalysed degradation of pesticides

Chapter 4. Photocatalysis for water treatment

Chapter 6. Heterogeneous photocatalysed degradation of
2-(1naphthyl)acetamide by decatunsgtate anion
immobilized in layered double hydroxides

Part 3. General conclusions and experimental part

Chapter 7. General conclusions and perspectives

Chapter 8. Materials and methods

Part 1

Photochemical behavior of

plant growth regulators

Chapter 1

Photophysical and photochemical processes of some pesticide water pollutants

1.1 Introduction

This chapter aims to give a general overview of the literature concerning the environmental problems posed by pesticides to the environment. The definition, classification, properties, environmental fate and photodegradation methods of pesticides are described. Emphasis is given to the two plant growth regulators that are studied within this thesis, 2-(1-naphthyl) acetamide and 2-naphthoxyacetic acid. The application, fate, toxicity and physical-chemical properties of these two compounds are provided. Reference is also made to previous photodegradation studies reported in the literature for these two compounds.

A short mention is also given concerning the incorporation of pesticides in cyclodextrins and its effect on the environment since the encapsulation of pesticides in these molecules can be beneficial to agriculture practices. Finally, a brief description on is given on the photophysical and photochemical processes that molecules may undergo following absorption of light.

1.2 Pesticides as water pollutants

Fresh water is crucial for sustainable development but is a limited resource. In the last century, the overall consumption of fresh water increased at double the rate of population growth [1]. In the world, more than 1 billion people lack access to safe drinking-water supplies, while 2.6 billion lack adequate sanitation. Water contamination and lack of sanitation and hygiene cause approximately 1.7 million deaths every year [2]. The quality of surface and ground waters is being prejudiced by pollution arising from a variety of sources, including industrial discharges, landfilling domestic wastes and excessive use of agricultural pesticides [1]. The presence of pollutants may cause acute or chronic health effects on humans along with impacts on the environment, depending on the type of contaminant and degree of exposure.

Chemical substances have been used in agriculture for many years to control pests which interfere with the efficient growth of crops and that transmit diseases to human kind. However, the use of modern pesticides in agriculture dates back to the 19th century. The "first generation" of pesticides was introduced in the 1860's for the control of pests such as fungi, insects and bacteria, and involved mainly inorganic compounds like sulfur, arsenic, mercury, lead and a fumigant hydrogen cyanide. Their use was

abandoned as a result of their toxicity and ineffectiveness. With the Second World War in the 1940s, a dramatic change occurred when synthetic organic pesticides were introduced into the market. Dichlorodiphenylchlorethane (DDT) (Figure 1-1) was the first developed synthetic organic pesticide to be used. DDT was not only highly effective as an insecticide, but also controlled diseases such as malaria, by killing the mosquitoes that transmitted this disease. This feature led to Paul Muller being awarded the Nobel Prize of medicine in 1948. Due to its broad-spectrum activity, persistence, insolubility, inexpensive and ease of application [3], use of DDT quickly spread over the globe, and at least two billion kilograms of DDT have been used worldwide since about 1940. The first organochlorine herbicide, 2,4-dichlorophenoxyacetic acid (2,4-D) (Figure 1-1) was introduced shortly after, in 1944. This compound targeted weeds [4] thus allowing the farmer to increase the yield of a crop per unit area of land. It is one of the most widely used herbicides in the world.
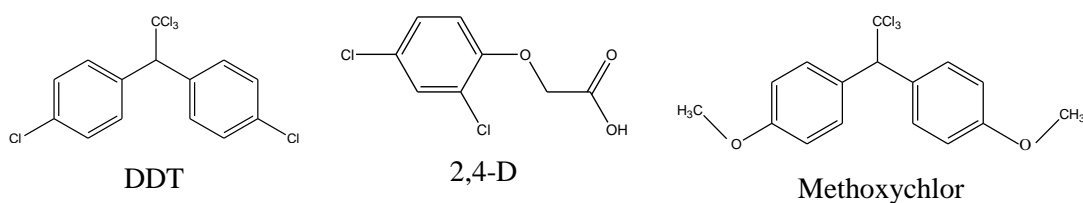
Figure 1-1 Chemical structures of DDT, 2,4-D and methoxychlor.

The so-called "second generation" of pesticides was developed in the period between 1945 and 1970. It started with the production of organophosphorous insecticides, carbamates and ureas (1940-1945s), followed by triazines and fungicides (benzimidazoles, pyrimidines, triazoles and imidazoles). Some pesticides of these groups are still used nowadays. The "third generation" of pesticides appeared in the period 1970-1980. It includes pyrethroids and sulfonylureas, which can be used at low dosage rates because of their strong biological action. Following this period, pesticides have been applied intensively up to today, although the introduction of strict legislation regarding their use has limited their application.

Despite the social and economic benefits of pesticides, such as increasing crops production, diminishing the price of food and controlling diseases like malaria and encephalitis, serious concerns about their risk appeared since once released, some of these compounds do not degrade in the environment and present toxicity. This was the

case with DDT and organochlorine pesticides. Because of their environmental persistence, some of these compounds have had unintended consequences. For instance, DDT caused egg shell thinning and thus affected the reproduction of certain types of birds. This problem was brought to the public's attention through the publication of the book Silent Spring in 1962 [5]. As a consequence, in the 1970s, DDT was banned for use in 86 countries and severe restrictions were imposed on the use of other pesticides, which were gradually replaced by compounds that are less environmentally persistent, but may be somewhat more toxic to mammals. DDT, however, is still produced and used to control malaria in some developing countries. Methoxychlor (Figure 1-1), a synthetic organochlorine used as an insecticide [6], was intended to be a replacement for DDT. Nonetheless, its degradation is very slow, it is ingested and absorbed by living organisms and accumulates in the food chain. This compound was, therefore, banned for use by the European Union in 2002 [7] due to its acute toxicity, bioaccumulation and endocrine disruption activity.

Pesticides show a high biological activity and toxicity (acute and chronic). As such, they can be best described as biocides since they are capable of harming all forms of life other than the target pest. Annually, and on the global scale, approximately 355 000 people are involuntary poisoned due to the excessive exposure and inappropriate use of toxic chemicals [8]. Acute exposure to pesticides can lead to death or serious illness [9]. Long term exposure can cause serious health problems such as reproductive disorders, immune-system disruption, endocrine disruption, impaired nervous-system function and even cancer [10-12].

The over-application or misuse of pesticides contributes to transport these compounds to habitats of non-target animals and to enter surface and ground water. Most of the pesticides are resistant to chemical and/or photochemical degradation, and may build up in animal tissues as well as contaminate food (fruits and vegetables) and drinking water, with consequent serious threat to human and animal health [13]. The combination of the increase of the global demand for food associated with the development of new chemical substances for agricultural application poses serious risks today.

The evaluation, marketing and use of pesticides (herbicides, insecticides, fungicides, etc.) for plant protection within the European Union (EU) were first regulated under the Council Directive 91/414/EEC [14]. The Directive aimed to harmonize the approval of agricultural pesticides within the EU members and also to

reevaluate the use of the 834 pesticides existing in the EEC at that time. This Directive lays out a comprehensive risk assessment and authorization procedure for active substances, and for products containing these substances. Each active substance has to be proven safe in terms of human health, including residues in the food chain, animal health and the environment, in particular related to groundwater and non-target organisms (such as birds, mammals, earthworms, bees), in order to be allowed to be marketed. Additionally, it is also stated that it is the responsibility of industry to provide the data showing that a substance can be used safely with respect to human health and the environment.

The Directive 91/414/EEC has been the subject of successive revisions being replaced by European Commission Directive EC 1107/2009. This Regulation aims, amongst other things, to ensure a high level of human, animal and environmental protection as well as to provide clearer rules to make the approval process for pesticides more efficient. In 1999 a new Directive was established (1999/45/CE) [15], which starts to include the agricultural pesticides in the legislation of dangerous substances, establishing as mandatory its reference in the labels and the safety data sheets.

The problems associate with water pollution and quality within the European Members prompted the establishment of the EU Water Directive Framework (WDF) in 2002 [16]. This WDF defined a new legislative approach to manage and to protect water by the coordination of different EU policies based on geographical and hydrological formation (river basins). WDF takes account all the aspects of water use and consumption. The goal is that all European waters have to achieve "good ecological and chemical status" to protect human health, water supply, natural ecosystems and biodiversity. This Directive has been updated by a more recent one [17]. The limits and guideline values for pesticides in drinking water have been issued by the World Health Organization (WHO), EU and many countries. The EU has set standards for drinking water at a maximum permissible concentration (MCL) for any particular pesticide of 0.1 and 0.5 g L^{-1} for the sum of all pesticides [18], including their degradation products (Directive 98/83/EC of the council).

In Portugal, the first legislation on pesticides was introduced with the Portuguese decree law nº 47802 from 19 July 1967 [19] which established the mandatory approval of agricultural pesticides (also described at that time as phyto-pharmaceuticals). Since the adhesion of Portugal to the EU in 1986 an increase in the number of the active

substances and formulations of the order of 41% has been observed along with an expansion of 188% in the pesticide companies.

The EU seeks to reduce the overall impact of pesticides on health and on environment, and regulate their actual usage. Consequently, in 2006 the European Commission proposed a strategy to improve the way pesticides are used across the EU. This strategy aims to encourage low-input or pesticide-free cultivation, in particular through raising user awareness, promoting the use of codes of good practice and making financial means available for applied research and training. The potential for pesticide contamination of water resources can be reduced considerably through the use of carefully designed pesticide management practices, increasing awareness of farmers with regard to the handling and application of pesticides, guided by the following goals: i) the prevention of pest infestations, ii) the use of pesticides only when necessary, iii) the inclusion of environmental considerations in selection and application of pesticides, and iv) the use of management practices which reduce pesticide loss.

Knowledge on pesticide behavior under environmental conditions is essential to have a more accurate understanding of the hazard that these compounds may or may not possess and also to discover routes to remove them from water resources.

1.3 Pesticide characteristics

1.3.1 Definition and classification

Pesticides are natural or synthetic substances that are used to prevent, eliminate, or control a variety of agricultural pests (insects, weeds, microbes, fungi, slugs, plant diseases, etc.) that compete with humans for food, destroy assets and spread disease [20-23]. Most of the pesticides are chemical substances; nevertheless, they may also be biological agents such as viruses or bacteria. Due to their nature, pesticides are potentially toxic to other organisms, including humans, and need to be used safely and disposed of properly. The term pesticide includes chemicals used as growth regulators, defoliants, desiccants, fruit thinning agents, or agents for preventing the premature fall of fruits, and substances applied to crops either before or after harvest to prevent deterioration during storage or transport [23].

Pesticides are often applied in agriculture as formulations. A formulation is a mixture of the active ingredient of the pesticide with inactive substances - the adjuvants [24]. The adjuvant is a specific substance, other than water, which itself has no

pesticidal properties but that enhances or is intended to enhance the efficiency of a particular pesticide to which it is added. It can only be used with a pesticide in accordance with the conditions of approval of that pesticide. Adjuvants can be surfactants, mineral, vegetable oils, emulsifiers and salts. Many commercial formulations contain adjuvants to improve pesticide retention and absorption by leaves or shoots and have to be diluted with water prior to its application. The combination of various adjuvants such surfactants, oils, and fertilizer salts have shown to be effective in improving the activity of some herbicides [24,25]. Formulations should be as effective as possible in order to make handling and application safer, easier, and more accurate to the target.

Pesticides may be classified into several categories since they vary in physical-chemical properties and identity. However, most of the literature classifies pesticides in three main categories according to their: chemical structure, mode of action and usage (target pest species) [21,23].

- *MODE OF ACTION*:

Pesticides are classified based on the way in which they act to bring about the desired effect. In this way pesticides are classified as contact (non-systemic) and systemic pesticides.

- The *non-systemic pesticides* are those that do not appreciably penetrate plant tissues and consequently are not transported within the plant vascular system. They will only bring about the desired effect when they come in contact with the targeted pest, hence the name contact pesticides. Examples of compounds: paraquat, diquat and dibromide.

- The *systemic pesticides* are those which effectively penetrate the plant tissues and move through the plant vascular system in order to bring about the desired effect.

- *CHEMICAL STRUCTURE:*

The classification of pesticides according to their chemical structure is the most widely used and useful since the physical-chemical properties of the pesticides will allow an understanding of their efficacy, mode of application and the precautions that

need to be taken during application. Pesticides are divided in four main groups: organochlorines, organophosphorous, carbamates and pyrethroids:

1) *Organochlorines*: are organic compounds with five or more chlorine atoms. They were the first synthetic organic pesticides to be used in agriculture and in public health, as earlier mentioned. The largest part of them was widely used as insecticides and they are resistant to most chemical and microbial degradation, remaining in the environment for a long period. Examples are the compounds: DDT, dieldrin, chlordane, endosulfan, aldrin, helptachlor, etc.

2) *Organophosphorous:* contain a phosphate group in their basic structure and are used as insecticides. In contrast to the organochlorines these pesticides are highly toxic to humans but do not remain in the environment for long periods of time [22]. Examples of compounds are: parathion, malathion, thimet, diazinon, trichlorphone, glyphosate, etc.

3) *Carbamates*: are organic pesticides derived from carbamic acid (see general formula). Carbamates were developed into commercial pesticides in the 1950s and are considered highly toxic to humans. It is a very large family with compounds that are effective as insecticides, herbicides, and fungicides. Nonetheless, the most commonly used application is as insecticides. Examples of compounds include: carbaryl, aldicarb, asulam, carbofuran, carbetamid, carbosulfan, chlorpropham, ethiofencarb, isoprocarb, methomyl, oxamyl, phenmedipham, etc.

$$HNR_1 \overset{\displaystyle \overset{O}{\|}}{\underset{}{-\!\!-C-\!\!-}} OR_2$$
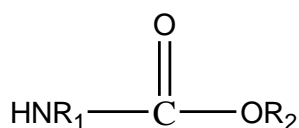
R_2 = aromatic or aliphatic moiety; If R_1 = methyl group, carbamate insecticide; If R_1 = aromatic moiety, carbamate herbicide; If R_1 = benzimidazole moiety, carbamate fungicide.

4) *Pyrethroids*: are synthetic analogues of the naturally occurring pyrethrins, a product of flowers from pyrethrum plant. Pyrethroids are very efficient against insect pests, present low mammalian toxicity and are readily biodegradable. Their fast photochemical degradation prevents them from being used as agricultural insecticides. Examples of compounds are: permethrin, cypermethrin and deltamethrin (synthetic compounds).

• *TARGET PEST SPECIES (USE):*

Pesticides are named according to the type of pests they control such as herbicides, insecticides, fungicides, rodenticides, nematicides, microbicides, and both plant and insect growth regulators [21,23]. Other types of pesticides such acaricides, molluscicides, nematicides, pheromones, repellents, rodenticides, etc., are listed in Table 1-1. Yet, most of the literature considers three main groups: *herbicides* - used to kill weeds and other plants growing in places where they are unwanted, rather than to protect them; *insecticides* - employed to kill insects and other arthropods and *fungicides* - used to kill fungi which cause molds, rots, and plant diseases.

Table 1-1 General classification of pesticides according to their target pest [23].

Type of pesticide	Target pest/organism
Insecticides	control insects
Algaecides	killing and/or slowing the growth of algae
Fungicides	control fungal problems like molds, mildew and rust
Herbicides	kill or inhibit the growth of unwanted plants, weeds
Rodenticides	rodents
Insect Growth Regulators	disrupt the growth and reproduction of insects
Plant Growth Regulators	alter the growth or reproduction of plants (ex: induce or delay flowering). Some growth regulators are used to move up or move back the normal harvest date for the crop and to obtain better quality and/or yield of the crop.
Molluscicides	control slugs, snails and other molluscs
Wood Preservatives	make wood resistant to insects, fungus and other pests
Repellents	repel unwanted pests, often by taste or smell
Ovicides	control eggs of insects and mites
Rodenticides	control rats, mice, bats and other rodents
Defoliants	cause plants to drop their leaves
Pheromones	biologically active chemicals used to attract insects or disrupt their mating behavior
Miticides	control mites that feed on plants and animals (mites are tiny insecticides spider-like animals)
Mothballs	insecticides used to kill fabric pests by fumigation in sealed containers
Antimicrobials	control germs and microbes such as bacteria and viruses
Herbicide safeners	antifeedants
Desiccants	dry up living plant tissues

1.3.2 Physical-chemical properties

When a pesticide is applied in the environment, it becomes distributed among water, soil, air and biota (living organisms) compartments (Figure 1-2). Therefore, the physical-chemical properties of a particular pesticide are very important for providing information on its fate in the environment (mode of action, dosage, mode of application, bioaccumulation and degradation) and will indicate the fraction of the pesticide that will move into each compartment. The physical properties of pesticides vary significantly according to their chemical nature and formulation. Properties such as water solubility, vapour pressure, volatility, *n*-octanol-water partition coefficient and soil adsorption are characteristic properties of each pesticide. Their definition and environmental significance are given below.
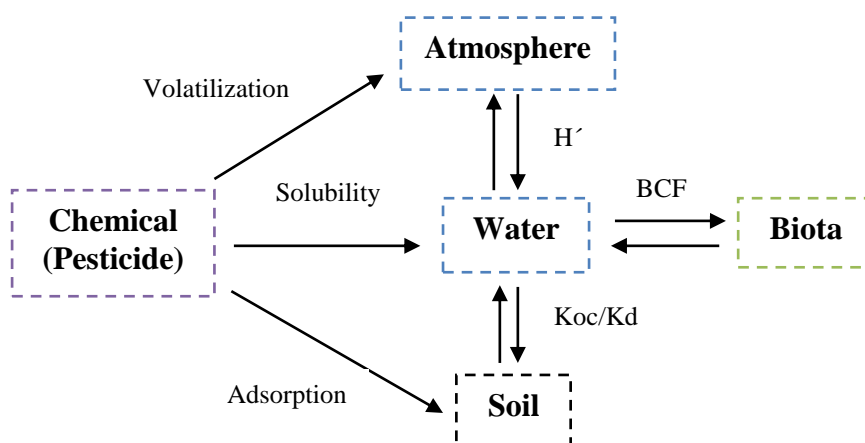
Figure 1-2 Environmental compartments and physical-chemical properties.

1.3.2.1 Water solubility

Water solubility is a fundamental chemical property defined as the concentration of a chemical dissolved in water (usually given in mg L^{-1} = ppm (parts per million)). Solubility expresses the tendency of a pesticide to be removed from soil by runoff or irrigation water and to reach the surface water [23]. Pesticides with low solubilities, below the threshold value of 30 mg L^{-1} are considered to have relatively low potential for leaching or runoff. Very water soluble pesticides with solubility values greater than 30 mg L^{-1} tend not to accumulate in soil or biota due to their strongly polar nature, and have a high leaching potential if the degradation rate and the soil adsorption coefficient are low. This suggests that they will degrade via hydrolysis which is a favored reaction

in water. Nonetheless, this parameter alone cannot be used to predict leaching through soil although the distribution of pesticides in the environment is conditioned by a variety of partition coefficients into water.

1.3.2.2 Octanol-water partition coefficient

The *n*-octanol-water partition coefficient K_{ow} is an indicator of the environmental fate of a chemical substance since it gives a general idea of how a chemical will be distributed in the environment [23]. This parameter is characteristic of the liphophility of the chemical and gives an indication of the compound's tendency to accumulate in biological membranes and living organisms. Apart from this prediction of the bioaccumulation in aquatic and terrestrial organisms, K_{ow} has also been used to indicate the mobility and persistence in soils and of soil sorption [26,27].

K_{ow} is defined as the ratio of a chemical's concentration in the *n*-octanol phase to its concentration in the aqueous phase of a two-phase *n*-octanol/water system (equation 1.1). It is usually expressed as log K_{ow} [28].

$$K_{ow} = \frac{chemical\ concentration\ in\ n\text{-}octanol\ phase}{chemical\ concentration\ in\ water\ phase} \qquad (1.1)$$

Chemicals (pesticides, in this case) with log K_{ow} values greater than 4 are regarded as of great concern since they can be adsorbed in soils and living organisms leading to bioaccumulation. The polarity of a molecule is strongly correlated with K_{ow}. Polarity refers to the extent to which charge is unevenly distributed within the molecule and to the occurrence of polar functional groups in it. As a rough rule, non-polar substances are characterized by log K_{ow} values above 4-5 whereas polar substances have log K_{ow} values below 1 or 1.5. Between these two values, compounds are classified as moderately polar.

In a general way, the bioaccumulation of pesticides in aquatic organisms is related to their K_{ow}. Bioaccumulation can be determined by measuring the bio concentration factor (BCF) which is defined as the concentration of the pesticide in tissue per concentration of chemical in water. This describes the accumulation of pollutants through chemical partitioning from the aqueous phase into an organic phase. The BCF show a linear relationship with log K_{ow}, but only up to a value of log K_{ow} of 5-6. Pesticides have rather different log K_{ow} values, depending on their structural family.

Triazine pesticides have values of log K_{ow} between 1.95 and 3.38 which suggests a low bioaccumulation potential while organophosphates and carbamates have log K_{ow} values in the range of 0.7 to 5.9 [29].

1.3.2.3 Soil adsorption coefficient

Adsorption of pesticides on soils or sediments is a major factor in their transportation and eventual degradation. Adsorption can be defined as the binding of a chemical (in this case a pesticide) to soil particles, mostly due to organic matter that coats the soil particles [23]. The richer is a soil in organic matter the higher is the binding by less-soluble pesticides. The tendency of a pesticide to be adsorbed by soil is expressed by its adsorption coefficient, K_{oc}, as given by equation (1.2):

$$K_{oc} = \frac{K_d \times 100}{\% \ Organic \ matter} \qquad (1.2)$$

Where K_d is the sorption coefficient and it measures the concentration of pesticide adsorbed onto soil per concentration of pesticide dissolved in water. Values for K_d vary greatly because the organic content of soil is not considered in the equation. Therefore, and since pesticides bond mainly to soil organic matter (organic carbon) it is necessary to divide K_d by the percentage of organic carbon in soil in order to obtain the final soil's adsorption coefficient K_{oc}. This makes the adsorption coefficient a pesticide-specific property, independent of soil type.

High K_{oc} values indicate a tendency for the pesticide to be adsorbed by soil particles rather than remaining in the soil solution. Nevertheless, they can be carried with eroded soil particles by surface runoff. The pesticides may subsequently desorb from soil particles and become surface water contaminants. K_{oc} values < 500 indicate a considerable potential for losses through leaching.

1.3.2.4 Vapour pressure and volatility

The vapour pressure is defined as the partial pressure of a chemical, in the gas phase, in equilibrium with solid or liquid [23]. Vapour pressures are very temperature-dependent. The potential for a pesticide to volatilize, *i.e.*, to become a gas, is expressed by its Henry's Law constant H. Henry´s Law involves a partition coefficient defined as

the ratio of a chemical's concentration in air to its concentration in water at equilibrium. The Henry´s Law constant for a chemical is generally expressed by H (eq. 1.3) when it is dimensionless (equation 1.3),

$$H = \frac{\text{concentration of chemical in air}}{\text{concentration of chemical in water}} \qquad (1.3)$$

or is represented by H´ when given with units, equation (1.4):

$$H´ = \frac{\text{liquid vapour pressure}}{\text{chemical solubility in water}} \ (\text{Pa m}^3 \text{ mol}^{-1}) \qquad (1.4)$$

It is generally accepted that compounds with H values $< 10^{-5}$ Pa m^3 mol^{-1} have little tendency to volatilize and persist in water. High value of H indicates volatilization of the pesticide from water into the atmosphere with consequent distribution over a large area. Gaseous losses can be reduced through soil incorporation. Although exchange of soil with the atmosphere does take place, the rate is so slow that volatilization losses of incorporated pesticides are very low. Pesticides which have volatilized can be redeposited through rain and thereby reach off-target areas. For most pesticides, loss through volatilization is insignificant compared with leaching or surface losses. The main pathway for atmospheric loss of a pesticide is through drift of spray mist under windy conditions, which is relatively independent of a pesticide's chemical characteristics.

1.3.2.5 Persistence

Persistence refers to the amount of time a pesticide remains in the environment. It is measured by its half-life time ($t_{1/2}$) [23]. The more persistent pesticides, having longer half-lives, can pose a greater threat to the environment since they remain there longer. Persistence is a function of the chemical and biological degradation processes which break down the pesticide into less harmful compounds. The rate of hydrolysis, photochemical and free radical reactions of a pesticide is usually expressed in terms of half-life $t_{1/2}$, which is defined as the time required for the pesticide to undergo dissipation or degradation (hydrolysis or photolysis) to half of its initial concentration. For example, the hydrolysis half-life values helps to estimate how long a chemical will

persist in an aqueous environment. If the chemical resists to hydrolysis then it may degrade via some other pathway such as microbial metabolism. In general, pesticides with a long half-life have a higher potential of reaching surface or groundwater because they are exposed to the hydrologic forces for a longer period of time.

Most of the degradation kinetics of pesticides follows a first order behaviour with a half-life time given by $t_{1/2} = \ln(2)/k$. The measurements of the half-life depend strongly on the environmental conditions in which they are measured (soil, site, light, temperature, soil microbial activity, etc.). Therefore, it is possible to find in the literature different values for the same compound depending on the experimental conditions under which it was measured.

1.3.2.6 Toxicity

The toxicity of a pesticide is defined as its capacity to cause injury to a living system [23]. The dose-time relationship is fundamental to determine the type of toxicity presented by the pesticide. This relationship indicates two types of toxicity: acute or chronic.

Acute toxicity is due to short-term exposure and happens within a relatively short period of time. The acute toxicity of a chemical refers to its ability to do systemic damage as a result of a single exposure to relatively large amounts of the chemical. A pesticide with a high acute toxicity may be deadly if even a very small amount is absorbed. Acute toxicity may be measured as acute oral, acute dermal and acute inhalation. Acute toxicity of a pesticide is measured by its lethal dose at fifty percent, LD_{50} (mg of substance/kg of body weight of the test animal). For example, an acute oral LD_{50} indicates the amount of pesticide swallowed that has killed half of the animals tested. LD_{50} is given for acute oral and dermal toxicity while the acute inhalation toxicity is measured by the lethal concentration at fifty percent LC_{50} (mg L^{-1}). The lower the LD_{50} or LC_{50} of a pesticide, the greater it is its toxicity to humans and animals. Pesticides with a high LD_{50} are the least toxic to humans if used according to the directions on the product label.

The *chronic toxicity* refers to harmful effects produced by long-term exposure to pesticides over a longer period of time. The chronic toxicity of a pesticide is more difficult to determine through laboratory analysis than acute toxicity. There is no standard measure like the LD_{50} for chronic toxicity. Some of the suspected chronic

effects from exposure to certain pesticides include birth defects, production of tumors, blood disorders and neurotoxic effects.

The World Health Organization (WHO) has developed a classification of pesticides by chemical hazard which groups pesticides according to the potential risks to human health. The classification is based primarily on the acute oral and dermal toxicity to the rat, LD_{50} (mg/kg body/weight). There are five classes of toxicity [30]. These are: class Ia - extremely hazardous, class Ib - highly hazardous, class II - moderately hazardous, class III - slightly hazardous and class IV - products unlikely to present acute hazard in normal use. The classification distinguishes between the more and the less hazardous forms of each pesticide in that it is based on the toxicity of the technical compound and on its formulations. Despite the fact that some pesticide products are considered only slightly toxic or relatively nontoxic, all pesticides can be hazardous to humans, animals, other organisms and the environment if the instructions on the product label are not followed.

Toxicology studies have demonstrated specific neurodegenerative effects from exposure to certain pesticides. Human case reports have also suggested causal relations between pesticide exposure and Parkinson disease [31].

1.4 Distribution and environmental fate of pesticides

The goal of pesticide use is to apply products that will remain in the target area long enough to control the specific pest(s) and then degrade into harmless compounds in the soil, air or water, without contaminating the environment. However, when a pesticide is spread in the environment only a small percentage of it reaches its target. Most of it remains on soil or plants or is washed out in natural waters causing adverse effects on plants, wildlife and even in humans. This movement can be beneficial if the pesticide is carried to a specific target area, like a plant's root zone, or if it helps to ensure that degradation occurs at the proper time and place. Sometimes, however, non-target insects, plants and other organisms come into contact with the pesticide. This can result in reduced control of the target pest and injury to non-target plants, animals and ultimately to humans through consumption of contaminated water or food.

How persistent these pollutants are in a given environmental system depends on transport and degradation processes. Any remaining pesticide or pesticide residue can be transported between the environmental compartments and through one, several or all

of the pathways, as shown in Figure 1-3.
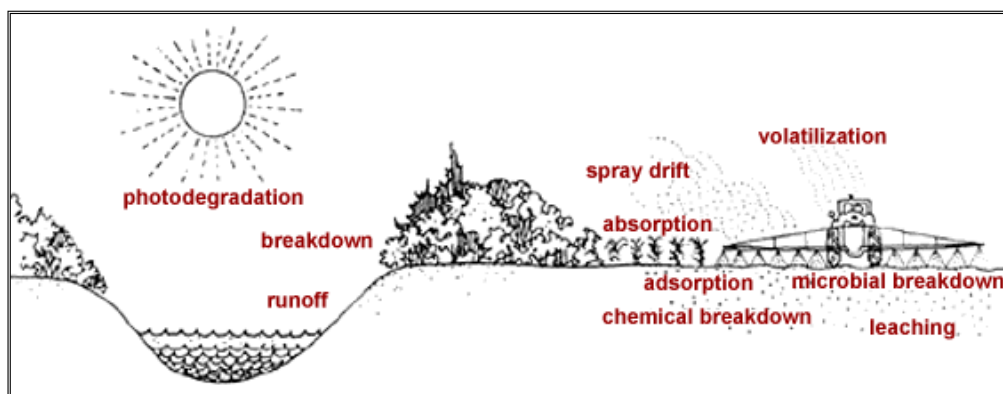
Figure 1-3 Environmental fate of pesticides in the environment. Redrawn from reference [32].

This movement of the pesticide is a complex process affected by weather, soil, and geological conditions, in addition to physical-chemical characteristics of the pesticide itself (given in previous section). The main distribution processes of pesticides in the environment involve surface runoff, leaching or erosion, adsorption and volatilization. The degradation processes include chemical, microbiological and degradation by sunlight.

Pesticides can be transported into the atmosphere by drift, volatilization and wind erosion. From there they can precipitate into surface waters contaminating lakes and streams. Surface waters can also be polluted by agricultural chemicals through irrigation and rainfall runoff. Runoff occurs when water carries pesticides either mixed in the water or bound to eroding soil to off target points. Rain carries pesticides off plant leaves to foliage near the ground and into the soil. The amount of pesticide runoff depends on the grade or slope of an area, the properties of the soil, the amount and timing of irrigation or rainfall, and the properties of the pesticide. Pesticides which have entered into soil may be taken up by plants and degraded into other chemical forms. However, if the pesticide is not readily degraded it may percolate and leach downward through the soil reaching groundwater sources. If, however, the pesticide is either insoluble or tightly bound to soil particles then it is more likely to be retained in the upper soil layers and small amounts may be lost to surface waters through runoff or erosion. For most pesticides the potential for surface loss or leaching to groundwater depends mainly on the half-life, solubility and adsorption coefficient. In general, pesticides with a long half-life have a higher potential of reaching surface or

groundwater because they are exposed to the hydrological forces for a longer period of time. Pesticides which are insoluble or have high adsorption coefficients tend to remain near the soil surface and are more susceptible to surface loss. Soluble pesticides with low adsorption coefficients have higher leaching potentials.

Possible ways to reduce the contamination of water sources are by careful management of the pesticides and by using suitable dosage and application methods.

1.5 Plant growth regulators

Plant growth regulators (PGRs), also known as growth regulators or plant hormones, are naturally occurring or synthetic chemicals used to alter the growth of a plant or plant part [33,34]. PGRs are employed in agriculture, horticulture and viticulture to alter the growth of plants/fruits, leading to improved morphological structure, facilitation of harvesting, quantitative and qualitative increases in yield, and modification of plant constituents [34]. Hormones are substances naturally produced by plants, substances that control normal plant functions such as root growth, fruit set and drop, growth and other development processes [33,35]. PGRs are small organic compounds that influence physiological responses to environmental stimuli at very low concentration, and are often transported from one part of the plant to another.

PGRs are applied in agricultural crops [33,36] (distinct from herbicidal action which destroys the plant) to obtain specific advantages such as: 1) regulating the chemical composition of the plant and/or the color of fruit, 2) controlling plant or organ size, 3) promoting rooting and propagation, 4) initiating or terminate the dormancy of seeds, buds and tubers, 5) promoting, delaying or preventing flowering, 6) inducing or preventing leaf and/or fruit drop by abscission, 7) controlling fruit set and further fruit development, 8) changing the timing of crop development, 9) influencing mineral uptake from the soil, 10) preventing postharvest spoilage, 11) increasing plant resistance to pests and 12) enhancing plant resistance to such environmental factors as temperature, water, and air pollution.

The use of PGRs began in the 1930s when ethylene and acetylene were used to induce flowering and fruit formation in pineapples. Since then many other plant growth regulators have been used, and some of these compounds have become indispensable in modern crop growing [37,38]. Many targets for plant growth regulators are also goals for reproduction, either by employing conventional methods or by genetic engineering.

However, in spite of the possibilities that reproduction offers, plant growth regulators often enable faster and better solutions to many problems. PGRs allow for an active regulation of plant processes, thereby adjusting a given genotype to its particular growing conditions. In other words, PGRs can be highly flexible for the fine-tuning of crop plants that grow at a given site under largely uncontrollable and unpredictable. Consequently, PGRs have great promise to increase the world food supply.

There are some herbicides and insecticides that although they are not true PGRs can cause some plant-growth-regulating effects. This is the case of the widely used insecticide carbaryl which is used to thin apple fruit from trees and to aid in encouraging annual bearing [34].

PGRs are classified in six main classes: *auxins, cytokinins, ethylene generators, gibberellins, growth inhibitors and growth retardants* [34]. Table 1-2 lists the classes of plant growth regulators, its main functions and gives as example some types of compounds belonging to each group.

Table 1-2 Plant growth regulator class, examples of compounds, functions and applications [34].

Class	Examples of compounds	Functions	Applications
Auxins	*1H*-indole-3-acetic acid (natural compound); 1-Naphthol; 2-(1-Naphthyl) acetamide; 1-Naphthylacetic acid; (2-Naphthoxy) acetic acid	Shoot elongation	Thin tree fruit, increase rooting and flower formation
Cytokinins	Benzyladenine, kinetin	Stimulate cell division	Prolong storage life of flowers and stimulate bud initiation and root growth
Ethylene generators	1-Methylcyclopropene	Ripening	Induce uniform ripening in fruit and vegetables
Gibberellins	Gibberellic acid	Stimulate cell division and elongation	Increase stalk length, increase flower and fruit size
Growth inhibitors	Carbaryl; propham; brutalin	Slows growth	Promote flower production by shortening internodes
Growth retardants	Daminozide; Flurprimidol	Slows growth	Retard tobacco sucker growth

Auxins were the first class of PGRs discovered. They stimulate cell elongation and cell division, autumnal loss of leaves, and the formation of buds, roots, flowers and fruit. Auxin action is inhibited by light which is an important role of the growth of stems toward light (phototropism) against the force of gravity (geotropism) and positively hydrotropic (moisture-seeking). The cells exposed to light do not grow as quickly as those on the shaded side and thus the plant grows toward the light source.

Auxins are usually synthetic compounds. The exception is the naturally occurring Indole-3-acetic acid (IAA). The synthetic auxins are widely used in vegetative propagation of plants from stem and leaf cutting. They are resistant to oxidation by enzymes that degrade IAA. In addition to their greater stability, they are often more effective than IAA in specific applications. The synthetic auxins are favoured in commercial applications due of their low cost and greater chemical stability [34].

Auxins usually have a ring system with at least one double bond and are linked by a side-chain that terminates in a carboxyl group. Members of the Auxin group are [34]: Indole-3-acetic acid, Indole-3-butyric acid, 1-naphthalene acetic acid, 2-(1-naphthyl) acetamide, 2-(naphthoxy) acetic acid, 1-naphthol, tris [2-(2,4-dichlorophenoxy)ethyl] phosphate, 1-(naphthloxy) acetic acid, 4-chlorophenoxyacetic acid, (2,4-dichlorophenoxy) acetic acid, 4-(2,4-dichlorophenoxy) butyric acid, 2-(2,4-dichlorophenoxy) propanoic acid, 2-(2,4,5-trichlorophenoxy) propanoic acid, naphthenic acid and (2,4,5-trichlorophenoxy) acetic acid. Carbaryl, although widely used as insecticide, has also been used as thinning agent in apple production. However, its pronounced insecticide activity led it to be banned for use as a PGR.

● *Indole-3-acetic acid (IAA):* is the only naturally occurring auxin that has the exact structure of auxin activity. IAA is the major auxin involved in many of the physiological processes in plants. LD_{50} rat oral: > 500 mg/kg; Trade name: Rhizopon A (Rhizopon B.V.). Preparations containing these compounds are mainly used for the rooting of cuttings.

● *4-(1H-indol-3yl) butyric acid or Indole-3-butyric acid (IBA):* is more stable than IAA. LD_{50} mice oral: 100 mg/kg. Trade name: Seradix (Bayer CropScience); Rhizopon AA (Rhizopon B.V.). Preparations containing these compounds are mainly used for the rooting of cuttings.

● *1-Naphthaleneacetic acid (1-NAA):* it is used to encourage root development in cuttings. 1-NAA is widely used in vegetative propagation of plants from stem and leaf

cutting. LD_{50} rat oral: > 1000 mg/kg. Trade names: Obsthormon 24a (L. Gobbi s.r.l.), Fruit Fix (AMVAC Chemical Corp.).

• *2-(1-Naphthyl) acetamide (NAD or NAAm):* LD_{50} rat oral: 1690 mg/kg, Trade names: Diramid (L. Gobbi s.r.l.), Amid Thin W (Bayer CropScience, AMVAC Chemical Corp.). 1-NAA and NAD are used at lower dosages for fruit setting and fruit retention in apples. Higher dosages are used for thinning. There is also some use of these compounds for the rooting of cuttings.

Figure 1-4 illustrate the chemical structures of some naphthalene based pesticides with auxin, herbicide, insecticide and growth activity. This choice was made because these naphthalene derivatives are structurally related, which can be helpful to compare their behavior in the environment regarding the two plant growth regulators that are subject of study within this thesis, the 2-(naphthyl) acetamide and 2-naphthoxy acetic acid. Therefore, the next section gives information on the physical-chemical properties and degradation processes of these two PGRs.
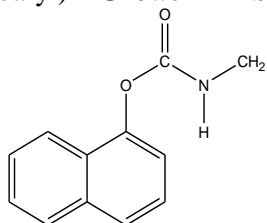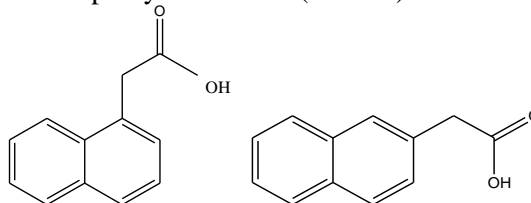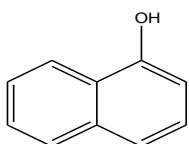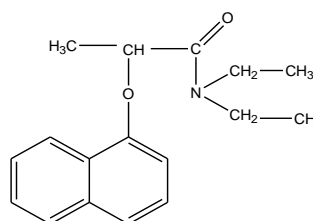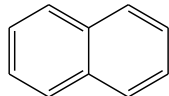
Figure 1-4 Chemical structures of naphthalene based pesticides (plant growth regulators, insecticides and herbicides compounds).

1.5.1 2-(1-Naphthyl) acetamide

2-(1-Naphthyl) acetamide (IUPAC nomenclature) is a plant growth regulator which is described in the literature by several names and abbreviation, such as α-naphthaleneacetamide, NAA Amide, 1-naphthylacetamide, NAD, naphthylacetamide, etc [21,39,40]. Some of its formulation names are Amid-Thin, Amid-Thin W, Frufix, Rootone, Amcotone, Fruitone, etc.

In this thesis the name adopted is in accordance with IUPAC nomenclature, and the common abbreviation NAD has been used throughout the thesis. NAD (Figure 1-5) has been widely used for more than 60 years in agriculture as a component in many commercial plant rooting and horticultural formulations [41,42]. It is used i) as fruit thinning agent for a variety of fruits such as apple, pear, peach, grape, ii) for root cuttings iii) and to prevent fruit drop shortly before harvest [21,41,42]. Its action mainly occurs by inducing abscission of flower buds. In 1941 Gardner reported for the first time the use of plant growth regulators to decrease preharvest abscission on citrus fruits [41]. He discovered that the application of NAD to pineapple oranges early in the harvest season at a concentration of 100 ppm (mg L^{-1}) reduced fruit drop for twelve weeks or longer.
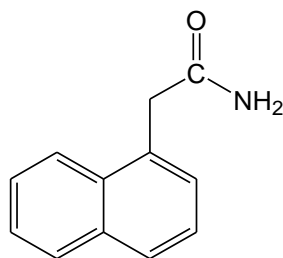
Figure 1-5 Chemical structure of 2-(1-naphthyl) acetamide (NAD).

NAD is used in crops as formulations [21,39]. The representative formulated products are "Amid-Thin W", a wettable powder containing 8.2% (w/w) 2-(1-naphthyl) acetamide and "Amcotone", a wettable powder containing 1.2% (w/w) of 2-(1-naphthyl) acetamide and 0.45 % (w/w) of 1-naphthylacetic acid (1-NAA), registered under different trade names in Europe. NAD is often mixed with carbaryl and is slightly less toxic than 1-NAA. The US Environmental Protection Agency (EPA) indicates that approximately 20.000 lbs of these naphthalene acetate active ingredients (NAD, 1-NAA, etc.) are applied annually in USA [39]. NAD is one of the 295 substances under the regulation of the European Commission (EC) No 2229/2004 [43], as amended by

the Commission Regulation (EC) No 1095/2007 [44] and was recently evaluated in the framework of the Directive 91/414/EEC [14].

NAD has a solubility in water of 164 mg L^{-1} (at 20 ℃, pH 7, 99.6 %), a vapour pressure of 9.4×10^{-7} Pa (at 20 ℃, 98.9 % purity), a Henry´s law constant equal to 1.02×10^{-8} Pa m^3 mol^{-1} (at 20 ℃) and a *n*-octanol-water partition coefficient of 1.58 (log K_{ow} at pH 7, at 25 ℃, 98.8 % purity) [40]. NAD is not bioaccumulative, and is not persistent in the environment.

Half-lives of NAD in soil and water were estimated to be 38 days [40] while the half-lives in sediment were 150 days. The degradation of NAD was investigated in laboratory incubations in dark aerobic water systems. Under these conditions NAD exhibited low persistence forming the major metabolite 1-naphthylacetic acid (1-NAA), most probably by hydrolysis.

NAD is "harmful if swallowed" based on LD50 oral: 1655 mg/kg bw/day (males rats), LD50 dermal: > 2000 mg/kg bw/day (rat), LC50 inhalation: > 2.17 mg L^{-1} (whole body, rats) [40]. Severe over exposure can result in injury or death. It is not acutely toxic via dermal and inhalation routes. It is not a skin irritant or a skin sensitiser but it is an eye irritant [40]. NAD is harmful to aquatic organisms, end point driving the aquatic risk assessment: acute fish LC_{50} = 44 mg a.s./L (regulatory concentration including a safety factor of 100 = 0.44 mg a.s./L) [40].

The Acceptable Daily Intake (ADI), Acceptable Operator Exposure Level (AOEL) and the Acute Reference Dose (ARfD) have been established as 0.1 mg/kg bw/day, 0.07 mg/kg bw/day and 0.1 mg/kg bw, respectively [40]. A maximum residue level (MRLs) for NAD in apples was proposed at the limit of quantification (LOQ) of 0.02 mg/kg.

Most of the analytical methods previously published for the determination of this compound are based on fluorescence or phosphorescence [45-47] detection taking advantage of the good spectrophotometric properties and sensitivity of this type of aromatic compounds. Moreover, chromatographic techniques such as high performance liquid chromatography (HPLC) with UV or diode array detection (DAD) have also been employed to identify and quantify NAD in fruits/vegetables and in water [48,49]. There is insufficient information in the literature concerning the transformation pathways of NAD in water. However, EPA reported 1-NAA as a metabolite resultant from NAD hydrolysis [39].

1.5.2 2-(Naphthoxy) acetic acid

2-Naphthoxyacetic acid (IUPAC nomenclature), or β-(naphthyloxy) acetic acid, abbreviated as 2-NOA (Figure 1-6), is a synthetic auxin-like plant growth regulator that is absorbed by leaves and roots. It is applied on several crops to promote the growth of roots, to encourage fruit set and to prevent fruit from falling prematurely [21,50]. It is used a fruit setting spray on tomatoes, strawberries, blackberries, aubergines, grapes and pineapples [22].
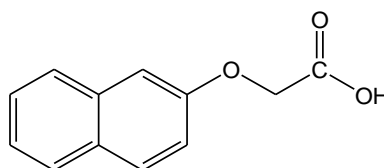
Figure 1-6 Chemical structure of 2-(naphthyloxy) acetic acid (2-NOA).

2-NOA is one of the 295 substances under the regulation of the European Commission (EC) No 2229/2004 [43], as amended by the Commission Regulation (EC) No 1095/2007 and was recently evaluated in the framework of the Directive 91/414/EEC [14]. France and Italy provided to the European Food Safety Authority (EFSA) a Draft Assessment Report (DAR) on 2-NOA in 2007 and later in 2010 [50]. The role of EFSA is to gather all the documentation provided by EC and make a risk assessment report on 2-NOA in order to send it to EC. A first decision on non-inclusion of the active substance 2-NOA in Annex I to Directive 91/414/EEC was therefore published by means of Commission Directive 2009/65/EC [51], which entered into force on 16 February 2009. This decision was based on the clear evidence of harmful effects regarding the consumer and operator exposures as well as the ecotoxicological assessment. In addition, it was also decided to withdraw the authorization of products containing this substance. Therefore, the use of 2-NOA is no longer authorized within the EU since 2009.

2-NOA has a solubility in water of 203 mg L^{-1} (at 20 ºC, pH > 3, 99.5% purity, pure water), a pKa of 3.35 (weak acid), a *n*-octanol-water partition coefficient of 2.50 (calculate by log K_{ow} at pH 3), a Henry´s law constant of 1.06×10^{-4} Pa m^3 mol^{-1} (20 ºC and pH > 3) and a vapour pressure of 2.89×10^{-6} Pa (at 25 ºC, 99.2 % purity) [50]. These properties indicate that 2-NOA has low potential for volatilization, no potential for accumulation and low risk of bioconcentration. The estimated atmospheric half-life is

shorter than 2 days, eliminating the hypothesis of transport through atmosphere at long range [50].

According to an EFSA report, 2-NOA is stable to hydrolysis [50] and its aqueous photolysis led to the formation of two major metabolites named DP-3 and DP-4. However, neither their structure nor their chemical nature was identified. In addition, laboratory incubation of 2-NOA in aerobic natural sediment water systems led to the formation of a major metabolite named M6. Once again it was not possible to identify this metabolite. The metabolite M6 was only found in the sediment while the major part of 2-NOA was found in the water phase. In soils, 2-NOA showed very high to high mobility and no metabolites were found upon 2-NOA photolysis. However, a minor metabolite named [(6-hydroxy-2-naphthyl)oxy] acetic acid was found in rat urine.

2-NOA is considered to be slightly toxic (class III) by the World Health Organization (WHO) based on its acute toxicity in rats (LD_{50} oral: 1417 mg/kg bw (rat), LD_{50} oral: 1557 mg/kg bw (mice), LD_{50} dermal: 2000 mg/kg bw (rat), LC_{50} inhalation = 4.87 mg/L (rat)). However, no maximum residue levels (MRLs) have been fixed for this compound [50]. The toxicological profile of 2-NOA was evaluated in the framework of Directive 91/414/EEC and toxicological reference values were established by EFSA [50], which resulted in an acceptable daily intake (ADI) and an acute reference dose (ARfD) being established at 0.01 mg/kg bw per day and 0.6 mg/kg bw, respectively. 2-NOA is considered toxic to fish, daphnids and algae, and very toxic to aquatic plants. In surface and ground water, 2-NOA is considered to be very toxic to aquatic organisms with an end point driving the aquatic risk assessment: aquatic plants EC_{50} = 3.85 mg a.s./L (regulatory concentration including a safety factor of 10 = 0.385 mg a.s./L).

Several analytical techniques have been employed to detect and quantify 2-NOA and its residues in water and in food. For this purpose, luminescence methods such as fluorescence and phosphorescence [51-53] have been extensively used, as well as chromatographic methods such as HPLC and gas chromatography (GC) [54-56].

In contrast, little information was found in literature concerning the photochemical degradation of 2-NOA in aqueous solution. In fact, and to our knowledge, only one paper was published on the degradation of 2-NOA in aqueous solution [56]. The authors of this paper described the degradation of 2-NOA in aqueous solution upon excitation with light of λ > 290 nm using GC-MS and GC-FTIR analysis [56]. The photoproducts were identified and a possible mechanism pathway was proposed, as depicted in Figure 1-7. Under aerobic conditions, the major photoproduct

obtained was 2-naphthol (1) along with minor amounts of 2-hydroxy-1-naphthaldehyde (3) and naphtho-[2,1-*b*]furan-2(1*H*)-one (5). Under these conditions, the cleavage of the aryloxy-carbon bond (route i) predominates to form 2-naphthol (1) or the rearranged hydroxy acid (2), which is detected as the corresponding lactone (4). Additionally, the cleavage of the C-C bond (route ii) also occurs, but to a lesser extent, with formation of 2-hydroxy-1-naphthaldehyde (3) due to a Photo-Fries rearrangement, as has been well documented in the literature [57,58] for this type of molecules. In contrast, under argon atmosphere only 2-naphthol (1) and naphtho-[2,1-*b*]furan-2(1*H*)-one (5) were detected.

EFSA [50] mentioned the formation of 2 metabolites upon 2-NOA photolysis in surface water named as DP-3 and DP-4. However, these compounds have not been identified. Additionally, in plants, 2-NOA is degraded to 2-naphthol followed by ring hydroxylation and ring opening [50].
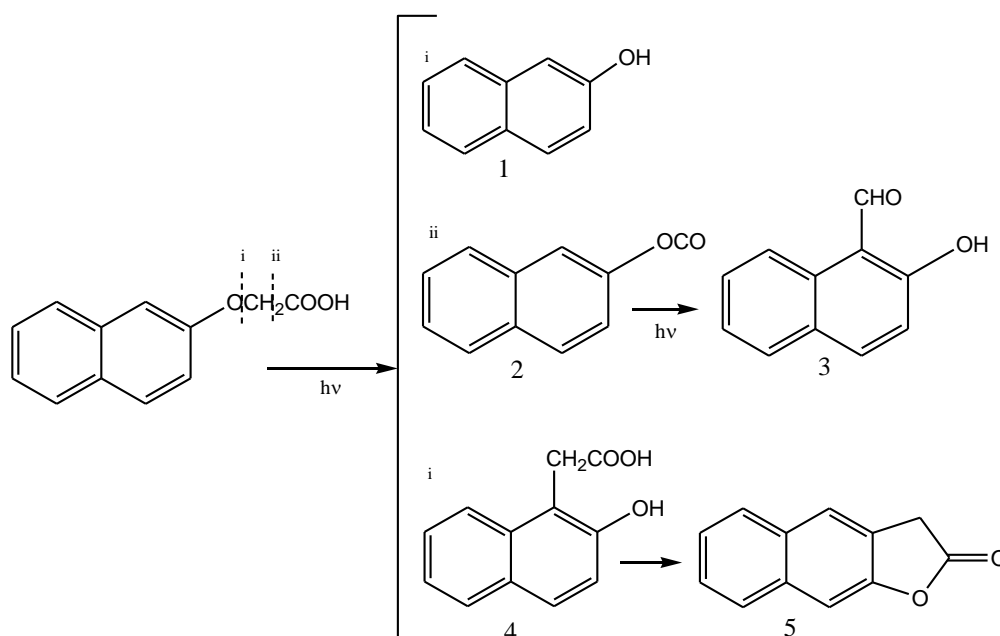
Figure 1-7 Proposed photodegradation pathway for 2-NOA in aqueous solution [56].

The lack of more deep scientific studies regarding the photochemical transformation of the plant growth regulators NAD and 2-NOA has prompted the interest in the study of its photochemical degradation in aqueous solution, either by direct or photocatalysed means in order to find possible routes towards environmental remediation. To help interpret the data, the photophysical characterization of these two compounds was also object of study in this thesis in order to obtain information of the reactive species involved in the mechanism of degradation.

1.6 Photochemical degradation of pesticides in water

The sun (in particular, its photons) is a cheap and abundant reagent that can initiate a large number of reactions in water. This process of degradation by light is one of the factors controlling the fate and persistence of pesticides and other chemicals in the environment [59]. Knowledge on the photoproducts formed is also important since enable to establish the involved photolytic pathways, thus providing valuable information on possible ways of protecting the environment.

Photodegradation, which is the breakdown of a chemical compound by light, is one of the most common methods for the elimination of organic pollutants from aqueous environment. Photodegradation may take place on plant leaves, surface of soils, water and air. Several types of pesticides have been subject of study concerning their kinetics of degradation, quantum yields, mechanisms, photoproducts and toxicity [60,61,62].

All pesticides are susceptible to photodegradation, to some extent. The photodegradation rate of a pesticide is dependent on the amount of light absorbed by the compounds, environmental conditions such as intensity and spectrum of sunlight, length of exposure, pH of the media and presence of other occurring ions (humic substances, etc.), and on the chemical properties of the pesticide [62]. Pesticides that break down quickly generally do not persist in the environment or on the crop. However pesticides that break down too rapidly may only provide short-term control.

Photochemical reactions are carried out in the presence of either UV (200-400 nm) or visible light. The artificial irradiation sources used for the UV region are normally incandescent, fluorescent, deuterium and mercury lamps, with the last ones being the mostly used with excitation at 254 nm, 312 nm or 365 nm. The 254 nm radiation excites $\pi \rightarrow \pi^*$ transition and is useful for compounds with absorption bands < 300 nm. For the visible region (400-700 nm), tungsten halogen lamps are commonly used. They can excite $n \rightarrow \pi^*$ and other transitions and are useful for compounds with absorption bands > 300 nm. Most of the photodegradation experiments carried out in laboratory use deionised water while only a minority involve the use of natural waters. Thus, they may not accurately reproduce environmental conditions.

According to the literature, the degradation of pesticides in water can be classified into three main categories [61]: direct, photosensitized and catalysed by Advanced Oxidation Processes (AOPs). AOPs will not be the subject of discussion in

this section but will be considered in Chapter 4 of this thesis. In the next section is given the definition and some examples of direct and photosensitized degradation methods.

1.6.1 Direct degradation

Since almost all pesticides absorb light in the UV-vis region, they are susceptible to undergo direct degradation (or direct photolysis). Given that most of the pesticides absorb light with wavelengths shorter (< 290 nm) than that of the solar spectrum, and since the intensity of sunlight enclose only a small fraction of UV radiation (Figure 1-8), the majority of the studies concerning the direct degradation are performed using artificial irradiation sources at 254 nm. Nevertheless, those pesticides that do absorb a portion of solar light (λ> 290 nm) may undergo photolysis, as supported by various studies [63]. In some of these, solar light processes were modeled by using artificial solar light sources [64].
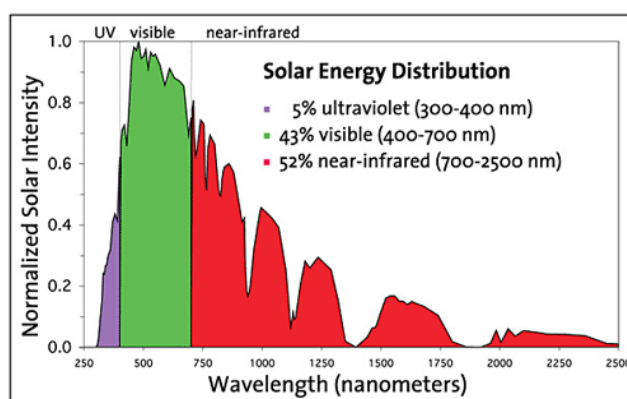
Figure 1-8 Solar energy distribution at the Earth´s surface [65].

Upon light irradiation, the ground state of a pesticide P is promoted to its singlet excited state $^1P^*$ which may decay by intersystem crossing to form its triplet excited state $^3P^*$. These excited states can then undergo several chemical reactions such as photooxidation, photoionization, photocycloaddition, photoisomerization, etc., producing reactive species such as singlet oxygen, hydroxyl radicals, hydrated electron, etc., that are responsible for the degradation processes [59,61]. Singlet oxygen can be involved in various processes. It is a moderately reactive electrophile known for oxidizing a wide range of electron rich organic compounds, such as pollutants containing polycyclic aromatic hydrocarbon [66] and other aromatic or heterocyclic

moieties present in pesticides. Singlet oxygen has been detected in natural waters and is naturally generated via sunlight initiated photochemistry [67].

The photochemical behavior of many different types of pesticides such as naphthalene and its derivatives, carbamates, organosphosphorous, triazines, amides, and chlorophenol compounds [68-74] have been subject of study over the last decades in relation to their direct degradation, either by UV or solar radiation.

Boule *et al.* [68] studied the photolysis of several aromatic herbicides, particularly phenylureas and halogenated derivatives, using artificial irradiation with different excitation wavelength (254, 290-350, 365 nm and simulated solar light sunlight). They concluded that the pesticides undergo various types of chemical reactions: carbon-halogen bond cleavage, other reactions involving the aromatic ring and reactions of the aliphatic moiety. The nature of the substituent's and their relative positions on the ring are directly related with the type of reaction. Toxicity experiments frequently show a higher toxicity to microorganisms of the formed intermediates than the parent compound.

The photochemical degradation of naphthalene in water, either by direct UV or sunlight, or sensitized degradation, has been the subject of interest [70,71]. Richard *et al.* studied the irradiation of aqueous naphthalene with simulated solar light ($\lambda > 290$ nm) [71]. The authors proved that naphthalene was transformed mainly via monophotonic ionization with formation of the transient species naphthalene radical cation and hydrated electrons. Three major photoproducts were formed and identified: 2-formylcinnamaldehyde, 7-hydroxy-1,4-naphthoquinone, 2-carboxycinnamaldehyde. Another intermediate product was formed, 1,4-naphthoquinone, but did not accumulate in the system. Using natural sunlight as light source, McConkey *et al.* [70] identified several products of naphthalene degradation, including 1-naphthol (major product), coumarin and two hydroxyquinones. Photocycloaddition reactions with subsequent oxidations (formation of endoperoxides) and/or rearrangements were involved. The products obtained were also similar to those resulting from naphthalene metabolism.

The photodegradation of other naphthalene based pesticides such as napropamide, nabumetone, carbaryl, etc., have also been investigated [74-76]. For example, the direct photolysis of aqueous napropamide solution [75] at different excitation wavelengths (254, 310 nm) led to the formation of three photoproducts with 1-naphthol as major byproduct. Toxicity assessment revealed an increase of toxicity of napropamide irradiated samples due to the formation of a photoproduct, which is more

toxic than its parent compound. As a consequence, it can be considered harmful to the surrounding environment. Brahmia *et al.* [74] described the direct degradation of the insecticide carbaryl in aqueous solutions using an irradiation system with maximum emission at 310 nm. Studies were carried out by steady state irradiation and also by laser flash photolysis in order to elucidate the reactive species involved in the degradation pathway. They observed the formation of the oxidation photoproducts 1,2-naphthoquinone, 2-hydroxy-1,4-naphthoquinone and 1,4-naphthoquinone. Traces of 1-naphthol were also found. However, when water was replaced by acetonitrile and methanol, 1-naphthol was found as the main photoproduct, accounting for 37 and 65 %, respectively, of converted carbaryl. The oxidation of carbaryl is likely to involve naphthoxyl radicals escaping the cage and solvated electrons and radical cations produced in the photoionisation process. In contrast to what is observed with other carbamates and aryl esters, no photo-Fries rearrangement was observed in this case.

1.6.2 Photosensitized degradation

Photosensitization is based on absorption of radiation by another molecule rather than the pesticide P [77]. This other molecule, the sensitizer (Sens), in its excited state can transfer its energy to the pesticide, or form other intermediates, leading to the formation of reactive species that will further induce the photochemical reactions. The different steps of degradation are given in Figure 1-9 where $Sens^*$ stands up for the sensitizer in its excited state (singlet or triplet), P^* is the pesticide in its excited state, Y represent other substances present in solution, and $P^{\bullet+}$, $P^{\bullet-}$, $Sens^{\bullet-}$ and $Sens^{\bullet+}$ represent the radical species of the pesticide and sensitizer, respectively.

$$Sens + h\nu \rightarrow Sens^*$$
$$Sens^* + P \rightarrow P^* + Sens$$
$$Sens^* + P \rightarrow P^{\bullet+} + Sens^{\bullet-}$$
$$or\ Sens^* + P \rightarrow P^{\bullet-} + Sens^{\bullet+}$$
$$P^* \rightarrow Products$$
$$P^* + Y \rightarrow Products$$
$$P^{\bullet-} + Y \rightarrow Products$$
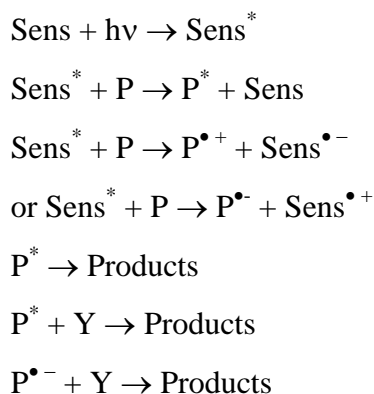
Figure 1-9 General mechanism of photosensitized processes.

In the presence of molecular oxygen two possible mechanisms have been distinguished in the literature, which are referred to as Type I and Type II [78-80], according to the type of reactive species that are formed. The type I mechanism involves the formation of superoxide anions $O_2^{\bullet-}$ through electron transfer from the excited triplet state of the sensitizer $^3Sen^*$ to molecular oxygen. Type II mechanism involves the formation of singlet oxygen $^1O_2$ through energy transfer from the excited triplet state of the sensitizer $^3Sen^*$ to molecular oxygen. These two reactive species of oxygen can then react with the pesticide leading to its degradation. Figure 1-10 illustrates, in an oversimplified way, the type I and type II mechanisms of degradation.

$$Sens + h\nu \rightarrow {}^1Sens^*$$
$${}^1Sens^* \rightarrow {}^3Sens^*$$
$${}^3Sens^* + {}^3O_2 \rightarrow Sens + \mathbf{{}^1O_2} \qquad \text{"Type II"}$$
$${}^3Sens^* + {}^3O_2 \rightarrow Sens^{\bullet+} + \mathbf{O_2^{\bullet-}} \qquad \text{"Type I"}$$
$${}^1O_2 + P \rightarrow PO_2 \rightarrow \rightarrow Products$$
$$O_2^{\bullet-} + P \rightarrow PO_2 \rightarrow \rightarrow Products$$
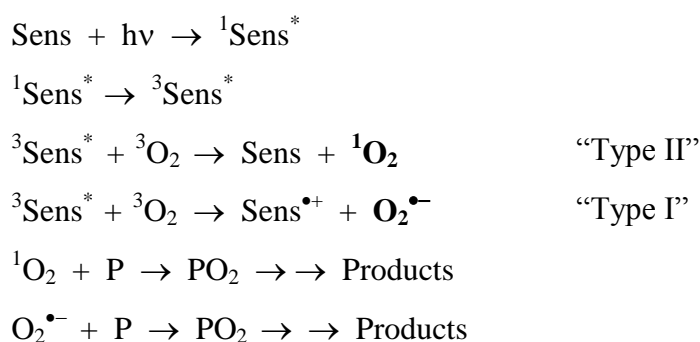
Figure 1-10 Schematic examples of Type I and type II mechanism.

Photosensitized degradation may be advantageous when pesticides absorb solar light poorly or when they are stable against direct photolysis. This process plays a major role in many natural waters where the presence of NO_3^-/NO_2^-, humic substances, natural organic matter, amino acids or metal anions (Fe(III)) [81] are responsible for the damage undergone by biological and chemical systems upon simultaneous action of visible light, molecular oxygen and a sensitizer. These natural substances can induce the generation of very reactive species such as singlet oxygen, hydroxyl and superoxide radicals, hydroperoxides and hydrogen peroxide [82,83] which then undergo further chemical reactions. In natural waters, $^1O_2$ can be produce in aerated aqueous solutions of an appropriate sensitizer that absorbs light and transfers the energy to dissolved triplet molecular oxygen. The dissolved organic matter is the primary sensitizer responsible for singlet oxygen formation [82]. Superoxide radical anion and hydrated electrons formed during photooxidation of aromatic compounds in near-UV light may also be produced by sensitizers [83].

The use of humic substances as photosensitizers to promote photooxidation of pesticides has been demonstrated [82]. For example, the photodecomposition of carbofuran was investigated in pure water and in the presence of various samples of organic matter (soil-extracted humic and fulvic acids) [84]. The presence of the dissolved organic matter was found to inhibit the carbofuran photolysis, ranging from 19 to 70 % for a concentration of dissolved organic matter of 5-30 mg L^{-1}.

In addition to natural substances, other compounds as Rose Bengal, methlyene blue, acetone, riboflavin, etc., have been used as sensitizers for the degradation of pesticides [85]. Photosensitized reactions have been demonstrated for different kind of pesticides using different types of sensitizers as is the case of aldrin [86], DDT [87], s-triazine herbicides, thiamethoxam and thiacloprid, etc. Significant degradation of pesticides can also be obtained in the presence of electron-acceptor sensitizers. For example, triadimenol, a pesticide applied in horticulture and viticulture that is very difficult to degrade by direct UV photolysis, could be significantly decomposed in the presence of 9,10-dicyanoanthracene or 2,4,6-triphenylpyrylium tetrafluoroborate [88]. This decomposition was accelerated by the presence of oxygen.

1.7 Inclusion complexes of cyclodextrins

1.7.1 Structure

Cyclodextrins (CDs) are cyclic oligosaccharides composed of more than five D-glucose units [89,90]. They were first discovered by Villiers in 1891 but it was only in the beginning of the twenty century that their properties were reported by Schardinger. The most common and commercial available CDs are constituted by six (α-), seven (β-) and eight (γ-) D-glucose units. As depicted in Figure 1-11 the glucose units are in C(1) chair conformation and are connected by 1,4-glycosidic bonds. CDs have a truncated cone shape structure with a height of approximately 8 Å and an inner central cavity diameter varying from approximately 5 Å (α-CD) to 8.5 Å (γ-CD) [89,90].

As a consequence of the chair conformation, the secondary hydroxyl groups on C(2) and C(3) atoms of the glucose are located on the larger rim of the truncated cone, whereas the primary hydroxyl groups are located on the opposite side. The interior of the cavity is composed by C-H groups and glycoside oxygen bridges [89,90]. The nonbonding electrons of the glycoside oxygen are directed toward the inside of the

cavity producing a high electron density, providing it some Lewis base character. As a result, the molecule has a hydrophilic exterior which helps increase water solubility of the guest molecule and an apolar cavity that provides a hydrophobic character ideal for solubilizing non-polar molecules [89].

The cavities of the α-, β- and γ-CDs possess on average 2, 6.5 and 12 water molecules, respectively. The water solubility of α- and γ-CDs is approximately 10^{-1} mol L^{-1} while for β-CD it is $< 2 \times 10^{-2}$ mol L^{-1}. Although β-CD presents the lowest solubility in water it is the most widely used cyclodextrin since it is non-toxic, biodegradable and relatively inexpensive [89,90]. In addition, the problem of solubility has been overcome by using derivatives of β-CD.
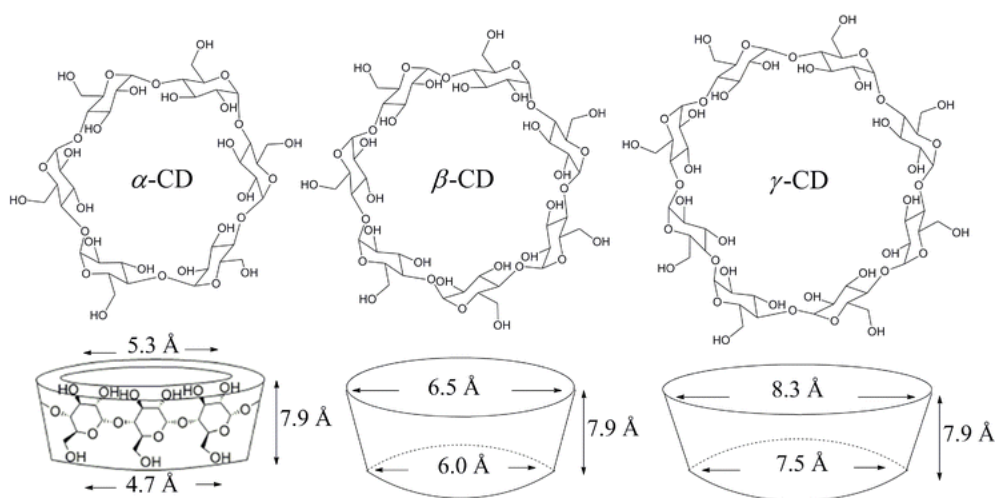
Figure 1-11 Chemical structure of CDs and schematic representation of the cone shape with the respective internal cavity diameter [90].

1.7.2 Formation of inclusion complexes

One of the most appealing characteristics of CDs is the ability of their central cavity to bind to a variety of organic and inorganic substrates forming host-guest inclusion complexes [92]. In aqueous solution the energetically unfavored (polar-apolar interaction) water molecules that occupy the slightly apolar CD cavity can easily be substituted in a fast, selective and reversible way by appropriate guest molecules, which are less polar then water (Figure 1-12).
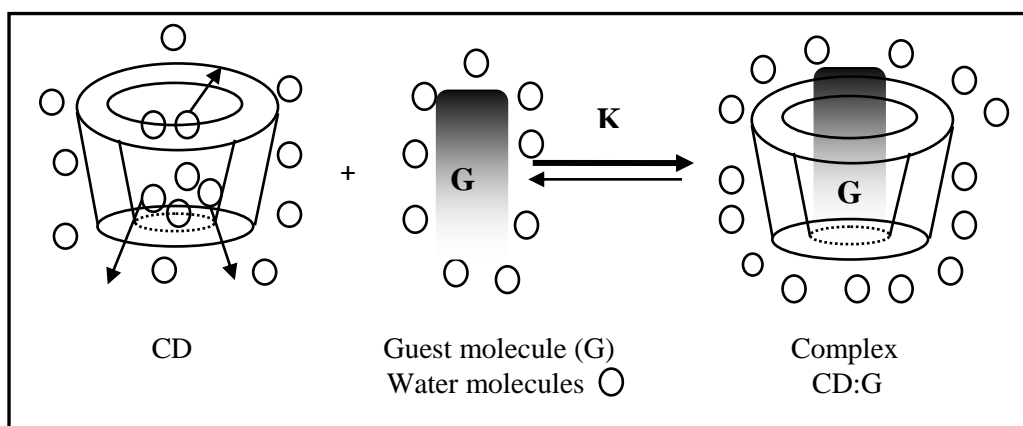
Figure 1-12 Schematic representation of the formation of inclusion complex of CD:Guest molecule.

The driving force for the formation of the inclusion complex comes from the substitution of the high entropy water molecules by a guest molecule (G). One, two or three CD molecules contain one or more entrapped guest molecules. The binding constant K (L mol^{-1}) of the inclusion complex is given by equation (1.5):

$$K = \frac{[CD:G]}{[CD][G]} \qquad (1.5)$$

The most frequent stoichiometry ratio of the host:guest inclusion complex is 1:1, although more complicated associations may occur (1:2, 2:1 2:2). Moreover, the binding of guest molecules with the host CD cavity induces important changes in the photophysical and photochemical properties of the guest molecules [93-95]. For instance, Monti *et al.* [95] observed an increase on the fluorescence quantum yields and lifetimes of dimethyl and trimethylphenols in the presence of β-CD, in agreement with the formation of 1:1 complexes with distinct photophysical properties.

Several intermolecular interactions such as van der Waals, hydrophobic and hydrogen bonding have been proposed for the formation of CD inclusion complexes in aqueous solution [91-93]. No covalent bonds are broken or formed during formation of the inclusion complex [91-93]. The stability of the inclusion complex is determined by the hydrophobic character of the guest molecule as well as its polarity, size and geometry [91-93]. For example, de La Peña *et al.* [95] studied the inclusion complexes of 2-naphthyloxyacetic acid (2-NOA) and 1-naphthylacetic acid (1-NAA) with β-CD in aqueous solution. A stoichiometric ratio 1:1 for the inclusion complex was observed for both compounds but their inclusion in the β-CD cavity was different. In the case of the

β-CD:2-NOA complex the naphthyl moiety is included in the CD and the acetic acid group protrudes from the cavity, while 1-NAA is only partially included due to the steric effect of the group in position 1.

This type of "molecular encapsulation" may lead to advantageous changes in the chemical and physical properties of the guest molecules such as:

• Improvement of the apparent solubility.

• Increase the stability of the compound in the presence of light, heat and oxidizing conditions.

• Decrease in the volatility.

• Modification of the chemical reactivity.

• Modification of liquid substances to powders.

• Protection against or enhancement of degradation.

• Masking of unpleasant smell and taste.

• Masking pigments or the colour of substances.

These properties have led to the widespread application of CDs in several fields such as food, pharmaceuticals, cosmetics, environment protection, bioconversion, packing and textile industry [96-102].

A wide variety of analytical techniques have been used to characterize the inclusion complexes formed in solution and in solid state. In solution, the most common techniques are phase-solubility and UV-vis, fluorescence, infrared, NMR and induced circular dichroism (ICD) spectroscopy [89,91,92]. Phase solubility allows determination of the stoichiometric ratio for the inclusion complex and the apparent binding constant K, given by equation (1.5) [103]. Additionally, computational modeling studies are also performed to obtain information concerning the spatial inclusion of the guest molecule on the CD cavity.

1.7.3 Application in agriculture

The inclusion of pesticides in CDs is attracting attention, not only due to the non-toxic nature of CDs, posing no risks either to humans or to the environment, but particularly due to the advantages that results from it [99-101]: improvement of pollutant solubilisation, elimination of organic pollutants by photodegradation and removal of heavy metals from water and soil. CDs are also applied in water treatment to

increase the stabilising action, encapsulation and adsorption of contaminants [99]. This can have an enormous influence on the residual persistence of pesticides in natural environments. It may also favor a more rational and efficient application of it, diminishing the environmental pollution of water sources and soils.

Literature data show that CDs form complexes with a wide variety of agricultural chemicals such as herbicides, insecticides, fungicides, repellents, pheromones and growth regulators [104-106]. Usually, the binding of pesticide with CDs is a dynamic equilibrium and the dissociation of the inclusion complex is a relatively rapid process [91]. The most common benefits of these applications in agriculture include alterations of the solubility of the pesticide, photodegradation or stabilization against the effects of light, biochemical degradation and a reduction of volatility.

The inclusion of a pesticide in CDs can influence its reactivity due to the interaction of the hydroxyl or substituted hydroxyl groups of the CD with the pesticide molecule [93]. This can either increase the rate of the reaction or stabilize the pesticide by preventing chemical reactions [102].

Studies of the catalytic effects of CDs on the degradation of pesticides are important to understand their persistence and fate in natural environments in order to promote the degradation of such hazardous pollutants. Additionally, it may also be used in pesticide formulations in order to stabilize it, leading to a more efficient use of the active substance. Ishiwata *et al.* [107 106] studied the inclusion-catalytic effect of α-, β- and γ-CDs on the degradation of eight organophosphorus pesticides in neutral aqueous media. An enhance of the degradation was observed, particularly for α-CD:diazinon and β-CD:chloropyrifos inclusion complexes. They also found that the differences in the catalytic effects of CD are dependent on the properties of the aromatic rings of pesticides and on the cavity size of the used CDs. Kamiya *et al.* [108,109] studied the effect of natural and methylated CDs on the hydrolysis rate of organophosphorus pesticides. Stabilization towards the degradation of the β-CD inclusion complexes with parathion, methyl parathion and fenitrothion was obtained; and at the same time the alkaline hydrolysis of paraoxon was accelerated. These results were explained in terms of the geometry of the inclusion complexes. The same group [110 109] also studied the inclusion effects of α-, β-, γ-CDs, hexa-2,6-dimethyl-α- and hepta-2,6-dimethyl-β-CDs on the photodegradation rates of the pesticide parathion and its oxidation product

paraoxon. Some of the CDs promoted the photodegradation of the pesticides while the others inhibited it. These different effects could be explained in terms of inclusion depth of the pesticides into CDs cavity. The deep inclusion of the phosphorus atom prevents the pesticide from interacting with the catalytic sites of the host cavity and the water or oxygen molecules from the solvent, slowing down the degradation. In 2001 the same authors studied the degradation of eleven organophosphorus pesticides in humic water complexed with α-, β- and γ-CDs [111]. The inclusion of the pesticides in humic water and CDs led to an increase on the degradation of these pesticides due to the photosensitized formation of hydroxyl radicals.

The contamination of soils and water has led to the development of formulations that prevent entry of the pesticides into the groundwater while maintaining effective pest control. Therefore, encapsulation of pesticides in CDs can change its characteristics. The group of Dailey *et al.* [112,113] prepared complexes with the herbicides metribuzin, atrazine, alachlor, simazine, and metolachlor. The idea was to develop formulations that prevent leaching while maintaining effective pest control. β-CD complexes of atrazine and simazine were prepared only after forcing reaction conditions, but they are resistant to dissociation owing to their high stability. In contrast, it was observed that a metribuzin-β-CD formulation controlled selected weed species in a greenhouse.

1.8 Photophysical and photochemical processes

1.8.1 Absorption of radiation

Photochemical reactions occur when molecules absorb radiation, normally of UV or visible range, resulting in the formation of excited states which then can undergo chemical reactions or physical deactivation. Two photochemical principles relate the absorption of light by molecules [114]:

The Grotthus-Draper law - only the radiation absorbed by a molecule can produce photochemical change within it.

The Stark-Einstein law - each absorbed photon will produce only one excited state (this refers to the primary steps of a reaction). The energy of a photon is given by the equation (1.6):

$$E = h\nu \tag{1.6}$$

where h is Planck´s constant (6.626×10^{-34} J s) and ν (cm^{-1}) is the frequency of the radiation. Therefore, the energy difference ΔE between two electronic levels is given by equation (1.7):

$$h\nu = \Delta E = E_n\text{-}E_0 \tag{1.7}$$

in which E_0 and E_n are the energy of the ground fundamental state and of the excited state n, respectively. The frequency of the radiation can be converted to wavelength (λ, nm) through the relation $\nu = c/\lambda$ where c represents the velocity of light ($\cong 3 \times 10^8$ m s^{-1}). As a consequence, equation (1.7) can be re-written to give the correlation between the energy required for photochemical transformation to occur at the wavelength of radiation used to excite electrons between molecular energy levels (equation 1.8):

$$\Delta E = \frac{1.196 \times 10^5}{\lambda \text{ (nm)}} \text{ kJ mol}^{-1} = \frac{1240}{\lambda \text{ (nm)}} \text{ eV} \tag{1.8}$$

Another important factor is that the transition between the two energy states must cause a change in the dipole moment of the molecule. The probability of occurrence of this electronic transition is given by the oscillator strength f as will be explained below in the text.

The absorption of light of hν energy by a molecule is given by the Beer-Lambert law according to equation (1.9):

$$A = \log_{10} \left(\frac{I_0}{I}\right) = \varepsilon \, c \, l \tag{1.9}$$

where A is the absorbance (or the optical density), I_0 and I is the light intensity before and after absorption (or the incident and transmitted radiant flux), respectively, ε is the molar absorption coefficient (L mol^{-1} cm^{-1}) at a certain wavelength and is characteristic of a molecule (commonly called the extinction coefficient), c (mol L^{-1}) is the concentration of the solution and l is the path length of the cell (normally 1 cm). This relation is only applicable in certain circumstances such as homogeneous medium, dilute solutions, etc.

In practical terms, the absorption of light is recorded as a function of the wavelength λ (or wave number $\nu = \lambda^{-1}$) by measuring the change in the intensity of the light beam passing through a sample in a cellule of 1 cm path length.

The measured extinction coefficient ε is a function of frequency, referring to the position of the maximum absorption band and the ability of a molecule to absorb is more adequately expressed by its oscillator strength f which is related to the integral of ε over all frequencies of absorption by equation (1.10):

$$f = \frac{2.3 \times 10^3 \; cm^2 \; m}{N \; e^2 \; \pi} \; F \int \varepsilon \; d\nu = \int 4.32 \times 10^{-9} \; F \int \varepsilon \; d\nu \tag{1.10}$$

where here c is the velocity of light ($c = \nu \times \lambda$), m and e are the mass and charge of an electron, N is Avogadro´s number (6.022×10^{23} mol^{-1}) and ε and ν have to be given in L mol^{-1} cm^{-1} and cm^{-1}, respectively. The factor F depends on the refractive index (n) of the absorbing medium, depicting solvent effects, with value close to unity when the band is allowed. Therefore, the absorption extinction coefficient given at a maximum wavelength of an absorption band ε_{max} measures the intensity of that band and gives also indication of the allowedness of the corresponding electronic transition (Table 1-3).

An electronic transition normally involves the promotion of an electron from an orbital of a molecule in the ground state to an unoccupied orbital by absorption of a photon. When a molecule in its ground state absorbs a photon, an electron occupying a σ, π or n orbital is promoted to a higher energy σ^* or π^* orbital. The type of electronic transitions is depicted in Figure 1-13 along with the molecular orbitals (MOs) [114].

Table 1-3 Correspondence between electron transition and molar absorption coefficient, ε.

Electron Transition	Absorption region (nm)	ε_{max} (L mol^{-1} cm^{-1})
$\sigma \rightarrow \sigma^*$	100-200	10^3
$n \rightarrow \sigma^*$	150-250	10^2-10^3
$\pi \rightarrow \pi^*$ (Isolated π-bonds) (Conjugated π-bonds)	180-250 220-IR	10^2-10^4
$n \rightarrow \pi^*$ (Isolated groups) (conjugated segments)	220-320 250-IR	1-400

As given in Figure 1-13a, the energy of these electronic transitions generally follows the order:

$$n \to \pi^* < \pi \to \pi^* < n \to \sigma^* < \sigma \to \sigma^*$$

Frequently, the MOs are classified as occupied (doubly), singly occupied and unoccupied: HOMO - Highest Occupied Molecular Orbital, LUMO - Lowest Occupied Molecular Orbital and SOMO - Singly Occupied Molecular Orbital (Figure 1-13b).
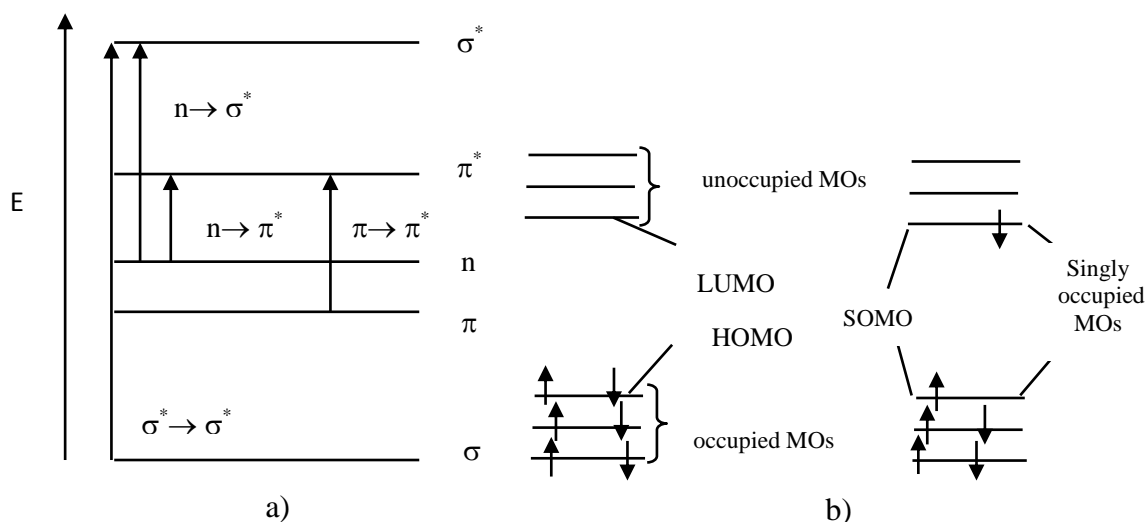
Figure 1-13 a) Molecular orbitals and electronic transitions induced by absorption of a photon. b) Classification of molecular orbitals with respect to electron occupancy.

1.8.2 Deactivation of the electronically excited states

A molecule is transformed to its excited state upon absorption of light in UV or visible region. In its excited state the molecule is unstable by nature relatively to its ground state. Therefore, the deactivation of the excited states must occur with consequent release of the excess energy. This energy can be released by radiative or non-radiative processes. The radiative transitions imply the emission of radiation from the electronically excited state to the ground state. This process of light emission is designated as luminescence. Luminescence is divided in two categories: fluorescence and phosphorescence, depending if the deactivation of the excited state has, respectively, the same multiplicity of the ground state (for example S_1-S_0) or not (for example T_1-S_0). In excited singlet states the electron in the excited orbital is paired (by opposite spin) to the second electron in the ground-state orbital. Consequently, return to the ground state is spin allowed and occurs rapidly by emission of a photon, with

emission rates of fluorescence in the order 10^8 s^{-1} (lifetimes near 10 ns). The non-radiative processes include internal conversion (*ic*) and intersystem crossing (*isc*). These processes are further elucidated in the next sections.

1.8.2.1 Perrin-Jablonski diagram

The Perrin-Jablonski diagram (Figure 1-14a) is convenient for visualizing in a simple way the possible molecular processes of absorption and deactivation of the excited states: *fluorescence, phosphorescence, ic, isc, vibrational relaxation and triplet-triplet transitions*. The absorption of light as well as the radiative transitions are depicted as vertical arrows while the non-radiative processes are represented by wavy arrows. The diagram puts in evidence the various electronic energy states of the molecule: the singlet electronic states are denoted as S_0 (fundamental ground state), S_1, S_2, ...S_n (excited states) and the triplet states as T_1, T_2, ...T_n. Vibrational levels are associated with each electronic state and are designated as v = 0,1,2,3,..n.
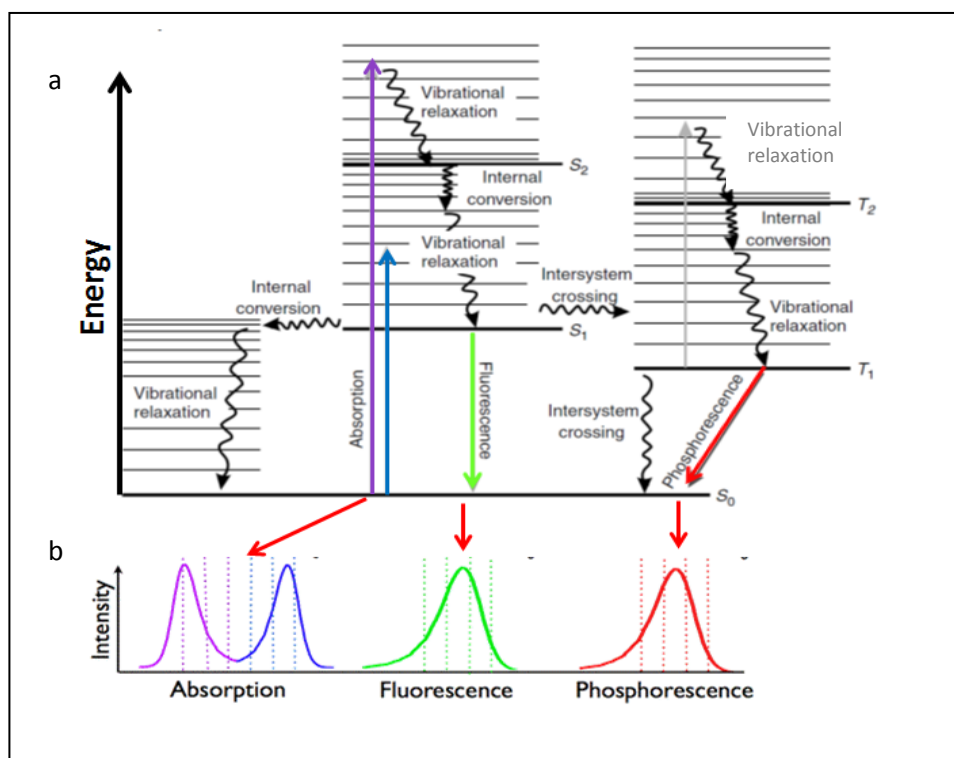
Figure 1-14 a) General Perrin-Jablonski diagram. Straight arrows represent radiative processes (fluorescence and phosphorescence) while wavy arrows represent the non-radiative processes (*ic* - internal conversion; *isc* - intersystem crossing, vr - vibration relaxation). b) Representative illustration of the relative position of the absorption, fluorescence and phosphorescence bands.

Absorption of light is a very fast process comparatively to all the other processes (typically it occurs in about 10^{-15} s), a time too short for significant displacement of the atomic nuclei of the molecule, according to the Franck-Condon principle. However, it is long enough to cause changes in the electronic structure of the absorbing molecule. The absorption of light starts from the lowest vibrational level (v=0) of the S_0 because the majority of molecules are in this level at room temperature. Upon absorption of light, the molecule reaches the first singlet excited state S_1 which can then undergo a spin conversion to the first triplet excited state T_1 by the nonradiative *isc* process. S_1 can also be deactivated to the singlet ground state through *ic* or fluorescence. The formation of excited states of different spin multiplicity from the singlet state, such as the triplet state, just after absorption of light are formally forbidden. However, it becomes partially allowed by effects such as spin-orbit coupling or vibronic coupling. The triplet excited state T_1 may be deactivated by light emission (phosphorescence) and/or by the non-radiative *isc* S_1-T_0 process.

In addition to the above photophysical deactivation processes, other deactivation pathways exist. It is convenient to divide the deactivation pathways into intramolecular and intermolecular processes, as depicted in Figure 1-15.
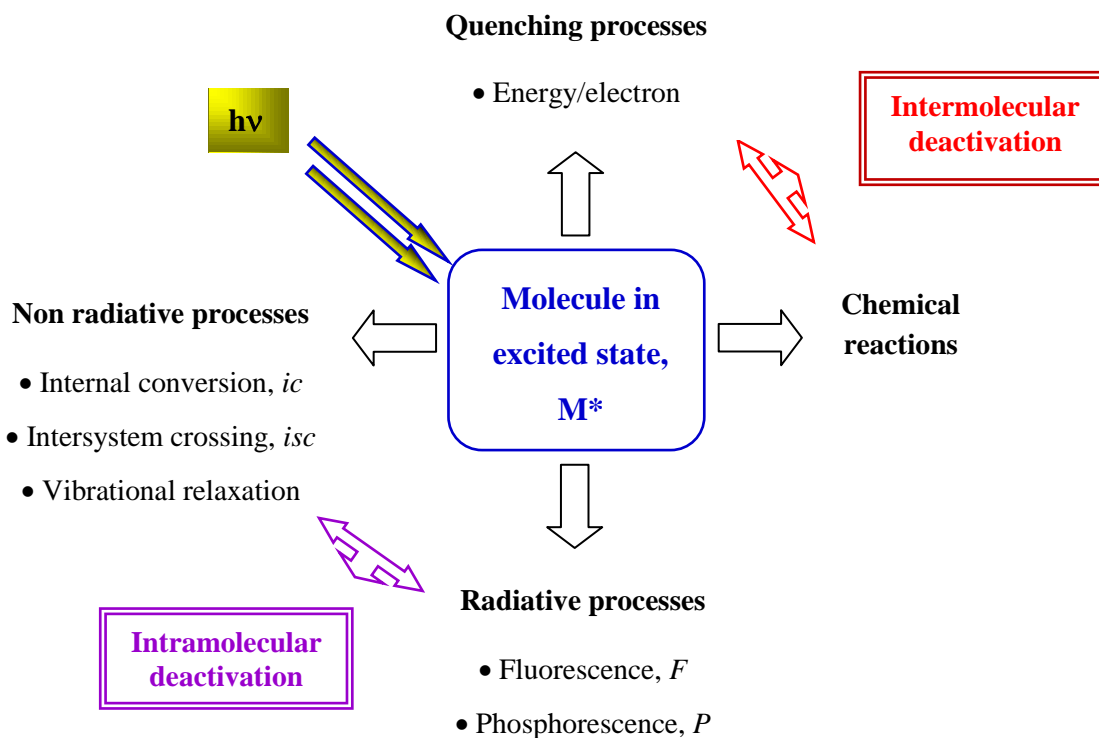
Figure 1-15 Possible deactivation (intermolecular and intramolecular) pathways of excited states.

1.8.2.2 Intramolecular deactivation processes

The intramolecular deactivation is a contribution of radiative and non-radiative (or non radiationless) processes to the photophysical desactivation of the excited states:

• **_Radiative decay processes_** involves emission of a photon. They are:

i. Fluorescence, _F_

is the spontaneous emission of UV or visible radiation from states of same multiplicity, this is, from the singlet excited state S_1 to the singlet ground state S_0:

$$S_1 \rightarrow S_0 + h\nu$$

The emission of fluorescence occurs at longer wavelengths (lower energies) than those of absorption, as shown in Fig. 1-14b. This shift in the energy between the absorption and emission is called the Stokes shift [114]. This parameter can give important information about the excited states. For example, it is known that when the dipole moment of a fluorescent molecule is higher in the excited state than in the ground state, the Stokes shift increases with solvent polarity. From a practical point of view, the detection of a fluorescent species is easier when the Stokes shift is larger. Some common fluorescent substances (fluorophores) are quinine sulfate, fluorescein, pyridine 1, rhodamine B and acridine orange. Fluorescence is typically observed from aromatic molecules such as naphthalene, anthracene, etc. [114]. The fluorescence emission of aromatic substances containing $-NO_2$ groups are generally weak, primarily as a result of large k_{nr} values (non-radiative rate constants). Fluorescence is also influenced by solvents, as will be referred ahead in the text.

ii. Phosphorescence, _P_

is the emission of a photon from the triplet excited state T_1 to the singlet ground state S_0:

$$T_1 \rightarrow S_0 + h\nu$$

Because the transition between states of different multiplicity is spin-forbidden (but it can be observed due to spin-orbit coupling), the emission is normally weak.

Since the energy of the lowest vibrational level of the triplet excited state T_1 is lower than the singlet excited state S_1, the phosphorescence spectrum is observed at longer wavelength (lower energy) values relative to fluorescence (Fig. 1-14b).

Phosphorescence is usually not observed in fluid solutions at room temperature since many deactivation processes exist that compete with emission. These processes can be the non-radiative decay and quenching processes (particularly by molecular oxygen). Therefore, most of the phosphorescence measurements are made at low temperature (77 K). The T→S transition is forbidden by symmetry and the rates of spontaneous emission are about 10^3 s^{-1} or less. Since k_{nr} values are near 10^9 s^{-1}, the quantum yields of phosphorescence are extremely small in liquid solutions at room temperature. However, the presence of heavy atoms such as bromine and iodine facilitate *isc* and thus enhance phosphorescence quantum yields. An example is given for the naphthalene molecule in Table 1-4 where the effect of heavy atom is clearly observed.

Table 1-4 Heavy atom effect on the emission properties of naphthalene [114].

Molecule	ϕ_F	k_{isc}/s^{-1}	ϕ_P	τ_T/s
Naphthalene	0.55	1.6×10^6	0.051	2.3
1-Fluoronaphthalene	0.84	5.7×10^5	0.056	1.5
1-Chloronaphthalene	0.058	4.9×10^7	0.30	0.29
1-Bromonaphthalene	0.0016	1.9×10^9	0.27	0.02
2-Iodonaphthalene	< 0.0005	$> 6 \times 10^9$	0.38	0.002

• *Non-radiative (or radiationless) decay processes* involves the transfer of excess energy into vibration, rotation, and translation of surrounding molecules resulting in heat to the surroundings. They are:

iii. Internal conversion, *ic*

is a non-radiative transition between two excited state of the same multiplicity, such as from singlet excited state S_n to the ground state S_0 with heat release to the surrounding molecules (such as solvents). Since these two states are of the same multiplicity the transformation is allowed and is often a favorable process with a very high rate constant.

$$S_n \rightarrow S_0 + \text{heat}$$

In solution this process involves transition between isoenergetic vibronic levels and is followed by vibrational relaxation towards the lowest vibrational level of the final electronic state (v=0). The excess vibrational energy is transferred to the solvent during collisions of the excited molecule with the surrounding solvent molecules. When a molecule is excited to an energy level higher than the lowest vibrational level (v=0) of the first electronic state, vibrational relaxation (and *ic* if the singlet excited state is higher than S_1) leads the excited molecule towards the vibrational level v=0 of the S_1 singlet excited state with a time scale of 10^{-13}-10^{-11} s. Internal conversion is more efficient from S_2 to S_1 than from S_1 to S_0 due to the much larger energy gap between S_1 and S_0. Therefore, the decay process of *ic* from S_1 to S_0 can compete with emission fluorescence and *isc* to the triplet excited state from which emission of phosphorescence can possibly be observed [114].

iv. Intersystem crossing, *isc*

is a non-radiative transition between electronic states of different multiplicity. It occurs, for example, from the singlet excited state S_1 to the triplet excited state T_1 with heat release:

$$S_1 \rightarrow T_1 + \text{heat}$$
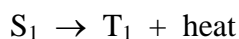
The transition between these two states of different multiplicity is spin forbidden and is usually 100 times or less than internal conversion. However, spin-orbit coupling, that is, the coupling between the orbital magnetic moment and the spin magnetic moment, can be large enough to make it possible. The probability of *isc* depends on the singlet and triplet states involved and also on the presence of heavy atoms on the molecule which favours the *isc* by enhancing spin orbit coupling (such as in the naphthalene example given in Table 1-4) [114]. Intersystem crossing may be fast enough (10^{-7}-10^{-9} s) to compete with the other pathways of de-excitation from S_1 as fluorescence and internal conversion.

Intersystem crossing can also occur from S_1 to T_0. Transition from T_1 to the singlet S_0 is forbidden and as a result the rate constants for triplet emission (phosphorescence) are several orders of magnitude smaller than those for fluorescence.

v. Vibrational relaxation, vr

A molecule may be promoted to several vibrational levels during the electronic excitation process. Collision of molecules with the excited species and solvent leads to rapid energy transfer and a slight increase in temperature of the solvent. Vibrational relaxation is so rapid that the lifetime of a vibrational excited molecule ($< 10^{-12}$) is less than the lifetime of the electronically excited state. For this reason the fluorescence from a solution always involves the transition of the lowest vibrational level of the excited state. Since the space of the emission lines are so close together, the transition of the vibrational relaxation can terminate in any vibrational level of the ground state.

1.8.2.3 Intermolecular deactivation processes

Intermolecular deactivation may involve both chemical reactions and physical quenching processes, this is, bimolecular processes.

The molecule M in its excited state M^* may react with other molecules that are in the surrounding media leading to the deactivation of the excited state by bimolecular processes through either physical quenching or chemical reactions (photoionization, photo-oxidation, photo-isomerization, redox reactions, photo-cycloaddtion, etc.). Therefore, the overall rate of deactivation of an excited state is the sum of the decay rates for intramolecular and intermolecular routes.

Quenching processes can be defined as any non-radiative deactivation of the excited state M* of a molecule by another molecule present in the system, the quencher Q (reaction 1.11). The term quenching will be used here as a photophysical process in which the M^* is restored unchanged to the ground state during a diffusive encounter with the quencher. Some examples of quencher molecules are oxygen, halogens, amines and electron-deficient molecules like acrylamide [114,115].

$$M^* + Q \overset{k_q}{\to} M + Q \text{ (+energy)} \tag{1.11}$$
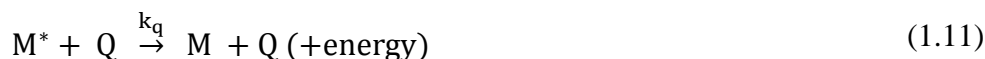
For this type of collisional quenching the decrease in intensity is described by the well-known Stern-Volmer equation (1.12), which for steady-state fluorescence intensities takes the form:

$$\frac{I_0}{I} = 1 + K_{SV} \times [Q] \hspace{4cm} (1.12)$$

where K_{sv} is the Stern-Volmer coefficient, [Q] stands for the concentration of the quencher and, I_0 and I are the fluorescence intensities of the molecule in absence and presence of the quencher, respectively. When studies are done for the triplet states, the ratio I_0/I is replaced by the ratio of the quantum yields ϕ_0/ϕ. The Stern-Volmer constant allows calculation of the quenching rate constant k_q of a bimolecular process through the following relationship (1.13):

$$K_{SV} = k_q \times \tau_S \hspace{4cm} (1.13)$$

where τ_S is the un-quenched fluorescence lifetime of the excited state determined experimentally.

The singlet or triplet excited states of a molecule can be quenched by several processes: energy transfer, electron transfer, effect of concentration, etc.

Energy transfer involves the energy transfer between the excited state of the donor molecule M* and the acceptor quencher Q (reaction 1.14). For this reaction to occur it is necessary that the energy level of Q is lower (or equal) to that of M^*.

$$M^* + Q \rightarrow M + Q^* \hspace{4cm} (1.14)$$

Energy processes are commonly used for the purpose of sensitization. Triplet-triplet (T-T) energy transfer is largely used for generation of triplet excited states of molecules which possess low quantum yields for triplet formation. The process can be given by reaction (1.15):

$$^3M^* + Q \rightarrow M + {}^3Q^* \text{ (triplet-triplet energy transfer)} \hspace{2cm} (1.15)$$

The triplet-triplet energy transfer only occurs efficiently when the energy of the donor molecule M in its triplet excited state $^3M^*$ is $\geq$ to the energy of the acceptor molecule Q. This means that the triplet state energies of the pesticides are determinant for the occurrence of the energy transfer. Naphthalene and its derivatives present triplet energies in the range < 78 kcal/mol, which being relatively low indicates that a wide range of sensitizers can transfer energy to them [114]. Singlet-singlet energy transfer

may also occur. For example, Dubois and his colleagues [114] observed singlet-singlet energy transfer from naphthalene to give sensitized biacetyl fluorescence in solution, with constant rates close to those predicted by the modified Debye equation.

Oxygen is one of the most effective quenchers of both singlet and triplet excited states of molecules [115-117]. The energy transfer between the triplet excited state of the molecule $^3M^*$ and molecular oxygen $^3O_2$ can lead to the formation of singlet oxygen $^1O_2$ (reaction 1.16). $^1O_2$ could also be formed from the singlet excited state of the molecule $^1M^*$, however, since singlet excited states are short lived - nanosecond time scale, there is, generally, only a low probability that the energy transfer can occur under these circumstances.

$$^3M^* + {}^3O_2 \rightarrow M + {}^1O_2 \text{ (triplet-triplet energy transfer)} \tag{1.16}$$

In general, the quenching rate constants by molecular oxygen of singlet excited states (k_q^S) of aromatic compounds such as naphthalene and its derivatives are around 10^{10} L mol^{-1} s^{-1} [116], this is, diffusion controlled. With triplet states, as has been found by L. K. Patterson et $al.$ [117] and various other scientists, the rate constant for energy transfer from triplet excited states to produce $^1O_2$ is normally 1/9 of the diffusion controlled rate in the solvent in agreement with what is expected from spin-statistical factors.

$Electron$ $transfer:$ involves the transfer of an electron between the excited state of the molecule M^* and the quencher with formation of new radical ion species. We present here the case in which the excited state is electron donor (reaction 1.17).

$$M^* + Q \rightarrow M^{\bullet+} + Q^{\bullet-} \rightarrow M + Q \text{ (+ energy)} \tag{1.17}$$
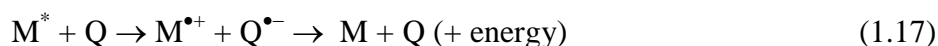
1.8.3 Kinetics and quantum yields of photophysical processes

The observed radiative lifetimes τ of an excited state (S_1, T_1) are related to the sum of the unimolecular rate constants k of the all decay processes originating from that state through the following equation (1.18):

$$\tau = \frac{1}{\sum k_i} \tag{1.18}$$

The extent to which each decay process (fluorescence, *ic*, *isc*, phosphorescence) contributes to the deactivation of the excited states to the ground state depends on the system being studied. Assuming that only the photophysical processes given in Jablonski diagram will contribute to the deactivation of the excited states, the radiative lifetimes of S_1 and T_1 states are given by equations (1.19) and (1.20), respectively:

$$\tau_{S_1} = \frac{1}{k_r^{S_1} + k_{nr}^{S_1}} = \frac{1}{k_F + k_{ic} + k_{isc}} \qquad (1.19)$$

$$\tau_{T1} = \frac{1}{k_{nr}^{T_1} + k_r^{T_1}} = \frac{1}{k_{isc} + k_P} \qquad (1.20)$$

where:

$k_r^{S_1} = k_F$; $k_r^{S_1}$ represents the sum of the rate constants for the radiative decay processes from singlet excited state S_1 and k_F is the rate constant for the radiative deactivation of S_1 by fluorescence;

$k_{nr}^{S_1} = k_{isc} + k_{ic}$; $k_{nr}^{S_1}$ represents the sum of the rate constants for the non radiative decay processes from S_1; k_{isc} and k_{ic} are the rate constants for the non radiative deactivation of S_1 by intersystem crossing and internal conversion, respectively.

$k_{nr}^{T_1} = k_{isc}$; $k_{nr}^{T_1}$ represents the sum of the rate constants for the non radiative decay processes from triplet excited state T_1 and k_{isc} is the rate constant for the non radiative deactivation of T_1 by intersystem crossing;

$k_r^{T_1} = k_P$; $k_r^{T_1}$ is the sum of the rate constants for the radiative decay processes from triplet excited state T_1 and k_P is the rate constant for the radiative deactivation of T_1 by emission of phosphorescence.

When the molecules under study emit fluorescence or phosphorescence, it is possible to measure the emission intensity as a function of time and obtain the observed experimental lifetime. The radiative lifetimes can be calculated from these if the quantum yields of fluorescence or phosphorescence are known. Fluorescence lifetimes (S_1 state) are frequently determined by the technique of time correlated single photon counting (TCSPC), while triplet state lifetimes (T_1 states) can be measure by laser flash

photolysis or by phosphorescence emission techniques. In Table 1-5 are presented the rate constants values of all photophysical processes.

Table 1-5 Schematic presentation of the physical excitation and decay processes of the excited state of a molecule and respective rate constants [114].

Process	Representation	Rate	Rate constant k (s^{-1})	Lifetimes τ (s)
Absorption	$S_0 + h\nu \rightarrow S_1$	I^*	-	10^{-5}
Fluorescence	$S_1 \rightarrow S_0 + h\nu_F$	$k_F [S_1]$	$k_F \cong 10^6$-10^9	10^{-7}-10^{-11}
Internal conversion	$S_1 \rightarrow S_0$	$k_{ic} [S_1]$	$k_{ic} \cong 10^6$-10^{12}	10^{-7}-10^{-11}
Intersystem crossing	$S_1 \rightarrow T_1$	$k_{isc} [S_1]$	$k_{isc} \cong 10^4$-10^{12}	10^{-8}-10^{-11}
Intersystem crossing	$T_1 \rightarrow S_0$	$k_{isc} [T_1]$	$k_{isc} \cong 10^{-2}$-10^5	10^1-10^{-6}
Phosphorescence	$T_1 \rightarrow S_0 + h\nu_P$	$k_P [T_1]$	$k_P \cong 10^{-2}$-10^4	10^1-10^{-5}

$* I$ is the rate of absorption of the incident radiation

If the emission of light is the only process deactivating the excited state then the time taken for the emission to decay to zero is the natural radiative lifetime τ_0 of the excited state. However, the observed (or experimentally measured) radiative lifetime of fluorescence or phosphorescence, τ, is frequently shorter than τ_0 since the lifetime of a state is given by the sum of all the processes deactivating the excited state, and the non-radiative processes compete with the emission decay processes.

Therefore, equation (1.21) gives the correlation between the natural radiative lifetimes τ_0 and the observed (or experimentally measured) radiative lifetimes τ for fluorescence (F) and phosphorescence (P):

$$\tau_{F,P}^0 = \frac{\tau_{F,P}}{\phi_{F,P}} \tag{1.21}$$

The rate constants $k_{F,P}$ for the fluorescence and phosphorescence processes can be calculated from the experimental values of $\tau_{F,P}$ and $\phi_{F,P}$ through the relation given by equation (1.22):

$$k_{F,P} = \frac{1}{\tau_{F,P}^0} = \frac{\phi_{F,P}}{\tau_{F,P}} \tag{1.22}$$

The relationship between the natural radiative lifetime and the absorption spectral properties of a transition is expressed approximately by the equation (1.23):

$$\tau = \frac{10^{-5}}{\varepsilon_{max}} \tag{1.23}$$

where ε is the molar absorption coefficient at the maximum wavelength of the absorption band. Allowed transitions from S_0 to S_1 usually have ε_{max} values in the region 10^3 L mol^{-1} cm^{-1} which gives radiative lifetimes of the S_1 state of approximately 10^{-8} s. Spin forbidden transitions from $S_0 \rightarrow T_1$ have ε_{max} values in the range 10^{-3} L mol^{-1} cm^{-1} which gives radiative lifetimes of approximately 10^{-2} s for the T_1 state.

For organic molecules, the values of ε_{max} for $S_0 \rightarrow S_1$ transitions are higher than for $S_0 \rightarrow T_1$ transitions leading to a shorter radiative lifetime of S_1 states than those of T_1 states. This means that the excited triplet states of molecules will remain longer time in the system, having higher probability of colliding with other molecules and take part of the photochemical reactions rather than the singlet excited state.

The *fluorescence quantum yield* ϕ_F is defined as the ratio of the number of emitted photons (over the whole duration of the decay) to the number of absorbed photons [114]. In other words, it is the fraction of excited molecules that return to the ground state S_0 with emission of fluorescence photons, and is given by equation (1.24).

$$\phi_F = \frac{k_F}{k_F + k_{ic} + k_{isc}} \tag{1.24}$$

were k_F is the rate constant for the radiative deactivation of $S_1 \rightarrow S_0$ by emission of fluorescence, and k_{ic} and k_{isc} are the rate constants for the non radiative deactivation of $S_1 \rightarrow S_0$ by internal conversion and of $S_1 \rightarrow T_1$ by intersystem crossing, respectively.

Using the radiative lifetime given by equation 1.21, ϕ_F can also be written by equation (1.25):

$$\phi_F = k_r^{S_1} \times \tau_{S_1} \tag{1.25}$$

If there is no quenching processes of the excited states and no photochemical reaction, then the sum of the quantum yields for the deactivation processes originating from S_1 are equal to unity, as shown by expression (1.26):

$$\phi_F + \phi_{ic} + \phi_{isc} (S_1\text{-}T_1) = 1.0 \qquad (1.26)$$

with ϕ_F, ϕ_{ic} and ϕ_{isc} being the quantum yields of fluorescence, internal conversion and intersystem crossing, respectively.

The T_1 state will be deactivated by *isc* and phosphorescence to the ground state S_0, considering the absence of chemical reactions or quenching processes. Therefore, the following expression is applicable (1.27):

$$\phi_{isc} (S_1\text{-}T_1) = \phi_P + \phi_{isc} (T_1\text{-}S_0) \qquad (1.27)$$

The ϕ_{isc} and ϕ_P can then be given by equations (1.28) and (1.29):

$$\phi_{isc} = \frac{k_{isc}}{k_r^{S_1} + k_{nr}^{S_1}} = k_{isc} \times \tau_{S_1} \qquad (1.28)$$

$$\phi_P = \frac{k_{isc}}{k_r^{T_1} + k_{nr}^{T_1}} \phi_{isc} \qquad (1.29)$$

1.8.4 Effect of solvents on UV-vis absorption and emission spectra

It is well recognized that the nature of the solvent (polarity, dielectric constant, hydrogen bond ability, etc.) in which a molecule is dissolved leads to shifts in electronic absorption and luminescence spectra [114,116]. This effect of the solvent is correlated with the interaction forces between the solvent and solute.

1.8.4.1 UV-vis absorption spectra

The position, shape and intensities of absorption bands are modified when solvents of different polarity are used [114]. This effect of the solvent is correlated with the interaction forces (hydrogen bonding, dipole-dipole, ion-dipole, etc.) between the solvent-solute which will affect the energy difference between the ground and excited state of the absorbing species.

The change in the position (and sometimes in intensity) of the UV-vis absorption band of the compound originated by changing the polarity of the solvent is called *solvatochromism*. The solvatochromic shifts represent the difference in the solvation

energies of the excited state and ground state of a transition. Solvents with higher polarity lead to a hypsochromic effect (or blue shift), also known as negative solvatochromism, while a bathochromic effect (or red shift) is a positive solvatochromism.

The solvent effect on the spectra resulting from electronic transitions is dependent on the chromophore and the nature of the transition (σ-σ*, n-σ*, π-π*, n-π* and charge transfer absorption). Only molecules with transitions in which the charge distribution in ground state is very different from excited states present pronounced solvatochromism. The increase of solvent polarity causes n-π* bands to shift to shorter wavelength (higher energies) while π-π* bands are shift to longer wavelengths. Generally, aromatic molecules with more π-electron system (naphthalene, anthracene) lead to an increase in the molar absorption coefficient and a shift to longer wavelengths in absorption spectra.

1.8.4.2 Emission spectra

The interaction between the excited states of a molecule with the surrounding solvent can cause changes on the quantum yield and lifetimes of the fluorescence emission and on the spectral position and shape of the emission bands [114].

Solvent effects shift the emission to even lower energy due to stabilization of the excited state by the polar solvent molecules. Typically, the fluorophore has a larger dipole moment in the excited state (μ_E) than in the ground state (μ_G). Following excitation, the solvent dipoles can reorient or relax around μ_E which lowers the energy of the excited state. As the solvent polarity is increased, this effect becomes larger, resulting in emission at lower energies (longer wavelengths). In general only fluorophores that are themselves polar display a large sensitivity to solvent polarity. Nonpolar molecules such as unsubstituted aromatic hydrocarbons are much less sensitive to solvent polarity. Fluorescence lifetimes (1-10 ns) are usually much longer than the time required for solvent relaxation. For fluid solvents at room temperature, solvent relaxation occurs in 10–100 ps. For this reason the emission spectra of fluorophores are representative of the solvent relaxed state.

An increase in the extent of the π-electron system of aromatic molecules shifts the fluorescence spectra to longer wavelengths and leads to an increase in the fluorescence quantum yield [114]. This is the case of aromatic hydrocarbons such as

naphthalene, anthracene, naphthacene and pentacene which emit fluorescence in the ultraviolet, blue, green and red, respectively. In general, molecules with electron-donating groups (-OH, -OR, -NH$_2$, -NHR, -NR$_2$) shift the fluorescence spectra to longer wavelengths [114]. Moreover, these spectra are broad and often structureless compared to the parent aromatic hydrocarbons (as is the case of 1- and 2-naphthol compared to naphthalene).

1.8.5 Quantum yield and kinetics of photochemical reactions

The rate of a photochemical transformation can be indicated by its quantum yield or quantum efficiency (ϕ). The Stark-Einstein law leads to the definition of quantum yield, which is defined as the ratio between the number of moles which are transformed and the number of photons which are absorbed. For monochromatic light and for solutions of low absorbance the quantum yield is given by equation (1.30):

$$\phi_\lambda = \frac{\text{number molecules undergoing transformation}}{\text{number of photons absorbed}} \qquad (1.30)$$

This relation is often given by:

$$\phi_\lambda = \frac{k}{I\,(\lambda)}$$

where ϕ_λ is the photodegradation quantum yield at a certain wavelength λ, k is the disappearance rate of the irradiated molecule (mol L^{-1} s^{-1}) and I is the photon flux or the absorbed light intensity (photons cm^2 s^{-1}) of the molecule in solution at the monochromatic wavelength λ. The photon flux for a system with monochromatic light and a specific geometry is calculated by using actinometry. The most commonly used actinometer involves aqueous solutions of potassium ferrioxalate [114,116].

The quantum yield of a primary photochemical process range between 0 and 1 since it represents the probability that the excited state will undergo the reaction. However, the overall quantum yield (primary and secondary processes) can be greater than 1, depending on the secondary reactions.

The quantum yield of a photochemical reaction is dependent of factors such as wavelength of radiation, maximum amount of light absorbed by the compound, solvent properties and pH [114,116]. The pH of a solution can cause a shift in the maximum of

absorption and even on the hydrolysis constant, leading to effects on the degradation process.

Another factor affecting the fate of a compound in the environment is its lifetime τ given by $\tau = 1/k$, where k (s^{-1}) is the pseudo-first order rate constant of the direct photolysis. The half-life, $\tau_{1/2}$, corresponds to the time which a molecule is reduced to half its initial concentration, and because it can readily be determined analytically is preferred to the lifetime [114]. The relation between these two factors, for a first order rate constant, is given by equation (1.31):

$$\tau_{1/2} = \tau \times \ln 2 = \frac{\ln 2}{k} = \frac{0.693}{k} \tag{1.31}$$

In liquid solutions the bimolecular reactions are controlled by the diffusion of the reactants. The diffusion controlled bimolecular rate constant is given by the Smoluchowski equation [114] (1.32):

$$k_{diff} = \frac{8RT}{3000\eta} \tag{1.32}$$

where R is the gas constant (8.314 J K^{-1} mol^{-1}), T is the temperature (K) and η is the viscosity of the solvent (N s m^{-2}). For water, at room temperature, k_{diff} has a value of 10^{10} L mol^{-1} s^{-1} ($\eta = 10^{-3}$ N sm^{-2}) [116]. As observed, in this form the rate is only dependent on the viscosity and temperature and can be related with the quenching rate constant k_q. While it is not relevant for this study, diffusion controlled rates do also depend on molecular size and charge. Although the quenching rate approaches the diffusion-controlled limit, it is not necessarily true that every molecular collision leads to deactivation. The diffusive process limits the rate at which the excited species and the quencher come together but prolongs each encounter so that several hundred collisions are possible before the two species diffuse apart.

1.8.6 Singlet oxygen as a reactive species

Molecular oxygen ($^3O_2$) is a paramagnetic molecule with triplet state (multiplicity 2S+1=3; $^3\Sigma_g^-$). It is the most recognized quencher of singlet and triplet excited states of organic molecules [116,118]. In excited state, oxygen presents two

electronically states with singlet multiplicity, $^1\Delta_g$ and $^1\Sigma_g^+$, that are located respectively at 0.98 eV (94.5 kJ mol^{-1}, 7882.1 cm^{-1}, 1268.7 nm) and 1.63 eV (157.2 kJ mol^{-1}, 13121 cm^{-1}, 762.1 nm) above the ground state [118]. The more stable of these two excited states is $^1\Delta_g$, commonly called singlet oxygen and simply designated as $^1O_2$ [118].

As previously mentioned, the electronically excited states of molecule M ($^1M^*$ or $^3M^*$) produced by UV or visible light are able to transfer their energy to molecular oxygen in its fundamental state and generate singlet oxygen $^1O_2$. The formation of $^1O_2$ may occur through two pathways (reaction 1.33 and 1.34):

$$^1M^* + {}^3O_2 \rightarrow {}^3M^* + {}^1O_2 \tag{1.33}$$

$$^3M^* + {}^3O_2 \rightarrow {}^1M^* + {}^1O_2 \tag{1.34}$$

Since the singlet excited states are often short lived (ns time scale) and the value of the energy difference ΔE (S_1-T_1) is frequently insufficient, the most probable pathway for $^1O_2$ generation is reaction (1.34) between the lowest excited triplet state of the sensitizer and oxygen. The quenching of $^3M^*$ by molecular oxygen involves other reactions that are in competition with the formation of $^1O_2$ such as formation of superoxide anion ($O_2^{\bullet-}$) through electron transfer, enhanced triplet decay and formation of products. These reactions are represented in equations (1.35 to 1.39):

$$^3M^* \rightarrow M \qquad\qquad \text{Intrinsic decay} \tag{1.35}$$

$$^3M^* + M \rightarrow M + M \qquad\qquad \text{Quenching by ground state} \tag{1.36}$$

$$^3M^* + {}^3O_2 \rightarrow M + {}^1O_2 \qquad\qquad \text{Triplet-triplet energy transfer} \tag{1.37}$$

$$^3M^* + {}^3O_2 \rightarrow M^{\bullet+} + O_2^{\bullet-} \qquad\qquad \text{Electron transfer} \tag{1.38}$$

$$^3M^* + {}^3O_2 \rightarrow M + O_2 \qquad\qquad \text{Enhanced triplet decay} \tag{1.39}$$
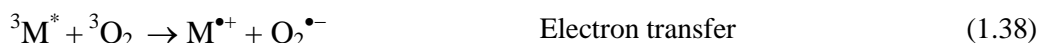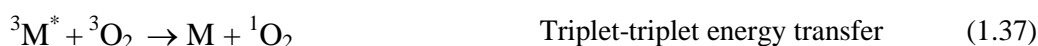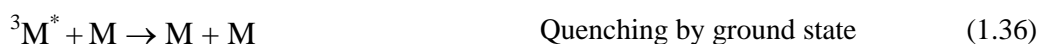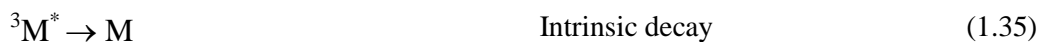
It has been described in the literature that the interaction of $^1O_2$ with aromatic molecules such as phenols, naphthalene and some naphthalene derivatives leds to the formation of endoperoxides and also that, via a mechanism resulting in one- or two-electron transfer, a superoxide radical or hydrogen peroxide, respectively, is formed [119,120].

An important property of $^1O_2$ that should be taken into consideration when studying its reactivity is the singlet oxygen lifetime. The $^1O_2$ lifetime is solvent dependent [121,122], as evidenced by the values listed in Table 1-6.

Table 1-6 Lifetimes of singlet oxygen in several solvents [122].

Solvent	$\tau/\mu s$
H_2O	4.4
D_2O	64.4
Methanol	10.0
Ethanol	14.5
1,4-Dioxane	27.1
Acetonitrile	83.7
Chloroform	232
Benzene	31.2
Acetone	55.6
n-Heptane	31.1
CCl_4	34000

The method most commonly used for the generation of $^1O_2$ is photosensitization [123,124]. This consists in using photosensitizers molecules such as rose Bengal, methylene blue, eosine, humic and fulvic acids, metallophthalocyanine [85,125], etc., either by continuous irradiation or by using pulsed excitation. The quantum yields of singlet oxygen formation can be determined in aerated solutions by measuring its quantum yield near Infrared phosphorescence emission at 1270 nm.

1.8.7 Photophysical data of naphthalene and naphthalene based compounds

The photophysical properties of naphthalene and of some naphthalene derivatives are well characterized in literature [116]. Therefore, and since NAD and 2-NOA have in common with these compounds the same aromatic structure, Table 1-7 lists the values of some photophysical properties of these compounds in order to facilitate the comparison of NAD and 2-NOA photophysical results with those of naphthalene and its derivatives.

Table 1-7 Photophysical properties of naphthalene and some naphthalene derivatives in non polar solvents (n) and in polar solvents (p): energy of singlet excited state (E_s), energy of triplet excited state (E_T), quantum yield and lifetime of fluorescence (ϕ_F and τ_S) [116].

Compound	E_S (kJ mol^{-1}; eV)		E_T (kJ mol^{-1}; eV)		τ_S (ns)		ϕ_F	
	n	p	n	p	n	p	n	p
Naphthalene	385; 3.99	384; 3.98	253; 2.62	255; 2.64	96	105	0.15	0.21
Naphthalene, 1-amino	348; 3.61	324; 3.36	-	229; 2.37	6.0	19.6	0.47	0.57
Naphthalene, 1-amino	-	306; 3.17	-	239; 2.48	6.9	16.6	0.33	0.46
Naphthalene, 1-hydroxy	372	371	-	-	10.6	7.5	0.17	-
Naphthalene, 2-hydroxy	362; 3.75	362; 3.75	-	252; 2.61	13.3	8.9	0.27	-
Naphthalene, 1-methoxy	-	374; 3.88	-	250; 2.59	-	-	0.36	0.53
Naphthalene, 1-nitro	313; 3.24	-	-	238; 2.47	0.012	0.0008	-	-
Naphthalene, 1-methyl	377; 3.91	377; 3.91	-	254; 2.63	67	97	0.21	0.19

1.9 References

[1] The state of the environment; freshwater. GEO-2000: Global Environment Outlook. Nairobi, United Nations Environment Programme, **1999**.

[2] The World Health Report: Reducing Risks, Promoting Healthy Life. Ed. World Health Organization (WHO), Geneva, **2002**.

[3] M. Keneth, *The DDT Story*, The British Crop Protection Council, London, UK, **1992**.

[4] http://water.epa.gov/drink/contaminants/basicinformation/2-4-d-2-4-dichlorophenoxyacetic-acid.cfm (accessed July 2013).

[5] L. Carson, *Silent Spring*. The Riverside Press, Boston, MA, **1962**.

[6] United States Environmental Protection Agency (2006-11-26). "Consumer Factsheet on: Methoxychlor (accessed July 2013).

[7] European Union - DG SANCO. "EU Pesticides Database". Retrieved 2009-10-02.

[8] The world health report 2003 - shaping the future. Geneva, World Health Organization, **2003**.

[9] Public health impact of pesticides used in agriculture. Geneva, World Health Organization, **1990**.

[10] A. Blair, M. Dosemeci, E. F. Heineman, Cancer and other causes of death among male and female farmers from twenty-three states. *Am. J. Ind. Med.*, **1993**, 23, 729-742.

[11] R. W. Tanner, J. W. Langston, Do environmental toxins cause Parkinson´s disease? A critical review. *Neurology*, **1990**, 40, 17-30.

[12] L. Yáñez, Overview of human health and chemical mixtures: problems facing developing countries. *Environ. Health Persp.*, **2002**, 110, 901-909.

[13] Childhood pesticide poisoning: information for advocacy and action. Food and Agriculture Organization of the United Nations/United Nations Environment Programme/World Health Organization. Geneva, United Nations Environment Programme, **2004**.

[14] Directive 91/414/EEC.

[15] Directive 1999/45/CE.

[16] Water Directive Framework (WDF 2002).

[17] Water Directive Framework (WDF 2013).

[18] Directive 98/83/EC.

[19] Portuguese law nº 47802 from 19 July 1967.

[20] http://www.alanwood.net/pesticides/class_pesticides.html (accessed June 2013).

[21] C. D. S. Tomlin, *The Pesticide Manual*, edition no. 12, British Crop Protection Council, **2000.**

[22] Food and Agriculture Organization (FAO), International code of conduct on the distribution and use of pesticides, Rome, Italy, **1989**.

[23] K. H. Buchel, *Chemistry of Pesticides*, John Wiley & Sons, Inc. New York, USA, **1983**.

[24] R. C. Kirkwood, Use and mode of action of adjuvants for herbicides: a review of some current work. *Pest. Manag. Sci.*, **1993**, 38, 93-102.

[25] R. F. Davis, R. D. Wauchope, A. W. Johnson, B. Burgo, A. B. Pepperman, Release of fenamiphos, atrazine, and alachlor into flowing water from granules and spray deposits of conventional and controlled-release formulations. *J. Agric. Food Chem.*, **1996**, 44, 2900-2907.

[26] L. Pussemier, G. Szabó, R. A. Bulman, Prediction of the soil adsorption coefficient Koc for aromatic pollutants. *Chemosphere*, **1990**, 21, 1199-1212.

[27] W. de Wolf, J. H. M. de Bruijn, W. Seinen, J. L. M. Hermens, Influence of biotransformation on the relationship between bioconcentration factors and octanol-water partition coefficients. *Environ. Sci. Technol.*, **1992**, 26, 1197-1201.

[28] P. Isnard, S. Lambert, Estimating bioconcentration factors from octanol-water partition coefficient and aqueous solubility. *Chemosphere*, **1988**, 17, 21-34.

[29] B. T. Bowman, W. W. Sans, Determination of octanol‑water partitioning coefficients (K_{OW}) of 61 organophosphorus and carbamate insecticides and their relationship to respective water solubility (S) values. *J. Environ. Sci. Health*, **1983**, 18, 667-683.

[30] The WHO Recommended Classification of Pesticides by Hazard, World Health Organization (WHO). **2009**.

[31] J. A. Firestone, T. S. Weller, G. Franklin, P. H. Swanson, Pesticides and risk of Parkinson disease. *Arch. Neurol.*, **2005**, 62, 91-95.

[32] http://www.agf.gov.bc.ca/pesticides/c_2.htm7 (accessed July 2013).

[33] L. G. Nikell, *Chapter1 - Plant growth regulators in agriculture and horticulture*. In: Bioregulators for crop protection and pest control. Ed. P. Hedin, pp 1-14, ACS Symposium Series; American Chemical Society, Washington D.C., **1994.**

[34] L. Brahm, W. Rademacher, *Plant Growth Regulators*. In: Ullmann´s Encyclopedia of Industrial Chemistry. John Wiley and Sons, **2012,** 27, 573-586.

[35] P. W. Zimmerman, Growth regulators of plants and formative effects induced with β-naphthoxy compounds. *Botany*, **1941**, 27, 381-388.

[36] H. Link, Significance of flower and fruit thinning on fruit quality. *Plant Growth Reg.*, **2000**, 31, 17-26.

[37] G. K. Shrestha, Effects of growth regulators on the growth and yield of detached and transplanted potato (*Solanum tuberosum L.*) sprouts. *Potato Res.*, **1986**, 29, 173-175.

[38] R. Untiedt, M. Blanke, Effects of fruit thinning agents on apple tree canopy photosynthesis and dark respiration. *Plant Growth Reg.*, **2001**, 35, 1-9.

[39] Environmental Protection Agency from United States of America (EPA), 738-R-07-07017 (October 2007) Registration eligibility decision (RED) for naphthaleneacetic acid, its salts, ester and acetamide, **2007**.

[40] European Food Safety Authority (EFSA), Conclusion of the peer review of the pesticide risk assessment of the active substance 2-(1-naphthyl) acetamide (notified as 1-napthylacetamide), *EFSA Journal*, **2011,** 9, 2020.

[41] F. E. Gardner, Practical applications of plant growth substances in horticulture. *Proc. Fla. State Hort. Soc.*, **1941**, 54, 20-26.

[42] A. E. Clarke, W. C. Edmundson, P. M. Lombard, Seed-setting in potatoes as affected by spraying with α-naphthaleneacetamide and by light. *Am. Potato J.*, **1941**, 18, 273-279.

[43] European Commission (EC) No 2229/2004.

[44] Commission Regulation (EC) No 1095/2007.

[45] R. Sigrist, A. Temperli, J. Hurter, A fluorometric method for the determination of residues of 1-naphthaleneacetamide and 1-naphthaleneacetic acid on apples. *J. Agr. Food Chem.,* **1974**, 22, 568-570.

[46] A. S. Carretero, C. C. Blanco, A. F. Gutiérrez, Experimental studies of the factors that influence 1-naphthaleneacetamide determination by micelle-stabilized room-temperature phosphorescence. *Analyst*, **1997**, 122, 563-566.

[47] C. C. Blanco, A. S. Carretero, M. I. R. García, A. F. Gutiérrez, A simple and rapid phosphorimetric method for the determination of α-naphthaleneacetamide in fruit samples. *Intern. J. Environ. Anal. Chem.*, **1999**, 75, 377-385.

[48] M. M. Galera, P. P. Vázquez, J. L. M. Vidal, J. Fernández, J. L. P. Gómez, Large-volume direct injection for determining naphthalene derivative pesticides in water using a restricted-access medium column in RPLC-LC with fluorescence detection. *Chromatographia*, **2004**, 60, 517-522.

[49] T. D. Bucheli, O. P. Haefliger, R. Dietiker Jr., R. Zenobi, Analysis of water contaminants and natural water samples using two-step laser mass spectrometry. *Anal. Chem.*, **2000**, 72, 3671-3677.

[50] European Food Safety Authority (EFSA), Conclusion on the peer review of the pesticide risk assessment of the active substance 2-naphthyloxyacetic acid, *EFSA Journal,* **2011**, 9, 2152.

[51] Directive 2009/65/EC.

[52] S. C. Terrones, J. F. F. Sánchez, A. S. Carretero, A. F. Gutiérrez, The development and comparison of a fluorescence and a phosphorescence optosensors for determining the plant growth regulator 2-naphthoxyacetic acid. *Sensor Actuator B*, **2005**, 107, 929-935.

[53] A. S. Carretero, C. Cruces Blanco, A. F. Gutiérrez, Heavy atom induced room temperature phosphorescence method for the determination of the plant growth regulator β-naphthoxyacetic acid. *J. Agric. Food Chem.*, **1998**, 46, 3683-3686.

[54] T. E. Archer, J. D. Stokes, Levels of β-naphthoxyacetic acid and β-naphthol on field sprayed strawberries as analyzed by high-pressure liquid chromatography. *J. Agric. Food Chem.*, **1978**, 26, 1465-1466.

[55] V. Gökmen, J. Acar, Liquid chromatographic determination of β-naphthoxyacetic acid in tomatoes. *J. Chromatogr. A*, **1998**, 798, 167-171.

[56] M. J. Climent, M. A. Miranda, Photodegradation of dichlorprop and 2-naphthoxyacetic acid in water. Combined GC-MS and FTIR study. *J. Agric. Food Chem.*, **1997**, 45, 1916-1919.

[57] I. F. Molokov, Y. P. Tsentalovich, A. V. Yurkovskay, R. Z. Sagdeev, Investigation of the photo-Fries rearrangement reactions of 1- and 2-naphthyl acetates. *J. Photochem. Photobiol. A: Chem.*, **1997**, 110, 159-165.

[58] J. P. Da Silva, E. V. Bastos, L. F. V. Ferreira, R. G. Weiss, Surface photochemistry of the berbicide napropamide. The role of the media and environmental factors in directing the fates of intermediates. *Photochem. Photobiol. Sci.*, **2008**, 7, 69-75.

[59] M. C. López, M. I. Fernández, C. Martínez, J. A. Santaballa, Photochemistry for pollution abatement. *Pure Appl. Chem.*, **2013**, 85, 1437-1449.

[60] D. Vialaton C. Richard, Phototransformation of aromatic pollutants in solar light: Photolysis versus photosensitized reactions under natural water conditions. *Aquat. Sci.*, **2002**, 64, 207-215.

[61] H. D. Burrows, M. L. Canle, J. A. Santaballa, S. Steenken, Reaction pathways and mechanisms of photodegradation of pesticides. *J. Photochem. Photobiol. B: Biol.*, **2002**, 67, 71-108.

[62] P. Meallier, *Chapter 9 - Phototransformation of Pesticides in Aqueous Solution*. In: The Handbook of Environmental Chemistry. Ed. P. Boule, vol. 2, Part L, Environmental Photochemistry, Springer-Verlag Berlin Heidelberg, **1999**.

[63] N. Mikami, K. Imanishi, H. Yamada, J. Miyamoto, Photodegradation of fenitrothion in water and on soil surface, and its hydrolysis in water. *J. Pestic. Sci.,* **1985,** 10, 263-272.

[64] A. T. Halle, C. Richard, Simulated solar light irradiation of mesotrione in natural eaters, *Environ Sci. Technol.*, **2006**, 40, 3842-3847.

[65] http://continuingeducation.construction.com/article_print.php?L=68&C=79 (accessed July 2013).

[66] M. P. Fasnacht, N. V. Blough, Mechanisms of the aqueous photodegradation of polycyclic aromatic hydrocarbons. *Environ. Sci. Technol.*, **2003**, 37, 5767-5772.

[67] R. C. Zepp, N. L. Wolfe, G. L. Baughman, R. C. Hollis, Singlet oxygen in natural waters. *Nature*, **1977**, 267, 421-423.

[68] P. Boule, L. Meunier, F. Bonnemoy, A. Boulkamh, A. Zertal, B. Lavedrine, Direct phototransformation of aromatic pesticides in aqueous solution. *Inter. J. Photoenergy*, **2002**, 4, 69-78.

[69] M. K. Wong, C. Y. Mol, Comparative study on the quantum yields of direct photolysis of organophosphorus pesticides in aqueous solution. *J. Agric. Food Chem.*, **1994**, 42, 2625-2630.

[70] B. J. McConkey, L. M. Hewitt, D. G. Dixon, B. M. Greenberg, Natural sunlight induced photooxidation of naphthalene in aqueous solution. *Water, Air, Soil Pollut.*, **2002**, 136, 347-359.

[71] D. Vialaton, C. Richard, D. Baglio, A.-B. Paya-Perez, Mechanism of the photochemical transformation of naphthalene in water. *J. Photochem. Photobiol. A: Chem.*, **1999**, 123, 15-19.

[72] M. Czaplicka, Photo-degradation of chlorophenols in the aqueous solution. *J. Hazard. Mater.*, **2006**, B134, 45-59.

[73] J. Jirkovsk, V. Faure, P. Boule, Photolysis of diuron. *Pestic. Sci.*, **1997**, 50, 42-45.

[74] O. Brahmia, C. Richard, Phototransformation of carbaryl in aqueous solution. Laser flash photolysis and steady state studies. *J. Photochem. Photobiol. A: Chem.*, **2003**, 156, 9-14.

[75] J. P. Aguer, P. Boule, F. Bonnemoy, J. M. Chezal, Phototransformation of napropamide [*N,N*-diethyl-2-(1-naphthyloxy)propionamide] in aqueous solution: Influence on the toxicity of solutions. *Pestic. Sci.*, **1998**, 54, 253-257.

[76] M. Valero, S. M. B. Costa, Photodegradation of nabumetone in aqueous solutions. *J. Photochem. Photobiol. A: Chem.*, **2003**, 157, 93-101.

[77] G. O. Schenck, Photosensitization. *Ind. Eng. Chem.*, **1963**, 55, 40-43.

[78] C. S. Foote, Mechanisms of photosensitized oxidation. *Science*, **1968**, 162, 963-970.

[79] C. Tanielian, R. Mechin, R. Seghrouchni, C. Schweitzer, Mechanistic and kinetic aspects of photosensitization in the presence of oxygen. *Photochem. Photobiol.*, **2000**, 71, 12-19.

[80] K. Gollnick, Type II photooxygenation reactions in solution. *Adv. Photochem.*, **1968**, 6, 1-122.

[81] N. Burkhard, J. A. Guth, Photolysis of organophosphorus insecticide on soil surfaces. *Pestic. Sci.*, **1979**, 10, 313-319.

[82] C. Richard, S. Canonica, *Chapter: Aquatic phototransformation of organic contaminants induced by coloured dissolved natural organic matter*. In: The Handbook of Environmental Photochemistry, Part II Environmental Photochemistry, vol. 2M, pp 299-323, Springer-Verlag Berlin Heidelberg, **2005**.

[83] J. M. Burns, W. J. Cooper, J. L. Ferry, D. W. King, Brian P. DiMento, K. McNeill, C. J . Miller, W. L. Miller, B. M. Peake, S. A. Rusak, A. L. Rose, T. D. Waite, Methods for reactive oxygen species (ROS) detection in aqueous environments. *Aquat. Sci.*, **2012**, 74, 683-734.

[84] W. S. Ku; Y. H. Chiang; L. S. Lai, Degradation of carbofuran in water by solar photocatalysis in presence of photosensitizers. *J. Environ. Sci. Health, Part B*, **2006**, 41, 937-948.

[85] J. J. M. Lamberts, D. C. Neckers, Rose Bengal derivatives as singlet oxygen sensitizers. *Tetrahedron*, **1985**, 41, 183-2190.

[86] R. D. Ross, D. G. Crosby, The photooxidation of aldrin in water. *Chemosphere*, **1975**, 4, 277-282.

[87] N. L. Wolfe, R. G. Zepp, D. F. Paris, G. L. Baughman, R. C. Hollis, Methoxychlor and DDT degradation in water: rates and products. *Environ. Sci. Technol.*, **1997**, 11, 1077-1081.

[88] M. R. Iesce, M. L. Graziano, F. Cermola, S. Montella, L. di Gioia, C. Stasio, Effects of sensitizers on the photodegradation of the systemic fungicide triadimenol. *Chemosphere*, **2003**, 51, 163-166.

[89] J. Szejtli, Introduction and general overview of cyclodextrin chemistry. *Chem. Soc. Rev.*, **1998**, 98, 1743-1753.

[90] E. M. M. Del Valle, Cyclodextrins and their uses: a review. *Process Biochem.*, **2004**, 39, 1033-1046.

[91] G. Köhler, G. Grabner, C. TH. Klein, G. Marconi, B. Mayer, S. Monti, K. Rechthaler, K. Rotkiewicz, H. Viernstein, P. Wolschann, Structure and spectroscopic properties of cyclodextrin inclusion complexes. *J. Inclusion Phenom. Molec. Recog. Chem.*, **1996**, 25, 103-108.

[92] R. Singh, N. Bharti, J. Madan, S. N. Hiremath, Characterization of cyclodextrin inclusion complexes - a review. *J. Pharm. Sci. Technol. 2*, **2010**, 171-183.

[93] P. Bortolus, S. Monti, *Photochemistry in cyclodextrin cavities*. In: Advances in Photochemistry, Eds. D. C. Neckers, D. H. Vohnan, G. Von Bunau, John Wiley & Sons, Inc. **1996**, 21, 1-133.

[94] S. Monti, G. Kiihler, G. Grabner, Photophysics and photochemistry of methylated phenols in β-cyclodextrin inclusion complexes. *J. Phys. Chem.*, **1993**, 97, 13011-13016.

[95] A. Muñoz de La Peña, F. Salinas, M. J. Gómez, M. I. Acedo, M. Sánchez Peña, Absorptiometric and spectrofluorimetric study of the inclusion complexes of 2-naphthyloxyacetic acid and 1-naphthylacetic acid with β-cyclodextrin in aqueous solution. *J. Incl. Phenom. Molec. Recognit. Chem.*, **1993**, 15, 131-143.

[96] E. Schneiderman, A. M. Stalcup, Cyclodextrins: a versatile tool in separation science. *J. Chromatography B*, **2000**, 745, 83-102.

[97] M. M. Sojo, E. Nunez-Delicado, F. Garcia-Carmona, A. Sanchez-Ferrer, Cyclodextrins as activator and inhibitor of latent banana pulp polyphenol oxidase. *J. Agric. Food Chem.*, **1999**, 47, 518-23.

[98] A. Vyas, S. Saraf, S. Saraf, Cyclodextrin based novel drug delivery systems. *J. Inclusion Phenom. Macrocycl. Chem.*, **2008**, 62, 23-42.

[99] C. Wu, J. Fan, Applications of cyclodextrin to water treatment. *Shuichuli Jishu*, **1998**, 24, 67-70.

[100] S. Ishiwata, M. Kamiya, Cyclodextrin inclusion: catalytic effects on the degradation of organophosphorous pesticides in neutral aqueous solutions. *Chemosphere*, **1999**, 39, 1595-1600.

[101] S. Gao, L. Wang, Application of cyclodextrin in environmental science. *Huanjing Kexue Jinzhan*, **1998**, 6, 80-86.

[102] J. Szejtli, Utilization of cyclodextrins in industrial products and processes. *J. Mater. Chem.*, **1997**, 7, 575-587.

[103] K. Hirose, A practical guide for the determination of binding constants. *J. Phenom. Macrocycl. Chem.*, **2001**, 39, 193-209.

[104] R. Saikosin, T. Limpaseni, P. Pongsawasdi, Formation of inclusion complexes between cyclodextrins and carbaryl and characterization of the complexes. *J. Incusion Phenom. Macro. Chem.*, **2002**, 44, 191-196.

[105] J. M. Ginés, J. I. Pérez-Martínez, M. J. Arias, J. R. Moyano, E. Morillo, A. Ruiz-Conde, P. J. Sanchez-Soto, Inclusion of the herbicide 2,4-dichlorophenoxyacetic acid (2,4-D) with β-cyclodextrin by different processing methods. *Chemosphere*, **1996**, 33, 321-334.

[106] X. -L. Zhu, H. -B. Wang, Q. Chen, W. -C. Yang, G. -F. Yang, Preparation and characterization of inclusion complex of iprodione and β-cyclodextrin to improve fungicidal activity. *J. Agric. Food Chem.*, **2007**, 55, 3535-3539.

[107] S. Ishiwata, M. Kamiya, Cyclodextrin inclusion: catalytic effects on the degradation of organophosphorous pesticides in neutral aqueous solutions. *Chemosphere*, **1999**, 39, 1595-1600.

[108] M. Kamiya, K. Nakamura, Studies on the susceptibility to alkaline hydrolysis of inclusion complexes of organophosphorothioate pesticides with β-cyclodextrins. *Pestic. Sci.*, **1994**, 41, 305-309.

[109] M. Kamiya, K. Nakamura, C. Sasaki, Inclusion effects of β-cyclodextrins on the hydrolysis of the organophosphorus pesticides. *Chemosphere*, **1995**, 30, 653-660.

[110] M. Kamiya, K. Nakamura, C. Sasaki, Inclusion effects of cyclodextrins on photodegradation rates of parathion and paraoxon in aquatic medium. *Chemosphere*, **1994**, 28, 1961-1966.

[111] M. Kamiya, K. Kameyama, S. Ishiwata, Effects of cyclodextrins on photodegradation of organophosphorus pesticides in humic water. *Chemosphere*, **2001**, 42, 251-255.

[112] O. D. Dailey, C. C. Dowler, N. C. Glaze, In: *Pesticide formulations and application systems*. Eds. L. E. Bode, J. L. Hazen, D. G. Chasin, American Society for Testing and Materials, Philadelphia, P.A., **1990**.

[113] O. D. Dailey, In: *Biotechnology of Amylodextrin Oligosaccharides*. Eds. R. B. Friedman, ACS Symposium Series 458, American Chemical Society, Washington D.C., **1991**.

[114] A. Gilbert, J. Baggott, *Esssentials of Molecular Photochemistry*. Ed. P. J. Wagner, Black Well, **1991**.

[115] F. Wilkinson, Quenching of electronically excited states by molecular oxygen in fluid solution. *Pure Appl. Chem.*, **1997**, 69, 851-856.

[116] M. Montalti, A. Credi, L. Prodi, M. T. Gandolfi, *Handbook of Photochemistry*, third edition, Taylor & Francis Group, Florida, **2006**.

[117] L. K. Patterson, G. Porter, M. R. Topp, Oxygen quenching of singlet and triplet states. *Chem. Phys. Lett.*, **1970**, 7, 612-614.

[118] D. R. Kearns, Physical and chemical properties of singlet molecular oxygen. *Chem. Rev.*, **1971**, 71, 395-427.

[119] A. T. Soltermann, M. Luiz, M. B. Biasutti, M. Carrascoso, F. Amat-Guerri, N. A. Garcia, Monosubstituted naphthalenes as quenchers and generators of singlet oxygen. *J. Photochem. Photobiol. A: Chem.*, **1999**, 129, 25-32.

[120] C. Pierlot, S. Hajjam, C. Barthélémy, J.-M. Aubry, Water-soluble naphthalene derivatives as singlet oxygen ($^1O_2$, $^1\Delta_g$) carriers for biological media. *J. Photochem. Photobiol. B: Biol.*, **1996**, 36, 31-39.

[121] P. R. Ogilby, C. S. Foote, Chemistry of singlet oxygen. 42. Effect of solvent, solvent isotopic substitution, and temperature on the lifetime of the singlet molecular oxygen ($^1\Delta_g$). *J. Am. Chem. Soc.*, **1982**, 104, 2069-2070.

[122] K. I. Salokhiddinov, I. M. Byteva, G. P. Gurinovich, Lifetime of singlet oxygen in various solvents. *J. Appl. Spectroscopy*, **1981**, 34, 561-564.

[123] M. C. DeRosa, R. J. Crutcheley, Photosensitized singlet oxygen and its applications. *Coord. Chem. Rev.*, **2002**, 233-234, 351-371.

[124] F. Wilkinson, W. P. Helman, A. B. Ross, Quantum yields for the photosensitized formation of the lowest electronically excited singlet state of molecular oxygen in solution. *J. Phys. Chem. Ref. Data*, **1993**, 22, 13-262.

[125] R. W. Redmond, J. N. Gamlin, A compilation of singlet oxygen yields from biologically relevant molecules. *Photochem. Photobiol.*, **1999**, 70, 391-475.

Chapter 2

Photophysical and photochemical studies of the
plant growth regulator 2-(1-naphthyl) acetamide

2A. Photophysical characterization

2A.1 Introduction

In this chapter are presented the results concerning the photophysical characterization of ground and excited states of 2-(1-naphthyl) acetamide (NAD) by means of steady-state and time resolved techniques such as UV-vis absorption, fluorescence and phosphorescence spectroscopy, time correlated single photon counting and nanosecond laser flash photolysis. The study was carried out in solvents of different polarity in order to obtain information on the nature of the electronic states and assess the effect of the solvent on the ground and excited state properties of NAD. Water, ethanol, ethylene glycol and chloroform were used as polar hydrogen-bond donating solvents, acetonitrile was used as polar aprotic non-hydrogen-bond donating solvent and 1,4-dioxane was used as a non-polar and non-hydrogen-bond donating solvent. Most of the figures along the chapter are given for NAD in aqueous solution due to the interest in its behavior under environmental conditions. However, occasionally, some figures are also given for NAD in organic solvents, as comparative data, while all results are given in the tables.

2A.2 Characterization of the singlet ground state

2A.2.1 UV absorption spectra and determination of molar absorption extinction coefficients

The UV absorption spectrum of NAD was recorded in water, deuterated water (D_2O), ethanol, ethylene glycol, acetonitrile, chloroform and 1,4-dioxane. As shown in Figure 2A-1, the UV absorption spectrum of NAD in aqueous solution presents two main bands: a short wavelength absorption which has a maximum around 223 nm and a lowest energy band within the wavelength range 250-320 nm with the maximum centred at 280 nm. This last band shows vibrational structure typical of naphthalene and its derivatives. Both of these bands are characteristic of π-π* transitions of the aromatic ring.

Neither the shape of the low energy absorption band nor its vibronic structure was influenced by changing the solvent. However, a slight red shift was observed in the absorption maximum wavelength when passing from water to a non-polar organic

solvent, as can be seen from the results presented in Table 2A-1. This is in agreement with the polarizing effect of the solvent medium on the π-π^* transition [1-3].
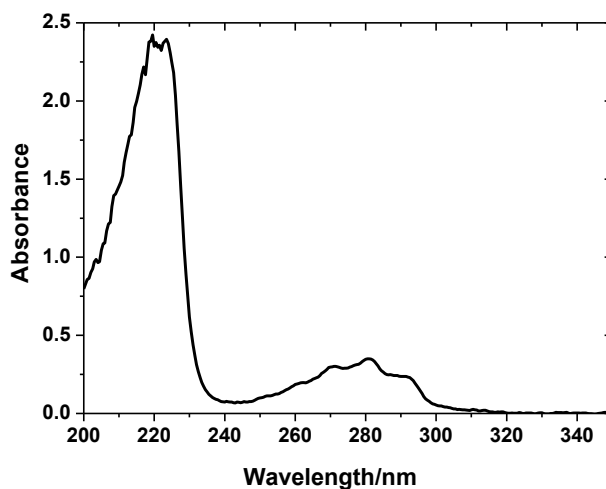
Figure 2A-1 UV absorption spectrum of aqueous NAD solution (5.0×10^{-5} mol L^{-1}; pH 5.6, 1cm cell).

The molar absorption coefficients of NAD, ε, were determined according to the Beer-Lambert law for each solvent at the maximum absorption wavelength, using at least six standard solutions with increasing concentrations. Figure 2A-2 gives, as illustrative example, the plot used for the determination of ε for NAD in acetonitrile while the spectral maxima and ε values in all the solvents are reported in Table 2A-1.
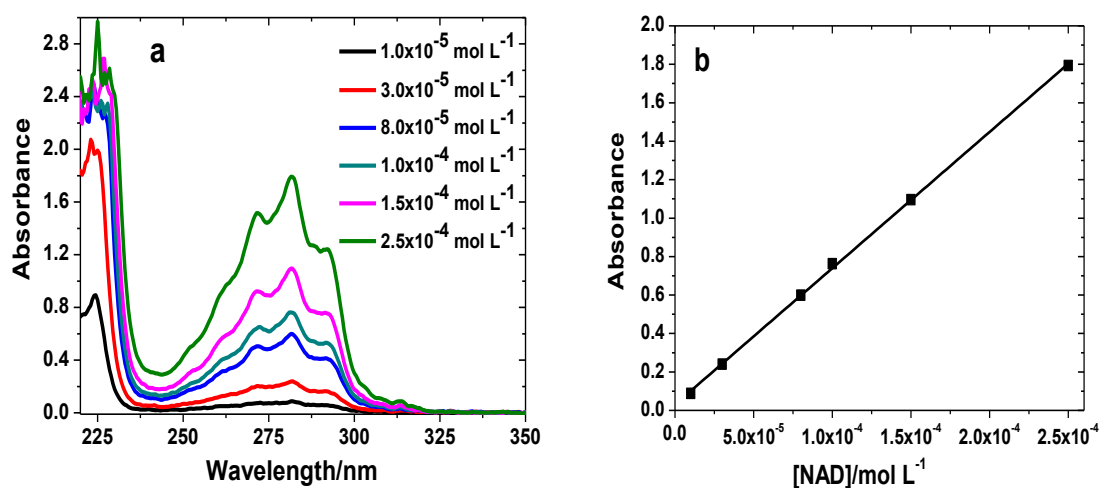
Figure 2A-2 a) UV absorption spectra of NAD in acetonitrile solution at different concentrations. b) Respective Beer-Lambert plot for the determination of ε (in 1 cm quartz cell).

The ε value obtained in water at the maximum absorption wavelength, $\varepsilon_{280\,nm}$, is in good agreement with previous reports (6747 L mol^{-1} cm^{-1}) [4], and is a typical value for a π-π* transition. A slight increase in ε with decrease of solvent polarity was observed for all solvents except chloroform. The low value obtained in this solvent, 4740 L mol^{-1} cm^{-1}, may well be associated with contact charge transfer contributions in this medium [5].

Table 2A-1 Maximum absorption wavelength (λ_{max}) and molar absorption extinction coefficient (ε) determined for NAD singlet ground state as function of solvent polarity. The refractive index (n_D), dielectric constant (ϵ) and viscosity (η) of solvents [6] are given for better clarity of discussion.

Solvent	Abs. λ_{max} (nm)	ε ^{a} (L mol^{-1} cm^{-1})	n_D	ϵ	η ($\times 10^{-3}$ Pa s)
Water	280	6540	1.333	80.1	1.00
D$_2$O	280	-	1.328	-	-
Ethylene glycol	283	6443	1.431	37.7	19.9
Ethanol	282	7477	1.361	24.5	1.20
Acetonitrile	282	7090	1.344	35.9	0.34
Chloroform	283	4740	1.445	4.81	0.58
1,4-Dioxane	283	7250	1.422	2.20	1.43

^{a} Estimated errors ± 5%

2A.3 Characterization of the first singlet excited state

2A.3.1 Fluorescence emission and excitation spectra and singlet excited state energy

Naphthalene and its derivatives are well known for presenting luminescence properties. Therefore, studies were undertaken to assess NAD fluorescence properties. NAD fluorescence emission and excitation spectra were measured in water, D$_2$O and in the organic solvents. Figure 2A-3 shows the fluorescence emission (λ_{ex} = 280 nm) and excitation spectra (λ_{em} = 324 nm) of aqueous NAD solution (1.0×10^{-5} mol L^{-1}) while Table 2A-2 summarizes the results in all the solvents. The fluorescence emission spectrum shows a broad band with vibronic structure extending from 300 to 400 nm. In

aqueous solution, two maxima at 324 and 338 nm were observed together with two shoulders at longer wavelengths. This is consistent with previous reports on the fluorescence spectra of this compound [7]. For all the solvents, the emission spectra was not affected when excitation was made at different wavelengths, confirming its origin from a single emitting species and that NAD does not contain any fluorescent impurities. No effect was observed on the shape of the emission or excitation spectra on going from H_2O to the other solvents, although, as seen in the results presented in Table 2A-2, there is a slight red shift in the emission maximum wavelength with decrease of solvent polarity. In all solvents, NAD excitation and absorption spectra were identical and were mirror images of the emission spectrum, confirming the lack of impurities and indicating that there is no significant geometrical change in the structure of NAD chromophore between the ground and excited state.
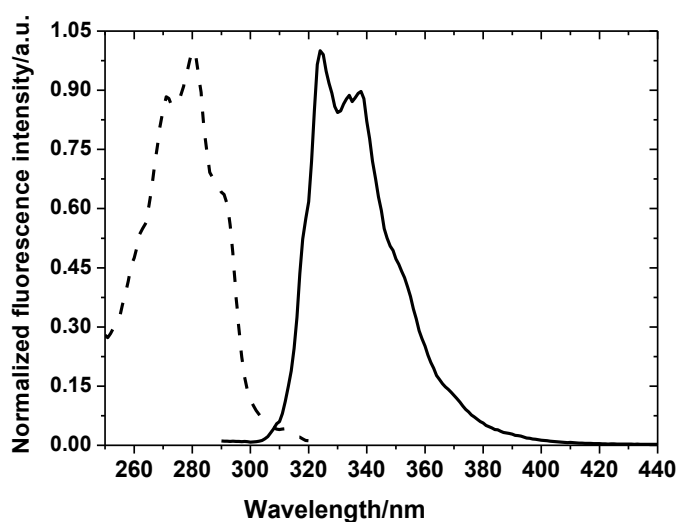
Figure 2A-3 Normalized excitation (dotted line) and emission (solid line) fluorescence spectra of aqueous NAD solution (1.0×10^{-5} mol L^{-1}).

The Stokes shifts, given as the difference between the maximum peak of normalized absorption and emission spectra, are also included in Table 2A-2. As can be noticed, no significant changes are observed on the Stokes shifts when replacing water by organic solvents. Another important parameter to be estimated is the energy of the lowest singlet excited state, E_S, which has been determined from the intersection of the normalized absorption and emission spectra (Table 2A-2). Within experimental error, E_S is independent on solvent and has a value of 4.00 eV (390 kJ mol^{-1}). This value is very similar to the E_S value of naphthalene, approximately 3.98 eV [6].

Table 2A-2 Maximum fluorescence emission wavelength (λ_{max}), Stokes shift, singlet excited state energy (E_S), determined fluorescence quantum yields (ϕ_F) and measured lifetimes (τ_F), chi squared factor (χ^2) and calculated radiative rate constant ($k_R = \phi_F/\tau_F$) for the emission decay of NAD in water, D_2O and organic solvents.

Solvent	Em. λ_{max} (nm)	Stokes shift (nm)	E_S (eV)	$\phi_F{}^a$	τ_F (ns)	χ^2	$k_R \times 10^6$ (s^{-1})
Water	324	44.0	3.99	0.066	35.0	1.09	1.89
D_2O	324	44.0	3.99	0.068	34.1	1.05	1.99
Ethylene glycol	325	42.0	3.99	0.096	52.9	0.98	1.81
Ethanol	325	43.0	4.09	0.096	49.0	1.05	1.96
Acetonitrile	325	43.0	4.00	0.186	54.0	1.08	3.44
Chloroform	325	42.0	4.09	0.022	6.77	1.10	3.25
1,4-Dioxane	326	43.0	3.95	0.357	51.0	1.01	7.00

^a Estimated errors ± 10%

2A.3.2 Determination of the fluorescence quantum yields and lifetimes

Both the fluorescence quantum yields, ϕ_F, and the singlet lifetimes, τ_F, were determined in de-aerated solutions since, as will be discussed latter, molecular oxygen quenches the singlet excited state. The results given in Table 2A-2 indicate that NAD fluoresces with reasonable quantum yields (≤ 0.357), with ϕ_F increasing on going to non-hydrogen bonding solvents. These values are similar to those reported in literature for naphthalene derivatives. For instance, Tamaki *et al.* reported a quantum yield of 0.14 for naphthyl acetic acid derivatives in acetonitrile [8]. The fact that the fluorescence quantum yields are less than unity indicates the relevance of non-radiative pathways in the deactivation of NAD singlet excited state, $^1NAD^*$. The low value obtained in water, 0.066, may be associated with hydrogen bonding effects involving the stretching modes of the hydroxyl group, which could facilitate the non-radiative decay to the ground state, and is consistent with quantum yields of other aromatics, such as benzene [9], that are markedly smaller in water than in other common solvents.

Although acetonitrile and ethylene glycol have comparable dielectric constants ($\epsilon \cong 36$), the fluorescence quantum yield in acetonitrile is twice than that in ethylene glycol. A comparison of the photophysical behavior in the two solvents is complicated by the observation of bi-exponential fluorescence decays in ethylene glycol, as will be discussed below. However, the results are consistent with hydrogen bonding enhancing non-radiative deactivation and decreasing the fluorescence quantum yield with ethylene glycol. The lowest value of fluorescence quantum yield is presented in chloroform, which again may indicate contact charge transfer [5] as was suggested above from the absorption spectra. Moreover, and as can be seen by the results in Table 2A-2, the replacement of H_2O by D_2O had no effect on NAD emission properties. With certain systems, notably lanthanides [10,11], different lifetimes are observed in D_2O compared with H_2O due to the effect of vibronic coupling on the non-radiative decay. However, the extent of coupling decreases with increasing separation between the electronic states, and the fact that no differences are observed between the fluorescence lifetimes of NAD in the two solvents indicates that this effect is insignificant here.

The fluorescence lifetimes, τ_F, in water, D_2O and organic solvents were measured with nanosecond time resolution with excitation at 282 nm and observation at the maximum emission wavelength. Figure 2A-4 shows the decay curve of NAD fluorescence in water while the results for all systems are summarized in Table 2A-2. The fluorescence decay of NAD could be fitted by a single exponential for all the solvents, except in ethylene glycol and ethanol, revealing a single emitting species. In those two solvents a better fit was obtained by a bi-exponential decay. To attempt to clarify the bi-exponential behavior seen in ethylene glycol and ethanol, NAD fluorescence decays were studied in three other alcohols: 1-propanol, 2-propanol and methanol. In methanol, the fluorescence decay of NAD followed a mono-exponential fit with a lifetime of 49.5 ns while in 1-propanol and 2-propanol the decays were well fitted using a bi-exponential decay, with the major components having lifetimes of 48.0 and 48.4 ns, respectively. In all the studied alcohols, except methanol, a small contribution was observed from a short lifetime component (≈ 4.5 ns). Although it has not yet been possible to attribute this, its contribution (5.0 %) is always small, and the lifetimes presented in Table 2A-2 for ethanol and ethylene glycol are those for the major component in the decay.
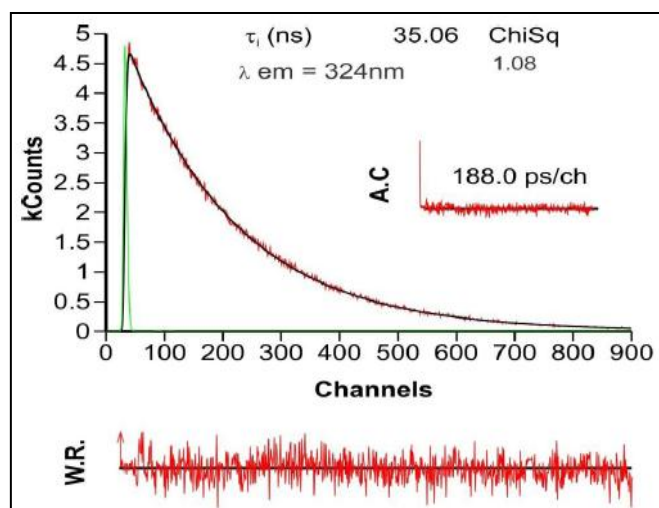
Figure 2A-4 Fluorescence decay of de-aerated aqueous NAD solution (1.0×10^{-5} mol L^{-1}) obtained with λ_{ex} = 282 nm at room temperature. The autocorrelation function (A.C.), weighted residual (W.R.) and chi-squared value (χ^2) are presented as insets. The green line in the decay is the pulse instrumental response.

τ_F is higher in organic solvents (around 50 ns) than in water (35 ns, *ca.* 70 % less than those in organic solvents). This may reflect a strong contribution of internal conversion induced by the water molecule in the decay of the singlet excited state of NAD in water, as was found with the fluorescence quantum yields. The replacement of water by deuterium oxide had no effect on the fluorescence lifetime, suggesting that it does not simply involve interaction with the O-H (O-D) groups. In general, although the values obtained for τ_F are close to those obtained for other naphthalene derivatives [6], they are somewhat smaller probably due to the effect of the substituent groups. The low value of τ_F observed in chloroform, 6.77 ns, indicates that another pathway may be involved in the deactivation, and is in agreement with the suggestion of contact charge transfer quenching of the singlet excited state by the solvent.

2A.3.3 Fluorescence quenching by inorganic anions

It is well known that a variety of species can induce the quenching of the fluorescence, leading to deactivation of the singlet excited states. These may be relevant to the degradation of NAD under environmental conditions. Many studies have been published concerning the involvement of electron transfer as a quenching mechanism of

fluorescence for aromatic molecules such as naphthalene, anthracene, biphenyl, etc.,
[12-15].

Therefore, the quenching of NAD fluorescence was studied with some halide, thiocyanate and azide ions, and with the known electron-transfer quencher triethylamine (TEA), to obtain insights on the mechanisms that may be involved in its excited state deactivation, with a consequent contribution to NAD photochemical degradation under environmental conditions.

Aqueous solutions of KBr, KI, KCl, KSCN, NaN_3 and a TEA solution in acetonitrile with different concentrations were added to a NAD solution (1.0×10^{-5} mol L^{-1}). Stern-Volmer plots of I/I_0 *vs* [quencher] was constructed in which the slope of the curve is equal to the Stern-Volmer constant K_{SV}. The quenching rate constant, k_q, was then determined by the relation $K_{SV} = k_q\times\tau_F$. Figure 2A-5 shows, as one example, the effect of the quencher KSCN in NAD fluorescence emission.
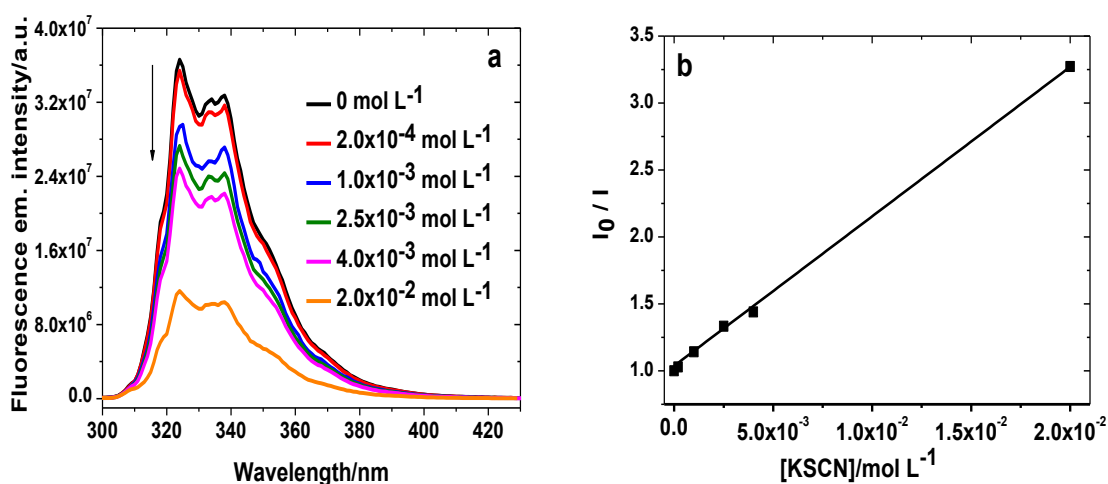
Figure 2A-5 a) Quenching of NAD fluorescence emission (1.0×10^{-5} mol L^{-1}) by KSCN in aqueous solution. b) Respective Stern-Volmer plot, $R^2 = 0.996$.

As given in the Figure 2A-5a, the addition of KSCN did not cause any change in the shape of emission spectra or formation of new bands, but only led to the decrease in fluorescence intensity due to the quenching process. Similar behavior was observed with the other quenchers. Furthermore, the excitation spectra in the presence of the quenchers resemble the excitation and absorption spectra in absence of the quenchers, confirming the lack of any ground state complexation. Good straight lines were observed in the Stern-Volmer plots within the concentration range 10^{-4}-10^{-2} mol L^{-1}, as

can be seen by the plot in Figure 2A-5b for the case of KSCN, strongly supporting a dynamic quenching mechanism. From the K_{SV} values reported in Table 2A-3 it is possible to calculate the fluorescence quenching rate constant for dynamic quenching, k_q, from the previous given relationship $K_{SV} = k_q \times \tau_F$, where τ_F values are taken from Table 2A-2. These quenching results are also included in Table 2A-3.

Table 2A-3 Stern-Volmer constants (K_{SV}) and fluorescence quenching rate constants (k_q) for NAD singlet excited state by anions in water and TEA in acetonitrile. The redox potentials of the quenchers are also given for better discussion of results.

Quencher	K_{SV} (L mol^{-1})	k_q (L mol^{-1} s^{-1})	Reduction potential (V) [a]
Cl$^-$	≤0.0038	≤1.08×10^5	2.41 [16]
Br$^-$	18.1	5.18×10^8	1.92 [16]
I$^-$	180	5.15×10^9	1.33 [16]
SCN$^-$	123	3.52×10^9	1.63 [16]
N$_3^-$	102	2.91×10^9	1.33 [16]
TEA	79.0	1.46×10^9	0.96 [6]

[a] E^o values for X$^\bullet$/X$^-$ *vs* the normal hydrogen electrode (NHE)

In aqueous solution k_q varies in the range 5.18×10^8 to 5.15×10^9 L mol^{-1} s^{-1}, indicating that there is a marked effect of the type of anion in the quenching of the fluorescence. This may be explained by the correlation between k_q and the reduction potential of the X$^\bullet$/X$^-$ couple given in Table 2A-3, with I$^-$ having the highest k_q, 5.15×10^9 L mol^{-1} s^{-1}, and Cl$^-$ the lowest. The low k_q value observed with Cl$^-$ is a limit since the fluorescence intensity of NAD was almost constant with increasing concentrations of KCl, showing that Cl$^-$ is not effective in quenching NAD fluorescence. Furthermore, N$_3^-$ has a very similar efficiency to SCN$^-$ in quenching the fluorescence of NAD, but is less effective than I$^-$. Both electron transfer and heavy atom effects may be responsible for the quenching. For electron transfer, the k_q values can be related to the free energy of reaction through the Rehm-Weller relationship [17]. The free energy depends on the electrochemical data, and a reasonable linear relationship between log k_q *vs* redox potential can be drawn for the anions I$^-$, Br$^-$ and

SCN^- (r = 0.856), with slope 1.6. A similar semilogarithmic relationship between the quenching rate and electrochemical data has been reported for the fluorescence quenching of naphthalene derivatives by halide ions [12,13], and suggests that the mechanism responsible for the quenching involves electron (or charge) transfer from the anion to $^1NAD^*$. It is necessary to point out that in both ref. 12 and our case the quenching efficiencies of N_3^- and SCN^- are very similar, although their redox potentials are different. However, the recommended value of 1.33 V for the reduction potential of the azide/azidyl couple is for buffered neutral solution [16]. Hydrazoic acid (HN_3) is a weak acid (pKa 4.65 at zero ionic strength) [18] and it is likely that the reduction potential for $N_3^\bullet/N_3^-$ in our unbuffered solution will differ from this recommended value. Additional support for an electron transfer mechanism comes from the fluorescence quenching of NAD in acetonitrile by the electron donor TEA. To obtain evidence for the fact that electron transfer is involved in the excited singlet state quenching, aerated and de-aerated solutions of NAD in the presence of KI and KSCN, respectively, were studied by laser flash photolysis with excitation of NAD at 266 nm. The transient bands corresponding to the formation of the radical anions $I_2^{\bullet-}$ at 380 nm and of $(SCN)_2^{\bullet-}$ at 480 nm [19] were observed as well as the formation of NAD triplet excited state, confirming parallel processes of electron transfer and intersystem crossing (isc). The study reported by Shizuka *et al.* in 50 % ethanol-water [13] shows no evidence for formation of the inorganic anion radical. However, this requires a second step where the initially formed radical pair reacts with halide ions [20], which may be inhibited in the mixed solvent medium used by Shizuka *et al*. [13]. A possible mechanism for the quenching process is given by reactions (2A-1) to (2A-3):

$$^1NAD^* + X^- \leftrightarrows \{^1NAD^*...X^-\} \leftrightarrows \{NAD^{\bullet-}\ X^\bullet\} \rightarrow {}^3NAD^* + X^- \qquad (2A.1)$$

$$\{NAD^{\bullet-}\ X^\bullet\} + X^- \rightarrow NAD^{\bullet-} + X_2^{\bullet-} \qquad (2A.2)$$

$$NAD^{\bullet-} + H_2O \leftrightarrows NADH^\bullet + OH^- \qquad (2A.3)$$
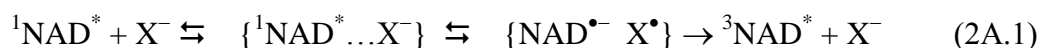
where X^- represents the halide anion. The fact that weak quenching was observed with bromide ion and no significant quenching with chloride ion allows to place a limit on the reduction potential of $^1NAD^*$ of E^o 2.1 ± 0.2 V.

2A.4 Characterization of the triplet excited state

2A.4.1 Phosphorescence spectra and triplet excited state energy

The phosphorescence emission spectra, quantum yields, ϕ_P, and lifetimes, τ_P, of NAD were measured at 77 K in ethanol, acetonitrile and ethylene glycol glasses. As depicted in Figure 2A-6, NAD presents well-resolved emission spectrum in acetonitrile with three main vibronic bands, which are comparable to those obtained in fluorescence spectrum. Similar trends are observed in ethylene glycol and ethanol glasses, although the spectra are not so well resolved due to problems with light scattering. The lowest wavelength band obtained in acetonitrile is assigned to the 0-0 transition between the lowest triplet excited state (T_1) and the ground state (S_0), and gives the energy of the triplet excited state E_T, 2.69 eV (260 kJ mol^{-1}). This value is close to the literature value for naphthalene (2.66 eV) [6].
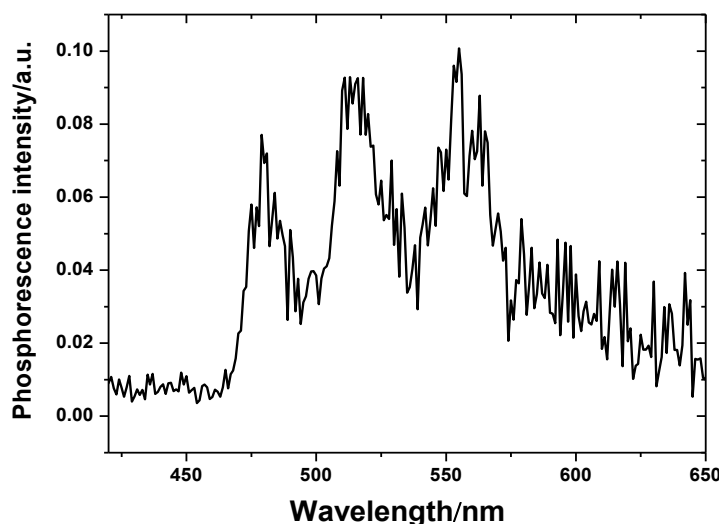
Figure 2A-6 Phosphorescence spectrum of NAD (1.0×10^{-5} mol L^{-1}) in acetonitrile at 77 K.

2A.4.2 Determination of the phosphorescence quantum yield and lifetimes

The ϕ_P was calculated in ethanol, ethylene glycol and acetonitrile at 77 K using benzophenone in ethanol at 77 K as reference ($\phi_P = 0.73$ [6]). The results presented in Table 2A-4 gave similar values in the three glasses, within the experimental error.

The lowest NAD triplet excited state, ^{3}NAD* (T_1) may be deactivated to the singlet ground state S_0 by radiative (phosphorescence) or non-radiative processes (isc). The rate constant for phosphorescence decay k_p (= ϕ_p/τ_P) as well as the non-radiative

quantum yield of intersystem crossing for the deactivation of $^3NAD^*$ state, ϕ_{isc} (T$_1$-S$_0$), were calculated according to the expression (2A.4), where determined ϕ_{isc} (T$_1$-S$_0$) values are given in Table 2A-5.

$$\phi_{isc}(S_1 - T_1) = \phi_P + \phi_{isc}(T_1 - S_0) \tag{2A.4}$$

The results given in Table 2A-4 show that the ϕ_{isc} (T$_1$-S$_0$) is ten times greater than ϕ_P indicating that the deactivation of $^3NAD^*$ state occurs preferentially by isc to the ground state rather than by the radiative process of phosphorescence.

Table 2A-4 Phosphorescence properties of NAD in ethanol, ethylene glycol and acetonitrile glasses at 77 K.

Solvent	ϕ_P [a]	τ_P (ms)	k_R (s^{-1})	ϕ_{isc} (T$_1$-S$_0$)
Ethylene glycol	0.043	210	0.22	0.57
Ethanol	0.052	64	0.79	0.50
Acetonitrile	0.043	0.12	400	0.65

[a] Estimated errors $\pm$ 10%

The phosphorescence lifetime of NAD, τ_P, was determined in the above glasses as the average of at least 10 measurements, with a relatively low measurement error. The obtained results are also presented in Table 2A-4 while Figure 2A-7 illustrates, as an example, the phosphorescence decay of NAD in ethanol at 77 K.
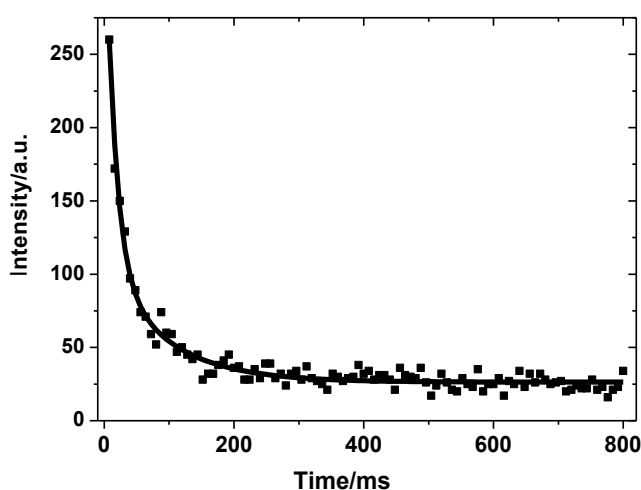
Figure 2A-7 Decay of NAD phosphorescence in ethanol at 77 K (λ_{ex} = 280 nm, λ_{em} = 478 nm).

The fact that the phosphorescence lifetime in ethylene glycol is in the hundreds of milliseconds time range is in agreement with the triplet excited state corresponding to a (π-π^*) transition, as reported for naphthalene and its derivatives [6]. The explanation for the decrease in lifetime on going from ethylene glycol to acetonitrile is not clear. However, this is completely reproducible. Given that similar quantum yields are observed with these two solvents while the lifetime is much shorter in acetonitrile, indicates that the magnitude of the effects involved must be similar with both radiative and non-radiative processes.

2A.4.3 Triplet-triplet absorption spectra and triplet lifetimes

Nanosecond laser flash photolysis studies were undertaken to obtain more detailed information on the reactive species that may be formed upon NAD photoexcitation. Excitation in the lowest energy absorption band of NAD (250-320 nm) was accomplished with frequency quadrupled (266 nm) pulses from a Nd/YAG laser.

The transient absorption (singlet-triplet difference) spectra were obtained in de-aerated NAD solutions in water, D_2O, ethylene glycol, ethanol, acetonitrile, chloroform and 1,4-dioxane, at different delays times after laser excitation. Figure 2A-8a shows the transient absorption spectra obtained for a de-aerated aqueous NAD solution.
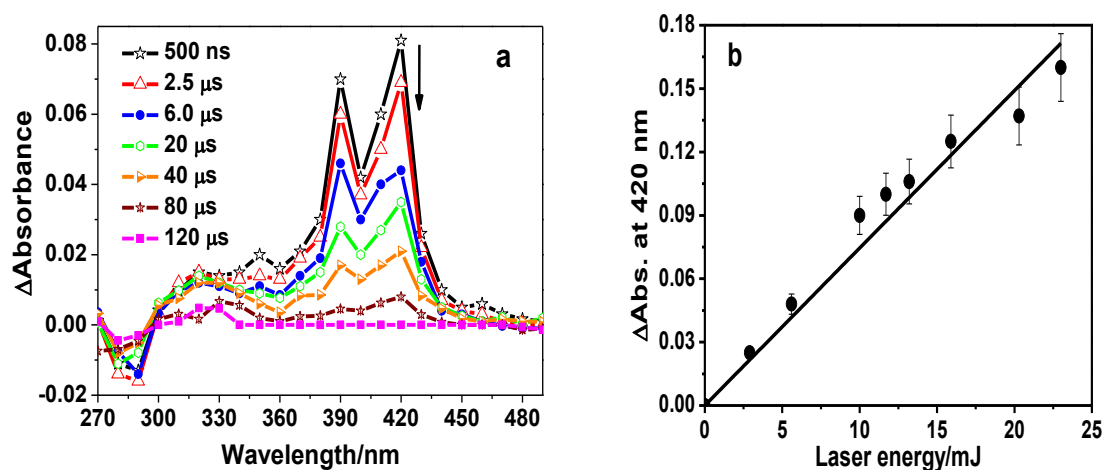
Figure 2A-8 a) Transient absorption spectra of de-aerated aqueous NAD solution (3.5×10^{-5} mol L^{-1}) obtained by nanosecond laser flash photolysis with excitation at 266 nm, recorded at 500 ns, 2.5, 6.0, 20, 40, 80, and 120 μs after pulse. b) Evolution of the absorbance for the band at 420 nm as function of laser energy.

Several transient absorption bands arising from NAD were observed: a negative band with maximum around 280 nm corresponding to the bleaching of the ground state, an intense band with maxima at 420 and 390 nm, and a third band with maximum absorption at 330 nm.

As clearly shown in Figure 2A-9, the absorption band at 330 nm presents a different kinetic profile when compared to the absorption band with maximum at 420 nm, with a rate constant of 8.5×10^3 s^{-1}, and may be attributed to the formation of the radical cation species of NAD (NAD$^{\bullet+}$) through ^{1}NAD*. The formation of the radical cation for naphthalene and naphthalene derivatives is well documented [21-24].
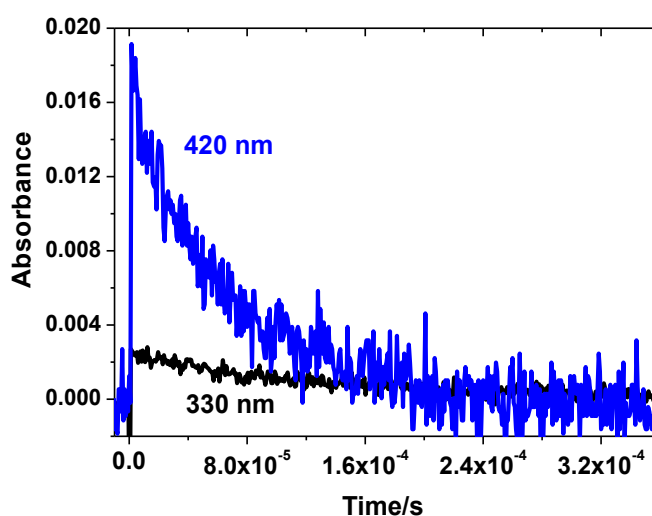
Figure 2A-9 Kinetics profile of NAD decay of the transient absorption band at 330 and 420 nm.

Furthermore, the formation of a fourth species attributed to hydrated electron was also observed at 720 nm just after the laser pulse, as can be seen in Figure 2A-10a, in agreement with several previous reports on naphthalene and its derivatives [22,23]. To determine whether the formation of the hydrated electron is due to a mono or bi-photonic process, the absorbance of the hydrated electron at 720 nm was measured as a function of the laser energy upon excitation of the NAD solution at 266 nm. As shown by Figure 12B-0b, at laser energies < 18 mJ the variation is linear and the hydrated electron is clearly formed through a monophotonic process. For laser energy greater than 18 mJ the absorbance starts to loss linearity with laser energy, suggesting the occurrence of biphotonic or multiphotonic processes. Therefore, all further nanosecond laser flash photolysis studies were carried out at laser energies < 18 mJ.
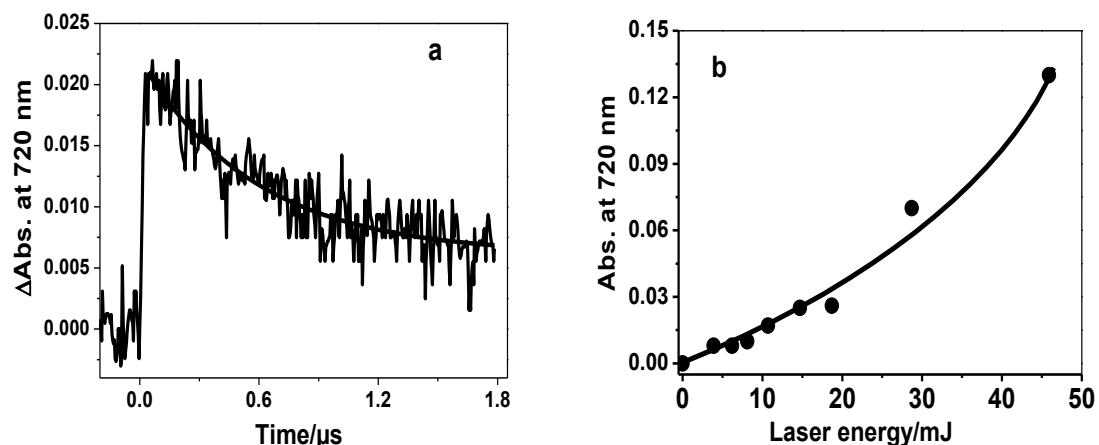
Figure 2A-10 a) Transient absorption signal of the hydrated electron at 720 nm measured with laser intensity of 15 mJ for a de-aerated aqueous NAD solution. b) Evolution of the absorbance at 720 nm of the hydrated electron as function of laser energy.

The formation of the hydrated electron is thought to occur mainly due to $^1NAD^*$ through a photoionisation process, as observed with similar compounds [25], forming the NAD cation radical, as shown in Scheme 1. In the presence of molecular oxygen, the hydrated electron leads to the formation of the superoxide anion radical ($O_2^{\bullet-}$) which can react with substrates or disproportionate to hydrogen peroxide (H_2O_2) and oxygen.

$$e^-\,(aq.) \quad + \quad \xrightarrow{\ O_2\ } \quad O_2^{\bullet-}$$

$$O_2^{\bullet-} + \ H^+ \ \rightleftharpoons \ HO_2^{\bullet} \quad (pKa = 4.8)$$

$$2\,HO_2^{\bullet} \ \rightleftharpoons \ H_2O_2 + O_2$$
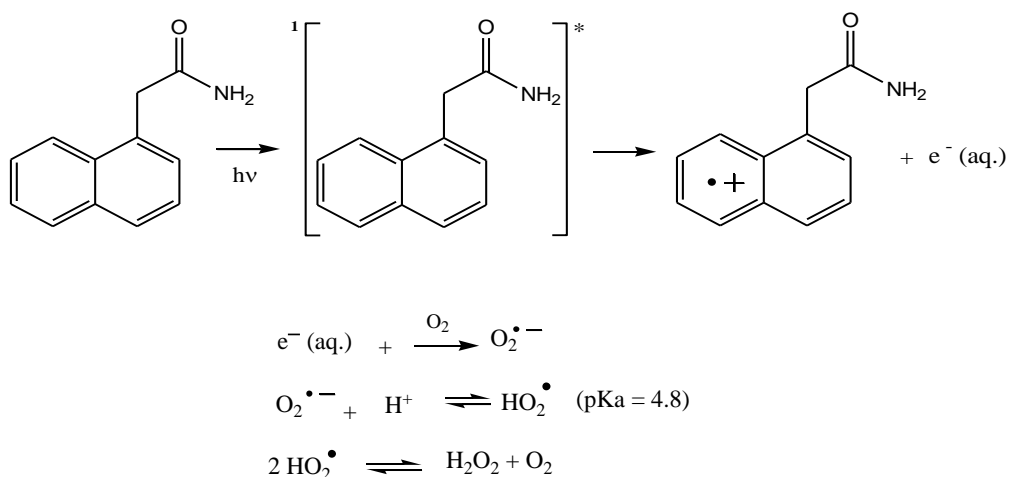
Scheme 2A-1 Photoionization process of NAD with formation of hydrated electron.

The decay of the solvated electron was dependent on oxygen concentration, as shown in Figure 2A-11, with a bimolecular rate constant of 1.8×10^{10} L mol^{-1} s^{-1} in perfect good agreement with the literature data, 1.9×10^{10} L mol^{-1} s^{-1} [26].
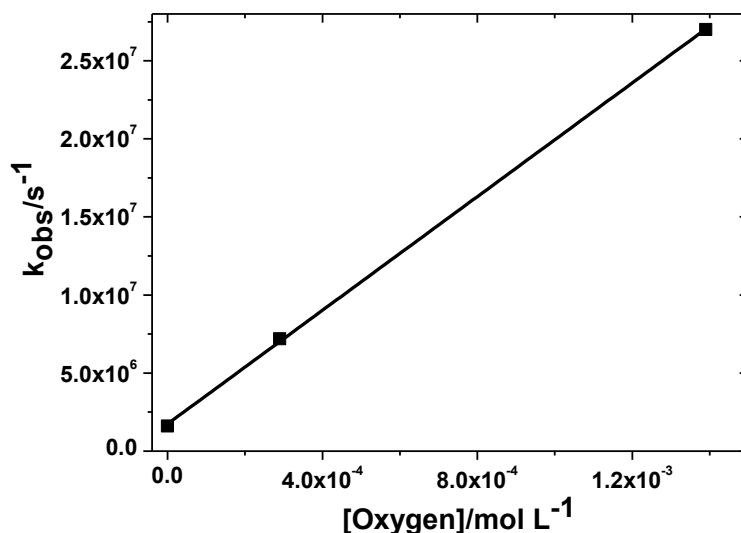
Figure 2A-11 Calculation of the bimolecular quenching rate constant for the hydrated electron at 720 nm as function of oxygen concentration.

The quantum yield of formation of the hydrated electron, ϕ_{e^-}, was also evaluated for NAD in water by using two chemical actinometers as references: benzophenone (BP) and cobalt complex $[Co(NH_3)_5 \ Br]^{2+}$. Aqueous solutions of NAD and of $[Co(NH_3)_5 \ Br]^{2+}$, and benzophenone solution in acetonitrile with absorbances $\cong 0.6$ were excited with the nanosecond laser at 266 nm at different laser energy. These measurements were made at the maximum absorption wavelength of each solution. For NAD this wavelength corresponds to the maximum wavelength of the hydrated electron (720 nm) while for BP corresponds to the maximum wavelength of the triplet excited state (525 nm) [6]. The photoexcitation at 266 nm of an aqueous solution of $[Co(NH_3)_5 \ Br]^{2+}$ results in the formation of the ligand derived radical intermediate Br_2^-, which has it maximum absorption wavelength at 360 nm [19]. The plot of the respective laser energy *vs* absorbance gave a linear line as shown in Figure 2A-12. The slope of each curve is equal to the product of $\varepsilon \times \phi$. Since the solutions have the same absorbance, the quantum yield of hydrated electron ϕ_{e^-} can be determined for NAD, for each actinometer, as follows (2A.5):

$$\varepsilon_{\text{actinometer}} \times \phi_{\text{actinometer}} \times \text{slope}_{e^-} = \varepsilon_{e^-} \times \phi_{e^-} \times \text{slope}_{\text{NAD}} \qquad (2A.5)$$

in which $\varepsilon_{360 \text{ nm}}([Co(NH_3)_5 \ Br]^{2+}) = 9900$ L mol^{-1} cm^{-1} [19] and $\phi = 0.3$ [27], while the actinometer BP has a extinction coefficient of 6250 L mol^{-1} cm^{-1} and a $\phi_T = 1.0$ [6]. The quantum yield of the hydrated electron ϕ_{e^-} was determined to be 10 % with the

actinometer BP and 12% with the actinometer cobalt complex, considering the extinction coefficient of the hydrated electron as 22700 L mol^{-1} cm^{-1} at 720 nm [28]. The two actinometers gave similar values, within the experimental errors.
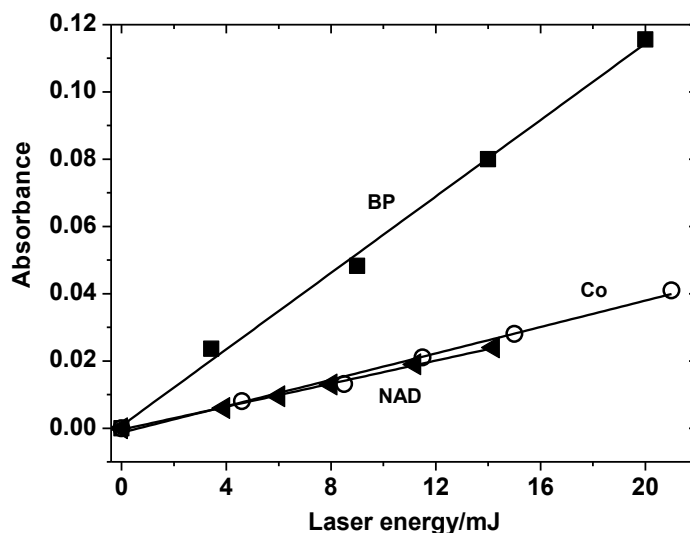
Figure 2A-12 Plot of the laser energy *vs* absorbance for de-aerated solutions of: (◄) NAD in water at 720 nm, (■) BP in acetonitrile at 525 nm and (○) cobalt complex in water at 360 nm.

The other transient species with maximum absorption wavelength around 420 nm (given in Figure 2A-8a) can be assigned to the NAD triplet-triplet absorption as will be discussed bellow, and is comparable to that seen for triplet states of naphthalene and derivatives [6,21,29]. The absorbance at 420 nm increased linearly with laser energy (Figure 2A-8b), within the range 1-15 mJ, indicating its formation occurs via a monophotonic process. To confirm the triplet-triplet nature of the absorption band with maximum around 420 nm, solutions of NAD in all solvents were excited at 266 nm as function of oxygen concentration since it is well known that molecular oxygen is a strong quencher of triplet excited states of aromatic molecules.

The decay rate constant of NAD absorption band at the maximum wavelength was measured in each solvent, and the triplet lifetimes τ_T calculated as the inverse of this rate constant. These results are summarized in Table 2A-5. A marked effect of oxygen was observed in the decay of the transient band at 420-425 nm, as shown in Figure 2A-13 for aerated and de-aerated aqueous NAD solution, and the decay of $^3NAD^*$ is faster in the presence of oxygen, confirming that it is acting as a quencher. This behavior was observed for all the solvents, supporting the idea that this band corresponds to $^3NAD^*$.

Table 2A-5 Photophysical parameters determined for NAD triplet excited state (lifetimes τ_T and quantum yield (ϕ_{isc} or ϕ_T)) as function of solvent polarity and oxygen concentration.

Solvent	Abs. λ_{max} (nm)	τ_T^{Argon} (μs)[a,b]	τ_T^{Air} (μs)[a]	$\tau_T^{O_2}$ (μs)[a]	ϕ_T [a,b]
Water	420	68	1.4	0.45	0.424
D$_2$O	420	65	1.5	0.39	0.414
Ethylene glycol	420	338	3.7	0.93	0.610
Ethanol	420	125	0.30	0.10	0.547
Acetonitrile	420	57	0.25	0.086	0.691
Chloroform	425	42	0.41	-	0.522
1,4-Dioxane	425	67	0.42	-	0.427

[a] Estimated errors $\pm$ 15%. [b] De-aerated solutions.

In aerated and oxygenated solutions the decay of the triplet excited state fitted a monoexponential rate law (Figure 2A-13). In contrast, in some cases, in de-aerated solutions, a better fit was achieved by a bi-exponential decay probably due to triplet-triplet annihilation as suggested by τ_T decreasing with an increase of laser energy. In water, τ_T values of 1.4, 67.7 and 0.454 μs were found in aerated, de-aerated and oxygenated solution, respectively. The replacement of H$_2$O by D$_2$O did not cause any significant changes on the triplet lifetimes, as can been seen by the results given in Table 2A-5.
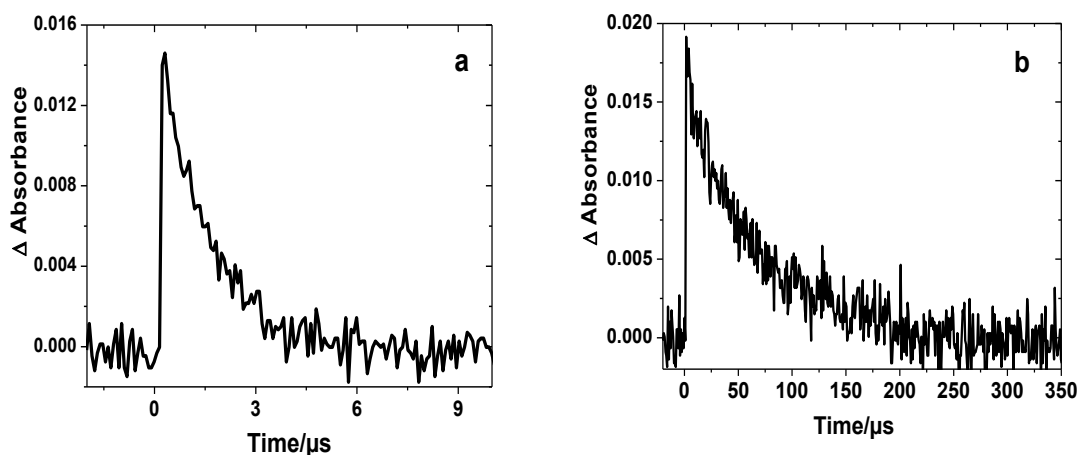
Figure 2A-13 Kinetic decay of aqueous NAD triplet excited state monitored at 420 nm in a) aerated and b) de-aerated solutions.

When water was replaced by 1,4-dioxane or chloroform, a 5 nm red shift of the main absorption band around 420 nm occurred (Table 2A-5). The band at 330 nm was not observed in any of the organic solvents, within the time scale studied.

Further confirmation of the triplet nature of the 420-425 nm transient species came from sensitization experiments using benzophenone (BP) as a high quantum yield triplet donor ($\phi_T = 1.0$, $E_T = 287$ kJ mol^{-1}, 2.98 eV) [6]. Figure 2A-14 gives the transient absorption spectra at different times after excitation by a 355 nm laser pulse of a de-aerated solution of BP in acetonitrile (2.0×10^{-3} mol L^{-1}) containing NAD (4.0×10^{-4} mol L^{-1}). Under these conditions the laser light is totally absorbed by BP to form its triplet excited state.
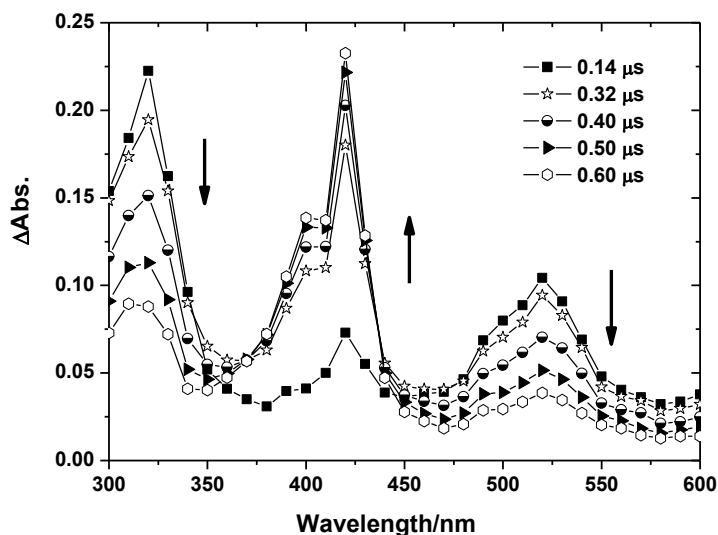
Figure 2A-14 Transient spectra observed at various times after exciting a de-aerated solution of benzophenone (2.0×10^{-3} mol L^{-1}) containing NAD (4.0×10^{-4} mol L^{-1}) in acetonitrile with pulsed laser radiation at 355 nm.

The spectra show three bands with absorption maxima at 320, 420 and 520 nm. The bands at 320 and 520 nm are attributed the formation of benzophenone triplet excited state ($^3BP^*$) in acetonitrile [6] while the band at 420 nm corresponds to $^3NAD^*$. This band is identical to that obtained upon excitation of de-aerated NAD solution with a 266 nm laser pulse given by Figure 2A-8. The spectra at successive times show a decrease of the absorption band at 520 nm and a consequent increase of the band at 420 nm. Additionally, the decay rate of the $^3BP^*$ donor at 520 nm (3.65×10^6 s^{-1}) is slower than the apparent acceptor $^3NAD^*$ build up rate at 420 nm (6.42×10^6 s^{-1}) due to the

simultaneous acceptor triplet decay. These results indicate that energy transfer occurs from $^3BP^*$ to NAD with formation of $^3NAD^*$ according to reactions (2A.6) and (2A.7):

$$BP + h\upsilon \longrightarrow {}^1BP^* \xrightarrow{\text{isc}} {}^3BP^* \qquad\qquad (2A.6)$$

$$^3BP^* + \text{NAD} \longrightarrow {}^3NAD^* + \text{BP} \qquad\qquad (2A.7)$$

This experiment was repeated with various concentrations of NAD (3.5×10^{-5}-4.0×10^{-4} mol L^{-1}) maintaining a constant BP concentration (2.0×10^{-3} mol L^{-1}). The decay rate at 520 nm of $^3BP^*$ was found to be linear with NAD concentration. A plot of the observed decay rates as function of NAD concentration allows the calculation of the quenching rate constant for the above reaction of 1.67×10^{10} L mol^{-1} s^{-1}, corresponding to diffusion controlled triplet-triplet energy transfer in a collisional process. From consideration of energetic effects on the rate [30] this indicates that the triplet energy of NAD must be significantly less than that of benzophenone (2.98 eV), in agreement with results from phosphorescence in this solvent which gives a $^3NAD^*$ energy of 2.69 eV.

2A.4.4 Determination of the triplet state molar absorption coefficient and quantum yield

The previous experiment on the energy transfer to benzophenone was used to calculate the triplet state molar absorption coefficient of NAD, ε_T, through the energy transfer method [31]. A molar absorption coefficient of 13820 L mol^{-1} cm^{-1} was obtained for $^3NAD^*$ in acetonitrile at 420 nm. Assuming that this coefficient is constant and independent of solvent, we have used this value to calculate the intersystem crossing quantum yield (or triplet quantum yield), ϕ_T, of NAD in the different solvents by the comparative method [32] using naphthalene in methylcyclohexane ($\varepsilon = 13200$ L mol^{-1} cm^{-1}, $\phi_T = 0.75$ [6]) as a reference. The results obtained of ϕ_T values for NAD in water, D$_2$O, ethylene glycol, ethanol, acetonitrile, chloroform and 1,4-dioxane are given in previous Table 2A-5. The ϕ_T values are relatively high and are dependent on solvent polarity ranging from 0.42 in water to 0.69 in acetonitrile, indicating that the formation of $^3NAD^*$ by intersystem crossing is an important decay pathway of $^1NAD^*$ and may be relevant to its photoreactivity. Changing water to deuterated water did not affect the triplet excited state properties (Table 2A-5).

2A.5 Quenching of singlet and triplet excited states of NAD by molecular oxygen

Molecular oxygen is an important quencher of both singlet and triplet excited states of molecules [6,33-35] leading to photophysical consequences such as fluorescence and triplet state deactivation, enhanced intersystem crossing and production of singlet oxygen, $^1O_2$ ($^1\Delta_g$). The rate constants for the quenching of $^1NAD^*$ by molecular oxygen, $k_S^{O_2}$, were determined in the various solvents through a Stern-Volmer plot of the fluorescence intensity ratios for oxygenated, aerated and de-aerated solutions vs oxygen concentration. A linear fit was obtained, with the slope giving the Stern-Volmer coefficient K_{SV} (= $k_{q\times}\tau_F$). Since the fluorescence lifetimes of NAD are already known (Table 2A-2), the $k_S^{O_2}$ values calculated are reported in Table 2A-6. In addition, the rate constants for oxygen quenching of NAD triplet excited state were calculated from the following equation (2A.8):

$$k_{obs} = k_0 + k_T^{O_2} [O_2] \qquad (2A.8)$$

where k_{obs} and k_0 are the observed first-order rate constants for the decay of NAD triplet excited state at the absorption maximum for each solvent in the presence and absence of oxygen, respectively, and $[O_2]$ is the oxygen concentration in each solvent [6]. The plot of the observed triplet rate constants k_{obs} vs the oxygen concentration gives a linear fit for all solvents with a slope equal to $k_T^{O_2}$. Table 2A-6 lists the quenching rate constants obtained for NAD singlet and triplet excited states by molecular oxygen for all the studied solvents.

Table 2A-6 Determined quenching rate constants of NAD singlet and triplet excited states, $k_S^{O_2}$ and $k_T^{O_2}$, respectively, by molecular oxygen as function of solvent polarity.

Solvent	$k_S^{O_2}$ (L mol^{-1} s^{-1})[a]	$k_T^{O_2}$ (L mol^{-1} s^{-1})[a]
Water	1.08×10^{10}	1.51×10^9
Ethylene glycol	6.50×10^8	1.82×10^9
Ethanol	8.55×10^9	9.46×10^8
Acetonitrile	1.81×10^{10}	1.21×10^9
Chloroform	1.47×10^{10}	1.00×10^9
1.4-Dioxane	1.18×10^{10}	1.82×10^9

[a] Estimated errors ± 10%

The results show that the bimolecular quenching rate constants of NAD excited states vary over a wide range (10^8-10^{10} L mol^{-1} s^{-1}), in agreement with literature data concerning aromatic molecules such as naphthalene and naphthalene derivatives [6]. The lowest value of $k_S^{O_2}$ presented in ethylene glycol is probably due to its high viscosity. Surprisingly, the rate for quenching NAD triplet excited state in this solvent is slightly higher than for the singlet excited state. Although we do not have at present any explanation for this, the measurement was repeated and the value is fully reproducible. In general, the quenching rate constants of $^1NAD^*$ by molecular oxygen, $k_S^{O_2}$, approach the diffusion controlled limiting rate constant, k_{diff}, and present higher values than those obtained for the deactivation of $^3NAD^*$, $k_T^{O_2}$. This difference is related with the spin statistical factor that in triplet excited state is $(1/9)\times k_{diff}$ while for singlet excited states it is 1. For example, in water, the quenching process of $^1NAD^*$ by molecular oxygen has a rate of 1.08×10^{10} L mol^{-1} s^{-1} while for $^3NAD^*$ it is 1.51×10^9 L mol^{-1} s^{-1}, about 1/9th that of $^1NAD^*$, as frequently observed in aromatic systems [36]. Although the details of the quenching mechanism are still not clear, there is a general agreement that this depends on the nature of the system and involves energy and/or charge transfer leading to the formation of the very reactive species singlet oxygen $^1O_2$ [33,37,38], and possibly superoxide radical anions ($O_2^{\bullet-}$). It is possible to presume that energy transfer between $^3NAD^*$ and molecular oxygen leading to $^1O_2$ formation will occur, base on previous studies on quenching of triplet state of naphthalene derivatives and formation of singlet oxygen [39]. However, since the reactive species $O_2^{\bullet-}$ was observed by laser flash photolysis, it is necessary to keep in mind that electron transfer may also contribute for quenching of NAD singlet and triplet excited states.

2A.6 Singlet oxygen measurements

Previous studies on naphthalene derivatives demonstrate that they are able to generate singlet oxygen, $^1O_2$ ($^1\Delta_g$), with relatively good yields [40-43]. Time resolved phosphorescence with emission monitored at 1270 nm has been used to determine NAD singlet oxygen formation quantum yields (ϕ_Δ). In addition, photosensitization experiments using phenalenone have been realized to study the rate constant for the singlet oxygen reaction with NAD.

For the determination of ϕ_Δ, optically matched aerated solutions of NAD in various solvents were irradiated with a laser pulse at 266 nm using as reference biphenyl solution in cyclohexane ($\phi_\Delta = 0.73$ [44]). This was chosen rather than the more commonly used phenalenone standard because of its stronger absorption at the excitation wavelength within the accessible concentration range. The time-resolved phosphorescence emission intensity of these samples at 1270 nm was measured at different laser pulse energies and extrapolated to the start of the decay. Since all solutions have the same absorbance at the excitation wavelength, for any given laser energy, the number of photons absorbed by any solution will be the same. Individual singlet oxygen luminescence traces were signal averaged and fitted using a single exponential function to yield the luminescence intensity. The phosphorescence intensity was then plotted against the laser energy [45] which gave straight lines whose slopes were compared with that obtained from the reference biphenyl, yielding relative singlet oxygen quantum yields, ϕ_Δ.

The relative ϕ_Δ values obtained for NAD given in Table 2A-7 show a dependence on solvent and vary between 0.097 and 0.396, in water and chloroform, respectively. Although these values are not high, we can say that they are within the range of values already reported for other naphthalene derivatives [46]. Though there may be technical difficulties with measurements in water due to the short singlet oxygen lifetime in this solvent (*ca.* 4 μs) the effect of this is small since the substitution of water by deuterated water had no effect on the ϕ_Δ value although the lifetime in deuterated water is 20 times higher than in H_2O [47].

Table 2A-7 Singlet oxygen quantum yield (ϕ_Δ) formation as function of solvent polarity.

Solvent	ϕ_T [a]	ϕ_Δ [a]
Water	0.424	0.097
D_2O	0.414	0.105
Ethylene glycol	0.610	0.261
Ethanol	0.547	0.394
Acetonitrile	0.691	0.269
Chloroform	0.522	0.396
1,4-Dioxane	0.427	0.346

[a] Estimated errors ± 10%

A comparison of the ϕ_Δ for NAD in the various solvents and the corresponding ϕ_T values (see Table 2A-5) indicates that the former are much lower than the ϕ_T values, providing evidence of a relatively low efficiency of energy transfer from $^3NAD^*$ to molecular oxygen to produce $^1O_2$. The case of water ($\phi_\Delta = 0.424$, $\phi_\Delta = 0.097$) is particularly striking. Therefore, it is likely that quenching of NAD triplet excited state by molecular oxygen in polar solvents also involves other pathways, such as electron transfer to produce $O_2^{\bullet-}$ and NAD radical cation, both of which could be implicated in the photodegradation of this compound in water.

To test the reactivity of NAD with $^1O_2$, this species was prepared by photosensitization [48,49] through energy transfer (E_{TR}) from the triplet excited state of a sensitizer (Sens) to molecular oxygen ($^3O_2$):

$$Sens \xrightarrow{h\upsilon} {}^1Sens^* \longrightarrow {}^3Sens^*$$

$${}^3Sens^* + {}^3O_2 \xrightarrow{E_{TR}} Sens + {}^1O_2$$
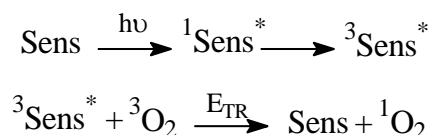
Phenalenone was used as sensitizer due to the high quantum yields of $^1O_2$ formation ($\phi_\Delta = 0.98$) [50], and chloroform was chosen as a solvent since it gives a sufficiently long singlet oxygen lifetime ($\tau_\Delta = 2.5 \times 10^{-4}$ s) to study the reaction conveniently [51]. Aerated solutions containing a constant concentration of phenalenone (3.0×10^{-5} mol L^{-1}) and concentrations of NAD varying within the range 1.0×10^{-4}-1.0×10^{-2} mol L^{-1} were excited at 355 nm and the $^1O_2$ phosphorescence decay was measured at 1270 nm. Rate constants of $^1O_2$ decay were obtained from the observed phosphorescence lifetimes ($k_{obs} = 1/\tau_\Delta$). A plot of the observed rate constants k_{obs} *vs* NAD concentration gave a straight line, as shown in Figure 2A-15, in agreement with the overall kinetic equation (2A.9):

$$k_{obs} = k_0 + k_q [NAD] \tag{2A.9}$$

where k_0 is the rate constant in absence of NAD and k_q is the quenching rate constant of $^1O_2$ by NAD.
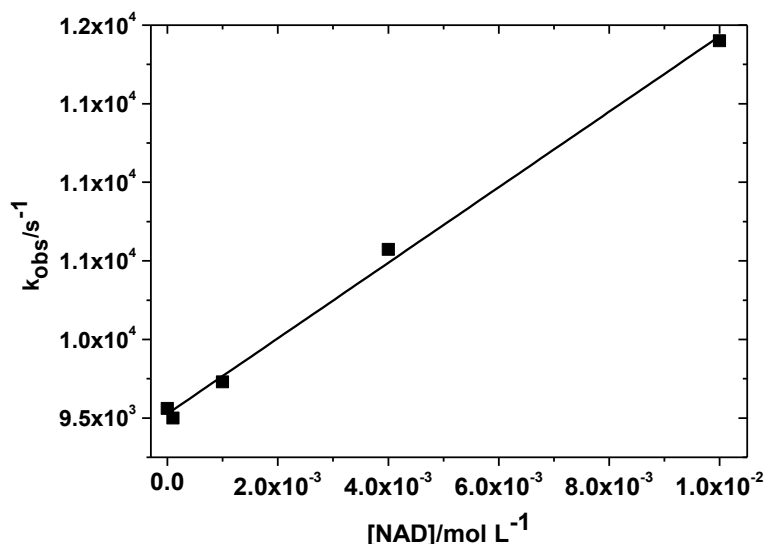
Figure 2A-15 Stern-Volmer plot of the observed rate constant *vs* NAD concentration.

From this, a second-order rate constant of 2.4×10^5 L mol^{-1} s^{-1} was obtained for the quenching reaction between $^1O_2$ and NAD in chloroform. Although this value of k_q is small, it lies between the values already reported for compounds within the same family such as 2-naphthol in chloroform (7.1×10^4 L mol^{-1} s^{-1}), dimethylnaphthalenes (values range from 10^4-10^5 L mol^{-1} s^{-1}) and various other hydroxynaphthalenes (values range from 10^6-10^7 mol^{-1} L s^{-1}) [46,52]. This indicates that NAD photodegradation in solution may occur through processes involving singlet oxygen, but these are probably less important than other routes.

2A.7 Deactivation pathways of NAD excited states

From all above data it has been possible to fully characterize the photophysical deactivation routes of NAD excited states. These include the radiative processes of fluorescence and phosphorescence, and the non-radiative processes of internal conversion (ic) and intersystem crossing (isc). In addition, photoionization to produce the radical cation and hydrated electron is also an important deactivation process in aqueous solutions.

Using NAD fluorescence quantum yields and the measured fluorescence lifetimes given in Table 2A-2, the natural radiative rate constant k_R ($= \phi_F/\tau_F$) and non-radiative rate constants k_{NR} ($= 1-\phi_F/\phi_F$) were determined for NAD in each solvent. The results are given in Table 2A-8. From these, the natural radiative lifetimes ($\tau^0_{nat} = 1/k_R$)

were calculated, which were found to vary in the range of 290 to 530 ns and are considerable greater than the experimental fluorescence lifetimes, τ_F, showing the major role that non-radiative processes play in deactivation of $^1NAD^*$. Furthermore, the quantum yield of internal conversion, ϕ_{ic}, can be calculated from the relationship (2A.10):

$$\phi_F + \phi_T + \phi_{ic} = 1 \tag{2A.10}$$

which assumes that only these three processes jointly deactivate $^1NAD^*$. In addition, the rate constants for the radiationless processes, k_{ic} $(= \phi_{ic}/\tau_F)$ and k_{isc} $(= \phi_T/\tau_F)$ are also calculated since the values of ϕ_F and of ϕ_T are known (Table 2A-2 and 2A-5). The photophysical parameters calculated for the deactivation of $^1NAD^*$ in the different solvents are presented in Table 2A-8. It can be noted that the ϕ_{ic} in water, 0.510, is greater than in the other solvents showing that this is the preferred deactivation pathway in this solvent. From comparison of ϕ_F, ϕ_{ic} and ϕ_{isc} values (Table 2A-2, 2A-5 and 2A-8) for the other solvents, ϕ_{ic} is greater than ϕ_F (except in acetonitrile) but the dominant pathway of $^1NAD^*$ deactivation involves intersystem crossing.

Table 2A-8 Radiative rate constants decay (k_R), natural radiative lifetimes (τ^0_{nat}), non-radiative rate constants decay (k_{NR}), non-radiative rate constants decay for internal conversion (k_{ic}) and for intersystem crossing (k_{isc}), and quantum yield of internal conversion (ϕ_{ic}) of $^1NAD^*$ in water, D_2O and in organic solvents.

Solvent	k_R (s^{-1})	τ^0_{nat} (ns)	k_{NR} (s^{-1})	ϕ_{ic}	k_{ic} (s^{-1})	k_{isc} (s^{-1})
Water	1.88×10^6	532	2.67×10^7	0.510	1.46×10^7	1.21×10^7
D_2O	1.94×10^6	515	2.66×10^7	0.518	1.48×10^7	1.18×10^7
Ethylene glycol	1.81×10^6	552	1.70×10^7	0.294	5.54×10^6	1.15×10^7
Ethanol	1.96×10^6	510	1.84×10^7	0.357	7.28×10^6	1.11×10^7
Acetonitrile	3.44×10^6	291	1.51×10^7	0.123	2.29×10^6	1.28×10^7
Chloroform	3.25×10^6	307	1.44×10^8	0.456	6.73×10^7	7.71×10^7
1,4-Dioxane	6.94×10^6	144	1.25×10^7	0.216	4.20×10^6	8.30×10^6

Given that all the deactivation pathways of the excited states have been characterized, it is possible to summarize these processes by a Perrin-Jablonski diagram. Figure 2A-15 shows, as example, the occurring processes for NAD in water.
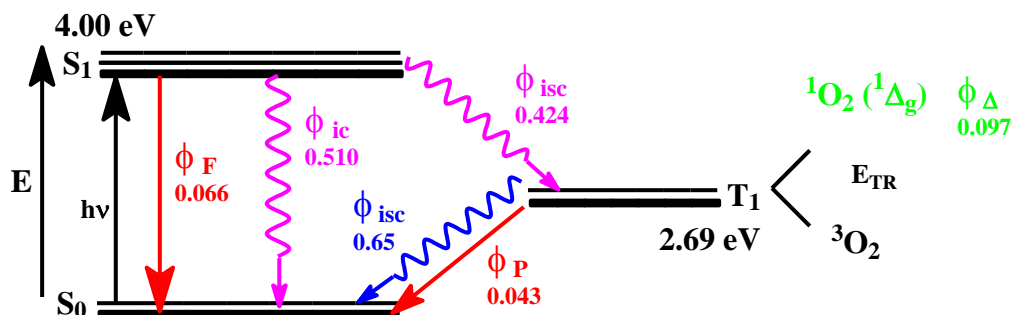
Figure 2A-15 Perrin-Jablonski diagram for de-aerated aqueous NAD solution.

2A.8 Conclusions

The photophysical properties of NAD in water and organic solvents have been fully investigated. The results show that the main deactivation of NAD singlet excited state is solvent dependent: i) in water, the non-radiative internal conversion process is predominant while in organic solvents the non-radiative intersystem crossing becomes the major process, ii) the radiative process of fluorescence is less important in all solvents when compared to the non-radiative ones, iii) NAD triplet excited state deactivates mainly by the non-radiative intersystem crossing process and the radiative conversion is very low in all solvents, iv) NAD singlet excited state is quenched more efficiently by molecular oxygen than NAD triplet excited state, as expected from spin-statistical factors, v) NAD excitation leads to formation of singlet oxygen through triplet sensitization, predominantly in non-aqueous solvents, vi) laser flash photolysis show the formation of NAD triplet states with reasonable quantum yields in all the solvents. In water, a photoionization process occurs yielding the formation of the reactive species hydrated electron, NAD radical cation and superoxide anion. Moreover, it has been shown that NAD singlet excited is also a relatively strong photooxidant, as it happens with most aromatics.

2A.9 References

[1] C. Pimentel, Hydrogen bonding and electronic transitions: the role of the Franck-Condon principle. *J. Am. Chem. Soc.*, **1957**, 79, 3323-3326.

[2] N. S. Bayliss, E. G. McRae, Solvent effects in organic spectra: dipole forces and the Franck-Condon principle. *J. Phys. Chem.*, **1954**, 58, 1002-1006.

[3] S. Nagakura, H. Baba, Dipole moments and near ultraviolet absorption of some monosubstituded benzenes-the effect of solvents and hydrogen bonding. *J. Am. Chem. Soc.*, **1952**, 74, 5693-5698.

[4] European Food Safety Authority (EFSA), Conclusion on the peer review of the pesticide risk assessment of the active substance 2-(1-naphthyl) acetamide (notified as 1-napthylacetamide), *EFSA Journal* 9, 2020, **2011**.

[5] K. M. C. Davis, M. F. Farmer, Charge transfer complexes. Part V. Nature of interaction of halogenomethanes and aromatic hydrocarbons. *J. Chem. Soc. B*, **1968**, 1968, 859-862.

[6] M. Montalti, A. Credi, L. Prodi, M. T. Gandolfi, *Handbook of Photochemistry*, third edition, Taylor & Francis Group, Florida, **2006**.

[7] A. B. Sánchez, Nuevos métodos luminescentes para la determinación de pesticidas en aguas. Dissertation, Universidad de Extremadura, Badajoz, **2001**.

[8] T. Tamaki, Intramolecular fluorescence quenching and photolysis of 1-naphthylacetic acid derivatives. *Chem. Lett.*, **1979,** 8, 575-578.

[9] J. W. Eastman, S. J. Rehfeld, Interaction of benzene molecule with liquid solvents. Fluorescence quenching parallels (0-0) ultraviolet absorption spectroscopy. *J. Phys. Chem.*, **1970**, 74, 1438-1443.

[10] W. D. Horrocks, D. R. Sudnick, Lanthanide ion probes of structure in biology - laser-induced luminescence decay constants provide a direct measure of the number of metal-coordinated water-molecules. *J. Am. Chem. Soc.*, **1979***, 101, 334-340.

[11] A. Beeby, I. M. Clarkson, R. S. Dickins, S. Faulkner, D. Parker, L. Royle, A. S. de Sousa, J. A. G. Williams, M. Woods, Non-radiative deactivation of the excited states of europium, terbium and ytterbium complexes by proximate energy-matched OH, NH and CH oscillators: an improved luminescence method for establishing solution hydration states. *J. Chem. Soc. Perkin Trans.* 2, **1999**, 493-503.

[12] A. R. Watkins, Kinetics of fluorescence quenching by inorganic anions. *J. Phys. Chem.*, **1974**, 78, 2555-2558.

[13] H. Shizuka, M. Nakamura, T. Morita, Anion-induced fluorescence quenching of aromatic molecules. *J. Phys. Chem.*, **1980**, 84, 989-994.

[14] A. R. Watkins, Quenching of biphenyl fluorescence by inorganic ions. *J. Phys. Chem.*, **1973**, 77, 1207-1210.

[15] J. Sujatha, A. K. Mishra, Fluorescence quenching of naphthalene and its substitutions by chloroethanes and -ethylenes. *J. Lumin.*, **1997**, 75, 135-141.

[16] D. M. Stanbury, Reduction potentials involving inorganic free radicals in aqueous solution. *Adv. Inorg. Chem.*, **1989**, 33, 69-138.

[17] D. Rehm, A. Weller, Kinetics of fluorescence quenching by electron and H-atom transfer. *Israel J. Chem.*, **1970**, 8, 259-271.

[18] J. Lin, J. Merryweather, L. B. Vitello, J. R. Erman, Metmyoglobin/azide: the effect of heme-linked ionizations on the rate of complex formation. *Arch. Biochem. Biophys.*, **1999**, 362, 148-158.

[19] G. L. Hug, *Optical spectra of nonmetallic inorganic transient species in aqueous solution*, National Standard Reference Data System, Washington, D. C., **1981**.

[20] H. D. Burrows, Electron transfer from halide ions to UO_2^{2+} excited-state ions in aqueous solution. Formation and decay of dihalide radical anions. *Inorg.Chem.*, **1990**, 29, 1549-1554.

[21] R. McNeil, J. T. Richards, J. K. Thomas, The laser flash photolysis of naphthalene and 1,2-benzanthracene. *J. Phys. Chem.*, **1970**, 74, 2290-2294.

[22] D. Vialaton, C. Richard, D. Baglio, A.-B. Paya-Perez, Mechanism of the photochemical transformation of naphthalene in water. *J. Photochem. Photobiol. A: Chem.*, **1999**, 123, 15-19.

[23] O. Brahmia, C. Richard, Phototransformation of carbaryl in aqueous solution. Laser flash photolysis and steady state studies. *J. Photochem. Photobiol. A: Chem.*, **2003**, 156, 9-14.

[24] F. Boscá, N. Canudas, M. L. Marín, M. A. Miranda, A photophysical and photochemical study of 6-methoxy-2-naphthylacetic acid, the major metabolite of the phototoxic nonsteroidal antiinflammatory drug nabumetone. *Photochem. Photobiol.*, **2000**, 71, 173-177.

[25] L. J. Martinz, J. C. Scaiano, Characterization of the transient intermediates generated from the photoexcitation of nabumetone: a comparison with naproxen. *Photochem. Photobiol.*, **1998**, 68, 646-651.

[26] E. J. Hart, M. Anbar, *The hydrated electron*, Wiley Interscience, **1970**.

[27] J. F. Endicott, G. J. Ferraudi, J. R. Barber, Charge transfer spectroscopy, redox energetics, and photoredox behavior of transition metal ammine complexes. Critical comparison of observations with mechanisms and models. *J. Phys. Chem.*, **1975**, 79, 630-643.

[28] P. M. Hare, E. A. Price, D. M. Bartels, Hydrated electron extinction coefficient revised. *J. Phys. Chem. A*, **2008**, 112, 6800-6802.

[29] G. Grabner, K. Rechthaler, B. Mayer, G. Köhler, K. Rotkiewicz, Solvent influences on the photophysics of naphthalene: fluorescence and triplet state properties in aqueous solution and in cyclodextrin complexes. *J. Phys. Chem. A*, **2000**, 104, 1365-1376.

[30] F. Scandola, V. Balzani, Energy-transfer processes of excited states of coordination compounds. *J. Chem. Educ.*, **1983**, 60, 814-823.

[31] R. Bensasson, E. J. Land, Triplet-triplet extinction coefficients via energy transfer. *Trans. Faraday Soc.*, **1971**, 67, 1904-1915.

[32] B. Amand, R. Bensasson, Determination of triplet quantum yields by laser flash absorption spectroscopy. *Chem. Phys. Lett.*, **1975**, 3, 44-48.

[33] J. B. Birks, *Photophysics of Aromatic Molecules*, Wiley-Interscience, London, New York, **1970**.

[34] F. Wilkinson, Quenching of electronically excited states by molecular oxygen in fluid solution. *Pure Appl. Chem.*, **1997**, 69, 851-856.

[35] L. K. Patterson, G. Porter, M. R. Topp, Oxygen quenching of singlet and triplet states. *Chem. Phys. Lett.*, **1970**, 7, 612-614.

[36] J. G. Calvert, J. N. Pitts, *Photochemistry*, Wiley, New York, **1966.**

[37] A. A. Abdel-Shafi, D. R. Worrall, F. Wilkinson, Singlet oxygen formation efficiencies following quenching of excited singlet and triplet states of aromatic hydrocarbons by molecular oxygen. *J. Photochem. Photobiol. A: Chem.*, **2001**, 142, 133-143.

[38] D. R. Kearns, Physical and chemical properties of singlet molecular oxygen. *Chem. Rev.*, **1971**, 71, 395-427.

[39] R. Schmidt, F. Shafii, C. Schweitzer, A. A. Adbel-Shafi, F. Wilkinson, Charge transfer and non-charge transfer processes competing in the sensitization of singlet oxygen: formation of $O_2(^1\Sigma g^+)$, $O_2(^1\Delta g)$ and $O_2(^3\Sigma g^-)$ during oxygen quenching of triplet excited naphthalene derivatives. *J. Phys. Chem. A*, **2001**, 105, 1811-1817.

[40] A. T. Soltermann, M. Luiz, M. B. Biasutti, M. Carrascoso, F. Amat-Guerri, N. A. Garcia, Monosubstituted naphthalenes as quenchers and generators of singlet oxygen. *J. Photochem. Photobiol. A: Chem.*, **1999**, 129, 25-32.

[41] C. Pierlot, S. Hajjam, C. Barthélémy, J.-M. Aubry, Water-soluble naphthalene derivatives as singlet oxygen ($^1O_2$, $^1\Delta_g$) carriers for biological media. *J. Photochem. Photobiol. B: Biol.*, **1996,** 36, 31-39.

[42] D. J. McGarvey, P. G. Szekeres, F. Wilkinson, The efficiency of singlet oxygen generation by substituted naphthalenes in benzene. Evidence for the participation of charge-transfer interactions. *Chem. Phys. Lett.*, **1992,** 199, 314-319.

[43] F. Wilkinson, D. J. McGarvey, A. F. Olea, Excited triplet state interactions with molecular oxygen: influence of charge transfer on the bimolecular quenching rate constants and the yields of singlet oxygen $[O_2^* (^1\Delta_g)]$ for substituted naphthalenes in various solvents. *J. Phys. Chem.*, **1994,** 98, 3762-3769.

[44] M. Kristiansen, R. D. Scurlock, K. Long Lu, P. R. Ogilby, Charge-transfer state and singlet oxygen ($^1\Delta_g$ O_2) production in photoexcited organic molecule-molecular oxygen complexes. *J. Phys. Chem.*, **1991**, 95, 5190-5197.

[45] R. Bonnett, D. J. McGarvey, A. Harriman, E. J. Land, T. G. Truscott, U. -J. Winfield, Photophysical properties of *meso*-tetraphenylporphyrin and *meso*-tetra(hydroxyphenyl)-porphyrins. *Photochem. Photobiol.*, **1988,** 48, 271-276.

[46] F. Wilkinson, W. P. Helman, A. B. Ross, Quantum yields for the photosensitized formation of the lowest electronically excited singlet state of molecular oxygen in solution. *J. Phys. Chem. Ref. Data*, **1993,** 22, 13-262.

[47] P. R. Ogilby, C. S. Foote, Chemistry of singlet oxygen. 42. Effect of solvent, solvent isotopic substitution, and temperature on the lifetime of the singlet molecular oxygen ($^1\Delta_g$). *J. Am. Chem. Soc.*, **1982,** 104, 2069-2070.

[48] M. C. DeRosa, R. J. Crutcheley, Photosensitized singlet oxygen and its applications. *Coord. Chem. Rev.*, **2002**, 233-234, 351-371.

[49] R. D. Scurlock, S. Nonell, S. E. Braslavsky, P. R. Ogilby, Effect of solvent on the radiative decay of singlet molecular oxygen ($^1\Delta_g$). *J. Phys. Chem.*, **1995**, 99, 3521-3526.

[50] R. Schmidt, Symposium in print: singlet oxygen invited review. Photosensitized generation of singlet oxygen. *Photochem. Photobiol.*, **2006**, 82, 1161-1177.

[51] K. I. Salokhiddinov, I. M. Byteva, G. P. Gurinovich, Lifetime of singlet oxygen in various solvents. *J. Appl. Spectroscopy*, **1981,** 34, 561-564.

[52] F. Wilkinson, W. P. Helman, A. B. Ross, Rate constants for the decay and reactions of the lowest electronically excited state of molecular oxygen in solution. An expanded and revised compilation. *J. Phys. Chem. Ref. Data 2*, **1995**, 663-1021.

2B. Direct and induced degradation in aqueous solution

2B.1 Introduction

The photochemical transformations that a pesticide can undergo under light exposure are import to assess its environmental fate. Therefore, in this chapter the direct photolysis is described of NAD in aqueous solution, mainly under excitation at 254 nm. In addition, for environmental considerations, a few results will also be given concerning NAD degradation using simulated solar light as excitation source. The disappearance of NAD and formation of photoproducts were followed by UV-vis absorption spectroscopy and by high performance liquid chromatography with diode array detection. Since the toxicity of the formed photoproducts is of great concern due to the adverse effects they can induce on the environment, toxicity of NAD and of its photoproducts was also assessed. The effect of oxygen concentration and excitation wavelength on the degradation, as well as the involvement of several reactive species such as singlet oxygen and superoxide anion radical on the transformation process is reported. A possible pathway for NAD degradation is proposed based on the combination of these results along with the photophysical results already reported in Chapter 2A concerning NAD transient species.

As mentioned in the Introduction (Chapter 1), cyclodextrins can form "host-guest" inclusion complexes with pesticides leading to changes in guest molecule (pesticide) photochemistry and photophysics, with consequent increase or decrease of pesticide degradation. This complexation is very interesting for the development of new catalytic techniques of photochemical cleaning in solutions. Therefore, the influence of β-cyclodextrin on NAD photodegradation in aqueous solution was also evaluated.

2B.2 Direct UV and sunlight degradation

2B.2.1 Observation by UV-visible absorption spectra

As already mentioned in Chapter 2A, NAD presents a main broad band extending with maximum absorption centred at 280 nm (ε = 6540 L mol^{-1} cm^{-1}). Under our experimental conditions, aqueous NAD solution (3.0×10^{-4} mol L^{-1}) presents a small absorbance at $\lambda > 290$ nm which overlaps to some extent with the emission spectrum of

solar light, as given in Figure 2B-1. This suggests that the direct photochemical transformation of NAD may occur under environmental conditions.
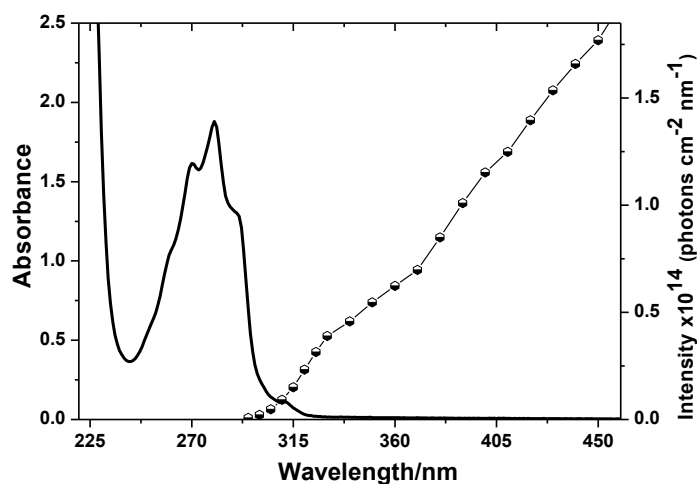
Figure 2B-1 UV-vis absorption spectrum of aqueous NAD solution (3.0×10^{-4} mol L^{-1}) and emission spectrum of solar light (dotted line).

Therefore, preliminary studies were conducted using a sunlight simulator system (Suntest) in order to mimic the degradation under environmental conditions, using aqueous NAD solutions with concentration of 3.0×10^{-4} mol L^{-1}. Figure 2B-2 depicts, as example, the evolution of the UV-vis absorption spectra of aerated aqueous NAD solution irradiated with the Suntest.
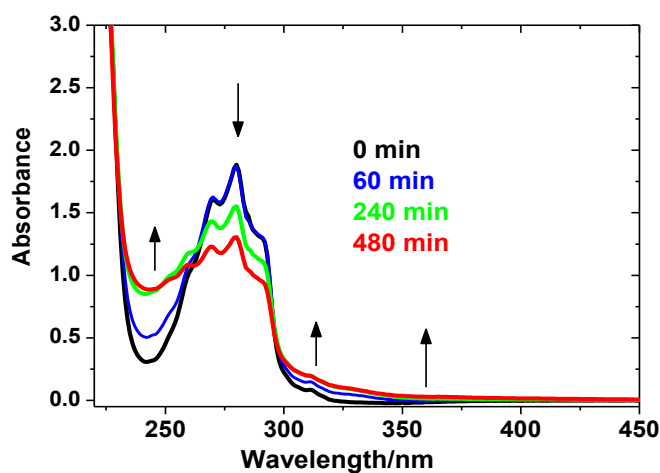
Figure 2B-2 Evolution of the UV-vis absorption spectra of aerated aqueous NAD solution (3.0×10^{-4} mol L^{-1}) under Suntest excitation as function of irradiation time.

A decrease of the absorbance within the wavelength range 270-290 nm with a concomitant increase at $\lambda < 270$ nm and at $290 < \lambda < 600$ nm is clearly observed, indicating not only the disappearance of NAD but also the formation of photoproducts. Under these conditions, only 51 % of NAD was transformed after 8 h of irradiation. These results show that NAD can be effectively transformed under environmental conditions. However, for analytical reasons (employing higher volumes of solution) further studies were performed using an irradiation system at 254 nm (see Chapter 8 for experimental details). Figure 2B-3 shows the evolution of the absorption spectra of an aerated aqueous NAD solution (3.0×10^{-4} mol L^{-1}) as a function of irradiation time upon excitation at 254 nm.
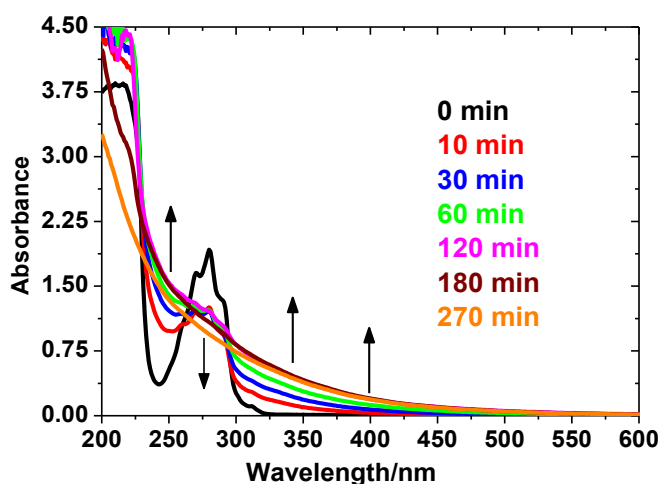
Figure 2B-3 Evolution of the UV-vis absorption spectra of aerated aqueous NAD solution (3.0×10^{-4} mol L^{-1}) under excitation at 254 nm as function of irradiation time.

This absorption spectra show the same shape and trends as the formerly reported for NAD degradation under Suntest irradiation (see Figure 2B-2). This suggests that similar photoproducts will be formed in both situations. The main difference between both UV spectral evolutions concerns the rate of NAD disappearance, which is faster under direct excitation at 254 nm then with Suntest. This is due to the stronger absorbance of NAD at the excitation wavelength and to the higher intensity emitted from the Hg lamps. Under 254 nm irradiation, the vibrational structure of NAD disappears after 3 h suggesting its complete degradation. These studies at 254 nm were also performed for aqueous NAD solutions in de-aerated and oxygen saturated conditions. Under these experimental conditions the absorption spectra show similar

behavior to those presented in Figures 2B-2 and 2B-3, regarding both the shape and trends of the spectrum (for visual simplicity it was decided not to present these graphs). However, from all the UV-vis spectral data it is possible to say that the rate of degradation is dependent both on the irradiation system and on the oxygen concentration present in the solution, as is discussed in the next section.

2B.2.2 Kinetics of degradation: effect of oxygen and excitation wavelength

NAD degradation was followed by high performance liquid chromatography (HPLC) with diode array detection (DAD). Figure 2B-4a illustrates the evolution of NAD degradation (C/C_0) in aerated conditions as a function of irradiation time for excitation with Suntest (corresponding UV-vis spectra in Figure 2B-2) and at 254 nm (corresponding UV-vis spectra in Figure 2B-3). Figure 2B-4b shows the plot of ln C/C_0 as function of irradiation time used for the determination of the respective pseudo-first-order rate constant, k.
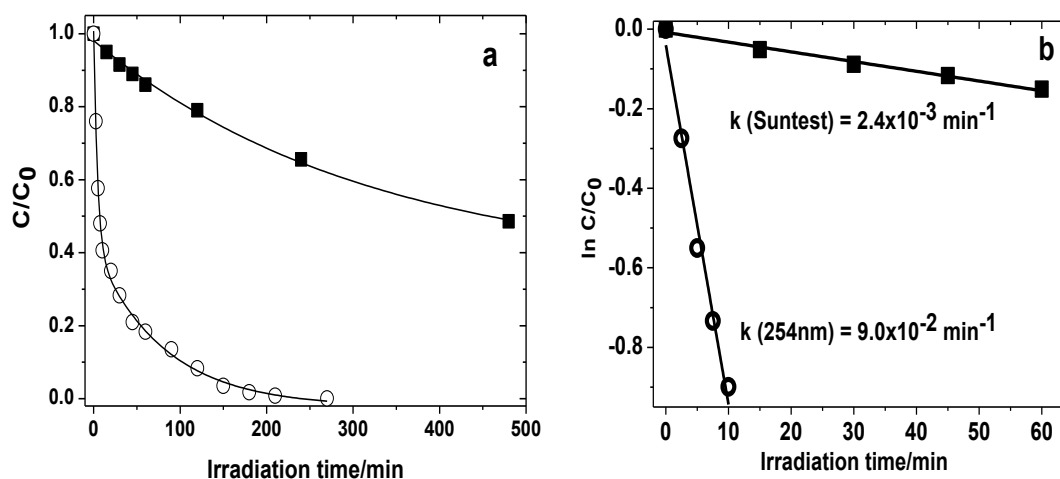
Figure 2B-4 a) Degradation kinetic profile of aerated aqueous NAD solution (3.0×10^{-4} mol L^{-1}) irradiated with Suntest (■) and at 254 nm (○) obtained by HPLC with diode array detection at 280 nm. b) Determination of the pseudo first order behavior of NAD irradiated with Suntest (■) for t < 60 min ($R^2 = 0.983$) and at 254 nm (○) for t < 10 min ($R^2 = 0.981$).

The kinetic decays given in Figure 2B-4a confirm the efficient disappearance of NAD using both irradiation systems, supporting the results from the UV-vis spectra changes. However, it is possible to see that NAD degradation is roughly two times faster with the irradiation system at 254 nm than with Suntest (Figure 2B-4b). With

Suntest, NAD degradation fits a mono-exponential decay with a pseudo-first-order rate constant of 2.4×10^{-3} min^{-1} and a half-life ($t_{1/2} = \ln 2/k$) of approximately 290 min (Figure 2B-4b). In turn, the irradiation of NAD at 254 nm leads to a kinetic profile that fits better a bi-exponential decay with an initial estimated first order rate constant of 9.0×10^{-2} min^{-1} and a half-life of 7.7 min (Figure 2B-4b). In this case a very fast degradation at early stages of the irradiation was observed, along with a slower degradation rate for prolonged irradiation, probably due to the formation of photoproducts which also absorb at the excitation wavelength. The stability of aqueous NAD solution was followed in the dark at room temperature (22 °C). No degradation was observed under these conditions for more than a month confirming the absence of thermal degradation.

The effect of oxygen concentration and excitation wavelengths (254, 300 and 310 nm) on NAD photodegradation was studied during the early stages of the irradiation using a monochromator system. This was evaluated by measuring the quantum yield of degradation, ϕ, which as previously mentioned is representative of the efficiency of a photochemical process. The results are presented in Table 2B-1.

Table 2B-1 Photolysis quantum yields (ϕ) of aqueous NAD solutions (3.0×10^{-4} mol L^{-1}) as function of oxygen concentration [1] and excitation wavelength.

Conditions	[O$_2$] (mol L$^{-1)}$ (20 ° C)	ϕ 254 nm ($\times 10^{-3}$)	ϕ 300 nm ($\times 10^{-3}$)	ϕ 310 nm ($\times 10^{-3}$)
Oxygen Saturated	1.39×10^{-3}	3.0 ± 0.2	3.6 ± 0.4	3.9 ± 0.4
Aerated	2.9×10^{-4}	5.0 ± 0.3	5.0 ± 0.5	4.7 ± 0.5
De-aerated	$< 10^{-5}$	15.0 ± 0.8	11.0 ± 0.9	10.9 ± 1.0

The results given in Table 2B-1 provide evidence that the disappearance quantum yield of NAD is independent of the excitation wavelength, within the experimental error, but strongly dependent on the amount of molecular oxygen present in the solution. The quantum yield is found to be approximately 5.0×10^{-3} under aerated conditions and increases by a factor of roughly 4 from oxygen saturated solution to de-aerated solution. These results suggest the possible involvement of the triplet excited state ^{3}NAD* in the degradation process. It has been demonstrated in Chapter 2A that the

deactivation of $^3NAD^*$ by molecular oxygen leads to the formation of singlet oxygen through triplet-triplet energy transfer. Moreover, it was also shown that $^3NAD^*$ is quenched by molecular oxygen, which can lead to the formation of the superoxide anion by electron transfer. Consequently, the reactive species such as singlet oxygen or the superoxide anion, or even both, can be involved in the mechanism of NAD degradation. Studies are discussed in the next section concerning these suggestions.

2B.2.3 Reactive species involved in NAD degradation

2B.2.3.1 Assessment of singlet oxygen participation

Although it has been demonstrated that NAD is able to produce $^1O_2$ in aqueous solution (Chapter 2A), its effective participation in NAD degradation process has not yet been shown. One way to study the reactivity of $^1O_2$ in a chemical reaction is by using $^1O_2$ quenchers, such as cholesterol, sodium azide (NaN$_3$), carotenes, diazobicyclooctane (DABCO), etc., [2]. Therefore, to address the question as to whether $^1O_2$ participates in NAD degradation pathway, sodium azide was used as $^1O_2$ physical quencher due to its high solubility in water. An aerated aqueous NAD solution (3.0×10^{-4} mol L^{-1}) in the presence of NaN$_3$ (2.0×10^{-3} mol L^{-1}) was irradiated at 254 nm. The reaction was followed by HPLC and the kinetic profile obtained is given in Figure 2B-5.
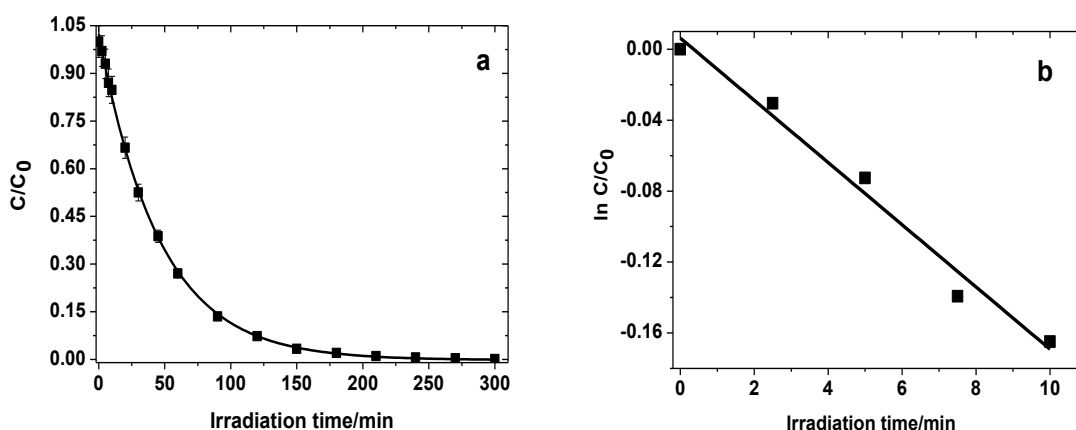
Figure 2B-5 a) Influence of NaN$_3$ (2.0×10^{-3} mol L^{-1}) on the degradation kinetic of aerated aqueous NAD solution (3.0×10^{-4} mol L^{-1}) as function of irradiation time ($\lambda_{irrad} = 254$ nm). b) First order behavior corresponding to the linear part of the kinetic given in a) ($R^2 = 0.974$).

A slower degradation of NAD was observed in the presence of NaN_3 when compared to its absence (see Figure 2B-4a), with a pseudo first order rate constant of 1.75×10^{-2} min^{-1} and a half-life of 40 min. This could suggest that $^1O_2$ may be involved to some extent in the degradation mechanism. However, NaN_3 is not only able to quench $^1O_2$ but can also deactivate excited states [3,4]. This was shown to be the case of $^1NAD^*$, which, as demonstrated in Chapter 2A, was effectively quenched by NaN_3 with a rate constant of 2.91×10^9 L mol^{-1} s^{-1}. In contrast, no effect on the rate constant of $^3NAD^*$ was observed when different concentrations of azide were added. These results indicate that azide effectively quenches some of the $^1NAD^*$ and is in line with the decrease of NAD photolysis rate in the presence of azide. As a consequence, inconclusive results on the involvement of $^1O_2$ were obtained and further studies were required.

In addition to the previously referred use of quenchers of $^1O_2$, dye molecules such as Rose Bengal, eosin and methylene blue can be used as very effective photosensitizers for the generation of $^1O_2$ since they possess appropriate energies of triplet states for oxygen sensitization [5,6]. Therefore, Rose Bengal was chosen as photosensitizer since it is water soluble, absorbs light outside the absorption region of most of molecules (maximum absorption wavelength at 547 nm) and has a quantum yield of singlet oxygen formation of 0.76 [7]. An aerated aqueous NAD solution (3.0×10^{-4} mol L^{-1}) was irradiated at 547 nm in the presence of Rose Bengal (6.0×10^{-6} mol L^{-1}). Under these conditions, no consumption of NAD was observed after 21 h of irradiation. This rules out any significant participation of $^1O_2$ in the photodegradation process.

2B.2.3.2 Assessment of superoxide anion radical participation

As already discussed in Chapter 2A, the superoxide anion radical $O_2^{\bullet-}$ may be formed through the reaction of hydrated electron with molecular oxygen or even by electron transfer between $^3NAD^*$ and molecular oxygen. $O_2^{\bullet-}$ can then undergo disproportionation in aqueous media to give hydrogen peroxide, H_2O_2. In order to assess the possible involvement of $O_2^{\bullet-}$ in the NAD transformation pathway, the formation of H_2O_2 was determined by using the Lazrus method [8]. This method is based on the reduction of H_2O_2 in the presence of 4-hydroxyphenylacetic acid (4-HPAC), a hydrogen donor, catalyzed by the enzyme peroxidase. Such a reaction leads

to the formation of a dimeric compound that can be easily detected by fluorescence at $\lambda_{max} = 400$ nm (Scheme 2B-1).
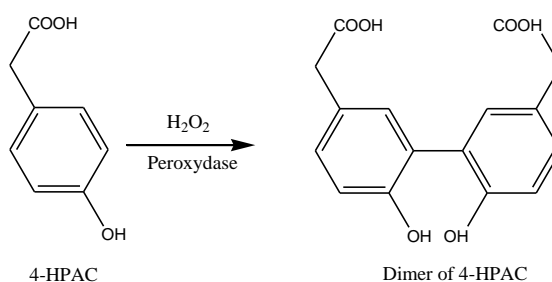
Scheme 2B-1 Reaction of H_2O_2 and 4-HPAC in the presence of enzyme peroxidase with formation of the 4-HPAC dimer detected by fluorescence at 400 nm ($\lambda_{ex} = 320$ nm).

Figure 2B-6 depicts the evolution of H_2O_2 concentration upon irradiation of aerated aqueous NAD solution (1.0×10^{-5} mol L^{-1}) at 254 nm. An increase on the H_2O_2 concentration with irradiation time was observed, even at early stages, supporting the previous suggestion concerning the participation of $O_2^{\bullet -}$ in the NAD degradation mechanism.
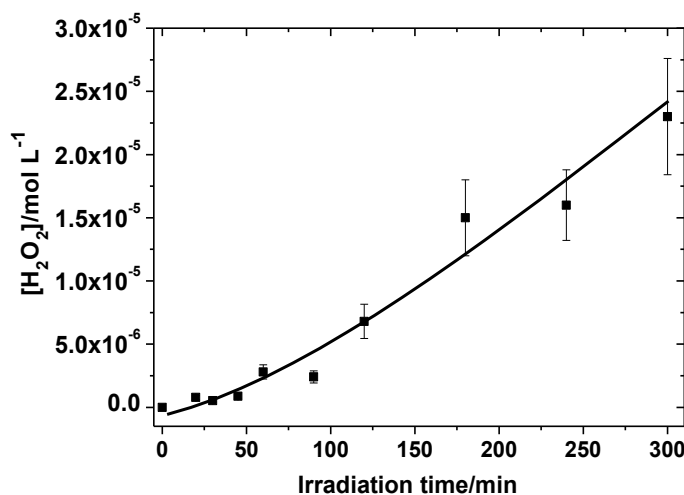
Figure 2B-6 Evolution of H_2O_2 formation of an aerated aqueous NAD solution (1.0×10^{-5} mol L^{-1}) irradiated at 254 nm.

2B.2.4 Photoproduct identification

The photoproducts formed upon irradiation of aqueous NAD solutions (at 254 nm and with Suntest) were detected and identified by HPLC-DAD and by HPLC/MS-
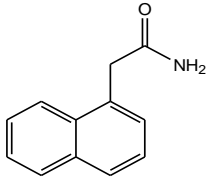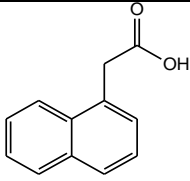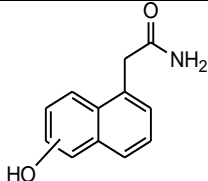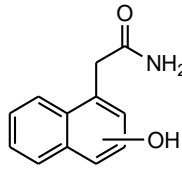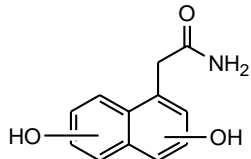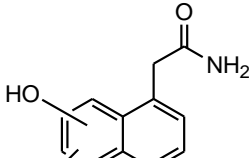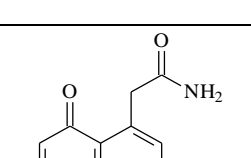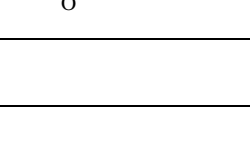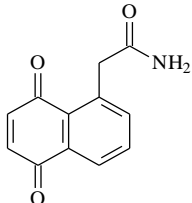
MS. Figure 2B-7 illustrates the LC-DAD chromatogram of aerated aqueous NAD solution obtained after 30 minutes of irradiation at 254 nm ($\cong$ 20 % conversion) and after a concentration step (see details in the experimental part). A large number of peaks was observed corresponding to NAD photoproducts. Under these analytical conditions, all of the products were eluted before NAD (t_{ret} = 24.1 minutes) pointing out the formation of compounds with higher polarity than NAD itself. The exception was a product with retention time of 25.0 min, which was also present at zero time.
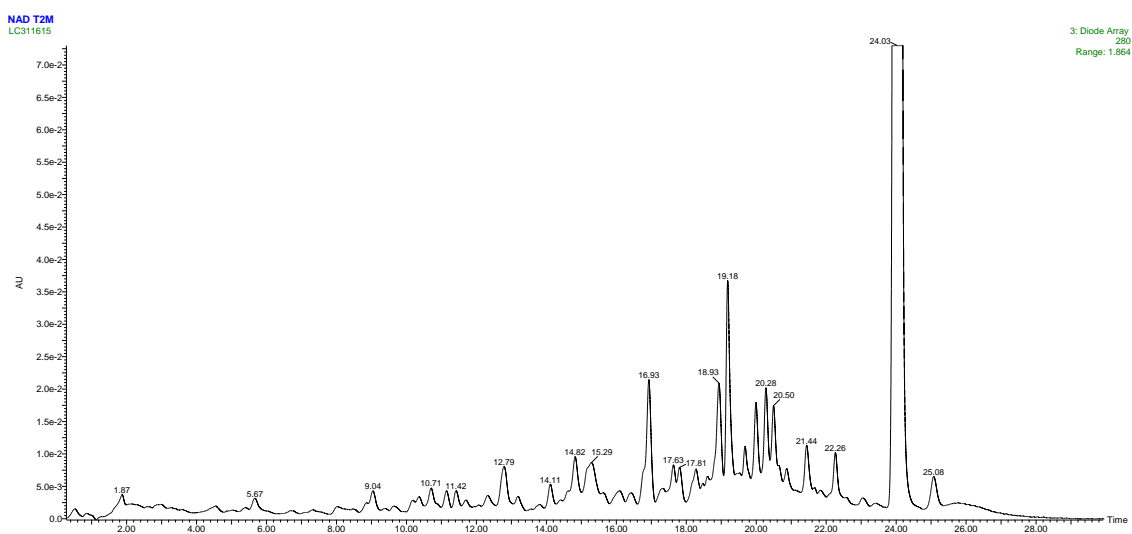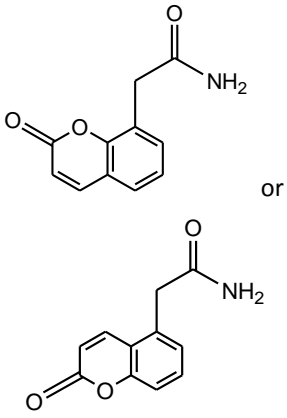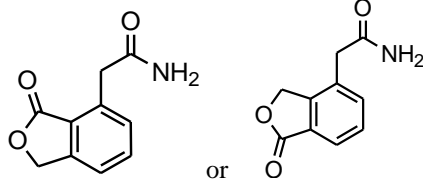
Figure 2B-7 LC-DAD chromatogram of an aerated aqueous NAD solution (3.0×10^{-4} mol L^{-1}) irradiated at 254 nm (λ_{det} = 280 nm).

The identification of these products was based on the results obtained by LC-MS with electrospray ionization (ESI) and LC-ESI-MS/MS in positive mode (ES$^+$) mode due to the presence of the amide group. Under our experimental conditions, no successful results were obtained in the ES$^-$ mode, except for the naphthoquinone compound. Several photoproducts were only identified by the molecular ion and mass fragment ions under aerated conditions since there were no standards commercial products available to allow their quantification. All the results concerning the retention times, [M+H]$^+$, UV data and suggested structures are gathered in Table 2B-2.

Table 2B-2 Retention time (t_{ret}), main fragments, UV data (obtained by LC-DAD (*a* - shoulder)) and proposed structure of the main photoproducts obtained by LC-MS/MS.

t_{ret} (min)	Main fragments (% abundance)	λ_{max} (nm)	Proposed chemical structure
24.1	[M+H$^+$] = 186 (15 %), 169 (10 %), 141 (100 %)	280	(NAD)
25.0	-	280	
19.4	[M+H]$^+$ = 202 (40 %), 184 (100 %), 156 (18 %), 140 (18 %)	290	
10.4	-	280	and/or
21.5	-	282	
11.1	[M+H]$^+$ = 218 (35 %), 201 (50 %), 173 (100 %), 159 (35 %)	252, 285^a	
12.6	[M+H]$^+$ = 218 (50 %), 201 (100 %), 173 (90%), 159 (50 %)	248,285^a	and
17.0	[M+H]$^+$ = 218 (25 %), 201 (50 %), 173 (50%), 159 (100%)	252	
19.5	[M+H$^+$]$^+$ = 218 (35 %), 201 (50 %), 173 (100 %), 159 (35 %)	289	
20.2	[M+H]$^+$ = 218 (60 %), 201 (10 %), 159 (50 %)	290	
20.1	[M+H]$^+$ = 216 (20 %), 199 (18 %), 171 (100 %), 143 (18 %), 115 (18 %)	240, 350	

Table 2B-2 (Continuation) Retention time (t_{ret}), main fragments, UV data (obtained by LC-DAD (*a* - shoulder)) and proposed structure of the main photoproducts obtained by LC-MS/MS.

t_{ret} (min)	Main fragments (% abundance)	λ_{max} (nm)	Proposed chemical structure
18.5	$[M+H]^+ = 204$ (85 %), 187 (50 %), 159 (100 %), 131 (32 %), 115 (13 %)	230; 322	or
15.3	$[M+H]^+ = 192$ (10 %), 175 (80 %), 147 (100 %), 133 (15 %), 105 (8 %)	231; 275	or

Characterization of the parent compound NAD

The mass spectrum of NAD in ES$^+$ mode is given in Figure 2B-9. In addition to the molecular ion of NAD $[M+H]^+$ with $m/z = 186$, a main fragment ion was observed at $m/z = 141$. This correspond to the loss of the amide group $[M+H-CONH_3]^+$ and is in agreement with literature data [9,10]. Another fragment with $m/z = 169$ was observed in the mass spectrum, although with a low abundance. This ion corresponds to the loss of ammonia $[M+H-NH_3]^+$. Further fragmentation of the molecular ion at 186 yields the ion with $m/z = 115$, as depicted in the inset of Figure 2B-8, which may be explained by the loss of an olefin group $[M+H-CONH_3-C_2H_2]^+$. Scheme 2B-2 shows the pattern of NAD fragmentation obtained by LC-MS/MS.
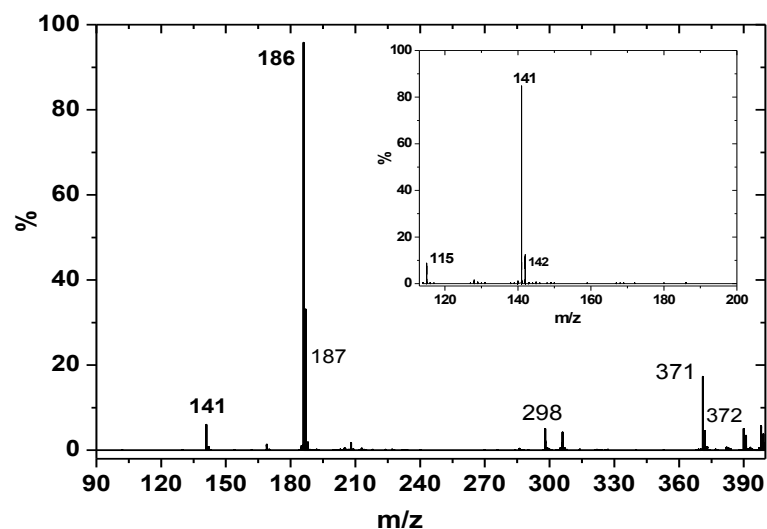
Figure 2B-8 LC-MS spectrum of NAD. Inset is given NAD MS-MS fragmentation (cone voltage = 35 V for both cases).
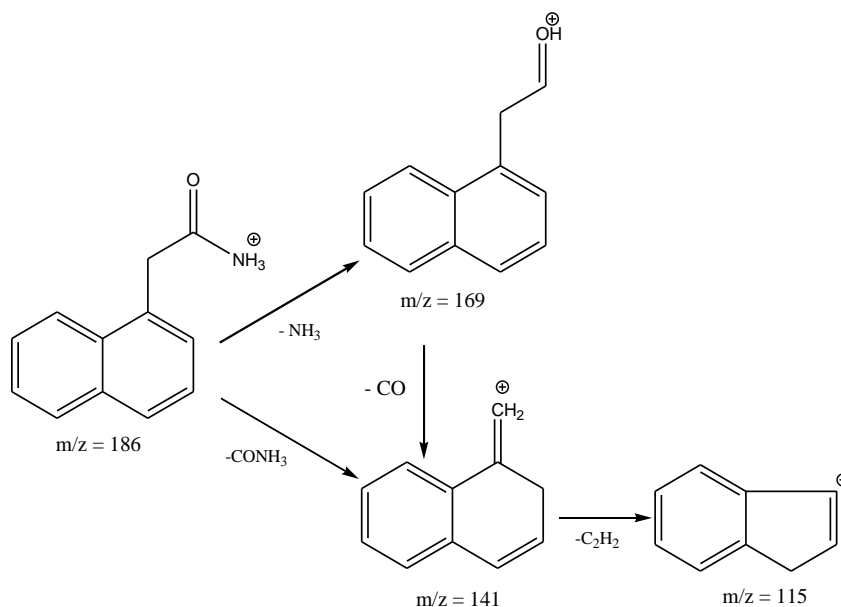
Scheme 2B-2 MS-MS fragmentation pattern of the parent molecule NAD.

Characterization of the product 1-naphthylacetic acid

The only product with retention time greater than NAD (25.0 min) corresponds to the compound 1-naphthylacetic acid (1-NAA). The amide group of NAD is hydrolyzed to yield the respective acid and NH_3 (Scheme 2B-3). Since 1-NAA compound is commercially available, its identification was made by comparing the obtained retention time of a sample injected in the HPLC-DAD in the same conditions as NAD. The UV-vis absorption spectrum ($\lambda_{max} \cong 280$ nm) of 1-NAA matches the

literature data and the elution time. This compound was observed at time zero and its concentration ($[1\text{-NAA}]_0 = 3.5\text{x}10^{-6}$ mol L^{-1}) decreases with irradiation time.
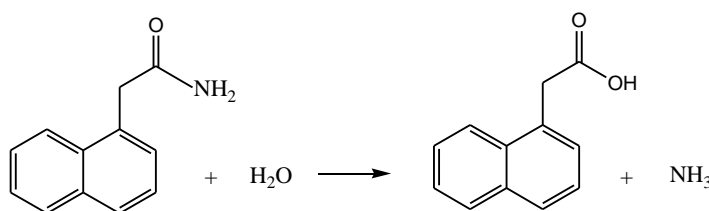
Scheme 2B-3 General scheme of NAD hydrolysis into 1-NAA and NH_3.

Characterization of hydroxylated products

Several photoproducts with $[M+H^+] = 202$ were detected from the early stages of the irradiation. The major ones that could be identified have retention times at 10.4, 19.4 and 21.5 minutes. These products have different fragmentation patterns, suggesting the formation of isomers corresponding to mono-hydroxylated forms of NAD. The main photoproduct observed at 19.4 min presents as main fragmentation m/z = 184, 156 and 140. The fragment ion at 184 clearly indicates the loss of a water molecule $[M+H-H_2O]^+$. The presence of several isomers suggests that hydroxylation may occur at the two aromatic moieties of NAD. Such hydroxylated compounds have previously been observed in photodegradation studies of naphthalene and naphthalene derivatives in solution [11-13].

Characterization of di-hydroxylated products

Several photoproducts with $[M+H^+] = 218$ were detected with retention times of 11.1, 12.6, 17.0, 19.5 and 20.2 minutes. The main fragments at 201, 173 and 159 correspond to the loss of NH_3, $CO-NH_3$ and $CH_2-CO-NH_3$, respectively.

Characterization of the naphthoquinone product

A photoproduct with $[M+H^+] = 216$ was observed at 20.1 minutes. It has fragments at 199, 171, 143 and 115 that show the loss of NH_3, $CO-NH_3$, $CO+CO-NH_3$ and also $CO+CO+CO-NH_3$, respectively. This is in complete agreement with the presence of three carbonyl groups. The proposed chemical structure given in Table 2B-2 for this compound is therefore attributed to a naphthoquinone derivative and

corresponds to the most stable structure 1,4-. The 1,2-position is unstable and leads to opening of the ring. Therefore, the presence of such naphthoquinone can be related to the fact that at least one of the di-hydroxylated derivatives may correspond to the 1,4-hydroquinone form as obtained with naphthalene and naphthalene derivatives [4,11].

Characterization of the furanone and coumarin products

Further products with $[M+H^+]$ = 192 and 204 were eluted at 15.3 and 18.5 minutes, respectively. They both give fragmentation with the loss of NH_3, $CO-NH_3$ and $CO+CO-NH_3$. The proposed structures (Table 2B-2), a furanone and a coumarin, respectively, are in agreement with the mass spectrometry findings. These types of compounds were also observed under photochemical oxidation of naphthalene in aqueous solutions [11].

LC-MS analysis in positive mode on irradiated NAD samples in de-aerated conditions was also performed. Under these conditions, only traces of these photoproducts were observed, even though the quantum yield of NAD degradation was higher under this condition. This probably indicates the formation of radicals that recombine to form oligomeric products (confirmed by LC/MS detection), where high molecular mass compounds at retention time greater than that of NAD were observed.

2B.2.5 Proposed mechanism

A mechanism summarizing the primary pathways involved in NAD degradation under environmental conditions is proposed in Scheme 2A-4, based on the present and previous results. Upon absorption of light in the UV-visible region, NAD is promoted to its first singlet excited state, $^1NAD^*$. This excited state may be deactivated by two main pathways:

pathway 1 - through a photoionization process giving rise to the formation of $NAD^{\bullet+}$ and hydrated electron, as already demonstrated in Chapter 2A. The hydrated electron can react with molecular oxygen leading to the formation of superoxide anion radical, $O_2^{\bullet-}$, which then after disproportionation leads to the formation of H_2O_2. The effective participation of $O_2^{\bullet-}$ in the degradation has been experimentally proved.

pathway 2 - by undergoing intersystem crossing (*isc*) to form the triplet excited state $^3NAD^*$.

In aerated or oxygenated conditions, ^{3}NAD* may lead to the formation of ^{1}O$_2$ through energy transfer to the dissolved molecular oxygen present in solution (pathway 3). However, although NAD is able to form ^{1}O$_2$ in aqueous solution, as reported in Chapter 2A, the use of Rose Bengal as ^{1}O$_2$ sensitizer ruled out any involvement of such reactive species in the degradation process. Additionally, the reaction of ^{3}NAD* with molecular oxygen can lead to the formation of NAD (pathway 4) or O$_2^{\bullet-}$ by an electron transfer process (pathway 5), which ultimately lead to products.

Therefore, and according to the experimental results, the main NAD degradation pathway in aerated and oxygenated conditions appears to be the photoinization process and consequent formation of superoxide anion radical (pathway 1). This process has also been observed with several polycyclic aromatic hydrocarbons [14-16]. Moreover, some minor contribution of pathway 4 and 5 may also be considered. In de-aerated condition, ^{3}NAD* decay leads to the formation of radical intermediates through bond scission to recombine and give NAD oligomers as photoproducts (pathway 6).
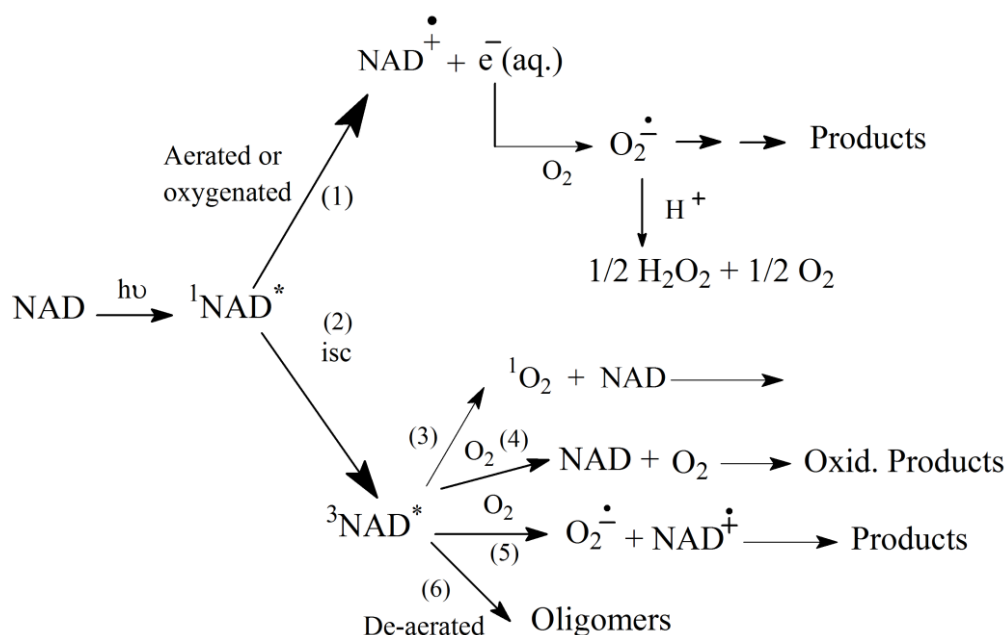
Scheme 2B-4 Primary steps of NAD photochemical degradation.

The exposure to light of aerated aqueous NAD solution led to the formation of several products; however, no change on the amide side chain -CH$_2$-CO-NH$_2$ was obtained. Thus, it is possible to say that the photochemical behavior of NAD mainly involves the naphthalene moiety. The presence of several isomers corresponding to

mono- and di-hydroxylated products suggests that the first step of the photodegradation is the hydroxylation of the aromatic ring. The formation of these may arise via the reactivity of NAD radical cation species with water leading to the formation the hydroxyl naphthalene derived radical(s) [17]. In the presence of oxygen, the latter species may lead to the final di-hydroxylated products (Scheme 2B-5).

$$e^- \text{ (aq.)} \quad + \quad \xrightarrow{\ O_2\ } \quad O_2^{\bullet -}$$

$$O_2^{\bullet -} \ + \ H^+ \ \rightleftharpoons \ HO_2^{\bullet} \quad (pKa = 4.8)$$

$$2\,HO_2^{\bullet} \ \rightleftharpoons \ H_2O_2 + O_2$$
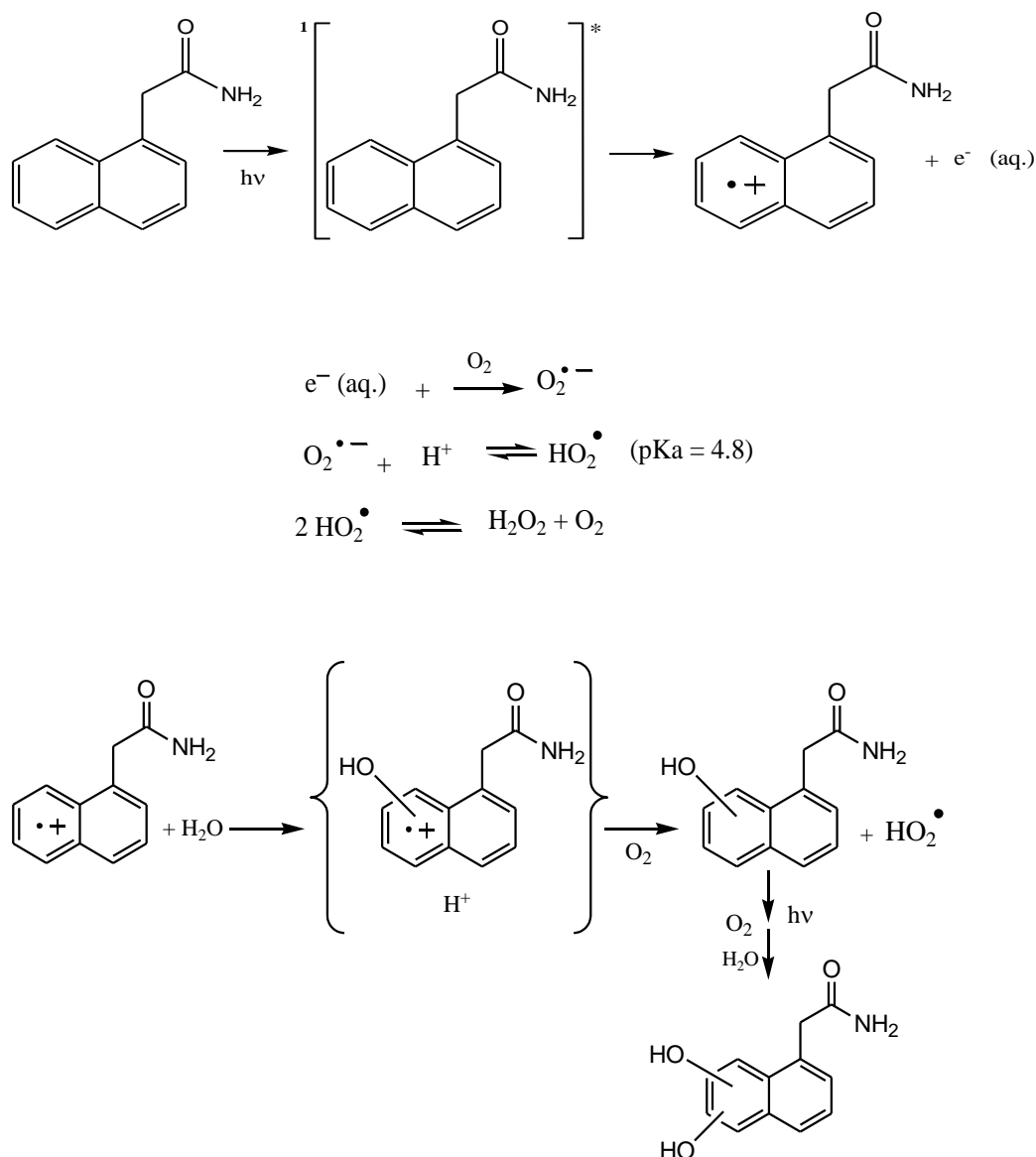
Scheme 2B-5 Probable pathways for the formation of mono- and di-hydroxylated products.

The proposed product naphthoquinone may arise from the 1,4-photocycloaddition of molecular oxygen or superoxide radical to NAD leading to an endoperoxide species [14], as shown by the following reaction:
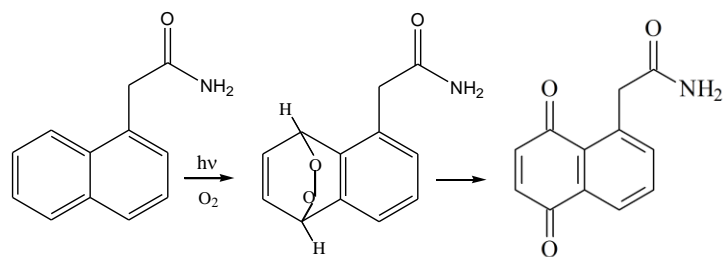
Alternatively, the naphthoquinone derivative may also be the result of the photochemical reactivity of the corresponding hydroquinone form, leading to the semiquinone radical, followed by a disporportionation process, as shown in Scheme 2B-6.
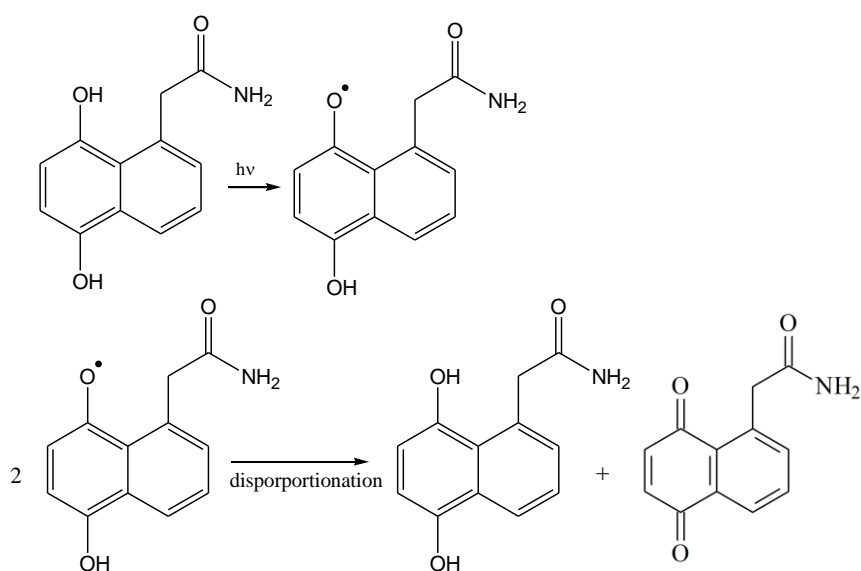
Scheme 2B-6 Possible pathways for naphthoquinone formation.

The homolytic scission of the generated 1,4-endoperoxide may lead to the formation of the furanone derivative by elimination of ethylene (Scheme 2B-7). Similar addition of molecular oxygen can also occur at 1,2 position leading to the formation of an unstable *ortho*-quinone derivative that leads after the monomolecular rearrangement to the coumarin product [11], as proposed in Scheme 2B-8.
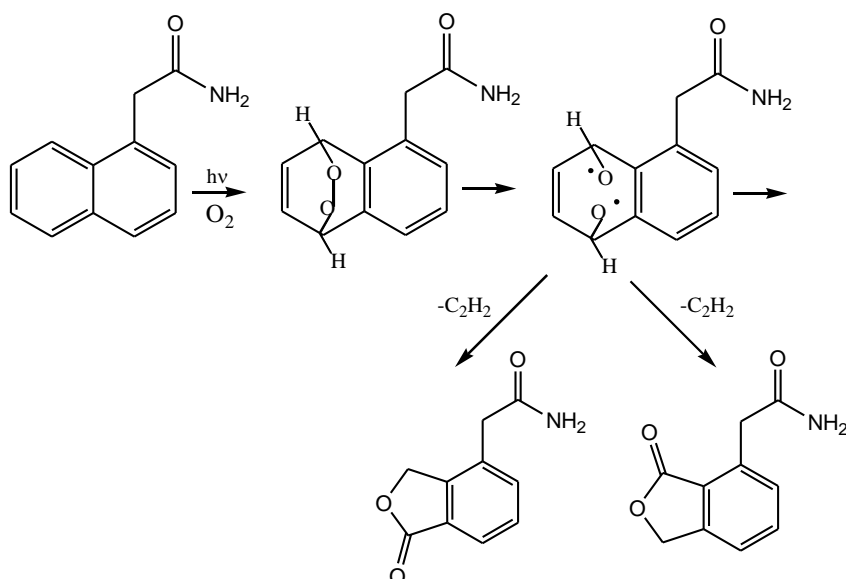
Scheme 2B-7 Possible pathways for the formation of furanone product.
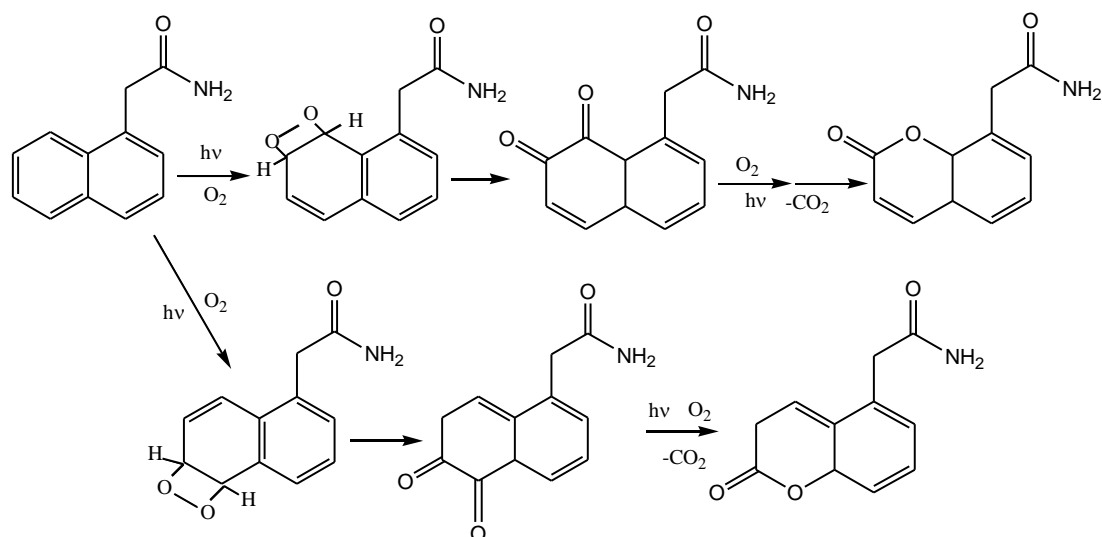
Scheme 2B-8 Possible pathways for the formation of coumarin product.

2B.2.6 Evaluation of toxicity

The influence of irradiation on the toxicity of organic compounds is an important factor in studies related to the fate of organic pollutants in the environment. Thus, the toxicity of aqueous NAD solution (3.0×10^{-4} mol L^{-1}) was assessed at several irradiation times upon excitation at 254 nm by measuring the % of luminescence inhibition (% I) of the bacteria *Vibrio fischeri* after 30 min of incubation (Figure 2B-9a). As shown, NAD by itself presents high toxicity since an inhibition of 73 % in the luminescence of the bacteria was observed before irradiation. Upon irradiation, an initial rapid increase on the toxicity was observed for the first 15 min (inset Figure 2B-

9a), after which the toxicity decreases, simultaneously with NAD degradation. In order to correlate this toxicity increase with photoproduct formation, the % I (photoproducts) was calculated for the first 20 min of irradiation (Figure 2B-9b). Additionally, the evolution of the formation of some primary products was also given for comparison. As clearly observed, there is a direct correlation between the increase on toxicity and the formation of these primary photoproducts. Therefore, we can postulate that these products (among them hydroxylated and di-hydroxylated photoproducts) are more toxic than the parent NAD. However, they do not seem to accumulate in solution since they are transformed in their turn with irradiation time in other less toxic compounds (Figure 2B-9a). Similar correlation of toxicity and formation of hydroxylated products has been observed by other groups [18].
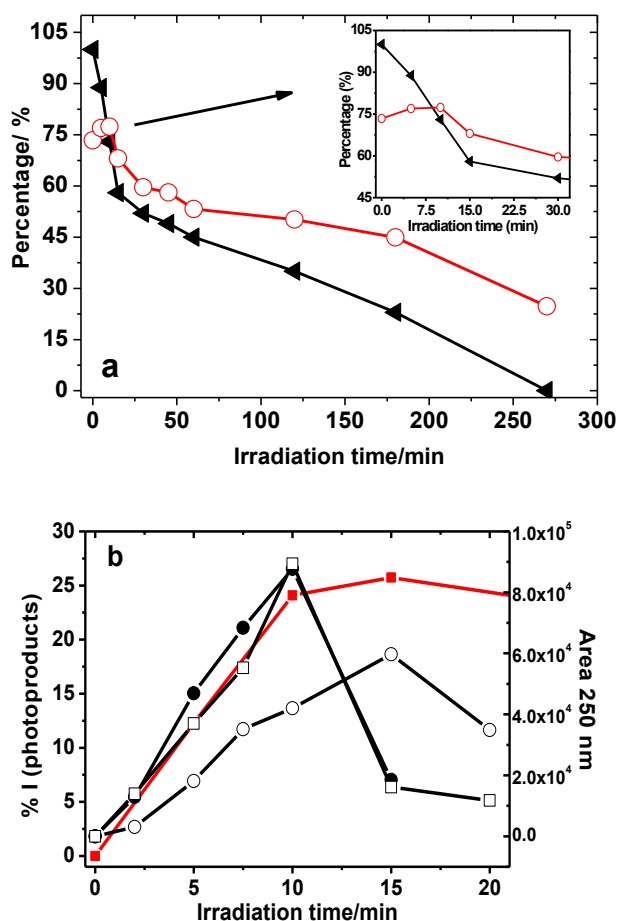
Figure 2B-9 a) Evolution of the % I of the luminescence of an aerated aqueous NAD solution $(3.0{\times}10^{-4}$ mol L^{-1}) upon excitation at 254 nm ($\bigcirc$), compared to the % of NAD degradation in the same conditions ($\blacktriangleleft$). b) % I (photoproducts) for the initial 20 minutes of irradiation ($\blacksquare$) and evolution of the formation of some di-hydroxylated photoproducts (11.1 min $\bigcirc$; 17 min $\bullet$; 19.5 min $\square$).

2B.3 Photodegradation in the presence of β-Cyclodextrin

As mentioned in the Introduction (Chapter 1, section 1.7), cyclodextrins (CDs) have been shown to provide an interesting environment for pesticide photodegradation, either protecting against it or increasing its degradation rate. Obviously, this will depend both on the structure of the pesticide and on its inclusion inside the cavity of the CD. Therefore, studies of NAD included in β-CD were carried out in order to assess the effect on NAD degradation process. Additionally, photophysical characterization of the inclusion complex followed by the photodegradation studies under UV and simulated solar light were carried out and the results are given below.

2B.3.1 Photophysical characterization of the system NAD:β-CD

The addition of β-CD (1.0×10^{-2} mol L^{-1}) to aqueous NAD solution (1.0×10^{-5} mol L^{-1}) induces changes in both the absorbance and fluorescence emission spectra, as shown in Figure 2B-10. An increase in NAD absorbance is observed in the UV absorption spectrum as well as a 1 nm bathochromic shift in the maximum wavelength upon β-CD addition (Figure 2B-10a). This is attributed to the inclusion of NAD in the CD cavity, as is frequently observed with β-CD.
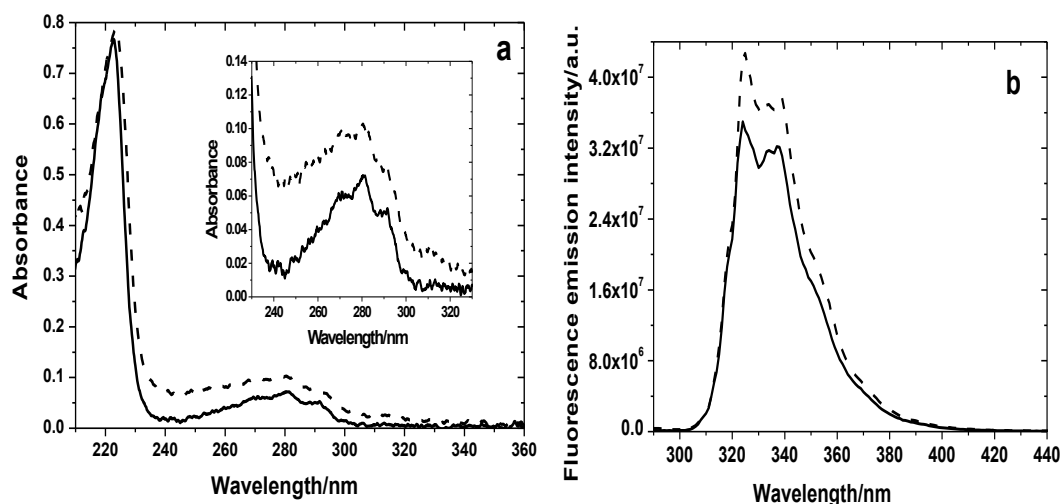
Figure 2B-10 a) UV absorption spectra of aqueous NAD solution (1.0×10^{-5} mol L^{-1}) in absence (solid line) and presence of β-CD 1.0×10^{-2} mol L^{-1} (dotted line). Inset is given the amplified graphic of the absorption in the range 230-330 nm. b) Fluorescence emission spectra ($\lambda_{ex} = 280$ nm) of the respective solutions described in a).

As with the absorption spectra, there is an increase in the fluorescence emission intensity of NAD and a very small bathochromic shift in the emission maximum from 324 to 325 nm, upon addition of the β-CD (Figure 2B-10b).

The influence of β-CD concentration on NAD fluorescence emission intensity was studied over the range 5.0×10^{-4} - 1.0×10^{-2} mol L^{-1}. The fluorescence emission intensity of NAD was enhanced with increasing concentration of β-CD, up to a constant value, as shown in Figure 2B-11. Water is known to quench the fluorescence of aromatic molecules in solution [19], and once NAD molecules enter the hydrophobic inner cavity of cyclodextrin this is diminished, leading to the increase of the fluorescence emission, reaching a constant value when all NAD has been entrapped in the hydrophobic cavity. In agreement with this, the fluorescence lifetime of NAD in aqueous solution was found to be 35 ± 2 ns ($\chi^2 = 1.09$) while in the presence of β-CD it increased to 41 ± 2 ns ($\chi^2 = 1.06$).
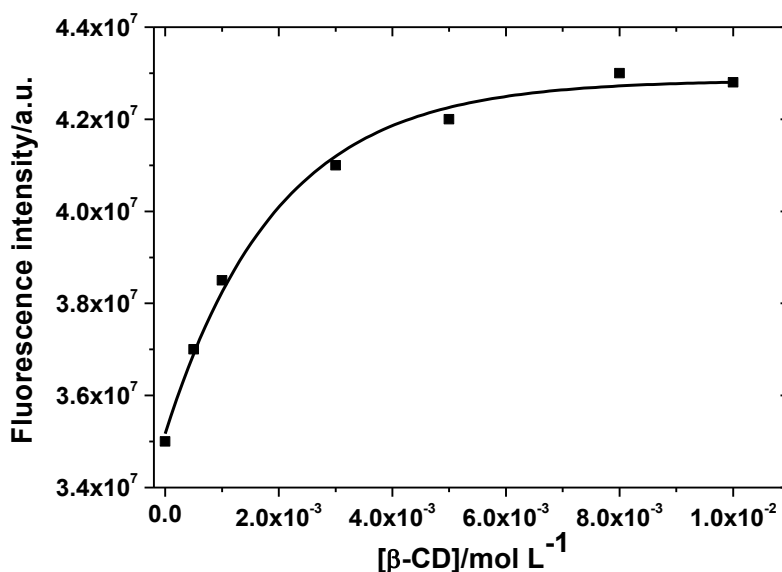
Figure 2B-11 Influence of β-CD concentration on the fluorescence emission intensity ($\lambda_{ex} = 280$ nm; $\lambda_{em} = 325$ nm) of aqueous NAD solution (1.0×10^{-5} mol L^{-1}).

The binding constant K for the inclusion complex NAD:β-CD was determined from the Benesi-Hildebrand equation [20] based on the fluorescence data presented in Figure 2B-12. A linear plot of $1/(I-I_0)$ as a function of $1/[\beta\text{-CD}]$ was observed suggesting the formation of a complex with a 1:1 stoichiometric ratio:

$$\beta\text{-CD} + \text{NAD} \xrightleftharpoons{K} \beta\text{-CD.NAD}$$

From this, a binding constant of 651 L mol^{-1} was determined, which is similar to that obtained for naphthalene inclusion in β-CD (685 L mol^{-1}) [21] and the naphthalene derivative 2-naphthyloxyacetic acid, (560 L mol^{-1}) [22].
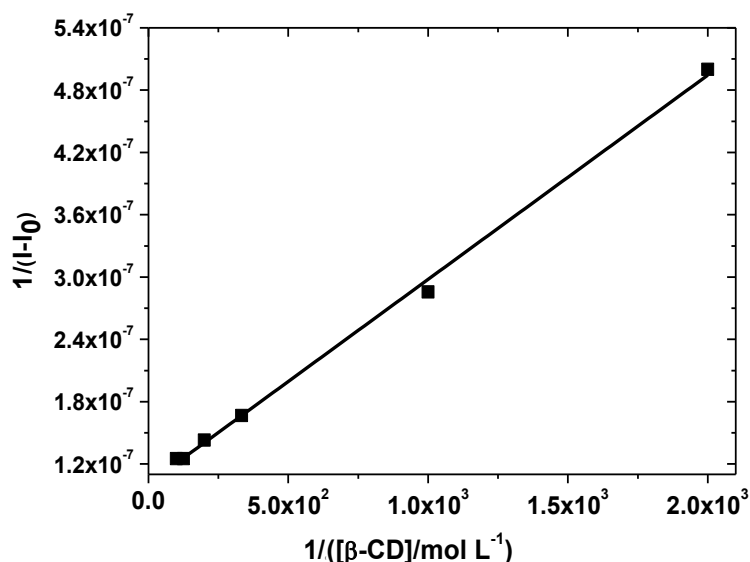
Figure 2B-12 Benesi-Hildebrand plot for the 1:1 complexation of NAD in β-CD ($R^2 = 0.998$).

Fluorescence quenching by inorganic anions

The quenching studies depicted in Chapter 2A have revealed that NAD fluorescence is effectively quenched by the anions I$^-$, Br$^-$, SCN$^-$ and N$_3^-$ through an electron transfer process. Therefore, we were interested to assess how the inclusion of NAD in β-CD will affect the quenching by these anions. The fluorescence emission of aqueous NAD solution (1.0×10^{-5} mol L^{-1}) in presence of β-CD (1.0×10^{-2} mol L^{-1}) was studied by adding different concentrations of the anions I$^-$, Br$^-$, SCN$^-$ and N$_3^-$ and the results were analyzed using the Stern-Volmer relationship. A comparison between efficiencies of NAD fluorescence quenching in presence and in absence of β-CD by the selected anions is summarized in Table 2B-3, while Figure 2B-13 shows, as an example, the Stern-Volmer plots for quenching by I$^-$ a) without and b) with β-CD (1.0×10^{-2} mol L^{-1}). Increasing concentrations of KI induce a decrease in NAD fluorescence, both with and without β-CD. Similar behavior was observed for all the

other anions. However, the quenching appears to be less efficient in the presence of β-CD.
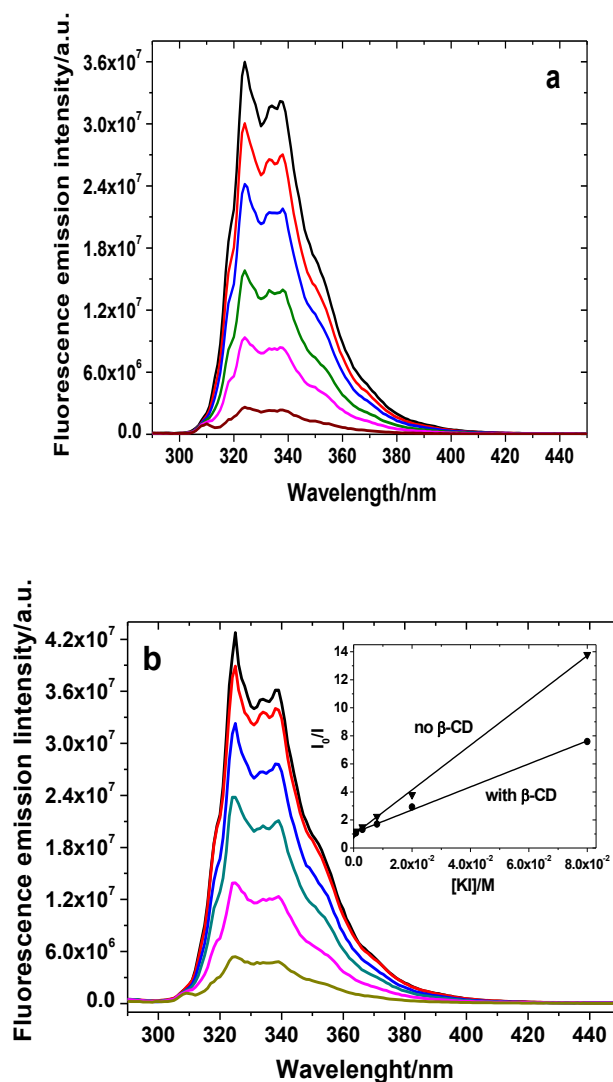
Figure 2B-13 Quenching effect of KI on fluorescence intensity (λ_{ex} = 280 nm) of aqueous NAD solution (1.0×10^{-5} mol L^{-1}) in a) absence and b) presence of β-CD (1.0×10^{-2} mol L^{-1}). Concentrations of KI from top to bottom: 0, 8.0×10^{-4}, 3.0×10^{-3}, 8.0×10^{-3}, 2.0×10^{-2} and 8.0×10^{-2} mol L^{-1}. Inset Figure 2B-14b are represented the Stern-Volmer plots in (▶) absence and (●) presence of β-CD (1.0×10^{-2} mol L^{-1}).

From the fluorescence quenching data given in Table 2B-3 it is possible to note a marked protective effect of the β-CD with all the anions. The ratio of K_{SV} for the systems (NAD +Q)/(NAD +Q+β-CD) presents the highest value for the anion I⁻. In this situation, the K_{SV} for NAD solution without β-CD is roughly 2.2 times higher (180 L

mol[-1]) than in presence of β-CD (82 L mol^{-1}). This quenching relation seems to follow the inverse order of the reduction potentials of the anions [23]. Fluorescence quenching in these cases is suggested to involve electron transfer, and these results corroborate the formation of the inclusion complex between β-CD and NAD and the protective effect of the cyclodextrin towards fluorescence quenching, as previously reported for naphthalene as well as its derivatives [21,24].

Table 2B-3 Stern-Volmer constants for NAD fluorescence quenching by I[-], Br^{-}, SCN[-] and N$_3$[-] in absence and presence of β-CD (1.0×10^{-2} mol L^{-1}).

Quencher (Q)	K_{SV} (L mol^{-1}) (NAD +Q)	K_{SV} (L mol^{-1}) (NAD +Q+β-CD)
Br^{-}	18	12
SCN[-]	123	76
N$_3$[-]	102	59
I[-]	180	82

2B.3.2 Influence of β-CD on photodegradation under simulated solar light

Aqueous NAD solutions (3.0×10^{-4} mol L^{-1}) were irradiated in the absence and presence of β-CD using two different systems: solar light simulator (Suntest) and UV irradiation at 254 nm. Figure 2B-14a shows, as an example, the evolution of the UV absorption spectra of NAD in the presence of β-CD (1.0×10^{-2} mol L^{-1}) upon Suntest irradiation. A decrease in the absorbance band with maximum wavelength centered at 280 nm is observed along with a simultaneous increase in the absorbance for wavelengths greater than 300 nm and less than 260 nm, indicative of NAD degradation and the formation of photoproducts that absorb in the same region. Some isobestic points are also observed in Figure 2B-14a, which provides further evidence of the suggested 1:1 inclusion complex. The same UV trends were observed either using different cyclodextrin concentrations or different irradiation system. Figure 2B-14b presents the degradation kinetics of aqueous NAD solution (3.0×10^{-4} mol L^{-1}) without and with addition of β-CD with different concentrations, upon irradiation with Suntest. All the curves fit first order kinetics. In the absence of β-CD, 51 % of NAD is

transformed after 8 h of irradiation, while in the presence of β-CD the transformation efficiency is reduced to about 22-27 % for the same irradiation time, depending on β-CD concentration. In the presence of β-CD, almost no degradation is observed in the first 120 min of irradiation, in contrast with the case in absence of cyclodextrin. The degradation of NAD increased with decreasing concentrations of β-CD in the range 1.0×10^{-2} - 1.0×10^{-3} mol L^{-1}, as shown in Figure 2B-14b.
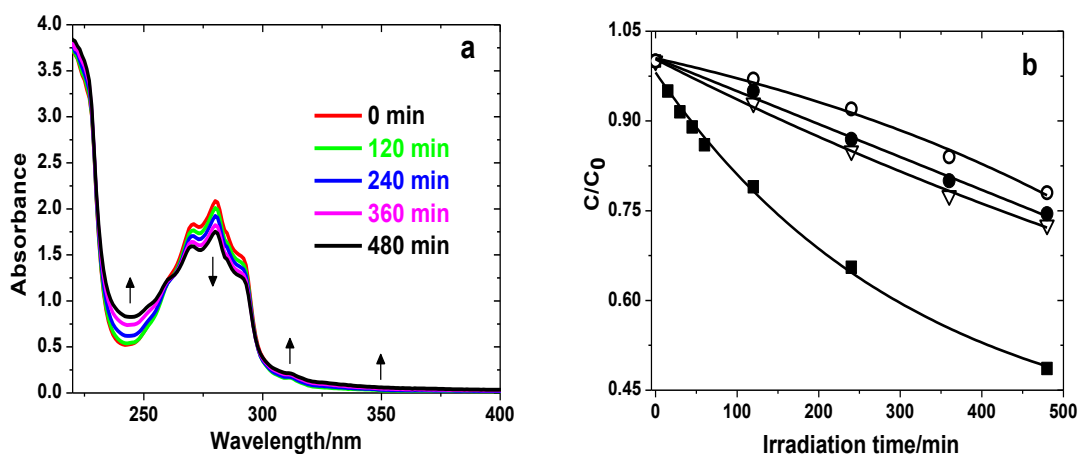
Figure 2B-14 a) UV absorption spectra of aqueous NAD solution (3.0×10^{-4} mol L^{-1}) evolution in the presence of β-CD (1.0×10^{-2} mol L^{-1}) upon irradiation with Suntest. b) Kinetics of NAD degradation (3.0×10^{-4} mol L$^{-}1$) upon irradiation with Suntest in absence (■) and in presence of β-CD with different concentrations: 1.0×10^{-2} mol L^{-1} (O); 5.0×10^{-3} mol L^{-1} (●) and 1.0×10^{-3} mol L^{-1} (▽), as function of irradiation time followed by HPLC-DAD (λ_{det} = 280 nm).

The estimated first order rate constants and half-live times obtained with Suntest in the absence and the presence of varying concentrations of β-CD are given in Table 2B-4. The half-life of NAD was enhanced by a factor of 8 in the presence of β-CD (1.0×10^{-2} mol L^{-1}), which clearly shows a stabilizing effect of the cyclodextrin, with NAD less prone to transformation with this high concentration of β-CD. This also suggests that the formation of the inclusion complex NAD:β-CD may be total at higher β-CD concentration and only partial at lower concentrations. It is well known that the mode of inclusion of a guest molecule in a cyclodextrin cavity depends on its structure. For example, the inclusion of the naphthalene derivatives 2-NOA and 1-NAA in β-CD are found to be dependent on the position of the substituent group [22]. For 1-NAA, a partial inclusion was observed due to the steric hindrance of the substituent group in

position 1 while for 2-NOA the total inclusion of the naphthalene moiety was observed to give a complex with axial orientation.

Table 2B-4 Pseudo first order rate constants (k) and half-lives ($t_{1/2}$) of aerated aqueous NAD solution (3.0×10^{-4} mol L^{-1}) in absence and presence of β-CD upon irradiation with the Suntest.

[β-CD] (mol L^{-1})	k (min^{-1})	$t_{1/2}$ (h)
0	2.4×10^{-3}	4.8
1.0×10^{-3}	7.0×10^{-4}	16.5
5.0×10^{-3}	6.0×10^{-4}	19
1.0×10^{-2}	3.0×10^{-4}	38.5

2B.3.3 Influence of β-CD on photodegradation under UV irradiation

An aqueous NAD solution (3.0×10^{-4} mol L^{-1}) was also irradiated at 254 nm in the absence and in the presence of β-CD (1.0×10^{-2} mol L^{-1}). The kinetic profiles obtained at this wavelength are presented in Figure 2B-15. A bi-exponential fit was observed for the kinetics in absence and presence of β-CD. In absence of β-CD, NAD is completely degraded after 4.5 h irradiation time with a pseudo first order rate constant of 9.0×10^{-2} min^{-1} and a half-life of 7.7 min. When the irradiation of NAD was carried out in presence of β-CD (1.0×10^{-2} mol L^{-1}), the transformation of NAD still occurs but to a lesser degree. Under these conditions, 74 % of NAD is transformed after 4.5 h. The rapid disappearance of NAD in the early stages of degradation is also observed with an initial estimated first order rate constant of 4.7×10^{-2} min^{-1} and a half-life of 14.7 min. This is roughly two times slower than in absence of β-CD (1.0×10^{-2} mol L^{-1}). Hence, we can say that although similar behavior was observed using the two different irradiation systems, the degradation process of NAD is faster at 254 nm than with the Suntest probably due to the high absorbance of NAD at this wavelength and to the higher intensity produced by the germicidal UV lamps.
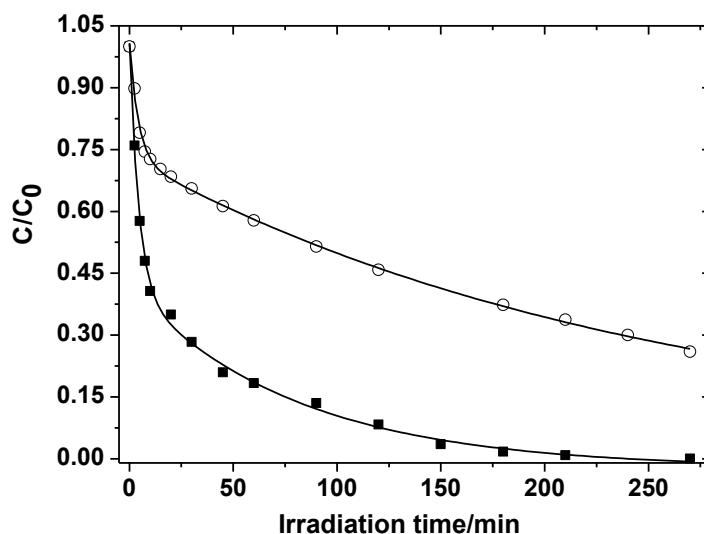
Figure 2B-15 Kinetics of NAD degradation (3.0×10^{-4} mol L^{-1}) in aqueous solution upon irradiation at 254 nm in absence (■) and in presence (○) of β-CD (1.0×10^{-2} mol L^{-1}) as function of irradiation time followed by HPLC-DAD (λ_{det} = 280 nm).

2B.3.3 Photoproduct identification

Several photoproducts were detected by HPLC-DAD upon NAD irradiation. All these photoproducts were eluted before NAD (24.1 min) indicating the formation of more polar products when compared to the parent compound. The same products were obtained either using Suntest or 254 nm irradiation step up. The main photoproducts of NAD formed in presence of β-CD (given in Table 2B-5) were compared with those already elucidated for direct NAD degradation (see Table 2B-2). These products correspond mainly to hydroxylated (mono- and di-) and coumarin products. In contrast with the behavior in the absence of the cyclodextrin, no furanone and di-hydroxylated compounds with hydroxyl group on the two aromatic rings were detected in presence of β-CD. This indicates that encapsulation also affects the photodegradation mechanism.

Table 2B-5 Retention time and proposed structure of NAD main photoproducts formed in the presence of β-CD.

Retention time (min)	Proposed chemical structure
24.1	
10.4 19.4	
11.1 17.0	
18.5	

2B.4 Conclusions

The photochemical degradation of NAD was studied in water under direct UV excitation and with simulated solar light. NAD was effectively transformed under these conditions with oxygen affecting the rate of degradation. The process was faster in the absence of oxygen, but not totally inhibited in oxygenated conditions highlighting the involvement of both triplet and singlet excited states in NAD photoreactivity, respectively. Although NAD was able to sensitize the formation of singlet oxygen, the participation of this species as a significant route in NAD degradation was ruled out by comparison with the behavior using Rose Bengal as singlet oxygen photosensitizer. In

contrast, superoxide anion and NAD radical cation seem to be involved in the degradation mechanism. The formation of these two species occurs through photoionization of NAD, as evidenced by laser flash photolysis studies. These species are considered to be the main intermediates responsible for NAD degradation in aerated conditions, yielding several photoproducts resultants from the hydroxylation and oxidation of the aromatic ring. A mechanistic pathway implying hydroxylation process through NAD radical cation species as well as an oxidation reaction by molecular oxygen is proposed. The photochemical behavior of NAD appears to mainly involve the aromatic moieties without any participation of the amide side chain. Additionally, toxicity tests clearly show that the generated primary photoproducts are responsible for a significant increase in the toxicity. However, upon prolonged irradiation this toxicity tends to decrease.

The photophysical properties of NAD as inclusion complex with β-CD and its photochemical degradation under UV and simulated solar light excitation were also studied in water. The inclusion complex of NAD:β-CD was characterized by fluorescence with a stoichiometric ratio of 1:1. The photodegradation of NAD as β-CD inclusion was carried out at different β-CD concentrations under 254 nm and simulated sunlight excitation. The results show that the NAD:β-CD complex increases NAD photostability towards photochemical degradation: the higher the β-CD concentrations, the less effective is the induced degradation of NAD. A comparison of NAD products formed in absence and presence of β-CD reveals some differences, indicating that encapsulation also affects the photodegradation, inhibiting some of the mechanistic pathways.

2B.5 References

[1] M. Montalti, A. Credi, L. Prodi, M. T. Gandolfi, *Handbook of Photochemistry*, third edition, Taylor & Francis Group, Florida, **2006**.

[2] C. S. Foote, *Photosensitized oxidation and singlet oxygen: consequences in biological systems*. In: Free Radicals in Biology. Ed. W. A. Pryor, vol. 2, pp. 85-133, Academic Press, New York, London, **1976**.

[3] R. S. Davidson, K. R. Trethewey, The role of the excited singlet state of dyes in dye sensitized photooxygenation reactions. *J. Am. Chem. Soc.*, **1976**, 98, 4008-4009.

[4] D. Vialaton, C. Richard, D. Baglio, A. B. Paya-Perez, Mechanism of the photochemical transformation of naphthalene in water. *J. Photochem. Photobiol. A: Chem.*, **1999**, 123, 15-19.

[5] J. J. M. Lamberts, D. C. Neckers, Rose Bengal derivatives as singlet oxygen sensitizers. *Tetrahedron*, **1985**, 41, 183-2190.

[6] M. C. DeRosa, R. J. Crutchley, Photosensitized singlet oxygen and its applications. *Coord. Chem. Rev.*, **2002**, 233-234, 351-371.

[7] R. W. Redmond, J. N. Gamlin, A compilation of singlet oxygen yields from biologically relevant molecules. *Photochem. Photobiol.*, **1999**, 70, 391-475.

[8] G. L. Kok, K. Thompson, A. L. Lazrus, S. E. McLaren, Derivatization technique for the determination of peroxides in precipitation. *Anal. Chem.*, **1986**, 58, 1194-1195.

[9] T. D. Bucheli, O. P. Haefliger, R. Dietiker Jr., R. Zenobi, Analysis of water contaminants and natural water samples using two-step laser mass spectrometry. *Anal. Chem.*, **2000**, 72, 3671-3677.

[10] X. Esparza, E. Moyano, J. R. Cosialls, M. T. Galceran, Determination of naphthalene-derived compounds in apples by ultra-high performance liquid chromatography-tandem mass spectrometry. *Anal. Chim. Acta*, **2013**, 782, 28-36.

[11] B. J. McConkey, L. M. Hewitt, D. G. Dixon, B. M. Greenberg, Natural sunlight induced photooxidation of naphthalene in aqueous solution. *Water, Air, Soil Pollut.*, **2002**, 136, 347-359.

[12] M. J. Climent, M. A. Miranda, Photodegradation of dichlorprop and 2-naphthoxyacetic acid in water. Combined GC-MS and GC-FTIR study. *J. Agric. Food Chem.*, **1997**, 45, 1916-1919.

[13] M. J. Garcia-Martinez, L. Canoira, G. Blazquez, I. Da Riva, R. Alcantara, J. F. Llamas, Continuous photodegradation of naphthalene in water catalyzed by TiO_2 supported on glass Raschig rings. *Chem. Eng. J.*, **2005**, 110, 123-128.

[14] M. P. Fasnacht, N. V. Blough, Mechanisms of the aqueous photodegradation of polycyclic aromatic hydrocarbons. *Environ. Sci. Technol.*, **2003**, 37, 5767-5772.

[15] M. P. Fasnacht, N. V. Blough, Aqueous photodegradation of polycyclic aromatic hydrocarbons. *Environ. Sci. Technol.*, **2002**, 36, 4364-4369.

[16] T. F. Kahan, D. J. Donaldson, Photolysis of polycyclic aromatic hydrocarbons on water and ice surfaces. *J. Phys. Chem. A*, **2007**, 111, 1277-1285.

[17] M. K. Eberhardt, Reaction of benzene radical cation with water. Evidence for the reversibility of hydroxyl radical addition to benzene. *J. Am. Chem. Soc.*, **1981**, 103, 3876-3878.

[18] J. P. Aguer, P. Boule, F. Bonnemoy, J. M. Chezal, Phototransformation of napropamide [*N,N*-diethyl-2-(1-naphthyloxy)propionamide] in aqueous solution: Influence on the toxicity of solutions. *Pestic. Sci.*, **1998**, 54, 253-257.

[19] J. W. Eastman, S. J. Rehfeld, Interaction of the benzene molecule with liquid solvents. Fluorescence quenching parallels (0-0) ultraviolet absorption intensity. *J. Phys. Chem.*, **1970**, 74, 1438-1443.

[20] H. A. Benesi, J. H. Hildebrand, A spectrophotometric investigation of the interaction of iodine with aromatic hydrocarbons. *J. Am. Chem. Soc.*, **1949**, 71, 2703-2707.

[21] S. Hamai, Association inclusion compounds of β-cyclodextrin in aqueous solution. *Bull. Chem. Soc. Jpn.*, **1982**, 55, 2721-2729.

[22] A. Muñoz de La Peña, F. Salinas, M. J. Gómez, M. I. Acedo, M. Sánchez Peña, Absorptiometric and spectrofluorimetric study of the inclusion complexes of 2-naphthyloxyacetic acid and 1-naphthylacetic acid with β-cyclodextrin in aqueous solution. *J. Inclusion Phenom. Molec. Recognit. Chem.*, **1993**, 15, 131-143.

[23] D. M. Stanbury, Reduction potentials involving inorganic free radicals in aqueous solution. *Adv. Inorg. Chem.*, **1989**, 33, 69-138.

[24] S. Hashimoto, J. K. Thomas, Fluorescence study of pyrene and naphthalene in cyclodextrin-amphiphile complex systems. *J. Am. Chem. Soc.*, **1985**, 107, 4655-4662.

Chapter 3

Photophysical and photochemical studies of the

plant growth regulator 2-naphthoxyacetic acid

3A. Photophysical characterization

3A.1 Introduction

It is well recognized that the polarity of a solvent can influence the absorption and fluorescence emission spectra of fluorophores. Therefore, in order to obtain information on the nature of the electronic states and assess the effect of the environment on the ground and excited state properties of the plant growth regulator 2-naphthoxyacetic acid (2-NOA), photophysical studies were undertaken in various solvents. Thus, in this Chapter the results are presented of the photophysical characterization of 2-NOA using steady-state and time resolved techniques. The study was carried out in water and in organic solvents, the same solvents used for the NAD studies presented in Chapter 2A with the exception that ethanol was replaced by methanol. Since the main interest is to learn more about the behavior of 2-NOA under environmental conditions, most of the figures along the chapter are given in aqueous solution. However, when justified, figures are also given in organic solvents, while data in all solvents is presented in tables.

3A.2 Characterization of the singlet ground state

3A.2.1 UV absorption spectra and determination of the molar absorption coefficients

The UV absorption spectrum of 2-NOA was recorded in water, methanol, ethylene glycol, acetonitrile, chloroform and 1,4-dioxane. As shown in Figure 3A-1, the UV absorption spectrum of 2-NOA in aqueous solution presents three bands: a short wavelength absorption band with maximum around 223 nm, a second band within the wavelength range 250-300 nm with maximum centred at 270 nm and a third absorption band with maximum at 324 nm. The absorption bands show vibrational structure typical of naphthalene and its derivatives, with π-$\pi*$ transitions of the aromatic ring. The replacement of water by the organic solvents did not affect either the shape of absorption bands or their vibronic structure. However, a bathochromic shift was observed in the absorption maximum wavelength with the decrease of solvent polarity, going from 270 to 273 nm, as depicted by the results presented in Table 3A-1. This is in agreement with the polarizing effect of the solvent medium (increase of refractive index) on the π-$\pi*$ transition [1-3].
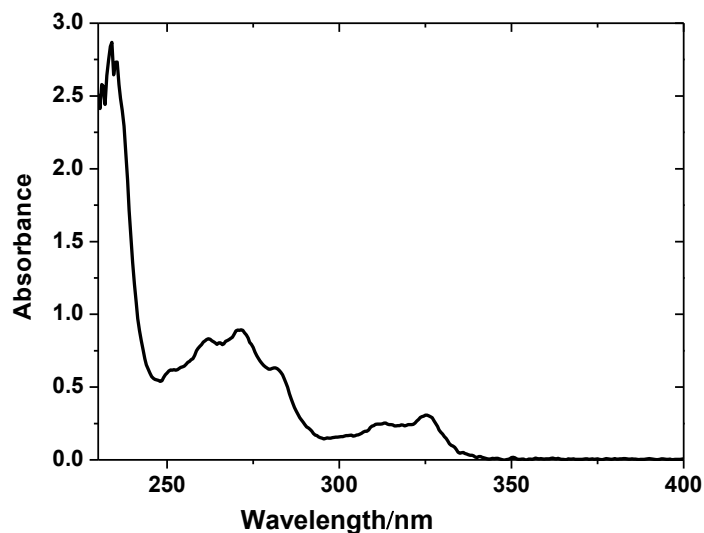
Figure 3A-1 UV absorption spectrum of 2-NOA aqueous solution (2.0×10^{-4} mol L^{-1}).

The molar absorption coefficients of the *ca.* 272 nm band of 2-NOA, ε, were determined according to the Beer-Lambert law for each solvent at the maximum absorption wavelength, using at least six standard solutions with increasing concentrations. Figure 3A-2 shows, as illustrative example, the plot used for the determination of $\varepsilon_{270\,nm}$ for 2-NOA in aqueous solution while the spectral maxima and ε values in all the solvents are reported in Table 3A-1. The ε values are in accordance with the literature (1711-4988 L mol^{-1} cm^{-1}, depending on the pH and on the solvent) [4] and are typical values for a π-π* transition.

Table 3A-1 Maximum absorption wavelength (λ_{max}) and molar absorption coefficient (ε) determined for 2-NOA singlet ground state as function of solvent polarity. The refractive index n_D, dielectric constant ϵ and viscosity η of solvents are given for better clarity of discussion [5].

Solvent	Abs. λ_{max} (nm)	ε [a] (L mol^{-1} cm^{-1})	n_D	ϵ	η ($\times10^{-3}$ Pa s)
Water	270	4440	1.333	80.1	1.00
Ethylene glycol	272	4896	1.431	37.7	19.9
Methanol	272	4870	1.328	32.7	0.59
Acetonitrile	272	4450	1.344	35.9	0.34
Chloroform	273	5710	1.445	4.81	0.58
1,4-Dioxane	273	4800	1.422	2.20	1.43

[a] Estimated errors ± 5%
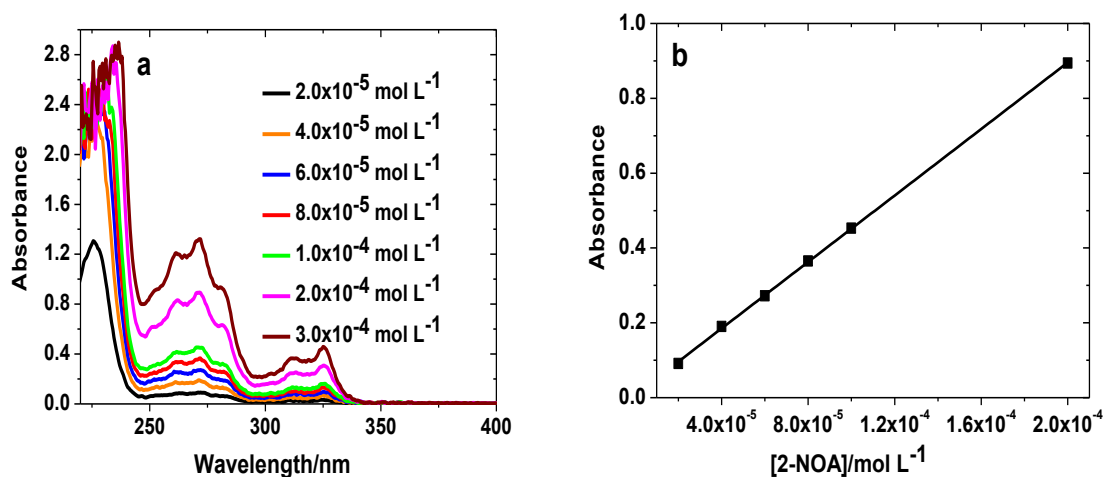
Figure 3A-2 a) UV absorption spectra of 2-NOA in aqueous solution at different concentrations. b) Respective Beer-Lambert plot for the determination of ε at 270 nm.

3A.3 Characterization of the first singlet excited state

3A.3.1 Fluorescence emission and excitation spectra and singlet excited state energy

The fluorescence emission and excitation spectra of 2-NOA was measured in water and in organic solvents under de-aerated conditions (Figure 3A-3). As observed in Figure 3A-3a, the maximum wavelength (λ_{max}) and the intensity of the fluorescence emission are dependent on the solvent type. In all the solvents, the fluorescence emission spectrum presents a single broad band extending from 320 to approximately 470 nm with a maximum emission wavelength in the region of 344-347 nm, depending on solvent, in agreement with literature [6]. The λ_{max} of fluorescence emission exhibits a bathochromic shift with increasing polarity of the solvent accompanied by a loss of vibronic structure (Figure 3A-3a and Table 3A-2). For all the solvents, the emission spectrum was not affected when excitation was made at different wavelengths confirming their origin from a single emitting species and that 2-NOA does not contain any fluorescent impurities. Furthermore, the excitation spectra of 2-NOA (Figure 3A-3b) is identical to the absorption spectra presenting similar vibronic structure. The Stokes shifts, given as the difference between the maximum peak of normalized absorption and emission spectra are given in Table 3A-2. As can be noticed, a small decrease of the Stokes shifts is observed when replacing water by organic solvents. The small Stokes shift obtained in all the solvents indicates that there is no significant

geometrical change in the structure of 2-NOA chromophore between the ground and excited states.
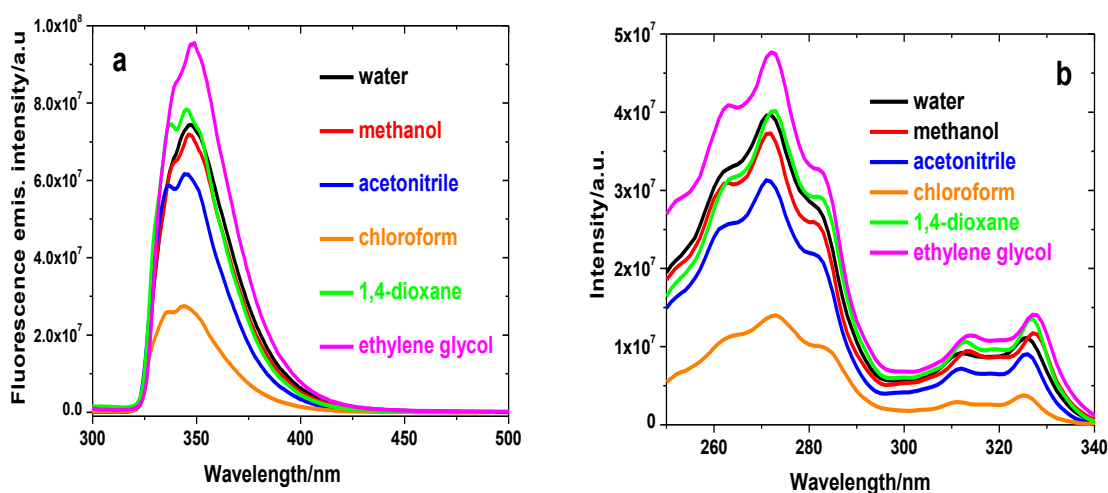
Figure 3A-3 Fluorescence a) emission and b) excitation spectra of 2-NOA de-aerated solutions (2.0×10^{-5} mol L^{-1}) in all the solvents (λ_{ex} = maximum absorption wavelength, λ_{em} = maximum emission wavelength).

The energy of the lowest singlet excited state of 2-NOA, E_S, has also been determined. E_S was estimated from the intersection of the normalized absorption and emission spectra (Table 3A-2). Within experimental error, E_S is independent on solvent and has a value of 3.78 eV ($\cong$ 365 kJ mol^{-1}). This value is somehow smaller then obtained for NAD (4.00 eV; 390 kJ mol^{-1}) or naphthalene (3.99 to 3.97 eV) but is within the range of energy values for naphthalene derivatives [5].

3A.3.2 Determination of the fluorescence quantum yields and lifetimes

The fluorescence quantum yields of 2-NOA, ϕ_F, were determined by steady state fluorescence measurements using naphthalene in ethanol as reference ($\phi_F = 0.21$ [5]), as explained in experimental section. Both the fluorescence quantum yields, ϕ_F, and the singlet lifetimes (or fluorescence lifetimes, τ_F) of 2-NOA were determined in de-aerated solutions in all the solvents since its known that molecular oxygen may be a quencher of excited states. The results presented in Table 3A-2 indicate that 2-NOA fluoresces with reasonable quantum yields, ranging from 0.13 in water to 0.33 in ethylene glycol. Chloroform is an exception, with a very low quantum yield of 0.028 which may indicate

contact charge transfer [7]. The ϕ_F value in water, 0.13, is approximately 2.5 times lower than in the organic solvents. This may be due to hydrogen bonding effects involving the stretching modes of the hydroxyl group, which could facilitate the non-radiative decay to the ground state, and is consistent with quantum yields of other aromatics, such as benzene [8], that are markedly smaller in water than in other common solvents. The quantum yield increases with the increase of the refractive index, with the exception of water and chloroform. For the organic solvents ethylene glycol, acetonitrile and methanol, the quantum yield follows the order of the dielectric constant of the solvent. These solvents are highly polar but differ in their hydrogen bonding donor ability. The fact that the fluorescence quantum yields are less than unity indicates the relevance of non-radiative channels in the deactivation of 2-NOA singlet excited state, ^{1}2-NOA*.

Table 3A-2 Maximum emission wavelength (λ_{max}), Stokes shift, singlet excited state energy (E_S), determined fluorescence quantum yields (ϕ_F), measured lifetimes (τ_F) and chi squared factor (χ^2) for the fluorescence emission decay of 2-NOA in water and in the organic solvents.

Solvent	Em. λ_{max} (nm)	Stokes shift (nm)	E_S (eV)	ϕ_F^*	τ_F (ns)	χ^2
Water	347	77	3.79	0.13	10.3	1.10
Ethylene glycol	347	75	3.77	0.33	11.4	1.06
Methanol	346	74	3.77	0.22	12.8	0.98
Acetonitrile	344	72	3.78	0.26	14.7	1.02
Chloroform	344	71	3.79	0.028	3.5	1.08
1,4-Dioxane	345	73	3.78	0.25	13.3	1.12

*Estimated errors $\pm$ 10%

The fluorescence lifetimes of 2-NOA in water and in the organic solvents were measured with nanosecond time resolution with excitation at 282 nm and observation at the maximum emission wavelength. All the results are summarized in the previous Table 3A-2 while Figure 3A-4 depicts, as an example, the decay curve of 2-NOA fluorescence emission in water. The fluorescence decay could be fitted well to a single exponential in all the solvents, revealing a single emitting species. The τ_F values range

from 10.3 ns in water (at pH of the solution, around 5.0) to 14.7 ns in acetonitrile, chloroform being the exception, where a much shorter fluorescence lifetime of 3.5 ns was observed. This low value in chloroform is in conformity with the suggestion of contact charge transfer quenching of the singlet excited state by the solvent [7]. The fluorescence lifetime of 2-NOA in water is $\cong$ 1.4 times less than those obtained in organic solvents, in accordance with the determined fluorescence quantum yields. This may reflect a stronger contribution of internal conversion process induced by water molecules in the decay of ^{1}2-NOA*. In general, solvents with OH group lead to smaller lifetimes than acetonitrile and 1,4-dioxane. However, unlike what was observed with the quantum yield, although ethylene glycol and acetonitrile have similar dielectric constants ($\cong$ 36), the lifetime in ethylene glycol is smaller than in acetonitrile, which seems to back up the previous hypothesis. The influence of the pH on the fluorescence decay of 2-NOA in aqueous solution was also measured, in addition to the previous fluorescence lifetime given in water (10.3 ns; pH around 5.0). The decays were measured at pH 1.35 and 9.40 and the kinetics fitted well a single exponential (χ^2 = 1.11) giving lifetimes of 8.42 and 9.66 ns, respectively.
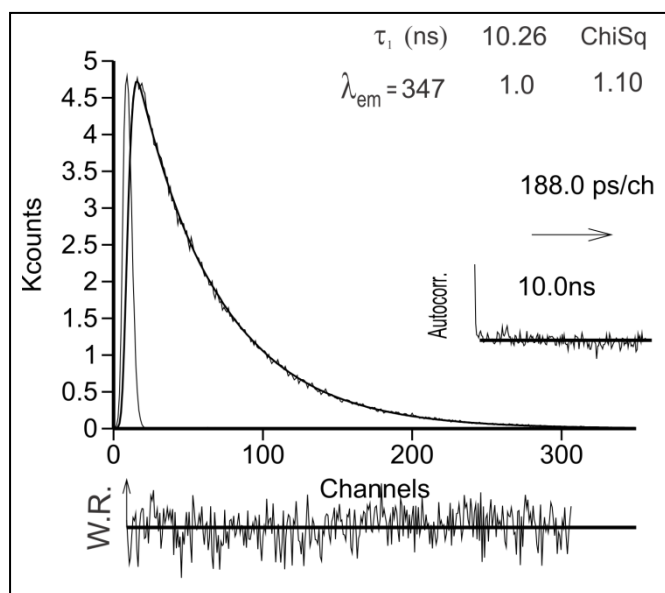
Figure 3A-4 Fluorescence emission decay curve of 2-NOA de-aerated aqueous solution (λ_{ex} = 282 nm at room temperature; 2.0×10^{-5} mol L^{-1}). The autocorrelation function (Autocorr.), weighted residual (W.R.) and chi-squared value (χ^2) are presented as insets. The vertical faintest line in the decay is the pulse instrumental response.

Although, in general, 2-NOA presents short fluorescence lifetimes, these values are in line with those reported in literature for other naphthalene derivatives [5]. For example, the lifetime of 2-hydroxy-naphthalene is 13.3 and 8.9 ns in non polar (n) and polar solvents (p), respectively, while naphthalene presents lifetimes of 96 (n) and 105 (p) ns. This puts in evidence the key role played by the substituent groups on the photophysical properties.

3A.3.3 Effect of pH on the fluorescence emission of aqueous solution

2-NOA is a relatively weak acid with a pKa of 3.55 [4]. The effect of pH on the fluorescence emission may be very significant since it will affect the existing forms of the luminescence moiety under environmental conditions. Consequently, the influence of pH on the fluorescence emission of 2-NOA aerated aqueous solution was studied by adding $HClO_4$ or NaOH (Figure 3A-5). Figure 3A-5a shows the fluorescence emission spectra of aqueous 2-NOA solution (2.0×10^{-5} mol L^{-1}) obtained when the pH ranged from 1.32 to 11.6 while Figure 3A-5b illustrates the observations taken from Figure 3A-5a.
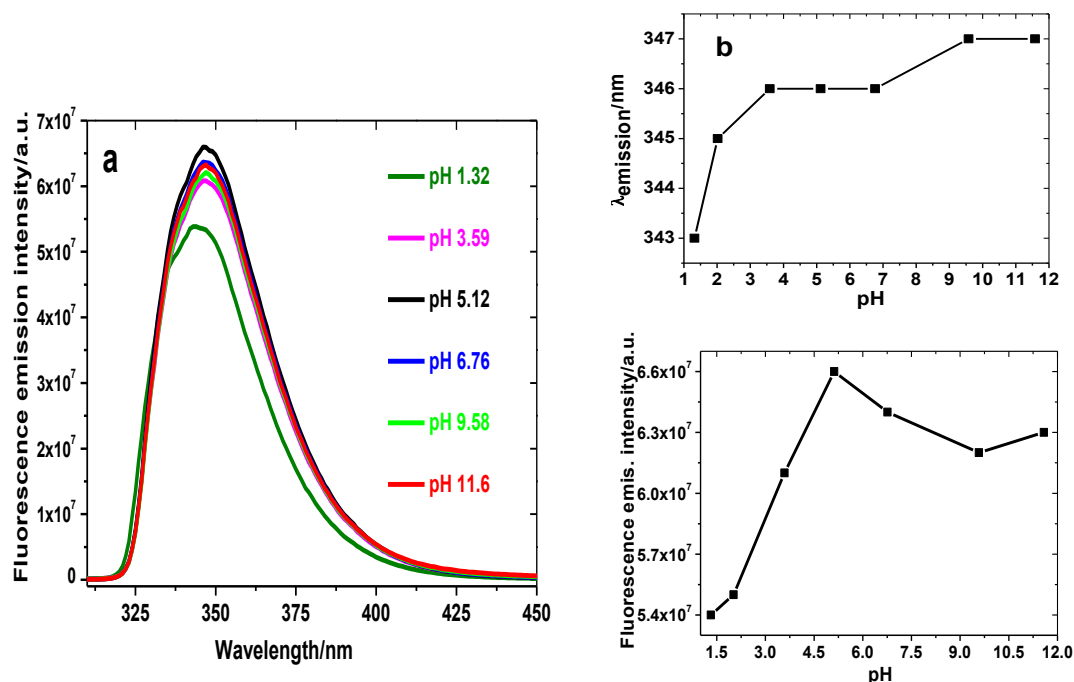
Figure 3A-5 a) Influence of pH on the fluorescence emission spectra of 2-NOA aqueous solution (λ_{ex} = maximum absorption wavelength). b) Respective maximum wavelength and intensity of fluorescence emission as function of pH of 2-NOA aqueous solution.

As observed, the increase of the pH leads to a red shift (from 343 to 347 nm) of the maximum emission wavelength of fluorescence and to a decrease of the vibrational structure of the band. Furthermore, the fluorescence intensity of the band is also dependent on pH increasing up to its highest value at pH 5.12, where 2-NOA exists in its anionic form in both ground and excited states.

3A.4 Characterization of the triplet excited state

3A.4.1 Phosphorescence spectrum and triplet excited state energy

The phosphorescence emission spectrum of 2-NOA was measured in acetonitrile at 77 K (Figure 3A-6). The phosphorescence presents well-resolved emission spectrum with three main vibronic bands which are comparable to those obtained in fluorescence spectrum, although with a very low intensity. The lowest wavelength band is assigned to the 0-0 transition between the lowest triplet state T_1 and the ground state S_0, and gives the energy of 2-NOA triplet excited state E_T, 2.72 eV (262 kJ mol^{-1}). This value is slightly higher than those of naphthalene 2.66 eV (256 kJ mol^{-1}) [6] and NAD (E_T, 2.69 eV or 260 kJ mol^{-1}), probably due to the effect of the substituent's groups.
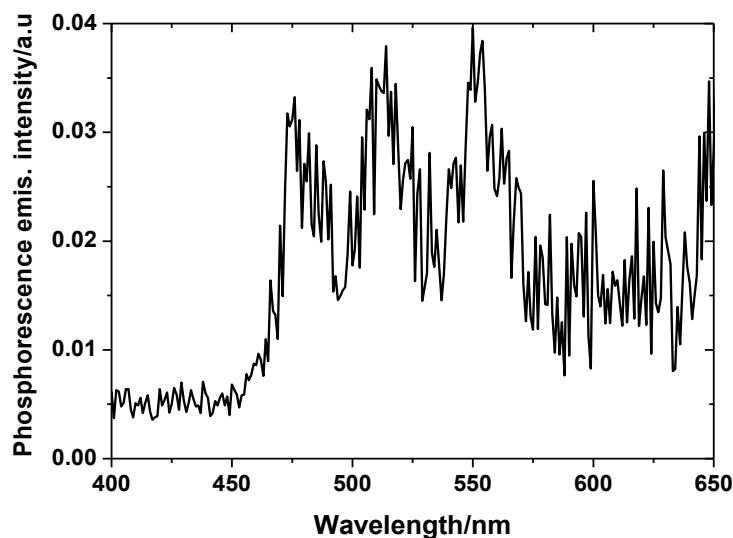
Figure 3A-6 Phosphorescence spectrum of 2-NOA in acetonitrile (2.0×10^{-5} mol L^{-1}) at 77 K.

3A.4.2 Determination of the phosphorescence quantum yield and lifetime

The phosphorescence quantum yield of 2-NOA, ϕ_P, was measured in acetonitrile at 77 K using as reference benzophenone in ethanol at 77 K ($\phi_P = 0.73$ [5]). Under these

conditions a value of 0.022 (± 10%) was obtained for the ϕ_P. The phosphorescence lifetime τ_P was also determined in the above glass as the average of at least 10 measurements, with a relatively low measurement error. The phosphorescence decay profile illustrated in Figure 3A-7 allows estimation of a lifetime of 311 ms. This lifetime in the timescale of milliseconds is in agreement with the triplet excited state of 2-NOA, ^{3}2NOA*, corresponding to a (π-π^*) transition, as expected from other reports for naphthalene and its derivatives [5].
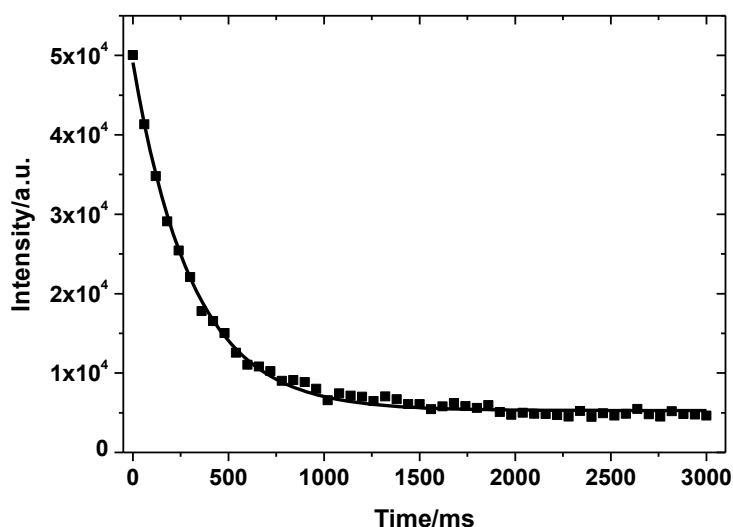
Figure 3A-7 Decay of phosphorescence of 2-NOA in acetonitrile glass at 77 K (λ_{ex} = 272 nm, λ_{em} = 510 nm).

The lowest ^{3}2NOA* (T$_1$), must lose its excess energy in order to return to the singlet ground state 2-NOA (S$_0$). This deactivation can occur by radiative (phosphorescence) or non-radiative (intersystem crossing, isc) processes. The radiative process is given by the rate constant for the phosphorescence decay k_p (= ϕ_p/τ_P), whereas the non-radiative process is given by the quantum yield of intersystem crossing ϕ_{isc} (T$_1$-S$_0$) determined according to the expression (3A.1), considering ϕ_{isc} (S$_1$-T$_1$) = 0.437 (at room temperature, as determined in next section):

$$\phi_{isc}(S_1 - T_1) = \phi_P + \phi_{isc} (T_1 - S_0) \qquad (3A.1)$$

Therefore, a rate constant of 7.07×10^{-2} s^{-1} was obtained for the phosphorescence decay as well as an intersystem crossing quantum yield for the triplet decay ϕ_{isc} (T$_1$-S$_0$)

of 0.42. This value is around twenty times greater than ϕ_P indicating that the deactivation of ^{3}2-NOA* occurs preferentially by *isc* to the ground state rather than by the radiative process of phosphorescence.

3A.4.3 Triplet-triplet absorption spectra and triplet lifetimes

Nanosecond laser flash photolysis studies were undertaken to obtain more detailed information on the reactive species that may be formed upon 2-NOA photoexcitation. Excitation in the lowest energy absorption band of 2-NOA (250-300 nm) was accomplished with frequency quadrupled (266 nm) pulses from a Nd/YAG laser. The transient absorption (singlet-triplet difference) spectra were obtained in de-aerated 2-NOA solutions in water, ethylene glycol, methanol, acetonitrile, chloroform and 1,4-dioxane, at different delays times after laser excitation. Figure 3A-8a displays the transient absorption spectra of 2-NOA de-aerated aqueous solution, in which various transient species are observed.
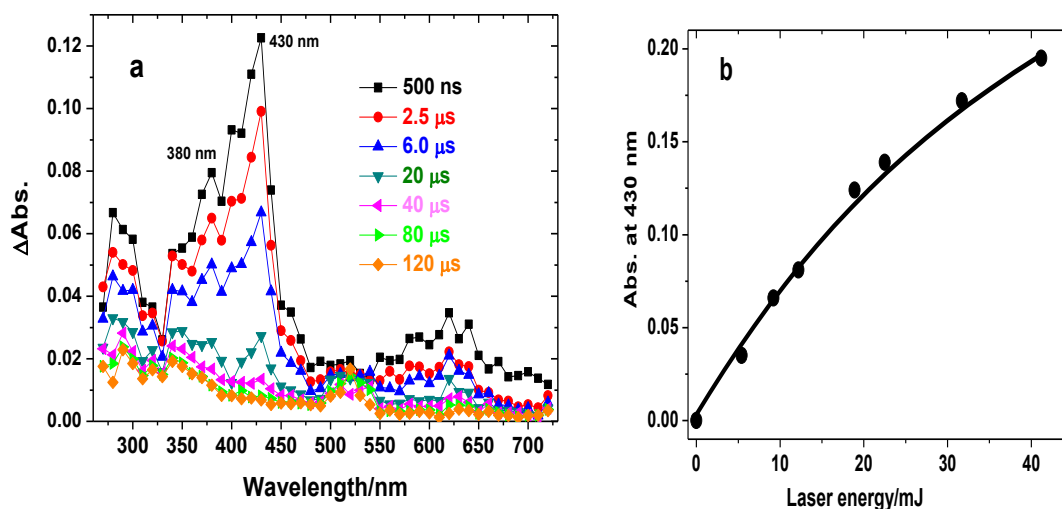
Figure 3A-8 a) Transient absorption spectra of 2-NOA de-aerated aqueous solution (2.0×10^{-5} mol L^{-1}) obtained by nanosecond laser flash photolysis with excitation at 266 nm, recorded at 500 ns, 2.5, 6.0, 20, 40, 80 and 120 μs after pulse. b) Evolution of the absorbance band at 430 nm as function of laser energy.

The intense and broad transient band with maxima absorption wavelength at 430 nm and 380 nm was assigned to 2-NOA triplet-triplet absorption (^{3}2-NOA*) as will be explained below, and corresponds closely to that seen for triplet states of naphthalene and derivatives [5,9,10]. This band did not undergo any shift when changing from water

to organic solvents, as given in Table 3A-3. The absorbance at 430 nm increased linearly with laser energy (see Figure 3A-8b) within the range 1-18 mJ, indicating its formation occurs via a monophotonic process. For higher energies the linearity is lost due to biphotonic or multiphotonic processes. Therefore, all the studies were performed at energies close to 15 mJ. To confirm the triplet-triplet nature of the absorption band at 430 nm, solutions of 2-NOA in all solvents were excited at 266 nm as function of oxygen concentration. It is well known that molecular oxygen is a strong quencher of triplet excited states of aromatic molecules [11]. The decay rate constant of ^{3}2-NOA* at 430 nm was measured in each solvent in aerated and de-aerated solutions and the triplet state lifetimes in solution, τ_T, was calculated as the inverse of this rate constant. The results summarized in Table 3A-3 confirm the marked effect of oxygen on the lifetimes of this transient band. This effect of oxygen was observed for all the solvents, supporting the idea that this band corresponds to ^{3}2-NOA*. In water, for example, ^{3}2-NOA* decays with lifetimes of 1.10 and 67.9 μs in aerated and de-aerated solutions, respectively (Figure 3A-9). The high value of the τ_T (680 μs) obtained in ethylene glycol in de-aerated conditions, although reproducible, may be explained by the high viscosity of the solvent, which reduces quenching by impurities present in the solution.

Table 3A-3 Determined photophysical parameters for 2-NOA triplet excited state (wavelength λ, lifetime τ_T and quantum yield ϕ_T) as function of solvent polarity and oxygen concentration [5].

Solvent	Abs. λ_{max} (nm)	τ_T^{Argon} (μs)[a,b]	τ_T^{Air} (μs)[a]	ϕ_T[a,b]
Water	430	67.9	1.10	0.318
Ethylene glycol	430	680	2.25	0.446
Methanol	430	19.6	0.144	0.333
Acetonitrile	430	39.1	0.154	0.437
Chloroform	430	27.2	0.309	0.393
1,4-Dioxane	430	63.4	0.312	0.490

[a] Estimated errors ± 15%. [b] De-aerated solutions
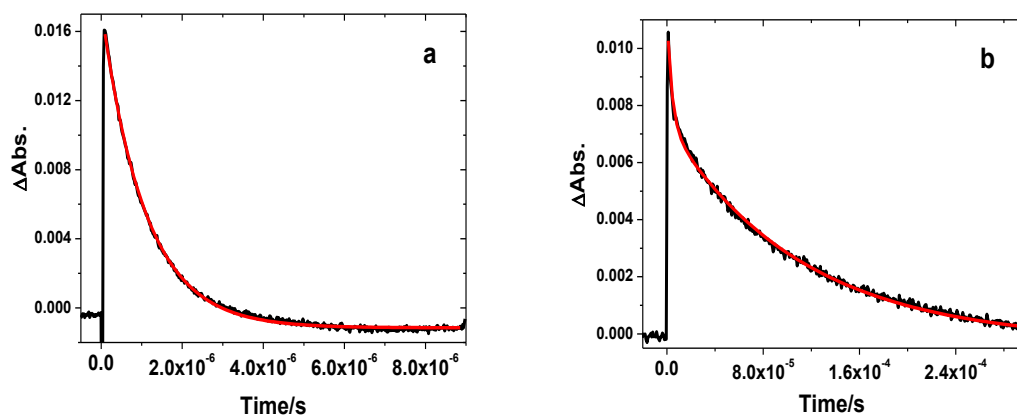
Figure 3A-9 Kinetic decay of 2-NOA triplet excited state monitored at 430 nm in a) aerated and b) de-aerated aqueous solutions.

In aerated solutions the decay of the triplet excited state (band at 430 nm) fitted well a mono-exponential rate law in all the solvents. In contrast, as illustrated in Figure 3A-9 for the decay of ^{3}2-NOA* in water, a better fit was achieved by a bi-exponential decay in de-aerated solutions, in which one component decays rapidly and the other decays on a longer time scale. This long component is attributed to the contribution with absorption maximum at 380 nm, as is discussed hereafter.

The transient species with maxima at 380 and 630 nm was assigned to the radical cation species of 2-NOA, 2-NOA$^{\bullet+}$, through ^{1}2-NOA*, as has been well documented for naphthalene and naphthalene derivatives [9,10,12-14]. As observed in Figure 3A-10a, in oxygen saturated solutions the signals at 380 and 630 nm still persist, contrary to the maximum at 430 nm that disappeared almost completely. The decay at 380 and 630 nm follows a bi-exponential fit with clear short and long components (Figure 3A-10b). At 380 nm, both the 2-NOA radical cation and the triplet excited state absorbs; however, the kinetic decays of the two species are very different (Figure 3A-10b). The radical cation is long lived, with lifetimes in the range of 10 μs, while the triplet state decays faster in oxygenated solutions. Moreover, in oxygenated solutions the decays fit well mono-exponential rate laws that correspond to the unique disappearance of the radical cation.
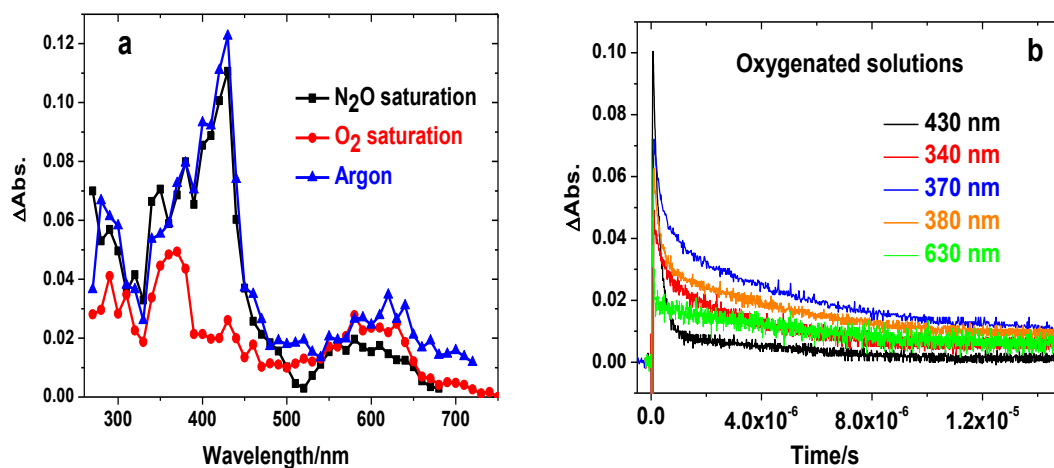
Figure 3A-10 a) Transient absorption spectra obtained 500 ns after laser flash excitation at 266 nm of argon, oxygen and N$_2$O saturated solutions of 2-NOA in water. b) Respective kinetic decay profiles of the transient absorption bands at 430, 340, 380 and 630 nm obtained 500 ns after laser pulse for oxygenated solutions of 2-NOA in water.

As observed in Figure 3A-10a, the band with maximum at 630 nm decays more rapidly in the presence of nitrous oxide (N$_2$O) than with oxygen. This is in agreement with the assignment to the absorption of the hydrated electron (e$^-$), which is known to start to occur at this wavelength. At 630 nm both the hydrated electron and the 2-NOA radical cation absorb, although with different kinetic decays. In oxygenated solutions the decay fitted well a bi-exponential with two clear behaviors, a fast and a slow component (Figure 3A-10b). The hydrated electrons disappear by reaction with oxygen (lifetime $\cong 4\times10^{-8}$ s) in the first μs following the pulse end, whereas the radical cations are long-lived species [10].

The formation of a transient species with maximum absorbance at 720 nm was observed just after the laser pulse which was attributed to hydrated electron, in agreement with several previous reports on naphthalene and its derivatives [10,14]. It rapidly disappeared in the presence of molecular oxygen and when N$_2$O was used as electron scavenger. Figure 3A-11a shows the decay profile at 720 nm of the hydrated electron in 2-NOA de-aerated solution with a constant rate of 3.38×10^6 s^{-1}. To determine whether the formation of the hydrated electron is due to a mono or bi-photonic process, the absorbance of the hydrated electron at 720 nm was measured as a function of the laser energy upon excitation of 2-NOA solution at 266 nm. As shown in Figure 3A-11b, at laser energies < 18 mJ the variation is linear and the hydrated electron is clearly formed through a monophotonic process. For laser energies greater

than 18 mJ the absorbance starts to loss linearity with laser energy, suggesting the occurrence of biphotonic or multiphotonic processes. Therefore, all further nanosecond laser flash photolysis studies were carried out in the monophotonic region, at laser energies < 18 mJ.
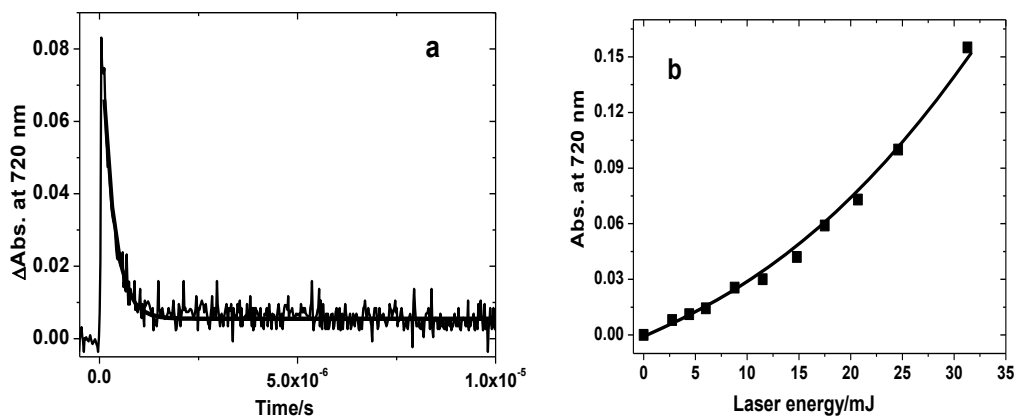
Figure 3A-11 a) Transient absorption signal of the hydrated electron at 720 nm measured with laser intensity of 15 mJ for a 2-NOA de-aerated aqueous solution (time scale 1 μs/div). b) Evolution of the absorbance of the hydrated electron as function of laser energy at 720 nm.

The formation of the hydrated electron (e⁻) is thought to occur mainly by formation of ^{1}2-NOA* through a photoionisation process, as observed with similar compounds [12,13], forming the 2-NOA cation radical (Scheme 3A-1). In the presence of molecular oxygen, the hydrated electron quickly reacts to produce superoxide anion radical ($O_2^{\bullet-}$). Superoxide anion has been shown to be capable of dehalogenating some pesticides and undergoes a variety of oxidation and reduction reactions with other organic and inorganic substrates [15,16]. However, its major fate in natural waters is probably disproportionation to hydrogen peroxide (H_2O_2) and oxygen.
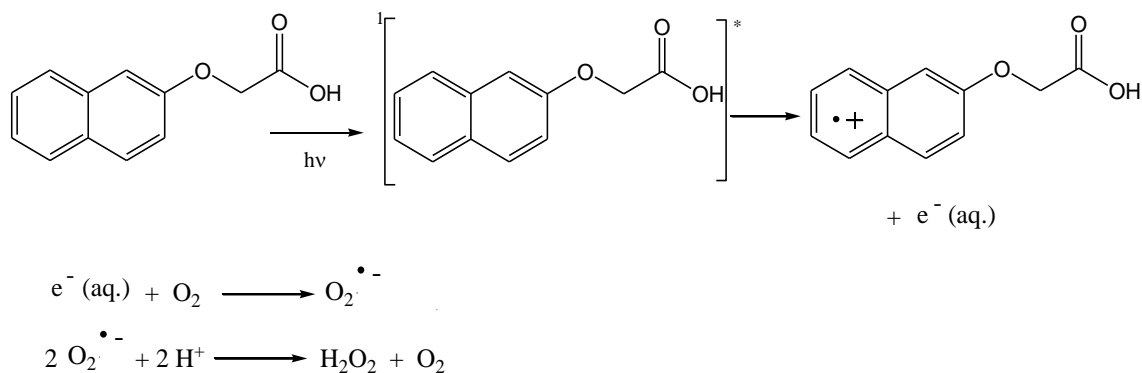
Sheme 3A-1 Photoionization process of 2-NOA in de-aerated aqueous solution.

The decay of the hydrated electron fitted a single exponential and was dependent on oxygen concentration, as shown in Figure 3A-12. From this, a bimolecular rate constant of 1.55×10^{10} L mol^{-1} s^{-1} was determined (reaction 3A.2), which is in good agreement with the literature data, 1.9×10^{10} L mol^{-1} s^{-1} [17].

$$e^{-}_{(aq.)} + O_2 \rightarrow O_2^{\bullet-} \qquad\qquad (3A.2)$$
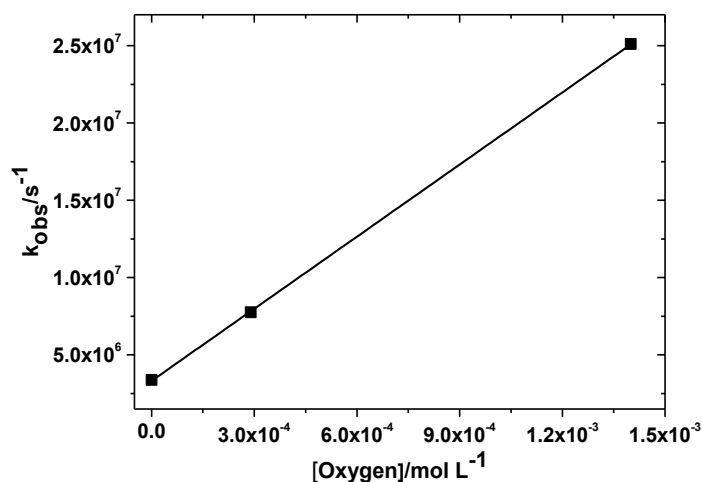
Figure 3A-12 Calculation of the bimolecular quenching rate constant k_q for the hydrated electron at 720 nm as function of oxygen concentration.

The quantum yield of formation of the hydrated electron, ϕ_{e^-}, was also evaluated for 2-NOA in water by using two chemical actinometers as reference: benzophenone in acetonitrile ($\varepsilon_{525\ nm} = 6500$ L mol^{-1} cm^{-1}; $\phi_T = 1.0$ [5]) and the cobalt complex [Co(NH$_3$)$_5$ Br]$^{2+}$ ($\varepsilon_{360\ nm} \cong 9300$ L mol^{-1} cm^{-1} [19]; $\phi_T = 0.30$ [18]). 2-NOA and [Co(NH$_3$)$_5$ Br]$^{2+}$ aqueous solutions, and benzophenone solution in acetonitrile were prepared with absorbances $\cong 0.6$. After de-aerating with argon, the solutions were excited with the nanosecond laser at 266 nm and the absorbance of each solution at the maximum absorption wavelength was measured as function of laser energy. For 2-NOA this corresponds to the maximum wavelength of the hydrated electron (720 nm) while for BP it corresponds to the maximum wavelength of the triplet excited state (525 nm) [5]. The photoexcitation at 266 nm of an aqueous solution of [Co(NH$_3$)$_5$ Br]$^{2+}$ results in the formation of the ligand derived radical intermediate Br$_2^-$, which has it maximum absorption wavelength at 360 nm [19]. The plot of the respective absorbance *vs* laser energy gave a linear line as displayed in Figure 3A-13.
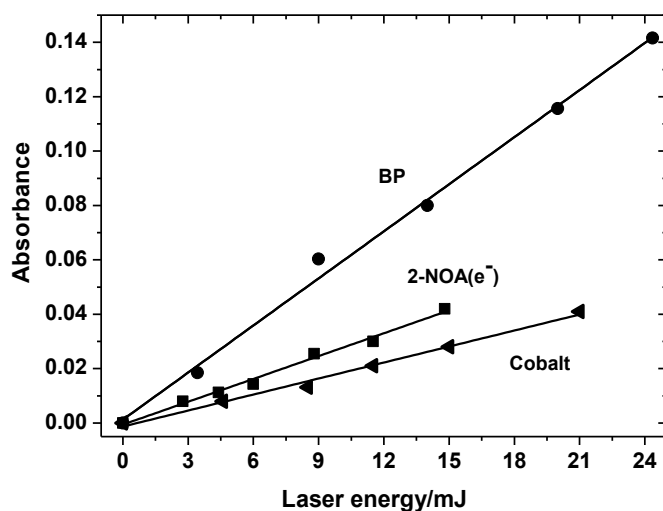
Figure 3A-13 Plot of absorbance *vs* laser energy for de-aerated solutions of: (■) 2-NOA in water at 720 nm (hydrated electron), (●) BP in acetonitrile at 525 nm and (◄) cobalt complex in water at 360 nm.

The slope of each curve is equal to the product of $\varepsilon \times \phi$. Since all the solutions have the same absorbance, the quantum yield of hydrated electron ϕ_{e^-} can be determined for 2-NOA, for each actinometer, by the following relation (3A.3):

$$\varepsilon_{actinometer} \times \phi_{actinometer} \times slope_{e^-} = \varepsilon_{e^-} \times \phi_{e^-} \times slope_{actinometer} \qquad (3A.3)$$

Taking the extinction coefficient of the hydrated electron as 22700 L mol^{-1} cm^{-1} [20], the quantum yield of the hydrated electron ϕ_{e^-} was determined to be 0.155 with the actinometer BP and 0.170 with the actinometer cobalt complex. The ϕ_{e^-} values obtained with these two actinometers, within experimental errors, suggest that this is a reliable value.

3A.4.4 Determination of the triplet state molar absorption coefficients and quantum yields

The triplet state molar absorption coefficients of 2-NOA, ε_T, in the various solvents were estimated by the energy transfer method [21] using benzophenone as triplet donor. This is chosen due to its high triplet quantum yield ($\varepsilon_{520\ nm} = 6500$ L mol^{-1} cm^{-1}; $\phi_T = 1.0$; $E_T = 287$ kJ mol^{-1} (2.98 eV) [5]). Figure 3A-14 shows the transient absorption spectra of a de-aerated solution of BP in acetonitrile (2.0×10^{-3} mol L^{-1})

containing 2-NOA (1.0×10^{-4} mol L^{-1}), determined at different times after excitation by a 355 nm laser pulse. Under these conditions the laser light is totally absorbed by BP to form its triplet excited state, $^3BP^*$ (reaction 3A.4).
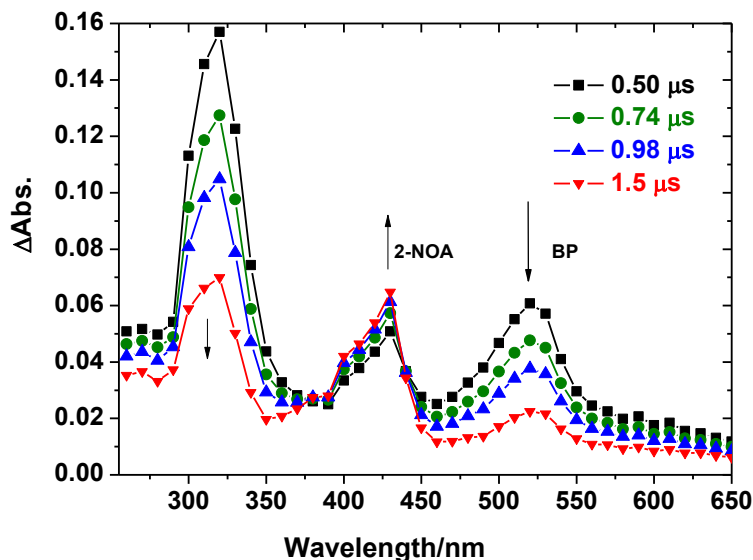
Figure 3A-14 Transient spectra observed at various times after exciting a de-aerated solution of benzophenone (2.0×10^{-3} mol L^{-1}) containing 2-NOA (1.0×10^{-4} mol L^{-1}) in acetonitrile with pulsed laser radiation at 355 nm.

The transient spectra show three bands with absorption maxima at 320, 430 and 520 nm. The bands at 320 and 520 nm are in good agreement with the formation of benzophenone triplet excited state in acetonitrile [5]. The band at 430 nm is identical to that obtained upon excitation with a 266 nm laser pulse of 2-NOA de-aerated aqueous solution (see Figure 3A-8a). This supports the earlier attribution of the band at 430 nm to the 2-NOA triplet excited state. Moreover, as illustrated in Figure 3A-14, the spectra of at successive times show a decrease of the absorption bands at 520 and 320 nm with a simultaneous increase of the band at 430 nm, indicative of triplet energy transfer from $^3BP^*$ to 2-NOA with formation of 2-NOA triplet excited state, ^{3}2-NOA*, according to reaction (3A.5):

$$BP + h\nu \longrightarrow {}^1BP^* \xrightarrow{\text{isc}} {}^3BP^* \tag{3A.4}$$

$$^3BP^* + 2\text{-NOA} \longrightarrow {}^3 2\text{-NOA}^* + BP \tag{3A.5}$$

This experiment was repeated with various concentrations of 2-NOA (6.0×10^{-5}-4.0×10^{-4} mol L^{-1}) maintaining a constant BP concentration (2.0×10^{-3} mol L^{-1}). The decay rate at 520 nm of $^3BP^*$ was found to be linear with 2-NOA concentration, as shown in Figure 3A-15. The quenching rate constant for the energy transfer process between BP and 2-NOA given by the slope of this curve is equal to 8.7×10^9 L mol^{-1} s^{-1}, corresponding to a diffusion controlled triplet-triplet energy transfer in a collisional process. From consideration of energetic effects on the rate [22] this indicates that the triplet energy of 2-NOA must be significantly less than that of benzophenone (2.98 eV), in agreement with results from phosphorescence in this solvent which gives a triplet state energy of 2.72 eV.
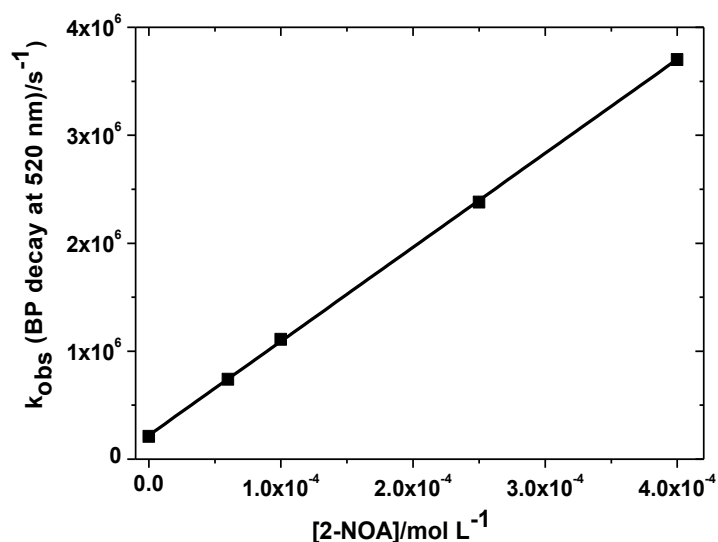
Figure 3A-15 Calculation of the bimolecular quenching rate constant of energy transfer process between benzophenone and 2-NOA.

The molar absorption coefficient of 2-NOA triplet excited state ε_T was calculated based on the previous experiment using benzophenone as donor (D) and 2-NOA as acceptor (A), according to the equation (3A.6):

$$\frac{\varepsilon_T^D}{\varepsilon_T^A} = \frac{\Delta OD^D}{\Delta OD^A} \tag{3A.6}$$

A molar absorption coefficient of 11550 L mol^{-1} cm^{-1} was obtained for ^{32}-NOA* in acetonitrile at 430 nm. Assuming that this coefficient is constant and independent of solvent, this value was used to calculate the quantum yield of triplet excited state

formation ϕ_T (or intersystem crossing quantum yield ϕ_{isc}) of 2-NOA in the different solvents by the comparative method [23], in which de-aerated naphthalene solution in methylcyclohexane ($\phi_T = 0.75$; $\varepsilon_T = 13200$ L mol^{-1} cm^{-1}) was used as reference [5]. The triplet quantum yield was calculated according to the equation (3A.7). Further details on these calculations are given in the experimental part, Chapter 8.

$$\phi_{T,S} = \frac{\varepsilon_T^R}{\varepsilon_T^S} \frac{\Delta OD_T^S}{\Delta OD_T^R} \frac{n_S^2}{n_R^2} \phi_{T,R} \qquad (3A.7)$$

The determined ϕ_T values for 2-NOA in water, ethylene glycol, methanol, acetonitrile, chloroform and 1,4-dioxane are summarized in previous Table 3A-3. The ϕ_T values are slightly dependent on solvent polarity, and vary from 0.318 in water to 0.490 in 1,4-dioxane. This indicates that the non-radiative process of intersystem crossing is an important solvent dependent decay pathway of 2-NOA single excited, which may be relevant to its photoreactivity.

3A.5 Singlet oxygen measurements

In order to ascertain if 2-NOA is able to produce singlet oxygen ($^1O_2$), time resolved phosphorescence with emission monitored at 1270 nm was used to determine the singlet oxygen formation quantum yield (ϕ_Δ) of 2-NOA in water and in the organic solvents. For the determination of ϕ_Δ, optically matched aerated solutions of 2-NOA in various solvents were irradiated with a laser pulse at 266 nm using as reference biphenyl solution in cyclohexane ($\phi_\Delta = 0.73$) [24], as explained in Chapter 8. Biphenyl was chosen rather than the more commonly used phenalenone standard because of its stronger absorption at the excitation wavelength within the accessible concentration range. The time-resolved phosphorescence emission intensity of these samples at 1270 nm was measured at different laser pulse energies and extrapolated to the start of the decay. Since all solutions have the same absorbance at the excitation wavelength, for any given laser energy, the number of photons absorbed by any solution will be the same. Individual singlet oxygen luminescence traces were signal averaged and fitted using a single exponential function to yield the luminescence intensity. The phosphorescence intensity was then plotted against the laser energy [25], which gave straight lines whose slopes (I^S) were compared with that obtained from the reference

biphenyl (I^R), yielding relative singlet oxygen quantum yields, ϕ^S_Δ, using the following equation (3A.8):

$$\phi^S_\Delta = \phi^R_\Delta \, \frac{I^S}{I^R} \, \frac{Abs^R}{Abs^S} \, \frac{n^2_S}{n^2_R} \tag{3A.8}$$

The relative ϕ^S_Δ values obtained for 2-NOA reported in Table 3A-4 show a dependence on solvent polarity and vary between 0.063 in water to 0.271 in non-polar solvent such as 1,4-dioxane. The ϕ^S_Δ appears to increase with the decrease of solvent polarity. Although these values are not high, they are within the range of values already reported for other naphthalene derivatives [26].

Table 3A-4 Singlet oxygen quantum yield formation (ϕ_Δ) for 2-NOA as function of solvent polarity.

Solvent	$\phi_\Delta{}^{*}$
Water	0.063
D_2O	0.060
Ethylene glycol	0.174
Methanol	0.152
Acetonitrile	0.232
Chloroform	0.184
1,4-Dioxane	0.271

*Estimated errors ± 10 %

No effect was observed on the ϕ_Δ value when water was replaced by deuterated water, even though the lifetime in deuterated water is 20 times longer than in H_2O [27]. The ϕ_Δ values are smaller than those of the triplet quantum yield ϕ_T (see Table 3A-3), providing evidence of a relatively low efficiency of energy transfer from ^{3}2-NOA[*] to molecular oxygen to produce $^1O_2$ (reaction 3A.9). Therefore, it is likely that quenching of 2-NOA triplet excited state by molecular oxygen in polar solvents (such as water) also involves other pathways such as electron transfer (to produce the superoxide anion radical and 2-NOA radical cation) (reaction 3A.10), both of which could be implicated in the photodegradation of this compound in water, although the contribution of singlet

oxygen for 2-NOA photodegradation will be less important than other routes due to its formation with low quantum yield.

$$^3\text{2-NOA}^* + {}^3\text{O}_2 \rightarrow \text{2-NOA} + {}^1\text{O}_2 \qquad \text{Triplet-triplet energy transfer} \qquad (3\text{A}.9)$$

$$^3\text{2-NOA}^* + {}^3\text{O}_2 \rightarrow \text{2-NOA}^{\bullet+} + \text{O}_2^{\bullet-} \qquad \text{Electron transfer} \qquad (3\text{A}.10)$$
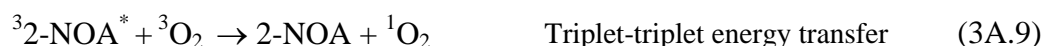
3A.6 Quenching of singlet and triplet excited states by molecular oxygen

The quenching of excited states of aromatic molecules by molecular oxygen is a well-recognized and an important process [11,28-30]. Therefore, studies were undertaken to assess to what extent oxygen quenches the singlet (^{1}2-NOA*) and triplet (^{3}2-NOA*) excited states of 2-NOA. The bimolecular rate constants for quenching of ^{1}2-NOA* by molecular oxygen, $k_S^{O_2}$, were determined in the various solvents through a Stern-Volmer plot of the fluorescence intensity ratios for oxygenated, aerated and de-aerated solutions *vs* oxygen concentration. A linear fit was obtained with a slope equal to the Stern-Volmer coefficient K_{SV} (= $k_S^{O_2} \times \tau_F$). Given that the fluorescence lifetimes of 2-NOA are already known (see Table 3A-2) it is possible to calculate the values of $k_S^{O_2}$. In addition, the bimolecular rate constants for quenching of ^{3}2-NOA* by molecular oxygen, $k_T^{O_2}$, were calculated from the following equation (3A.11):

$$k_{obs} = k_0 + k_T^{O_2} [O_2] \qquad (3\text{A}.11)$$

where k_{obs} and k_0 are the observed first-order rate constants for the decay of 2-NOA triplet excited state at the absorption maximum for each solvent in the presence and absence of oxygen, respectively, and [O$_2$] is the oxygen concentration in each solvent [5]. The plot of the observed triplet rate constants k_{obs} *vs* the oxygen concentration gives a linear fit for all solvents, with the slope equal to $k_T^{O_2}$. Table 3A-5 summarizes the quenching rate constants determined for both singlet and triplet excited states of 2-NOA by molecular oxygen.

Table 3A-5 Determined quenching rate constants by molecular oxygen of the singlet and triplet excited states of 2-NOA, $k_S^{O_2}$ and $k_T^{O_2}$, respectively, as function of solvent polarity.

Solvent	$k_S^{O_2}$ (L mol^{-1} s^{-1}) *	$k_T^{O_2}$ (L mol^{-1} s^{-1}) *
Water	1.54×10^{10}	3.08×10^9
Ethylene glycol	1.57×10^{10}	3.95×10^9
Methanol	1.69×10^{10}	3.13×10^9
Acetonitrile	1.38×10^{10}	3.40×10^9
Chloroform	1.51×10^{10}	1.33×10^9
1,4-Dioxane	1.78×10^{10}	2.46×10^9

*Estimated errors ± 10%

The results show that the bimolecular quenching rate constants of 2-NOA excited states vary over a wide range (10^8 to 10^{10} L mol^{-1} s^{-1}), in agreement with literature data for various aromatic molecules such as naphthalene and its derivatives [5]. Furthermore, the quenching rate constants of ^{1}2-NOA* by molecular oxygen, $k_S^{O_2}$, approach the diffusion controlled limiting rate constant, k_{diff}, and present higher values than those obtained for the deactivation of ^{3}2-NOA*, $k_T^{O_2}$. This difference is related with the spin statistical factor that in triplet excited state is $(1/9) \times k_{diff}$ while for singlet excited states it is 1, as frequently observed in aromatic systems [31]. Surprisingly, the $k_T^{O_2}$ presents the highest value in ethylene glycol, the most viscous solvent. If the process is truly diffusion controlled, according to the Debye-Smoluchowski equation (see Chapter 1) this relation should be the inverse. The value was reproducible, and it seems possible that in this solvent some static quenching may also be present. For oxygen quenching reactions, both energy transfer and electron transfer can be considered producing the very reactive species $^1O_2$ [32,33] and $O_2^{\bullet-}$, respectively (reactions 3A.9 and 3A.10). This suggestion is supported by the experimental results obtained by laser flash photolysis and by the results on singlet oxygen measurements. Literature studies on quenching of triplet state of naphthalene derivatives and formation of singlet oxygen [34] also corroborate this idea.

3A.7 Fluorescence quenching by inorganic anions

A variety of species can induce the quenching of the fluorescence of aromatic molecules such as 2-NOA through deactivation of the singlet excited states [35,36]. This may be relevant to the degradation of 2-NOA under environmental conditions. Therefore, the quenching of 2-NOA fluorescence with some halide ions was studied to obtain insights into mechanisms that may be involved in its excited state deactivation, with a consequent contribution to 2-NOA photochemical fate under environmental conditions. In addition, the effect of the pH on the fluorescence quenching was also assessed since 2-NOA can exist in anionic or cationic form. Aqueous solutions of different concentrations of KI, KBr and KCl were added to a 2-NOA solution (2.0×10^{-5} mol L^{-1}). These solutions were then de-aerated and the fluorescence emission spectra were recorded. The quenching rate constant, k_q, was determined by the known Stern-Volmer relationship (3A.12):

$$\frac{I_0}{I} = 1 + K_{SV}[Q] \qquad (3A.12)$$

where [Q] represents the quencher concentration, I_0/I is the ratio of 2-NOA emission fluorescence intensity without and with the respective quencher and K_{SV} is the Stern-Volmer coefficient ($= k_q \times \tau_F$). Figure 3A-16 shows, as example, the effect of the quencher KI in 2-NOA emission fluorescence.
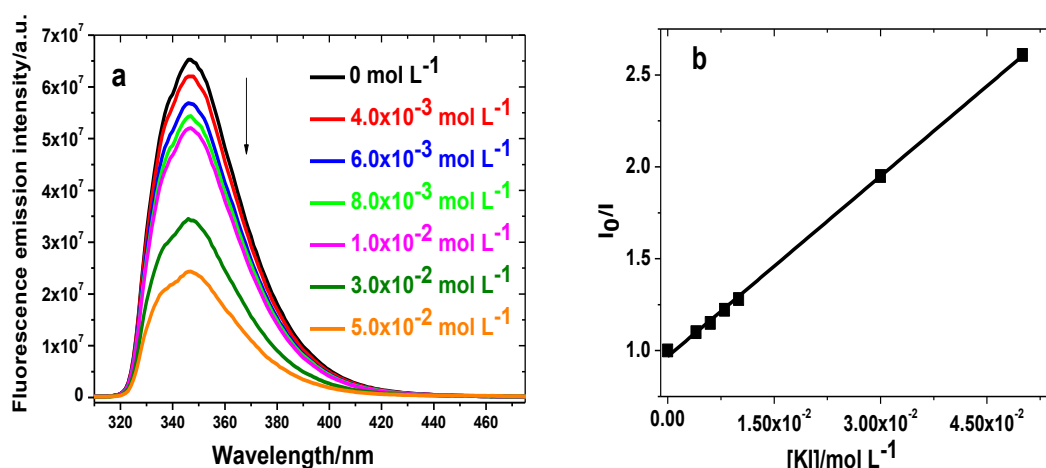
Figure 3A-16 a) Quenching of fluorescence emission of 2-NOA aqueous solution (2.0×10^{-5} mol L^{-1}) by KI at pH 5.5. b) Respective Stern-Volmer plot ($K_{SV} = 32.7$ L mol^{-1}).

As observed in the Figure3A-16a, the addition of increasing concentrations of KI causes the decrease of the fluorescence intensity due to the quenching process. The excitation spectra in the presence of KI are identical to the excitation and absorption spectra in absence of it, confirming no ground state complexation. A plot of I/I_0 *vs* [Q] gives a straight line with the slope equal to the Stern-Volmer constant (Figure 3A-16b), supporting a dynamic quenching mechanism.

Similar behavior was observed with KBr, however, no significant change on the fluorescence intensity of 2-NOA was observed upon KCl addition, showing that Cl^- is not effective in quenching 2-NOA fluorescence. Since the fluorescence lifetimes of 2-NOA have been measured at the three different pH it is possible to calculate the quenching rate constants of 2-NOA through the relation $K_{SV} = k_q \times \tau_F$. These results are summarized in Table 3A-6.

Table 3A-6 Fluorescence lifetimes (τ_F), Stern-Volmer constants (K_{SV}) and fluorescence quenching rate constants (k_q) for 2-NOA singlet excited state by KI and KBr in water as function of pH.

pH	$\tau_{(2\text{-NOA})}$ (ns)	K_{SV} (L mol^{-1}) KI	k_q (L mol^{-1} s^{-1}) KI	K_{SV} (L mol^{-1}) KBr	k_q (L mol^{-1} s^{-1}) KBr
1.35	8.42	55.9	6.64×10^9	4.08	4.85×10^8
5.5	10.3	32.7	3.17×10^9	1.97	1.91×10^8
9.4	9.66	37.3	3.86×10^9	2.95	3.14×10^8

KI is a more efficient quencher than KBr with quenching rates of the order of 10^9 L mol^{-1} s^{-1}. This is in agreement with the reduction potential of the $X^\bullet/X^-$ couple, which is 1.33 V for I^- [37], 1.92 V for Br^- [37] and 2.41 V for Cl^- [37] (E^o values *vs* the normal hydrogen electrode (NHE)) and suggest that electron transfer may be involved in the quenching. However, there may also be some contribution from the heavy atom effect. The Stern-Volmer constant presents a higher value in acidic conditions than at the two other pH values. This may be due in part to decreased collisional quenching by the anionic halide ions when 2-NOA is in its anionic and cationic form. These results support the existence of the anionic form at pH > pKa of 2-NOA. Consequently, studies were undertaken using $CuCl_2$ as quencher in order to check the effect of the cation,

particularly with the anionic form of 2-NOA. It was observed that $CuCl_2$ quenches more efficiently the fluorescence of 2-NOA at pH 5.5 (K_{SV} = 193 L mol^{-1}; k_q = 1.87×10^{10} L mol^{-1} s^{-1}) than at pH 1.35 (K_{SV} = 51.6 L mol^{-1}; k_q = 6.13×10^9 L mol^{-1} s^{-1}). However, when the studies were carried out in alkaline conditions (9.4) the solutions precipitate due to the formation of an insoluble copper complex.

To check if this behavior is still observed when 2-NOA is protected, 2-NOA was incorporated in β-CD and the quenching effect of $CuCl_2$ was measured at the different pH values. Lower quenching rates were obtained for the complex β-CD/2-NOA than in absence of β-CD, evidencing the protective effect of the β-CD. For pH 5.5 the k_q was of 1.12×10^{10} L mol^{-1} s^{-1} (K_{SV} = 116 L mol^{-1}) while for pH 1.35 a k_q value of 5.09×10^9 L mol^{-1} s^{-1} (K_{SV} = 43 L mol^{-1}) was obtained. However, for basic pH, the formation of a precipitate was still observed, which means that in this case the incorporation of 2-NOA in β-CD does not prevent the formation of the complex. The quenching effect of KI, the most efficient quencher under our experimental conditions, was also tested on the complex β-CD/2-NOA as function of pH. The results are given in Table 3A-7.

Table 3A-7 Fluorescence lifetimes (τ_F), Stern-Volmer constants (K_{SV}) and fluorescence quenching rate constants (k_q) for the complex β-CD/2-NOA in presence of the quencher KI as function of pH.

pH	$\tau_{(NOA+\beta\text{-}CD)}$ (ns)	K_{SV} (L mol^{-1}) (β-CD + KI)	k_q (L mol^{-1} s^{-1}) (β-CD + KI)
1.4	11.1	34.0	3.06×10^9
5.5	10.9	20.4	1.87×10^9
9.4	10.8	26.4	2.44×10^9

The results show an increase on the fluorescence lifetimes of 2-NOA as well as a decrease of the K_{SV} by a factor of approximately 1.6 when 2-NOA forms an inclusion complex with β-CD. These highlight the protective effect of β-CD on the 2-NOA fluorescence against the quencher KI.

3A.8 Deactivation processes of 2-NOA excited states

From all above data, it has been possible to fully characterize the photophysical deactivation routes of 2-NOA excited states. As discussed in Chapter 1, the deactivation channels include the radiative processes of fluorescence and phosphorescence and the non-radiative processes of internal conversion (ic) and intersystem crossing (isc). A further important process in deactivation of 2-NOA excited state is the photoionization process, as evidenced by laser flash photolysis.

The radiative rate constants k_R (= ϕ_F/τ_F) and non-radiative rate constants k_{NR} (= $1-\phi_F/\tau_F$) determined for 2-NOA singlet excited state in each solvent are summarized in Table 3A-8, using the fluorescence quantum yields and lifetime values taken from Table 3A-2. From k_R values, it was possible to calculate the natural radiative lifetimes (τ^0_{nat} = $1/k_R$) of ^{1}2-NOA* in each solvent. These were found to vary in the range of 33 to 124 ns, which are considerable greater than the experimental fluorescence lifetimes, τ_F. The reason relays in the fact that these theoretical values consider the emission of light as the only process deactivating the singlet excited state of 2-NOA, excluding the non-radiative processes. Consequently, this emphasizes that the non-radiative (ic or isc) routes play a main role in the deactivation process of ^{1}2-NOA*.

Table 3A-8 Determined radiative (k_R) and non-radiative (k_{NR}) rate constants decay, natural radiative lifetime (τ^0_{nat}), non-radiative rate constants decay for internal conversion (k_{ic}) and for intersystem crossing (k_{isc}) and quantum yield of internal conversion (ϕ_{ic}) of ^{1}2-NOA* in water and in organic solvents.

Solvent	k_R (s^{-1})	τ^0_{nat} (ns)	k_{NR} (s^{-1})	ϕ_{ic}	k_{ic} (s^{-1})	k_{isc} (s^{-1})
Water	1.20×10^7	83.4	8.54×10^7	0.559	5.45×10^7	3.10×10^7
Ethylene glycol	2.96×10^7	33.8	5.84×10^7	0.216	1.90×10^7	3.92×10^7
Methanol	1.68×10^7	59.2	6.13×10^7	0.447	3.49×10^7	2.60×10^7
Acetonitrile	1.79×10^7	55.9	5.04×10^7	0.303	2.06×10^7	2.98×10^7
Chloroform	8.90×10^6	123	2.81×10^8	0.579	1.67×10^8	1.14×10^8
1,4-Dioxane	1.87×10^7	53.4	5.63×10^7	0.261	1.96×10^7	3.68×10^7

Furthermore, the quantum yield of internal conversion, ϕ_{ic}, was calculated from the relationship $\phi_F + \phi_T + \phi_{ic} = 1$, which assumes that only these three processes jointly deactivate the ^{1}2-NOA*. Moreover, the rate constants for the non-radiative processes ic and isc, k_{ic} (= ϕ_{ic}/τ_F) and k_{isc} (= ϕ_T/τ_F), may be also calculated since the values of ϕ_F and of ϕ_T are known (see Table 3A-2 and Table 3A-3). Therefore, Table 3A-8 summarizes all the photophysical parameters estimated for the deactivation of ^{1}2-NOA* in the different solvents.

As noticed, the non-radiative rate constants k_{NR} are higher than the radiative rate constants k_R in all the solvents, with a different contribution of the ic or isc processes for the deactivation, depending on the solvent. Contrary to what was observed with the other solvents, chloroform presents a huge difference between the radiative rate constant (8.90×10^6 s^{-1}) and the non-radiative rate constant (2.81×10^8 s^{-1}), which can be explained by the low fluorescence quantum yield measured in this solvent. In water, in particular, the ic is the dominant deactivation mode of the singlet excited state of 2-NOA, as given by its high ϕ_{ic} (0.559), while in organic solvents the isc predominates, with the exception of chloroform and methanol. From comparison of ϕ_F, ϕ_{ic} and ϕ_{isc} values (Table 3A-2, 3A-3 and 3A-8) for the organic solvents, ϕ_{ic} is greater than ϕ_F (except in ethylene glycol), but the dominant pathway of ^{1}2-NOA* deactivation involves isc processes for ethylene glycol, acetonitrile and 1,4-dioxane.

Since all the deactivation pathways of 2-NOA excited states have been characterized, it is possible to summarize the processes by a Perrin-Jablonski diagram, as exemplified in Figure 3A-17 for the solvent water.
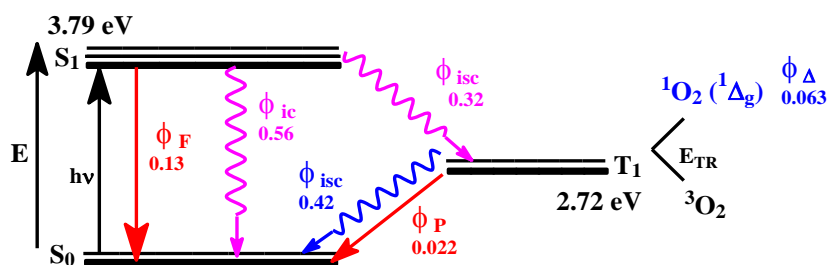
Figure 3A-17 Perrin-Jablonski diagram for 2-NOA de-aerated solution in water.

3A.9 Conclusions

A comprehensive study has been accomplished on 2-NOA photophysics in water and organic solvents from which several conclusions are made: i) although 2-NOA presents fluorescence, its singlet excited state decays preferentially by the non-radiative processes of internal conversion and intersystem crossing in all the solvents, ii) in water and methanol the predominant non-radiative deactivation process is the internal conversion, iii) laser flash photolysis shows the formation of 2-NOA triplet excited states with reasonable quantum yields in all the solvents, iv) the triplet excited state also decays mainly by intersystem crossing, v) in water, a photoionization process occurs yielding the formation of the reactive species hydrated electron (quantum yield of 0.16), 2-NOA radical cation and superoxide anion, vi) 2-NOA excitation leads to the formation of singlet oxygen through triplet sensitization, predominantly in non-aqueous solvents, but also occurs in water, vii) triplet excited state is quenched by molecular oxygen in all the solvents; the quenching mechanism in water may involve energy transfer with formation of singlet oxygen and electron transfer with formation of superoxide anion. These reactive species may be involved in the mechanism of 2-NOA degradation, although the contribution of singlet oxygen will be minor due to its formation with low quantum yield.

3A.10 References

[1] C. Pimentel, Hydrogen bonding and electronic transitions: the role of the Franck-Condon principle. *J. Am. Chem. Soc.*, **1957**, 79, 3323-3326.

[2] N. S. Bayliss, E. G. McRae, Solvent effects in organic spectra: dipole forces and the Franck-Condon principle. *J. Phys. Chem.*, **1954**, 58, 1002-1006.

[3] S. Nagakura, H. Baba, Dipole moments and near ultraviolet absorption of some monosubstituded benzenes-the effect of solvents and hydrogen bonding. *J. Am. Chem. Soc.*, **1952**, 74, 5693-5698.

[4] European Food Safety Authority (EFSA), Conclusion on the peer review of the pesticide risk assessment of the active substance 2-naphthyloxyacetic acid, *EFSA Journal* 9, 2152, **2011**.

[5] M. Montalti, A. Credi, L. Prodi, M. T. Gandolfi, *Handbook of Photochemistry*, third edition, Taylor & Francis Group, Florida, **2006**.

[6] A. B. Sánchez, Nuevos métodos luminescentes para la determinación de pesticidas en aguas. Dissertation, Universidad de Extremadura, Badajoz, **2001**.

[7] K. M. C. Davis, M. F. Farmer, Charge transfer complexes. Part V. Nature of interaction of halogenomethanes and aromatic hydrocarbons. *J. Chem. Soc. B*, **1968**, 1968, 859-862.

[8] J. W. Eastman, S. J. Rehfeld, Interaction of benzene molecule with liquid solvents. Fluorescence quenching parallels (0-0) ultraviolet absorption spectroscopy. *J. Phys. Chem.*, **1970**, 74, 1438-1443.

[9] R. McNeil, J. T. Richards, J. K. Thomas, The laser flash photolysis of naphthalene and 1,2-benzanthracene. *J. Phys. Chem.*, **1970**, 74, 2290-2294.

[10] O. Brahmia, C. Richard, Phototransformation of carbaryl in aqueous solution. Laser flash photolysis and steady state studies. *J. Photochem. Photobiol. A: Chem.*, **2003**, 156, 9-14.

[11] L. K. Patterson, G. Porter, M. R. Topp, Oxygen quenching of singlet and triplet states. *Chem. Phys. Lett.*, **1970**, 7, 612-614.

[12] R. McNeil, J. T. Richards, J. K. Thomas, The laser flash photolysis of naphthalene and 1,2-benzanthracene. *J. Phys. Chem.*, **1970**, 74, 2290-2294.

[13] D. Vialaton, C. Richard, D. Baglio, A.-B. Paya-Perez, Mechanism of the photochemical transformation of naphthalene in water. *J. Photochem. Photobiol. A: Chem.*, **1999**, 123, 15-19.

[14] F. Boscá, N. Canudas, M. L. Marín, M. A. Miranda, A photophysical and photochemical study of 6-methoxy-2-naphthylacetic acid, the major metabolite of the phototoxic nonsteroidal antinflammatory drug nabumetone. *Photochem. Photobiol.*, **2000**, 71, 173-177.

[15] W. M. Draper, D. G. Crosby, Photochemical generation of superoxide radical anion in water. *J. Agric. Food Chem.*, **1983**, 31, 734-737.

[16] J. M. Burns, W. J. Cooper, J. L. Ferry, D. W. King, B. P. DiMento, K. McNeill, C. J. Miller, W. L. Miller, B. M. Peake, S. A. Rusak, A. L. Rose, T. D. Waite, Methods for reactive oxygen species (ROS) detection in aqueous environments. *Aquat. Sci.*, **2012**, 74, 683-734.

[17] E. J. Hart, M. Anbar, *The hydrated electron*, Wiley-Interscience, **1970**.

[18] J. F. Endicott, G. J. Ferraudi, J. R. Barber, Charge transfer spectroscopy, redox energetics, and photoredox behavior of transition metal ammine complexes. Critical comparison of observations with mechanisms and models. *J. Phys. Chem.*, **1975**, 79, 630-643.

[19] G. L. Hug, *Optical spectra of nonmetallic inorganic transient species in aqueous solution*, National Standard Reference Data System, Washington, D. C., **1981**.

[20] P. M. Hare, E. A. Price, D. M. Bartels, Hydrated electron extinction coefficient revised. *J. Phys. Chem. A*, **2008**, 112, 6800-6802.

[21] R. Bensasson, E. J. Land, Triplet-triplet extinction coefficients via energy transfer. *Trans. Faraday Soc.*, **1971**, 67, 1904-1915.

[22] F. Scandola, V. Balzani, Energy-transfer processes of excited states of coordination compounds. *J. Chem. Educ.*, **1983**, 60, 814-823.

[23] B. Amand, R. Bensasson, Determination of triplet quantum yields by laser flash absorption spectroscopy. *Chem. Phys. Lett.*, **1975**, 3, 44-48.

[24] M. Kristiansen, R. D. Scurlock, K. Long Lu, P. R. Ogilby, Charge-transfer state and singlet oxygen ($^1\Delta_g$ O_2) production in photoexcited organic molecule-molecular oxygen complexes. *J. Phys. Chem.*, **1991**, 95, 5190-5197.

[25] R. Bonnett, D. J. McGarvey, A. Harriman, E. J. Land, T. G. Truscott, U. -J. Winfield, Photophysical properties of *meso*-tetraphenylporphyrin and *meso*-tetra(hydroxyphenyl)-porphyrins. *Photochem. Photobiol.*, **1988**, 48, 271-276.

[26] F. Wilkinson, W. P. Helman, A. B. Ross, Quantum yields for the photosensitized formation of the lowest electronically excited singlet state of molecular oxygen in solution. *J. Phys. Chem. Ref. Data*, **1993**, 22, 13-262.

[27] P. R. Ogilby, C. S. Foote, Chemistry of singlet oxygen. 42. Effect of solvent, solvent isotopic substitution, and temperature on the lifetime of the singlet molecular oxygen ($^1\Delta_g$). *J. Am. Chem. Soc.*, **1982**, 104, 2069-2070.

[28] J. B. Birks, *Photophysics of Aromatic Molecules*, Wiley-Interscience, London, New York, **1970**.

[29] F. Wilkinson, Quenching of electronically excited states by molecular oxygen in fluid solution. *Pure Appl. Chem.*, **1997**, 69, 851-856.

[30] F. Wilkinson, A. F. Olea, D. J. McGarvey, D. R. Worrall, Quenching of excited states of aromatic hydrocarbons and their derivatives by oxygen. *J. Braz. Chem. Soc.*, **1995**, 6, 211-220.

[31] J. G. Calvert, J. N. Pitts, *Photochemistry*, Wiley, New York, **1966**.

[32] A. A. Abdel-Shafi, D. R. Worrall, F. Wilkinson, Singlet oxygen formation efficiencies following quenching of excited singlet and triplet states of aromatic hydrocarbons by molecular oxygen. *J. Photochem. Photobiol. A: Chem.*, **2001**, 142, 133-143

[33] D. R. Kearns, Physical and chemical properties of singlet molecular oxygen. *Chem. Rev.*, **1971**, 71, 395-427.

[34] R. Schmidt, F. Shafii, C. Schweitzer, A. A. Adbel-Shafi, F. Wilkinson, Charge transfer and non-charge transfer processes competing in the sensitization of singlet oxygen: formation of $O_2(^1\Sigma g^+)$, $O_2(^1\Delta g)$ and $O_2(^3\Sigma g^-)$ during oxygen quenching of triplet excited naphthalene derivatives. *J. Phys. Chem. A*, **2001**, 105, 1811-1817.

[35] A. R. Watkins, Kinetics of fluorescence quenching by inorganic anions. *J. Phys. Chem.*, **1974**, 78, 2555-2558.

[36] H. Shizuka, M. Nakamura, T. Morita, Anion-induced fluorescence quenching of aromatic molecules. *J. Phys. Chem.*, **1980**, 84, 989-994.

[37] D. M. Stanbury, Reduction potentials involving inorganic free radicals in aqueous solution. *Adv. Inorg. Chem.*, **1989**, 33, 69-138.

3B. Direct UV and simulated solar light degradation

3B.1 Introduction

This chapter describes the results of the direct photodegradation of the plant growth regulator 2-naphthoxyacetic acid (2-NOA) in water under UV and simulated solar light excitation (Suntest). The influence of oxygen concentration and excitation wavelength on the rate of degradation, as well as the involvement of singlet oxygen and superoxide anion radical as reactive species on the transformation process is reported. The disappearance of 2-NOA and formation of photoproducts was followed by UV-vis absorption spectroscopy and by high performance liquid chromatography with diode array detection (HPLC-DAD). Furthermore, mass-mass spectrometry was used to identify the photoproducts formed. The identification of the photoproducts allows us to establish the photolytic pathways involved, thus providing valuable information on possible ways of protecting the environment. A mechanism of photodegradation for 2-NOA under direct UV excitation is proposed based on the combination of these results along with those obtained by laser flash photolysis studies reported in Chapter 3A.

3B.2 Direct UV and simulated solar light degradation

3B.2.1 Observation by UV-visible absorption spectra

As mentioned in Chapter 3A, 2-NOA presents two main absorption bands in aqueous solution with maximum wavelengths centred at 270 and 324 nm. As depicted in Figure 3B-1, under our experimental conditions ([2-NOA] = 3.0×10^{-4} mol L^{-1}) the lower energy absorption band of 2-NOA overlaps to some extent the solar light emission spectra. This suggests that 2-NOA is capable of undergoing photochemical degradation under environmental conditions. To assess this hypothesis, aerated aqueous 2-NOA solution (3.0×10^{-4} mol L^{-1}; pH 3.6) was irradiated using the Sunstest system. Figure 3B-2 presents the evolution of the UV-vis absorption spectra and the kinetics of degradation obtained under these conditions as function of irradiation time.
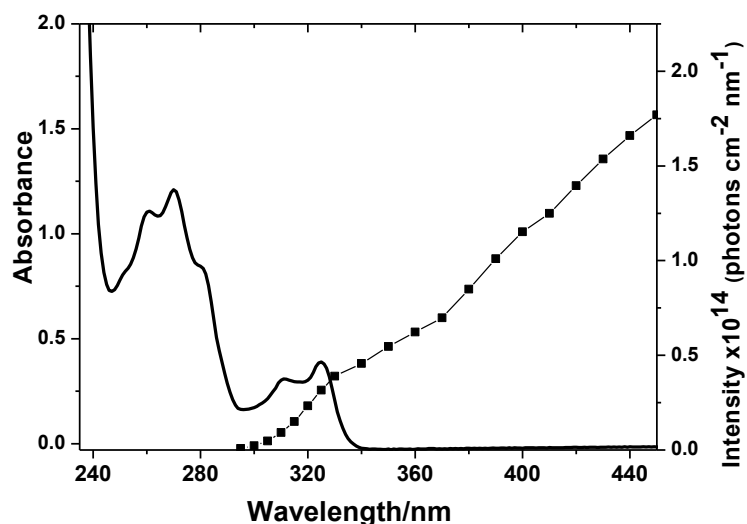
Figure 3B-1 UV absorption spectrum of 2-NOA aqueous solution $(3.0 \times 10^{-4}$ mol L^{-1}) and emission spectrum of solar light (dotted line).

Upon irradiation with the Suntest system, the UV spectra of 2-NOA given in Figure 3B-2a show an increase in absorbance in several regions of the spectra (280-500 nm and 220-260 nm) with irradiation time which can be attributed to the formation of photoproducts that absorb in this wavelength range. Additionally, a decrease in the absorbance at 270 nm is observed corresponding to the degradation of 2-NOA.
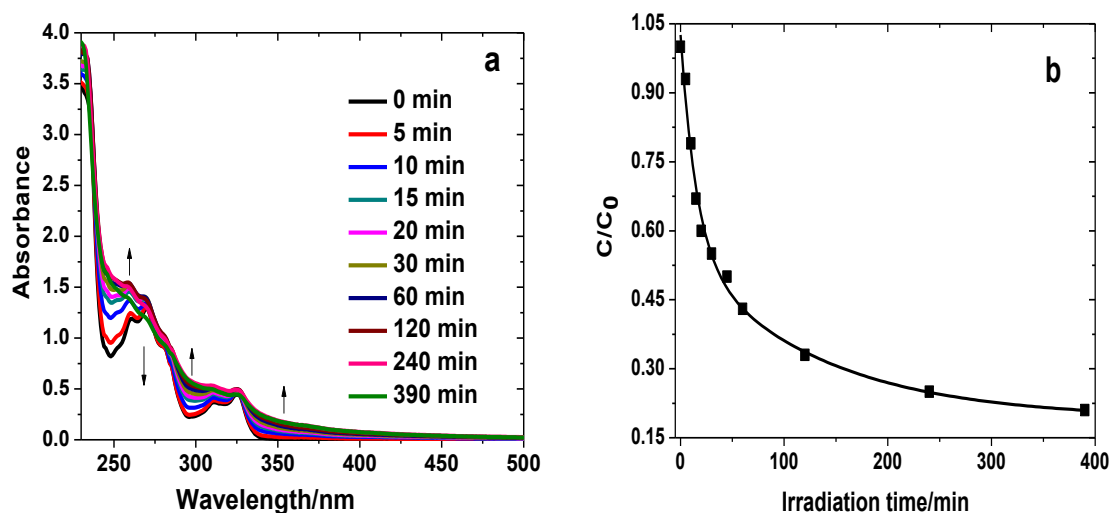
Figure 3B-2 a) Evolution of the UV-vis absorption spectra of aerated aqueous 2-NOA solution $(3.0 \times 10^{-4}$ mol L^{-1}) irradiated with the Suntest during 390 min. b) Respective kinetics of degradation as function of irradiation time followed by HPLC-DAD with detection at 270 nm.

The effective disappearance of 2-NOA is given by the kinetic curve obtained by HPLC analysis (Figure 3B-2b). After 6.5 h of irradiation, 79 % of 2-NOA was transformed into its photoproducts. The kinetics follows a bi-exponential decay and are faster at initial times of irradiation with an estimated first order rate constant of 2.7×10^{-2} min^{-1} and a half-life time of 26 min. For prolonged irradiation times, the degradation rate slows down and the first-order kinetic behavior is lost, probably due to formation of photoproducts that absorb in the same region.

The degradation of aqueous 2-NOA solution (3.0×10^{-4} mol L^{-1}) was further studied upon excitation at 254 nm by using two irradiation systems: i) monochromatic light ii) and a system with up to 6 germicidal lamps that allows working with a larger sample volume (See Chapter 8, section 8.5.2). A preliminary study was conducted in which aqueous 2-NOA solution was irradiated with the 254 nm system with 6 germicidal lamps. Under these conditions, 2-NOA was completely degraded within 90 min of irradiation. Therefore, in order to be able to follow the kinetics of degradation in a reasonable timescale, five lamps were removed and studies were carried out just with one lamp. Consequently, all the results presented hereafter concern the irradiation system at 254 nm with 1 germicidal lamp. Once again, UV-vis spectroscopy was used to follow the changes of 2-NOA spectrum as a function of irradiation time but only as a qualitative technique. For quantitative determinations HPLC-DAD was employed to follow the kinetics of 2-NOA degradation and the formation of photoproducts.

3B.2.2 Kinetics of degradation: effect of oxygen and excitation wavelength

Since it is well documented that oxygen plays an important role in the photodegradation process, the effect of oxygen concentration on 2-NOA transformation was evaluated. Aqueous 2-NOA solutions (3.0×10^{-4} mol L^{-1}) were irradiated under aerated, de-aerated and oxygenated conditions at 254 and 313 nm. The removal and addition of oxygen was carried out by bubbling argon and oxygen, respectively, before and during the course of irradiation. Figure 3B-3 presents the changes observed in the UV-vis absorption spectra of an aerated aqueous 2-NOA solution (3.0×10^{-4} mol L^{-1}) irradiated at 254 nm (1 germicidal lamp).

Figure 3B-3 a) Evolution of the UV-vis spectra of aerated aqueous 2-NOA solution $(3.0 \times 10^{-4}$ mol L^{-1}). b) Respective kinetics of degradation as function of irradiation time followed by HPLC-DAD (λ_{det} = 270 nm) upon irradiation at 254 nm with 1 lamp.

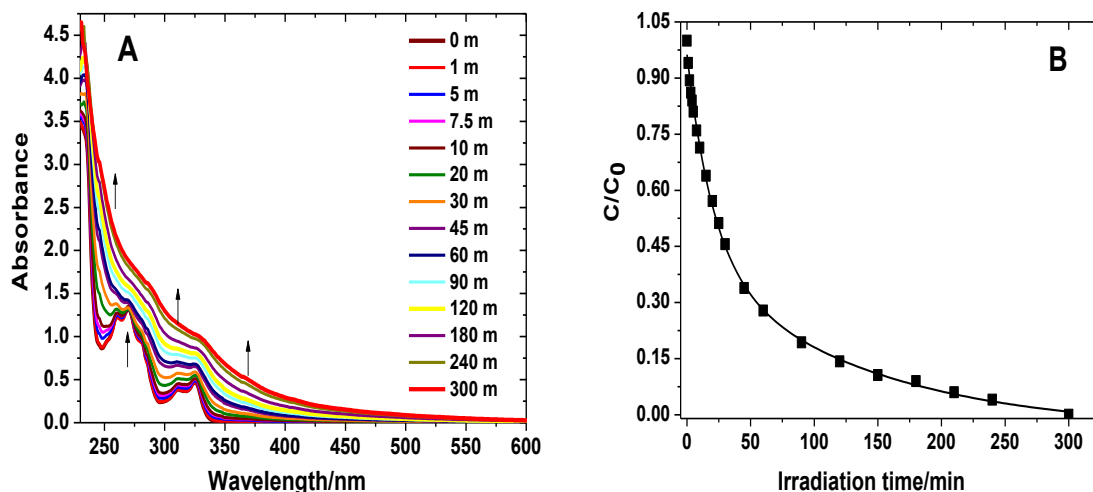An increase in the absorbance with irradiation time is observed over the entire spectrum, including at 270 nm, indicating the formation of products that also absorb at the excitation wavelength. The same trends on the UV-vis absorption spectra of 2-NOA were observed when oxygenated or de-aerated aqueous solutions were employed. The kinetic profile depicted in Figure 3B-3b shows that under aerated conditions 2-NOA is completely transformed after 5 h of irradiation. The degradation follows a bi-exponential decay and is faster at initial times of irradiation with an estimated pseudo-first order rate constant of 5.0×10^{-2} min^{-1} and a half-life of 14 min. The same study was performed for 2-NOA solution in oxygenated and de-aerated conditions and the respective rate constants were also calculated through the linear plot of ln (C/C$_0$) *vs* time (Table 3B-1). The given values express the role played by oxygen on 2-NOA degradation and indicate that the degradation is roughly 1.5 times faster in aerated than in oxygenated or even de-aerated conditions.

The effect of the excitation wavelength on 2-NOA degradation was also studied. The quantum yields of 2-NOA were determined using monochromatic light at 254 and 313 nm as function of oxygen concentration (Table 3B-1). The quantum yields at 313 nm are similar to those obtained at 254 nm, within the experimental errors, indicating that there is no effect of the excitation wavelength on 2-NOA degradation. This means

that the irradiation of 2-NOA at any of its two absorption bands will involve the participation of the same excited species in the degradation process.

Table 3B-1 Quantum yields (ϕ) of degradation and estimated first order rate constant (k) at 254 nm of aqueous 2-NOA solution (3.0×10^{-4} mol L^{-1}) irradiated at 254 and 313 nm as function of oxygen concentration [1].

Conditions	$[O_2]$ (mol L^{-1}) 20 °C	$\phi_{254\,nm}$*	k (min)** 254nm	$\phi_{313\,nm}$
Aerated	2.9×10^{-4}	$0.011 \pm 1.1 \times 10^{-3}$	5.0×10^{-2}	$0.012 \pm 1.4 \times 10^{-3}$
Oxygenated	1.39×10^{-3}	$0.0079 \pm 1.2 \times 10^{-3}$	3.1×10^{-2}	$0.0070 \pm 1.8 \times 10^{-3}$
De-aerated	$< 10^{-5}$	$0.0068 \pm 2.0 \times 10^{-3}$	2.7×10^{-2}	$0.0062 \pm 1.5 \times 10^{-3}$

* Monochromatic light at 254nm; ** 254 nm irradiation system with 1 germicidal lamp

The quantum yields at 254 and 313 nm in aerated conditions are roughly 1.5 times higher than in oxygenated and under de-aerated conditions. These results are consistent with the previous kinetics of degradation. This suggest that although 2-NOA triplet excited state (^{3}2-NOA*) may participate in the degradation process, it is not the main route of degradation.

3B.2.3 Reactive species involved in 2-NOA degradation

3B.2.3.1 Assessment of singlet oxygen participation

The photophysical studies given in Chapter 3A demonstrate that 2-NOA is able to produce $^1O_2$ in aqueous solution ($\phi_\Delta = 0.063$). Hence, in order to ascertain the involvement of $^1O_2$ on 2-NOA degradation process Rose Bengal was used as $^1O_2$ photosensitizer (as already explained in Chapter 2B for NAD). An aerated aqueous 2-NOA solution (3.0×10^{-4} mol L^{-1}) was irradiated with monochromatic light at 547 nm in presence of Rose Bengal (6.0×10^{-6} mol L^{-1}). The reaction was followed by HPLC-DAD with detection at 270 nm. The obtained kinetic profile is given in Figure 3B-4a. After 50 h 30 min of irradiation, 8.2 % of 2-NOA was transformed with the appearance of new peaks on the chromatogram corresponding to the formation of photoproducts (Figure 3B-4b). This suggests the involvement of $^1O_2$ in 2-NOA degradation, although as a

minor pathway, in agreement with the results given in Chapter 3A. $^1O_2$ is most probably formed through triplet-triplet energy transfer between molecular oxygen and triplet excited state of 2-NOA (reaction 3B.1). $^1O_2$ reacts then with 2-NOA to originate oxidation products (reaction 3B.2).

$$^3\text{2-NOA}^* \ + \ ^3O_2 \ \rightarrow \text{2-NOA} \ + \ ^1O_2 \tag{3B.1}$$

$$\text{2-NOA} \ + \ ^1O_2 \ \rightarrow \text{Oxidation products} \tag{3B.2}$$
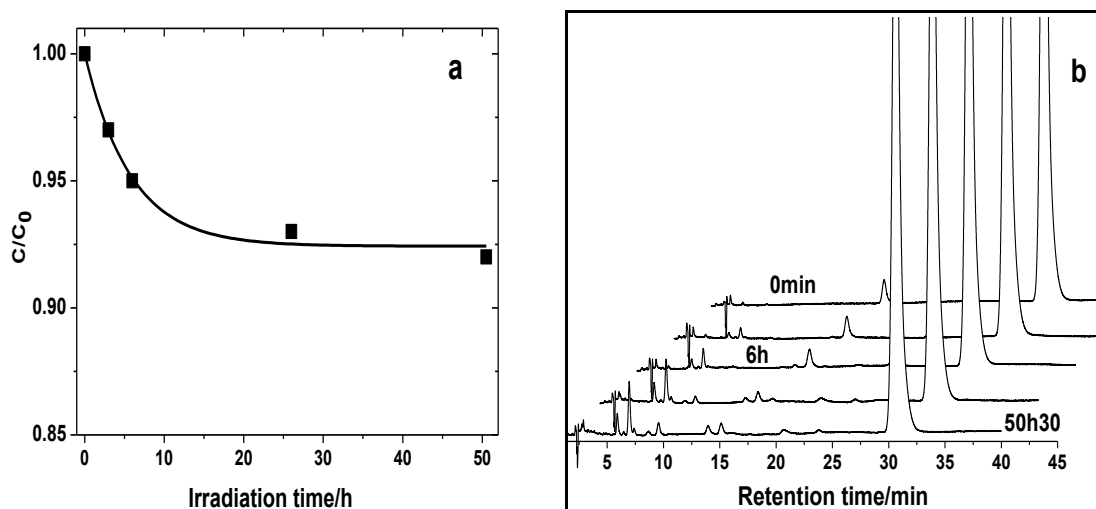
Figure 3B-4 a) Influence of Rose Bengal (6.0×10^{-6} mol L^{-1}) on the degradation kinetics of aerated aqueous 2-NOA solution (3.0×10^{-4} mol L^{-1}) as function of irradiation time ($\lambda_{ex} = 547$ nm). b) Respective HPLC-DAD chromatogram as function of irradiation time ($\lambda_{det} = 270$ nm, t_{ret} 2-NOA = 31 min).

3B.2.3.2 Assessment of superoxide anion radical participation

The previous results obtained by laser flash photolysis (Chapter 3A) provide evidence for the photoionization of 2-NOA to form its radical cation and the hydrated electron. It is well established that the latter species will react with molecular oxygen to form superoxide anion ($O_2^{\bullet -}$). Ultimately, hydrogen peroxide (H_2O_2) and oxygen will be formed by the disproportionation of $O_2^{\bullet -}$. Therefore, in order to evaluate the involvement of $O_2^{\bullet -}$ in 2-NOA transformation pathway, the formation of H_2O_2 was determined by the Lazrus method [2] as already explained in Chapter 2B. Figure 3B-5 reports the evolution of H_2O_2 concentration upon irradiation of aerated aqueous 2-NOA solution at 254 nm. An increase on the H_2O_2 concentration with irradiation time was

observed, even at early stages, supporting the previous assumption concerning the participation of $O_2^{\bullet-}$ in the degradation mechanism.
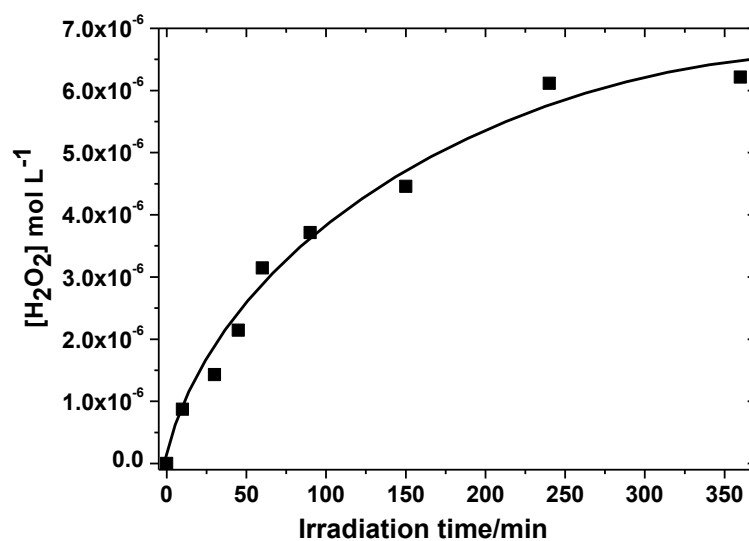
Figure 3B-5 Evolution of H_2O_2 formation of aerated aqueous 2-NOA solution (1.0×10^{-5} mol L^{-1}) upon 254 nm irradiation (system with 1 germicidal lamp).

3B.2.4 Photoproduct identification

The intermediate products formed upon excitation of an aqueous 2-NOA solution (3.0×10^{-4} mol L^{-1}, pH 3.6) under aerated, de-aerated and oxygenated conditions were analyzed. The HPLC-DAD chromatograms of aqueous 2-NOA solution excited at 254 nm as function of irradiation time under aerated and de-aerated conditions (retention time of 2-NOA = 31 min) are depicted in Figure 3B-6. Under these conditions the photolysis of 2-NOA generates several photoproducts. A careful inspection of the chromatograms reveals that eight main products with the same retention times are formed under the two conditions, although with different rates. Moreover, more products are formed under aerated than de-aerated media, as shown by the greater amount of peaks present in the region with retention times less than 8 min. Their earlier elution indicates that these products must be more polar then the main products. All these same products were observed when irradiation was carried out in oxygenated conditions (chromatogram not presented here). Moreover, these products were also identical to those formed when 2-NOA was subject to Sunstest irradiation in aerated conditions. Therefore, HPLC-MS/MS analysis with ES in negative and positive mode

was conducted only in aerated and de-aerated conditions. The products were identified by the molecular ion and mass fragment ions.
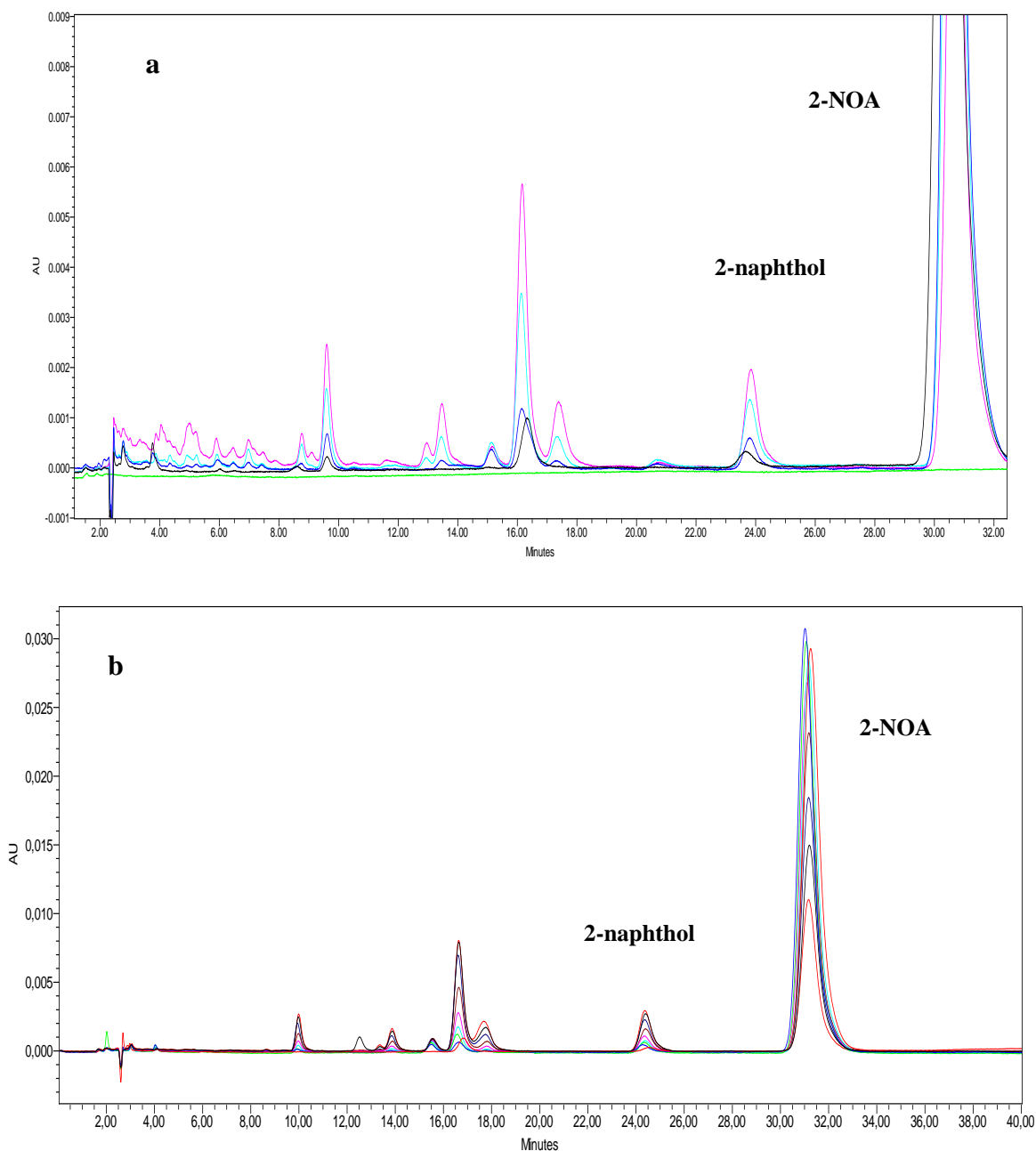
Figure 3B-6 HPLC-DAD chromatograms (λ_{det} = 270 nm) of aqueous 2-NOA solution (3.0×10^{-4} mol L^{-1}) irradiated at 254 nm as function of irradiation time in a) aerated (purple line - 10 min of irradiation) and b) de-aerated conditions (red line - 20 minutes of irradiation).

The kinetic evolution of 2-NOA products was followed under aerated and de-aerated conditions, as illustrated in Figure 3B-7. 2-NOA products are formed in higher amount in de-aerated than aerated solution, and also seems to disappear faster in the absence of oxygen.
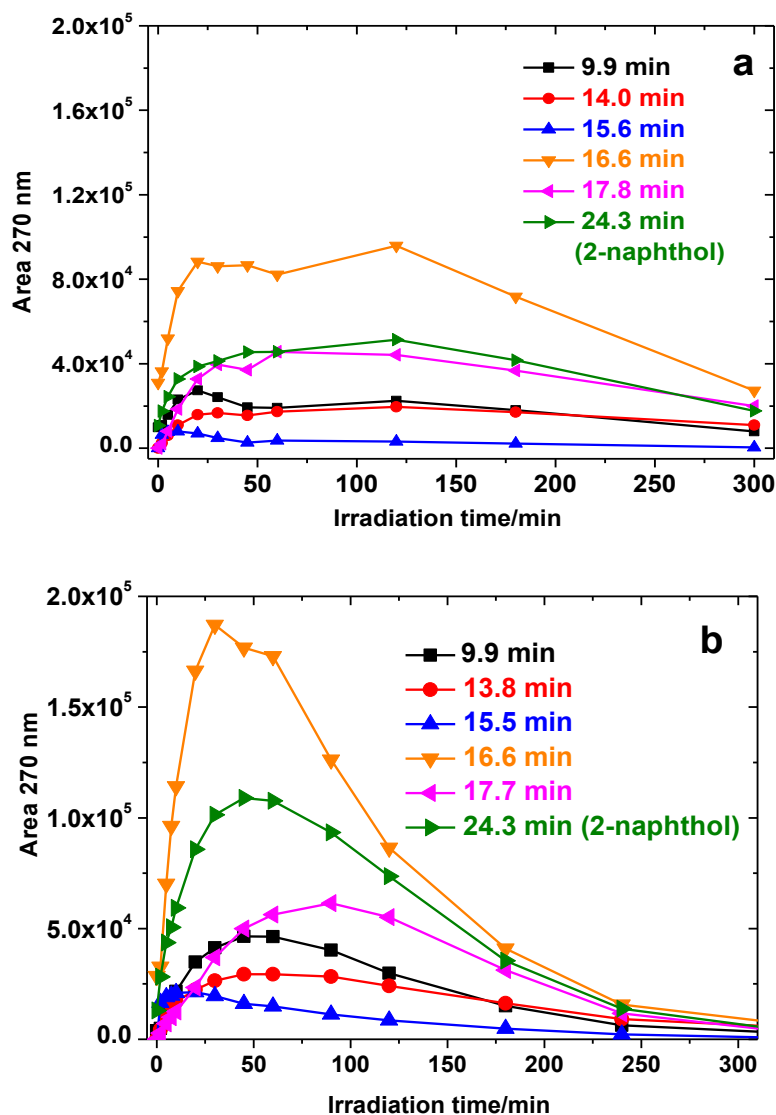
Figure 3B-7 Kinetics of products formation of aqueous 2-NOA solution irradiated at 254 nm in a) aerated and b) de-aerated conditions.

Characterization of the product 2-naphthol

The product with retention time 24.3 min was assigned to 2-naphthol by comparison of its UV-vis spectrum (λ_{max} = 273 and 324 nm) and retention time with that of the commercially available product. The initial solution of 2-NOA already contains small amount of 2-naphthol arising from 2-NOA hydrolysis. The quantification of 2-naphthol concentration formed during the first 60 min of irradiation under aerated and de-aerated conditions was done through construction of a calibration curve. As observed in Figure 3B-7, 2-naphthol is formed in larger amounts in de-aerated than in aerated solution which may be explained by the competing reaction with oxygen, leading to the

formation of radicals which inhibit this process. 2-naphthol is one of the major primary products of 2-NOA degradation accounting for 6.0 % of 2-NOA disappearance.
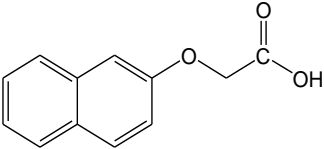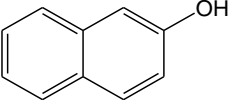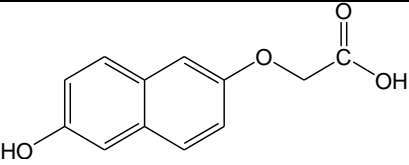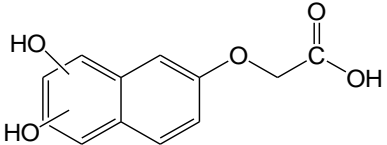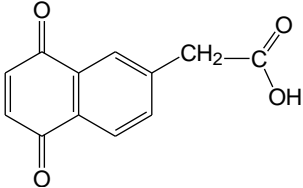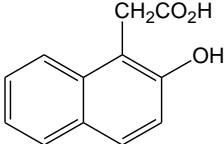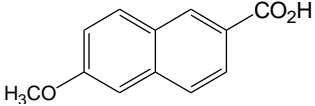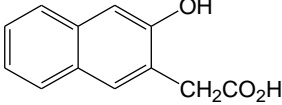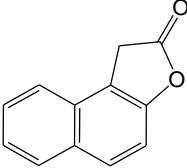
The irradiation of aerated aqueous 2-naphthol solution (1.0×10^{-4} mol L^{-1}) was also performed at 254 nm in order to verify if some of 2-NOA products arise from the degradation of 2-naphthol. The HPLC-DAD chromatograms depicted in Figure 3B-8 show common peaks at 9.9 and 17.7 min when 2-NOA (aerated and de-aerated) and 2-naphthol (aerated) are irradiated at the same wavelength. The 2-naphthol products with elution times less than 8.0 min also seem to be similar to those obtained for 2-NOA irradiated under aerated conditions (blue line).
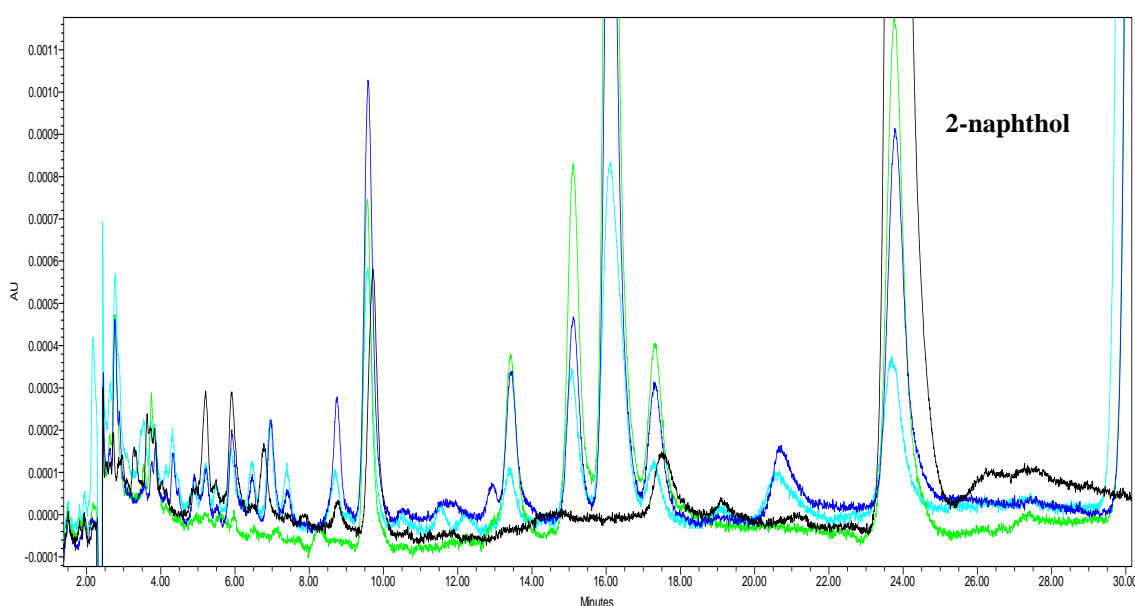
Figure 3B-8 HPLC-DAD chromatograms (λ_{det} = 270 nm) of aqueous 2-NOA solution (3.0×10^{-4} mol L^{-1}) irradiated under aerated (blue line, $t_{irrad\ 254\ nm}$ = 5 min) and de-aerated (green line, $t_{irrad\ 254\ nm}$ = 5 min) conditions, and 2-naphthol aqueous solution irradiated at 254 nm under aerated conditions (black line, $t_{irrad\ 254\ nm}$ = 5 min).

In Table 3B-2 are gathered the retention times, *m/z* ratio and suggested structures for some of the identified products analyzed by LC-MS/MS with ES⁻ and ES⁺ mode. The elution program used here is different from that used in the previous chromatograms and, therefore, the retention times are different. Under these conditions 2-NOA was eluted at 12.8 min whereas the products were eluted at lower retention times.

Table 3B-2 Retention time (t_{ret}), *m/z* and proposed structure of the main photoproducts identified by LC-MS/MS.

t_{ret} (min)	*m/z*	Molecular mass	Proposed structure
12.8	201/157/143/ (ES$^-$)	202	(2-NOA)
11.8	-	-	
8.79	217/173 (ES$^-$)	218	
10.48	233/175/159		
10.7	235/1597131 (ES$^+$)	234	
9.2	215/187/159 (ES$^-$) ($\lambda_{max.} = $ 316 nm)	216	
8.6	201/157		
9.8	201/157	202	
11.0	201/157 (ES$^-$)		
11.3	185/157/149 (ES+)	184	

(* more probable)

Characterization of products

The mass spectrum of 2-NOA with a retention time of 12.8 min presents a molecular peak [M-H]$^-$ with *m/z* = 201 and a main fragment ion at *m/z* = 143. This corresponds to the loss of the group –CH$_2$CO$_2$H. Three other products were identified with the same [M-H]$^-$ = 201 at times 8.6, 9.8 and 11.0 min. This can be attributed to products coming from a photo-Fries rearrangement, as reported in literature for similar compounds, such as naphthyl acetates [3], napropamide [4,5], 1-naphthyl esters [6], etc. The primary step in the photo-Fries rearrangement is the homolytic dissociation of C-O bond, yielding a pair of radicals. Consecutive rearrangements of these radicals originate products as the ones detected for 2-NOA. One of the products with m/z = 201 may be assigned to the most stable structure proposed in Table 3B-2, the 2-hydroxy-1-acid, in accordance with literature [7]. The product eluted at 11.3 with m/z = 185 can be attributed to naphtho[2,1-*b*]furan-2(1*H*)-one, as proposed in a degradation study performed by Climent *et al.*, in which the products were identified by GC-MS and GC-FTIR [7]. This may be originated from the previous rearranged 2-hydroxy-1-acid compound. The product with *m/z* = 217 eluted at 8.79 min can be assigned to a hydroxylated compound. The proposed structure, 6-hydroxy-(2-naphthoxy) acetic acid, corresponds to the most probable one. This compound was found as a minor metabolite in rat urine but no detection was achieved when the photolysis of 2-NOA was carried out in water [8]. Two compounds detected at 10.48 and 10.7 min with [M-H]$^-$ = 233 can be attributed to di-hydroxylated products based on the fragmentation patterns. Another product was detected (ES$^-$ mode) with elution time of 9.2 min. The fragments indicate the loss of two carbonyl groups and the compound was attributed to a naphthoquinone. The fact that the UV-Vis absorption spectrum presents a band with maximum absorption longer than 300 nm is in accordance with a naphthoquinone structure.

3B.2.5 Proposed mechanism

The following Schemes illustrate the possible steps involved in the formation of 2-NOA products. Under aerated conditions it seems that three reaction pathways are possible. One of the primary steps of 2-NOA degradation appears to be the photo-Fries rearrangement. This rearrangement involves the homolytic cleavage of C-O bond yielding a pair of radicals (Scheme 3B-1a) that further recombine to form rearrangement products. It is also possible to have the cleavage of the C-C bond (Scheme 3B-1b),

although the first predominate to yield 2-naphthol, one of the major products of 2-NOA degradation.
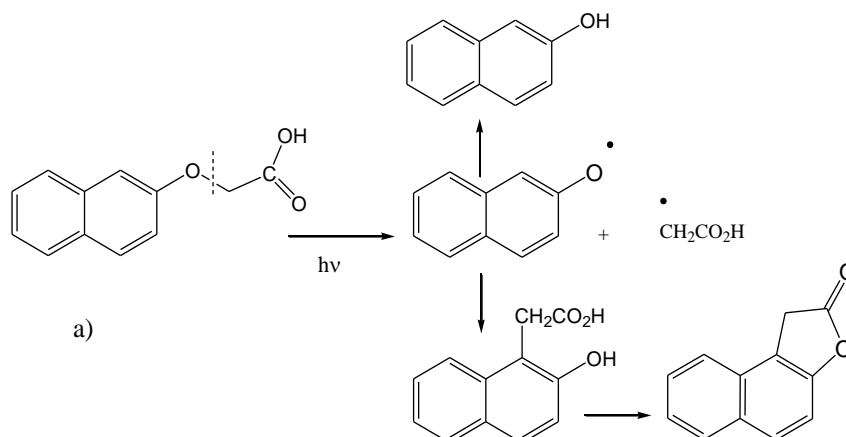
Scheme 3B-1 a) Proposed steps for the formation of 2-NOA products.
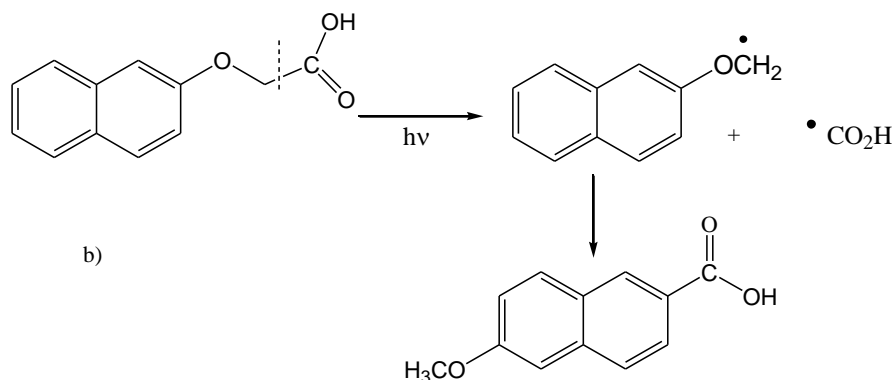
Scheme 3B-1 b) Proposed steps for the formation of 2-NOA products.

The involvement of superoxide anion and singlet oxygen also has to be taken in consideration for the degradation mechanism since their reactivity has been experimentally received evidence from laser flash photolysis studies and by using Rose Bengal as singlet oxygen sensitizer. The photoionization of 2-NOA (and consequently the singlet excited state), can be considered to be another degradation pathway. In this process, both the radical cation and the hydrated electron are produced (Scheme 3B-1c).

In the presence of oxygen, the hydrated electron generates the superoxide anion $(O_2^{\bullet-})$ which is in equilibrium with its protonated form $HO_2^{\bullet}$. These radicals may react with 2-NOA radical and lead to formation of hydroxylated products, after disproportionation. The subsequent reaction with water leads to the formation of di-hydroxylated products (Scheme 3B-1c). The identified naphthoquinone eluted at 9.2 min can be formed by triplet oxidation through the reaction of 2-NOA with $^1O_2$

(Scheme 3B-1d) since the effective participation of this species has been put in evidence with the irradiation in presence of Rose Bengal. This indicates that 2-NOA triplet excited state also participates in the degradation mechanism, although as a minor pathway. Nevertheless, in aerated solutions the formation of naphthoquinone may also involve the photoionization of 2-NOA. The hydrated electron formed in this process may be trapped by oxygen, preventing 2-NOA to be regenerated. Recombination of 2-NOA radical cations (or 2-naphthoxyl radicals) with superoxide anion will ultimately lead to the formation of naphthoquinone. No further in-depth studies were performed by laser flash photolysis to assess if 2-naphthoxyl radicals were formed; however, considering the 2-NOA products and based on literature data [9], it is probable that 2-naphthoxyl radicals are present and contribute to 2-NOA degradation.
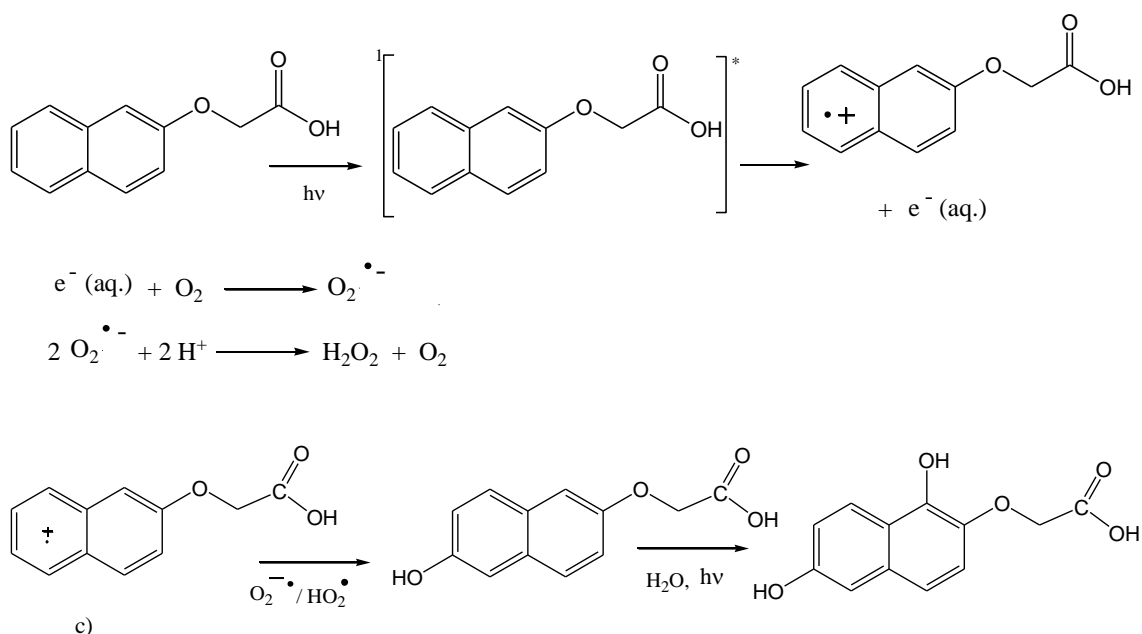
Scheme 3B-1 c) Proposed steps for the formation of 2-NOA products.
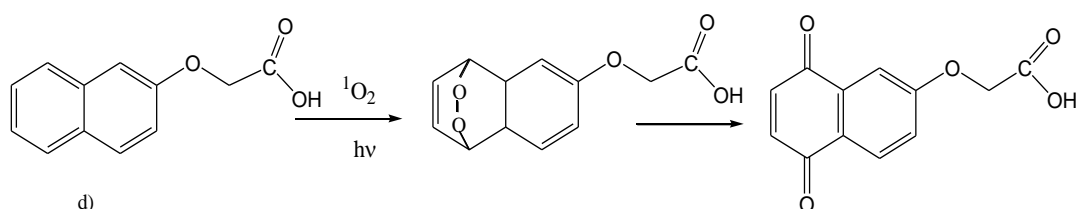
Scheme 3B-1 d) Proposed steps for the formation of 2-NOA products.

3B.3 Conclusions

The photochemical degradation of 2-NOA in water under direct UV and simulated solar light excitation was studied. 2-NOA was effectively transformed under these conditions with a higher rate and quantum yield of degradation in aerated conditions suggesting the involvement of the singlet excited state in 2-NOA photoreactivity. The photoionization of 2-NOA through the singlet excited state leads to the formation of hydrated electron and 2-NOA radical cation, with consequent formation of superoxide anion. These reactive species seem to be involved in the mechanism of degradation yielding several photoproducts. Another primary step of 2-NOA photochemical degradation is the photo-Fries rearrangement, leading to the formation of 2-naphthol as one of the major products, in addition to additional products. The involvement of 2-NOA triplet excited state may also be relevant in aerated solutions, with participation of singlet oxygen as reactive species, as evidenced by the photosensitization experiment with Rose Bengal, yielding the naphthoquinone product.

3B.4 References

[1] M. Montalti, A. Credi, L. Prodi, M. T. Gandolfi, *Handbook of Photochemistry*, third edition, Taylor & Francis Group, Florida, **2006**.

[2] G. L. Kok, K. Thompson, A. L. Lazrus, S. E. McLaren, Derivatization technique for the determination of peroxides in precipitation. *Anal. Chem.*, **1986**, 58, 1195-1194.

[3] I. F. Molokov, Y. P. Tsentalovich, A. V. Yurkovskay, R. Z. Sagdeev, Investigation of the photo-Fries rearrangement reactions of 1- and 2-naphthyl acetates. *J. Photochem. Photobiol. A: Chem.*, **1997**, 110, 159-165.

[4] J. P. Da Silva, E. V. Bastos, L. F. V. Ferreira, R. G. Weiss, Surface photochemistry of the berbicide napropamide. The role of the media and environmental factors in directing the fates of intermediates, *Photochem. Photobiol. Sci.*, **2008**, 7, 69-75.

[5] J. P. Aguer, P. Boule, F. Bonnemoy, J. M. Chezal, Phototransformation of napropamide [*N,N*-diethyl-2-(1-naphthyloxy)propionamide] in aqueous solution: Influence on the toxicity of solutions. *Pestic. Sci.*, **1998**, 54, 253-257.

[6] W. Gu, S. Bi, R. G. Weiss, Photo-Fries rearrangements of 1-naphthyl esters in the glassy and melted states of poly(vinyl acetate). Comparisons with reactions in less polar polymers and low viscosity solvents. *Photochem. Photobiol. Sci.*, **2002**, 1, 52-59.

[7] M. J. Climent, M. A. Miranda, Photodegradation of dichlorprop and 2-naphthoxyacetic acid in water. Combined GC-MS and GC-FTIR Study. *J. Agric. Food Chem.*, **1997**, 45, 1916-1919.

[8] European Food Safety Authority (EFSA), Conclusion on the peer review of the pesticide risk assessment of the active substance 2-naphthyloxyacetic acid, *EFSA Journal* 9, 2152, **2011**.

[9] O. Brahamia, C. Richard, Photochemical transformation of 1-naphthol in aerated aqueous solution. *Photochem. Photobiol. Sci.*, **2005**, 4, 454-458.

Part 2

Photocatalysed degradation of pesticides

Chapter 4

Photocatalysis for water treatment

4.1 Introduction

This Chapter aims to give a general overview of reported advanced oxidation processes (AOPs) employed for the treatment of water pollution, most particularly the branch of photocatalysis which is one of the themes explored within the scope of this thesis. A short introduction is given on polyoxometalates (POMs), a class of compounds that, due to their distinctive redox properties find applications in several fields including as photocatalysts for degradation of organic pollutants. The polyoxometalate decatungstate anion $W_{10}O_{32}^{4-}$ is one of the most widely applied in this field since its UV-vis spectrum partially overlaps that of solar light, which makes it a very interesting compound to be used as green photocatalyst for water treatment. However, its high solubility in water requires its immobilization on solid supports in order to be recyclable. For this, layered double hydroxide (LDH) materials have been chosen as solid support due to their excellent anionic exchange properties. The Chapter finishes with a description of LDHs (properties, applications, synthesis and characterization) and of the methods employed to intercalate POMs in LDH. Examples of practical application of these heterogeneous POM-LDH systems in the photocatalytic degradation of pesticides are also addressed.

4.2 Advanced oxidation processes for water remediation

The presence of pesticides in surface and groundwater has greatly increased over recent years due to their large-scale use in intensive agriculture. Possible sources of pesticide contamination in drinking water supply include agricultural and urban runoffs, pesticide treatment as routine agricultural practice, leaching from pesticide wastes, plant residues contaminated with pesticides and industrial scale pest control operations. Despite their benefits, pesticides still remain an issue of great concern as they are acutely toxic to birds and mammals, and persistent, ending up contaminating surface and ground waters. In view of this, providing clean water and a clean environment is a challenging task. Several classical treatment processes have been investigated for their possible implementation for reducing pesticide concentrations in water to minimize the potential health risks associated with exposure to these chemicals. However, these processes are not efficient since the pollutant is only transformed (sometimes to compounds with higher toxicity) and not mineralized. Therefore, there is great concern

to search for powerful methods to promote their complete degradation and mineralization to environmentally compatible products.

Among the methods described in the literature to reduce the impact of these pollutants in the environment, advanced oxidation processes (AOPs) [1-5] are well known for their oxidizing efficiency, even towards traces of the target compounds, either leading to total mineralization with formation of CO_2, H_2O and inorganic compounds, or at least to their transformation into more harmless products. Furthermore, these processes allow the use of solar light as an irradiation source, making their use more attractive for environmental applications [6,7]. The concept of advanced oxidation processes was first established by Glaze [8] in which "*Advanced oxidation processes are defined as those which involve the generation of hydroxyl radicals in sufficient quantity to affect water purification*".

The AOPs are generally characterized by the use of UV and UV-near visible radiation and/or strong oxidizing agents (O_3, H_2O_2, semiconductors such TiO_2, ZnO and WO_3, polyoxometalates, etc.) which produce the highly reactive hydroxyl radicals $HO^{\bullet}$ that are responsible for the transformation and mineralization of the organic pollutants. The $HO^{\bullet}$ radical is a very reactive, unselective chemical oxidant that attacks rapidly most organic compounds [1,2] often leading to their mineralization with formation of water, carbon dioxide and inorganic anions (reaction 4.1).

$$\text{AOPs} \rightarrow HO^{\bullet} \xrightarrow{\text{pollutant}} CO_2 + H_2O + \text{inorganic anions} \qquad (4.1)$$
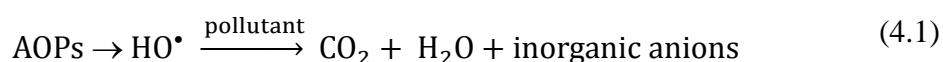
However, unlike the definition given by Glaze, nowadays the designation of AOPs also considers the involvement of other reactive species such as $HO_2^{\bullet}$ and its conjugate base $O_2^{\bullet-}$ in the degradation processes of organic pollutants (pesticides, pharmaceuticals, dyes, etc.). Nevertheless, these radicals are much less reactive than free hydroxyl radicals [2]. In fact, the $HO^{\bullet}$ possesses the highest oxidizing power (E° 2.80 V *vs* NHE (Normal Hydrogen Electrode)) among those species based on oxygen (Table 4-1). Only fluorine gas has a higher standard reduction potential (3.06 V) but it is not used in water treatment.

Table 4-1 Relative reduction potential of some oxidizing species *vs* NHE [9].

Oxidation species	Half-cell reaction	Reduction potential/V
HO$^\bullet$ (Hydroxyl radical)	HO$^\bullet$ + H$^+$ + e$^-$ → H$_2$O	2.80
F$_2$ (Fluorine)	F$_2$ + 2e$^-$ → 2F$^-$	3.06
O$_3$ (Ozone)	O$_3$ (g) + 2H$^+$ + 2e$^-$ → O$_2$ (g) + H$_2$O	2.07
H$_2$O$_2$ (Hydrogen peroxide)	H$_2$O$_2$ + 2H$^+$ + 2e$^-$ → 2H$_2$O	1.77
HO$_2$$^\bullet$ (Hydroperoxyl radical)	HO$_2$$^\bullet$ + H$^+$ + e$^-$ → H$_2$O$_2$ (protonation/deprotonation pK $\cong$ 4.8)	1.70
HClO (Hypochlorous acid)	2HClO + 2H$^+$ + 2e$^-$ → Cl$_2$ + 2H$_2$O	1.49
Cl$_2$ (Chlorine)	Cl$_2$ (g) + 2e$^-$ → 2Cl$^-$	1.36

The HO$^\bullet$ reacts strongly with most organic pollutants by hydrogen abstraction or by electrophilic addition to double bonds to generate organic free radicals. These free radicals can further react with molecular oxygen to give a peroxylradical, initiating a sequence of oxidative degradation reactions which may lead to complete mineralization of the pollutant [10]. In addition, hydroxyl radicals may attack aromatic rings at positions occupied by a halogen, generating a phenol homologue. Although hydroxyl radicals are among the most reactive radicals known, they react slowly with chlorinated alkane compounds.

AOP systems can be divided into photochemical processes (UV/O$_3$, UV/H$_2$O$_2$, etc., photocatalysis by semiconductor material/UV and photo-Fenton reactions), and into chemical oxidation processes in which light is not involved (O$_3$, O$_3$/H$_2$O$_2$, H$_2$O$_2$/Fe^{2+}, etc.). In both cases, the formation of the reactive hydroxyl radicals occurs.

Ozonation and ozone related processes (O$_3$/H$_2$O$_2$, UV/O$_3$), heterogeneous photocatalysis (for example, semiconductor TiO$_2$/UV and polyoxometalates/UV) and homogeneous photocatalysis (Fenton and Fenton-like processes) are considered to be the most efficient for pesticide degradation in water [4,5]. Among these processes, TiO$_2$ and POM photocatalysis exhibit the further advantage of triggering combined oxidation/reduction reactions in a one-pot system. So far, TiO$_2$ has been the most used photocatalyst for degradation of organic pollutants in waters [11,12]. Nevertheless, AOPs have also been widely applied with success in wastewater treatment [3,13] and as water disinfectants [14]. A short description of these processes is given below. More

focus will be given to this branch of photocatalysis since it has been used in this thesis to access the photocatalytic degradation of the pesticides under study.

4.2.1 Processes based on hydrogen peroxide and UV radiation

These processes can be: H_2O_2/UV, Fenton ($H_2O_2/Fe^{2+}(Fe^{3+})$) and photo-Fenton ($H_2O_2+Fe^{2+}/Fe^{3+}+UV$).

H_2O_2/UV

In this method, hydroxyl radicals are generated by the photolysis of H_2O_2 in presence of UV light at 253.7 nm (reaction 4.2):

$$H_2O_2 \overset{h\nu}{\rightarrow} 2\ HO^\bullet \tag{4.2}$$

with subsequent propagation reactions (4.3 to 4.5).:

$$H_2O_2 + HO^\bullet \rightarrow HO_2^\bullet + H_2O \tag{4.3}$$

$$H_2O_2 + HO_2^\bullet \rightarrow HO^\bullet + O_2 + H_2O \tag{4.4}$$

$$2HO_2^\bullet \rightarrow H_2O_2 + O_2 \tag{4.5}$$
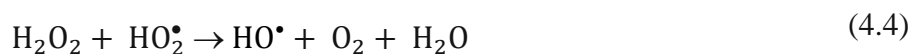
Hydrogen peroxide can decompose in another way, through the reaction (4.6):

$$H_2O_2 + H^\bullet \rightarrow H_2O + HO^\bullet \tag{4.6}$$

and the hydroxyl radical may also recombine (reaction 4.7):

$$2HO^\bullet \rightarrow H_2O_2 \tag{4.7}$$

The H_2O_2/UV system can totally mineralize any organic compound, transforming it into CO_2 and water.

4.2.2. Processes based in ozone and UV radiation

These processes include photo-ozonation (O_3/UV) and combination of photo-ozonation and hydrogen peroxide -UV irradiation ($O_3/H_2O_2/UV$).

O$_3$/UV

In the ozone-UV technology, hydroxyl radicals are produced from ozone, water and UV photons, as shown in the reactions (4.8) and (4.9):

$$H_2O + O_3 \overset{h\nu}{\rightarrow} 2HO^\bullet \rightarrow + O_2 \tag{4.8}$$

$$2HO^\bullet \rightarrow \rightarrow H_2O_2 \tag{4.9}$$

Generally, high-pressure mercury or xenon lamps emitting at 254 nm are employed since the extinction coefficient at this wavelength ($\varepsilon = 3.300$ L mol^{-1} cm^{-1}) for gas-phase ozone is higher than that of hydrogen peroxide ($\varepsilon = 18.6$ L mol^{-1} cm^{-1}) [15]. Several compounds have been degraded and even mineralized by this methodology.

O$_3$/H$_2$O$_2$/UV

The addition of hydrogen peroxide to an O$_3$/UV process enhances the decomposition of ozone and increases the generation of hydroxyl radicals. However, combining the two types of reagents is very expensive when compared to the use of one reagent. The combination of these two systems can be presented by reaction (4.10).

$$2O_3 + H_2O_2 \overset{h\nu}{\rightarrow} 2HO^\bullet + 3O_2 \tag{4.10}$$
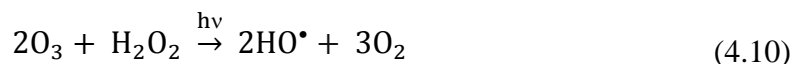
Despite the advantages presented by these AOPs such as high rates of pollutant oxidation, flexibility concerning water quality variations and small dimensions of the equipment, there are also drawbacks. The main disadvantages are relatively high treatment costs compared with other processes (particularly biological treatment), special safety requirements are necessary, both due to the use of very reactive chemicals (ozone, hydrogen peroxide), and high-energy sources (UV lamps, electron beams, radioactive sources) [16].

4.2.3 Photocatalysis

Photocatalysis can be defined as the combination of photochemistry and catalysis, a process where light and a catalyst are simultaneously used to promote or accelerate a chemical reaction [17,18]. Photocatalytic reactions can occur in homogenous or heterogeneous media; however, the largest number of studies reported

in the literature use heterogeneous photocatalysis [5,12,19], making it one of the most studied AOPs since the commonly used semiconductors such as TiO_2 are cheaper, more robust and more easily recovered and reused than soluble photocatalysis.

From an economic point of view, heterogeneous (as well as homogeneous) photocatalysis is likely to benefit from the use of renewable energy sources to power the process. In this direction, solar photocatalysis [6,7,19,20] has gained considerable attention as a route to green chemistry [21] and several studies report the use of natural sunlight irradiation for pesticide degradation [20,22,23].

4.2.3.1 Homogeneous photocatalysis

Homogeneous photocatalysis uses catalysts that are dissolved in water or other solvents (single phase system). This process involves the generation of highly oxidizing species that are responsible for the transformation of the pollutant. These species are often hydroxyl radicals $HO^\bullet$; however, depending on the system that is being used, other reactive species can be formed. A very good example of homogeneous photocatalysis is the photo-Fenton system [24]. Although homogeneous photocatalysis is more effective than heterogeneous photocatalysis it presents as a disadvantage the difficulty of separation of the catalyst from the reaction medium [24].

Fenton-like and Photo-Fenton system

The use of Fenton's reagent consists of a process in homogeneous aqueous phase, not activated by light, in which an aqueous H_2O_2 solution and Fe^{2+} (ferrous) ions in acidic conditions (pH = 2-4) generate $HO^\bullet$ (reaction 4.11) [25,26].

$$Fe^{2+} + H_2O_2 \rightarrow Fe^{3+} + OH^- + HO^\bullet \qquad (4.11)$$

Although the Fenton reaction is most often applied to remove recalcitrant compounds due to its management simplicity, it presents as a weakness the production of iron sludge wastes. This problem has been partially overcome by the photo-Fenton process which uses UV or solar light ($\lambda < 580$ nm) for the reduction of Fe^{3+} back to Fe^{2+} (reaction 4.12) resulting in a drastic reduction of the sludge waste. Photo-Fenton can be referred as a photocatalytic process since Fe^{2+} is regenerated. It has been proved that light accelerates the reaction, when compared with Fenton´s degradation, with

concomitant additional production of hydroxyl radicals (4.13) and photocatalyst reduction [25,26]:

$$Fe^{3+} + H_2O + h\nu_{UV-vis} \rightarrow Fe^{2+} + H^+ + HO^{\bullet} \qquad (4.12)$$

$$H_2O_2 \xrightarrow{h\nu} 2HO^{\bullet} \qquad (4.13)$$
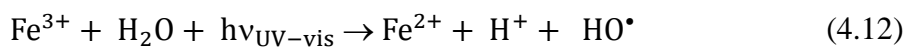
The main advantage of this process comparatively to heterogeneous photocatalysis (particularly with TiO_2) is its sensitivity to light up to 580 nm which enables a more efficient use of solar light. Furthermore, the contact between the pollutant and the oxidizing agent is also more effective in processes occurring in homogeneous phases. Nonetheless, the photo-Fenton poses as disadvantages the necessity to work with low pH (usually below 4), the high consumption of hydrogen peroxide and the need of removing iron at the end of the treatment. On the other hand, the use of solar light instead of artificial light for photo-Fenton activation, in addition to increasing the efficiency, also significantly decreases the cost of treatment. Hence, the development of the photo-Fenton is a great advance towards industrial implementation of photocatalytic processes [27]. The Photo-Fenton processes ability to treat water containing various pollutants has already been proved for the removal from waters of organic pollutants such as phenols, nitrophenols and dyes [28-30].

4.2.3.2 Heterogeneous photocatalysis

Heterogeneous photocatalysis is a light activated process that produces reducing and oxidizing species able to promote mineralization of organic pollutants using a solid semiconductor as catalyst [31]. Several articles, reviews and books have been published over the last few years on this topic reflecting the importance of this type of reactions in environmental remediation [18,32,33]. The main advantage of this process over homogeneous degradation is the possible recovery and recycling of the catalyst. Besides this application, heterogeneous photocatalysis (or semiconductor mediated photocatalysis), has also caught the attention of scientific community concerning its promising environmentally friendly applications for water splitting [34], solar energy conversion [35,36] and disinfection [37].

In the field of organic pollutant degradation, heterogeneous photocatalysis, particularly using the semiconductor TiO_2 as photocatalyst, is by far the most employed

method for removal of pollutants from water, as shown by the several studies carried out in pesticides, alkanes and alkenes, aliphatic alcohols, aliphatic carboxylic acids, alkenes, phenols, aromatic carboxylic acids, dyes, PCB's and surfactants [38-41]. The highly reactive $HO^{\bullet}$ formed during the irradiation process is the main species responsible for the degradation and mineralization of these pollutants, producing as final products carbon dioxide, water and inorganic anions.

4.2.3.2.1 Semiconductors

The electronic structure of a semiconductor (abbreviated as SC) is characterized by a filled valence band (abbreviated as VB) and an empty conduction band (abbreviated as CB). This typical semiconductor electronic structure enables the SC to act as sensitizer for light induced oxidation processes. The ideal properties of a semiconductor to be used as photocatalyst are that it should be: a) photoactive, b) able to absorb ultraviolet and visible radiation, c) photostable toward photocorrosion, d) reused several times without significant loss of activity, e) biologically and chemically inert and f) cheap and non-toxic [41]. Another important feature of the semiconductors is its redox potential. The redox potential of the photogenerated valence band hole (h_{VB}^{+}) must be sufficiently positive to generate $HO^{\bullet}$ which can consequently oxidize the organic pollutants, and the redox potential of the photogenerated conductance band electron (e_{CB}^{-}) must be sufficiently negative to be able to reduce adsorbed oxygen to superoxide anions $O_2^{\bullet-}$ [32,41]. That is, the VB and CB of the semiconductor photocatalyst should be positioned in such a way that the oxidation potential of the hydroxyl radicals (E^0 ($H_2O/HO^{\bullet}$) = 2.8 V *vs* NHE) and the reduction potential of superoxide anions (E^0 ($O_2/O_2^{\bullet-}$) = - 0.28 V *vs* NHE) lie well within the band gap.

Several semiconductors materials have been tested as potential photocatalysts. These include TiO_2, ZnO, WO_3, ZnS, α-Fe_2O_3, CdS, etc., [42] which are able to generate a colloidal suspension stable under radiation. Some of the most common semiconductors and their band gap energies are depicted in Table 6-2 [43]. Even though the metal sulfide and iron oxide (α-$Fe_2O_{3)}$ semiconductors have nominally high band gap energies and are inexpensive, they are unsuitable because the sulfide readily undergoes photo anodic corrosion (not fulfilling the stability requirement) while the iron oxide polymorphs readily undergo photo cathodic corrosion [44]. In addition, ZnO was proven to be unstable with respect to incongruous dissolution [45] to yield $Zn(OH)_2$ on

the ZnO particle surfaces, leading to catalyst inactivation over time. From these semiconductors, TiO_2 satisfies the previous mentioned criteria since it presents high photo-activity, low cost, low toxicity and good chemical and thermal stability. Owing to this, it is one of the most investigated semiconductors for widespread environmental applications [11,12,38].

Table 4-2 Band gap energies of some semiconductors [43].

Semiconductor material	Band gap energy (eV)	Activation wavelength (nm)
ZnS	3.7	336
SnO_2	3.9	318
SrTiO3	3.4	365
TiO_2 (anastase)	3.2	387
ZnO	3.2	390
WO_3	2.8	443
CdS	2.5	497
Fe_2O_3	2.2	565
CdO	2.1	590
CdSe	1.7	730

TiO_2 has three crystalline forms, anatase, rutile and brookite, but only the first two are stable [46]. Even though rutile has a lower band gap energy (3.0 eV) than the anastase form (3.2 eV) indicating the possibility of absorption of longer wavelength radiation, TiO_2 in the anatase form is known to be more active for photocatalysis applications [47]. This is because the CB position of the anatase form is more negative when compared to rutile form, which results in the higher reducing property of anatase. A major drawback of pure TiO_2 is the large band gap (3.2 eV) meaning it can only be activated upon irradiation with photons of light in the UV domain ($\lambda \leq 387$ nm for anatase) limiting the practical efficiency for solar applications. However, approaches have been made to modify the surface material (doping, immobilization, etc) in order to enlarge its range of light absorption [48].

4.2.3.2.2 Principles of photocatalysis

The basic photophysical and photochemical principles underlying photocatalysis by semiconductors have been broadly reported, mainly for TiO_2 [17,19,33,42], although the narrative can be expanded to other semiconductors such ZnO, WO_3, CdS, ZnS, etc. Below is presented a succinct description of the primary steps involved on semiconductor photocatalysis backed by a visual image (Figure 4-1) withdraw from reference [17].
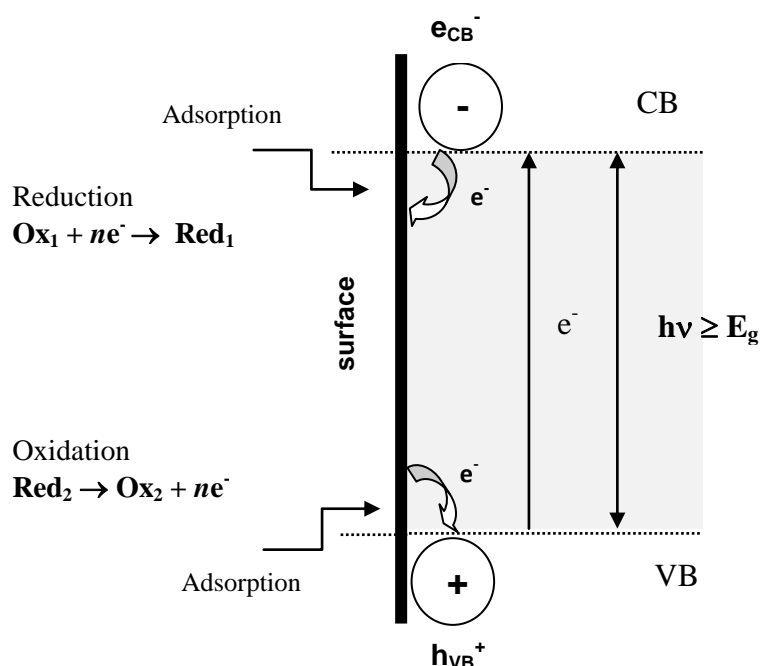
Figure 4-1 Electron energy plotted upwards as a function of the distance from the surface to the bulk of the semiconductor [17].

The excitation of the SC by absorption of a photon with energy $h\nu$ greater than or equal to the band gap energy (Eg) of the SC ($h\nu \geq Eg$) promotes an electron from the VB to the CB (e_{CB}^-), thus leaving an electron deficiency or hole (h_{VB}^+) in the VB (reaction 4.14). As a result, electron/hole (e_{CB}^--h_{VB}^+) pairs are generated. In the absence of proper e_{CB}^- and h_{VB}^+ scavengers, the generated pair can recombine and the excited electron reverts to the VB non-radiatively or radiatively, dissipating the energy as heat or light within a few nanoseconds (reaction 4.15). However, if a suitable scavenger or surface defect state is available to trap the e_{CB}^- or h_{VB}^+ the recombination does not occur. In these situations, the e_{CB}^- and h_{VB}^+ migrate to the surface of the SC and undergo oxidation and reduction reactions with any species which might be adsorbed on the

surface. The electrons e_{CB}^- are good reducing agents (+0.5 to -1.5 V *vs* NHE) and under aerated conditions they can react with adsorbed oxygen (electron acceptor molecule) to form superoxide anion $O_2^{\bullet-}$ (reaction 4.16) and its protonated form, the hydroperoxyl radical $HO_2^\bullet$ (reaction 4.17), which subsequently lead to the formation of H_2O_2 (reaction 4.18 and 4.19). The formed hydroperoxyl radical also has scavenging properties like oxygen, thus doubly prolonging the lifetime of the photo-hole. These reactive oxygen species may also contribute to the oxidative pathways such as the degradation of a pollutant. The photogenerated holes h_{VB}^+ are powerful oxidants (+1.0 to +3.5 V *vs* NHE depending on the semiconductor and pH) and can oxidize the adsorbed water molecules (reaction 4.20) or hydroxide anions derived from water ionization to produce hydroxyl radicals $HO^\bullet$. Both oxidation and reduction reactions occur at the surface of the SC. The generated hydroxyl radicals and the other formed reactive species will then react with the pollutant, leading to its mineralization (reaction 4.21).

$$SC + h\nu \xrightarrow{h\nu \geq E_g} h_{(VB)}^+ + e_{(CB)}^- \qquad (4.14)$$

$$h_{VB}^+ + e_{CB}^- \rightarrow energy \qquad (4.15)$$

$$(O_2)_{ads} + e_{CB}^- \rightarrow O_2^{\bullet-} \qquad (4.16)$$

$$(O_2^{\bullet-})_{ads} + H^+ \rightarrow HO_2^\bullet \qquad (4.17)$$

$$HO_2^\bullet + e^- \rightarrow HO_2^- \qquad (4.18)$$

$$HO_2^- + H^+ \rightarrow H_2O_2 \qquad (4.19)$$

$$h_{VB}^+ + (H_2O)_{ads} \rightarrow HO^\bullet + H^+ \qquad (4.20)$$

$$HO^\bullet + Org. \rightarrow oxidation\ products \rightarrow\rightarrow$$
$$\rightarrow\rightarrow CO_2 + H_3O + inorg.\ anions \qquad (4.21)$$
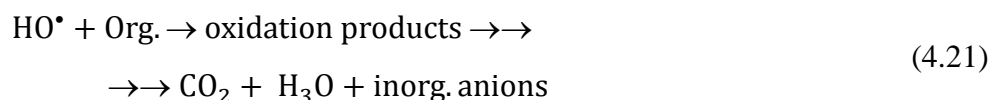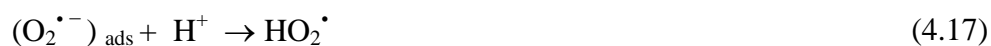
Although TiO_2 is the most widely used photocatalyst, it presents several drawbacks [48], as earlier mentioned: 1) recombination processes of the photo-generated charge carriers (e^-/h^+) with consequent reduction of the overall quantum efficiency of the process, 2) difficult and expensive liquid-solid separation due to the formation of milky dispersions after mixing the powder catalyst in water and, 3) in solar photocatalysis only the small UV fraction of solar light (about 3-5%) can be utilized due to the large band gap of TiO_2 anstase (3.2 eV). Therefore, it is necessary to find a way to use sunlight, which represents a valuable source of renewable energy, and to increase

its photocatalytic activity. The approaches undertaken to overcome these limitations consist on modifying the surface of TiO_2: doping with metal cations and anions, immobilization and coupling with other semiconductors (TiO_2/polyoxometalate, etc.) and metals, etc. [49].

The efficiency of a photocatalytic process [17,32], this is, its kinetic rate *r*, is dependent on factors such as nature and concentration of the reactant, radiant flux (light intensity), pH, wavelength, temperature and amount of catalyst (Figure 4-2). For example, heterogeneous photocatalytic reactions are known to show a proportional increase in photodegradation with catalyst loading. The catalyst concentration should be optimized in order to avoid excess catalyst and ensure total absorption of efficient photons since high amounts of catalyst can cause reduction of light penetration into the solution, largely through light scattering. Therefore, these parameters should be optimized when performing photocatalytic tests. The kinetics rates *r* of photocatalytic degradation of organic compounds usually follows the Langmuir-Hinshelwood scheme (equation 4.22) ([17]):

$$r = -\frac{dC}{dt} = \frac{kKC}{1 + KC} \tag{4.22}$$

where r represents the initial rate of photooxidation, C the concentration of the reactant, t the irradiation time, k the rate constant of the reaction and K is the adsorption coefficient of the reactant. This equation can be simplified to the apparent first order equation (4.23):

$$\frac{\ln C_0}{C} = kKt = K_{app}t \quad \text{or} \quad C_t = C_0 \, e^{-Kapp \, t} \tag{4.23}$$

where C_0 and C_t are concentration of the organic pollutant at the initial time (t=0) and at a certain time t, respectively, and K_{app} is the apparent first order rate constant given by the slope of the graph of $\ln C_0/C$ *vs.* time. Consequently, under the same condition, the initial degradation rate could be written in a form conforming to the apparent first order rate law given by equation (4.24):

$$r_0 = K_{app} \, C \tag{4.24}$$
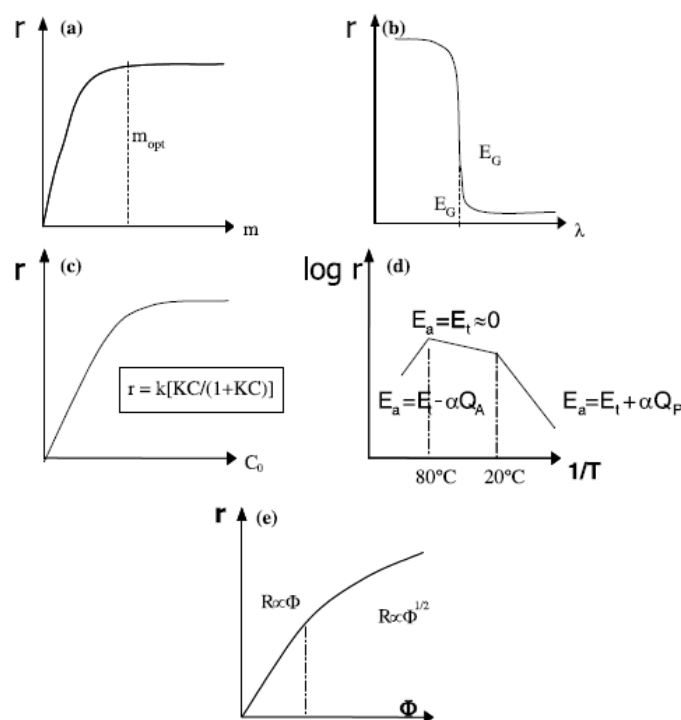
Figure 4-2 Influence of the different physical parameters which govern the kinetics of a photocatalytic reaction rate, r [17]: a) mass of catalyst m, b) wavelength λ, c) initial concentration of reactant C_0, d) temperature T and e) radiant flux ϕ.

4.2.3.3 Photocatalytic degradation of pesticides in water

In addition to the widely used semiconductor TiO_2 for the degradation of pesticides in water, another important type of AOPs has been developed in last decades involving the use of polyoxometalates (POMs) and light. This has yielded promising results for water remediation [50-52]. Comparative studies regarding the mode of action of UV/TiO_2 *vs* UV/POMs suggest that POMs present the same photochemical characteristics as the semiconductor photocatalyst TiO_2 [53,54] with production of hydroxyl radicals. Below are given some examples for the photocatalytic degradation of pesticides in the presence either of TiO_2, POMs, or both, in order to have an idea of the degradation obtained with these catalysts. More detailed information on POMs and their properties, applications, and photochemical activity for degradation of pesticides is given in the next section since the catalyst used during this research work was a POM. No deep information will be given on TiO_2 photocatalysis as it is outside the scope of this thesis. Nevertheless, the information given for the semiconductor titanium dioxide can be applied to POMs.

Pelizzeti *et al.* [55] studied the degradation of the highly persistent s-triazine herbicides (atrazine, simazine, trietazine, prometone, and prometryne) using TiO_2 as photocatalyst under simulated solar light. It was observed that these pollutants are singularly resistant to complete mineralization. In all cases the starting material is degraded to the very stable six-membered ring cyanuric acid. Since cyanuric acid has a very low toxicity, these partial mineralization results are encouraging. Pathways for atrazine degradation such as dehalogenation, dealkylation and deamination were proposed by the authors. Atrazine solution (pH 2-4) degradation was also studied in the presence of TiO_2 and the POM $Na_4W_{10}O_{32}$ [56]. Both catalysts were efficient even though the mechanisms of degradation were different. The authors suggested that in the presence of TiO_2 hydroxyl radicals are the oxidizing species while in the case of $Na_4W_{10}O_{32}$ hydrogen abstraction on the alkyl side chains of atrazine and dehalogenation by electron transfer on the dealkylated metabolites take place. Neither of the catalysts was able to mineralize the aromatic ring of atrazine, in agreement with results reported by other authors. Lindane, an insecticide that persists in environment, was completely mineralized to CO_2 and HCl when photocatalysed in homogeneous solution in the presence of the polyoxometalate $[PW_{12}O_{40}]^{3-}$ [57]. These results are promising in what concerns using polyoxometalates as catalysts for the degradation of pesticides.

4.3 Polyoxometalates

4.3.1 History and structure

The discovery of polyoxometalates (POMs) goes back to the year of 1826 when Berzelius [58] described the formation of a yellow precipitate resulting from a mixture of ammonium molybdate and phosphoric acid, later on identified as the ammonium salt of the anion $[PMo_{12}O_{40}]^{3-}$. In 1862 Marignac published one of the first systematic studies on POMs determining the analytical composition of the silicotungstate and several correspondents salts, as well as analyzing two isomeric forms of the heteropolyoxyanion $[SiW_{12}O_{40}]^{4-}$ (nowadays designated as α and β isomers). Research studies conducted by Pauling [59], Keggin [60], Anderson [61], Evans [62] and Lindqvist [63] are fundamental in the chemistry of POMs, and lead to the well-known compounds designated with their names (Keggin structure, etc.). Since then the development of new synthetic approaches and new characterization methods (X-ray diffraction, infrared, Raman and NMR spectroscopy) has contributed to the vast growth

of POM chemistry, leading to the discovery of a large number of new POM structures and the development of molecular and composite materials applied in different areas, as evidenced by the large number of publications in the literature. The reviews published in 1991 by Pope *et al.* [64] and by Hill in 1998 [65] have elucidated the advances at those times. The chemistry of POMs has expanded over the last few years to a very large field, as evidenced by the huge amount of published works since then [66-69].

POMs, or early transition metal oxygen clusters, are inorganic molecular aggregates based on the metal-oxygen bonds that exhibit a wide variety of alterable shapes, sizes, and surface charge densities [70]. POMs are constituted by polyhedral MO_x units, generally MO_6 octahedrons, which can share their vertices, edges or less frequently, corners (Figure 4-3) [71].

Figure 4-3 Different assemblies of union between two octahedral units in a POM (a) vertice, (b) edge and (c) share corners.

POMs are constituted primarily of d^0 early transition metal cations and oxide anions. The principal d^0 transition metal ions that form the molecular structural framework or scaffolding of polyoxometalates are W^{6+}, Mo^{6+}, V^{5+}, Nb^{5+}, Ta^{5+} and Ti^{4+}. POMs are divided in two generic families based on their chemical composition, isopolyoxianions and heteropolyoxyanions [64]. The isopolyoxianions contain only transition metal cations M (W^{6+}, V^{5+}, Nb^{5+}, Mo^{6+}, Ta^{5+}) and oxide anions with the general formula $[M_mO_y]^{n-}$. The heteropolyoxyanion compounds are defined by the general formula $[X_xM_mO_y]^{p-}$ (x < m) and contains one or more *p* (Al^{3+}) or *d* (Co^{2+}, Fe^{3+}, Si^{4+}) block elements as "heteroatoms" (X) located at structurally well-defined sites in the polyanion. The heteroatoms X can be classified as primary or secondary. The primary or central heteroatoms are fundamental in the whole structure of POMs and their removal implies the destruction of the anion. The secondary or peripheral heteroatoms are not essential to maintain the POMs structure and may be removed leading to the formation of other stable anionic species [64]. Besides the heteroatom, the heteropolyoxyanions also contains transition metal M and oxide ions. The transition metal M is present in its highest oxidation state (electronic configuration *d^0* or *d^1*) and

its atoms are designated by addenda atoms because they are the major constituents responsible for the POMs structure [70]. Listed below in Figure 4-4 are some examples of isopolyoxianions (such as decatungstate anion $W_{10}O_{32}^{4-}$) and heteropolyoxyanions structures (such as those of Keggin, Dawson and Preyssler). The decatungstate anion $W_{10}O_{32}^{4-}$ has been used in the scope of the research work developed in this thesis. Further information on this compound is provided in the next sections.
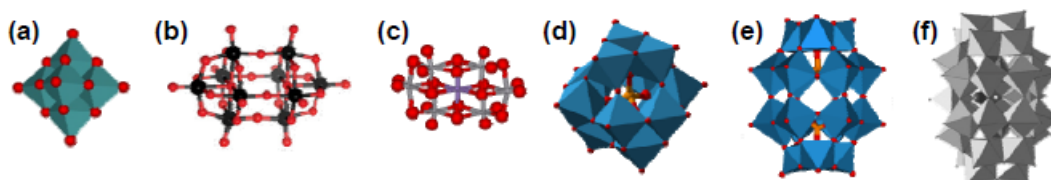
Figure 4-4 Examples of POMs structures. Isopolyoxianions (a, b) and heteropolyoxyanions (c, d, e, f). a) Lindqvist $[M_6O_{19}]^{n-}$, b) $[M_{10}O_{32}]^{n-}$ (such as decatungstate anion $W_{10}O_{32}^{4-}$), c) Anderson-Evan $[XM_6O_{24}]^{n-}$, d) Keggin $[XM_{12}O_{40}]^{n-}$, e) Wells-Dawson $[X_2M_{18}O_{62}]^{n-}$, f) Preyssler $[XP_5W_{30}O_{110}]^{n-}$.

The oxygen atoms can be classified as O_a, O_b, O_c and O_d according to their position in the POM structure. O_a is a oxygen atom bonded to a heteroatom (in the case of the heteropolyoxyanions), O_b and O_c stands for atoms that share a vertice or an edge, respectively, and O_d designates a not shared oxygen atom (terminal oxygen) [71].

Although IUPAC has defined a nomenclature for POMs, the most used nomenclature system for POMs is the same as used to designate the coordination compounds [72] due to its simplicity. In the case of the heteropolyoxyanions, the heteroatom is considered as the central atom of a coordination complex and the addenda atoms as the ligand. POMs formulas are usually given by the heteroatom followed by the addenda atoms, as given by the Wells-Dawson anion formula, $[P_2W_{18}O_{62}]^{6-}$.

4.3.2 Properties and applications

The great diversity of structures, size, charge and the huge number of elements that can constitute POMs, as well as their acidity and unique electronic versatility allow POMs to undergo photoinduced multi-electron transfer without any change in their structure, broadening the range of POM application [68,73]. The most important property of POMs is their capacity to participate in redox reactions as electron and oxygen relays without structural rearrangement, yielding well-known "blue" reduced

forms (heteropolyblue). The oxidized forms of POMs can accept and release several electrons without decomposing or undergoing changes in their structures, while the reduced forms of POMs can be regenerated by oxygen. POMs have been applied in fields such as electrochemistry [74] catalysis, clinical chemistry and medicine [75], environmental remediation, material science, including nanotechnology [67-69], corrosion protection, dye, pigments as well as analytical chemistry. However, the most frequent application of POMs is in the field of catalysis due to their diverse properties such as redox potential and acidity, molecular composition and high thermal stability [65,73,76].

In recent decades many issues about energy, environment and sustainable development have become clearer and the search for desirable solutions is essential. Fortunately, POM-based catalytic materials present such capacities as highlighted above and thus may play significant roles in these up-to-date developments. However, although many catalytic oxidation reactions utilizing POM-based catalytic materials have been developed, most of them are homogeneous and share common drawbacks for catalyst/products separation and difficulty of the reuse of expensive catalysts. The exploration of easily recoverable and recyclable heterogeneous catalysts through covalent linkage, encapsulation, adsorption and substitution are necessary for applications in industrial and environmental catalysis. POMs have also been used as photocatalysts for environmental remediation namely for degradation of organic pollutants from waters [51,77] and water oxidation [78].

4.3.3 The decatungstate anion

4.3.3.1 Structure and characteristics

The polyoxometalate sodium decatunsgtate, $Na_4W_{10}O_{32}$, from now on designated as decatungstate anion or $W_{10}O_{32}^{4-}$, is composed of ten WO_6 octahedra sharing edges and corners with a pseudo point symmetry D_{4h} [79] (Figure 4-5). The tungsten metal atoms in the decatungstate anions can be separated into "axial" (W1) and "equatorial" (W2) centers, and the oxygen atoms can be grouped in three different categories, terminal (Ot: O1, O2), two-coordinate (O2c: O3, O4, O5) and five coordinate (O5c: O6) sites [80]. The decatungstate anion is stable in acid media and exhibits electrochemically reversible oxidation-reduction steps [81] with a first ground-state reduction potential of -0.780 V vs Ag/Ag$^+$ (CH$_3$CN) [82].
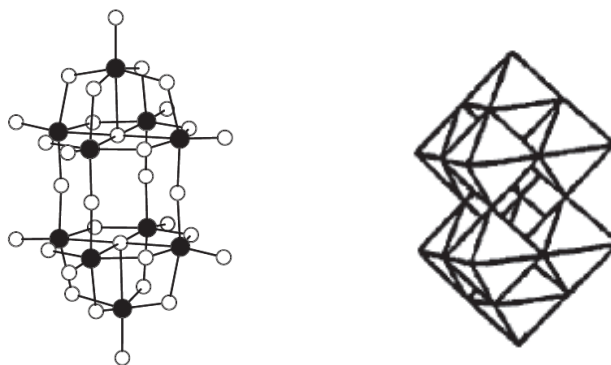
Figure 4-5 Chemical (left) and polyhedral (right) structure of the polyoxometalate decatungstate anion, $W_{10}O_{32}^{4-}$ (filled circles represent W atoms and empty circles O atoms).

In water, the UV-vis absorption spectrum of decatungstate anion presents two main absorption bands around 260 and 323 nm, as shown in Figure 4-6. The first band is attributed to the form $H_2W_{12}O_{40}^{6-}$ which is in equilibrium with $W_{10}O_{32}^{4-}$ [83] while the later absorption band with maximum wavelength of 323 nm (325 nm in acetonitrile) is attributed to a ligand-to-metal-charge-transfer (LMCT) transition in the quasi-linear W-O-W bridges linking both halves of the anion [84-86]. The reduced form of decatunsgate anion, $W_{10}O_{32}^{5-}$, presents a main absorption band around 780 nm with blue coloration [87]. The formation of these decatungstate species was supported by a recent density function theory (DFT) study performed by Ravelli *et al.* [88].
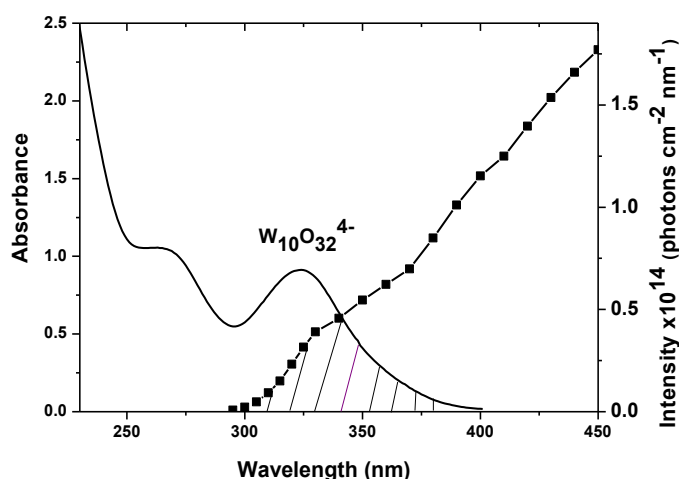
Figure 4-6 UV-vis absorption spectrum of $W_{10}O_{32}^{4-}$ in aqueous solution (pH 5.5) and emission of solar light (dotted line).

4.3.3.2 Applications

$W_{10}O_{32}^{4-}$ has been recently investigated mainly for its catalytic versatility, both in organic chemistry [89] and in environmental application [90]. In organic chemistry, $W_{10}O_{32}^{4-}$ has been extensively used in oxidation reactions of diverse substrates such as alkanes, alcohols and alkenes [91-94]. Current examples of application of heterogeneized decatungstate on free radical functionalization of the unactivated C-H bonds of alkenes, amides, aldehydes, and on the functionalization of nanocarbon chemistry, reflect the ongoing synthetic interest in this matter [95]. In environmental studies, $W_{10}O_{32}^{4-}$ has largely been employed as a "green" catalyst in the field of water contamination treatment, especially as homogeneous photocatalyst for the degradation of organic pollutants to minimize their environmental persistence and hazardous effects [90]. Pesticides, dyes and representative aromatic systems such as phenols, chlorophenols, p- cresol, etc., are some of the compounds that have been studied [96,97]. Further on in the text some examples are described of $W_{10}O_{32}^{4-}$ application on the degradation of organic pollutants in homogenous and heterogeneous media, along with the description for other POMs. Following this line, a short summary of the photocatalytic mechanism involving $W_{10}O_{32}^{4-}$ is given below.

4.3.3.3 Decatungste as photocatalyst - mechanism

The $W_{10}O_{32}^{4-}$ anion is one of the most photochemically active polyoxometalates and exhibits attractive properties as a photocatalyst [90] since its absorption spectrum overlaps, although in to a small extent, the UV solar emission spectrum (see Figure 4-6). This diminishes the consumption of energy that is required when UV lamps are employed opening the potential route for environmentally benign solar photoassisted applications [98]. Furthermore, its low toxicity and cost, makes it a promising compound to be applied in decontamination technology.

Over the last two decades the molecular and electronic structures of $W_{10}O_{32}^{4-}$ and its mechanistic aspects in photocatalysis have been extensively studied by several groups in acetonitrile and water solution on the nanosecond and picosecond time scales [84-86,99,100]. Figure 4-7 exemplifies the general steps that occur once decatungstate anion is irradiated by UV-vis light. A brief explanation of the process is given below.

It is established in literature that the absorption of light by $W_{10}O_{32}^{4-}$ leads to the formation of a charge transfer excited state $W_{10}O_{32}^{4-*}$ [84,86] which decays in

approximately 30 ps [100] to a longer-lived state extremely reactive and non-emissive transient designated as wO (reaction 4.25) [85,99]. This transient species, which is a relaxed excited state, exhibits oxyradical-like character due to the presence of an electron deficient oxygen center and has a lifetime of 35 ns in water [85,99] and 65.5 ns in acetonitrile [84]. This species wO does not react with oxygen but exclusively with organic compounds (RH) through hydrogen atom abstraction (HA) or electron transfer (ET) mechanisms, originating radicals. These radicals when in presence of oxygen may lead to the formation of peroxyl compounds. Nevertheless, there are cases in which a molecule may react by both ET and HA mechanism [93].

Both mechanisms (HA or ET) give rise to the formation of the one electron reduced form of decatungstate $W_{10}O_{32}^{5-}$ [83] or its protonated form $HW_{10}O_{32}^{4-}$, and to the corresponding substrate-derived radical ($R^{\bullet}$). Oxygen, the most common and benign oxidant plays a major role in the process since it oxidizes the $W_{10}O_{32}^{5-}$ [100] to restore the starting catalyst $W_{10}O_{32}^{4-}$, completing the catalytic cycle (reaction 4.29). Oxygen undergoes reductive activation in the process and the superoxide anion formed initiates further oxidations. In the absence of oxygen, the blue color of the reduced species $W_{10}O_{32}^{5-}$ develops and the photoreaction is easily followed spectrophotometrically due to the formation of its characteristic absorption band around 780 nm [83].
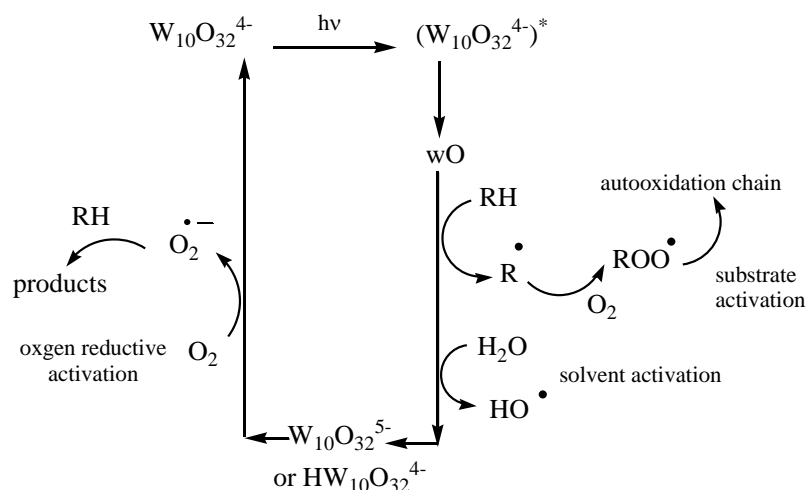
Figure 4-7 Mechanism of action of decatungstate photocatalysis (RH - organic substrate).

The formation of the highly reactive hydroxyl radicals $HO^{\bullet}$ during the photo-irradiation of decatungstate anion in water, and POMs in general, has been subject of study and debate in recent years as doubts come up among researchers. This question is

still a matter of discussion even though several authors [52,102,103] proposed its formation through the direct reaction of the reactive species wO with water molecules (reaction 4.26), the so called solvent activation. This hypothesis has been supported by: EPR detection of $HO^\bullet$ radicals, the detection of hydroxylation products in photolysis experiments with aromatic hydrocarbons and the excited state potentials of decatungstate (and practically all POMs) which are more positive than the one-electron oxidation of water [$OH + H^+ + e^- \rightarrow H_2O$ (E = 2.8 V *vs* NHE)].

A very recent study performed by Molinari *et al.* [103] on decatungstate photocatalysis further support the formation of $HO^\bullet$ from water molecules, as evidenced by the EPR spin-trapping data. Additionally to this pathway of $HO^\bullet$ radical formation the authors also suggest that the reduced form of decatungstate $W_{10}O_{32}{}^{5-}$ is able to initiate reductive activation processes of oxygen leading to H_2O_2. Therefore, the one-electron reduction of H_2O_2 (reaction 4.27) should be considered as an additional source of hydroxyl radicals, according to these authors. The highly reactive $HO^\bullet$ generated by reaction of POM with H_2O play a key role in the degradation process, which is characteristic of AOP technologies. These radicals can initiate oxidation reactions by hydrogen abstraction of the organic substrate, with subsequent reactions that lead to the degradation and mineralization of the pollutants (reaction 4.28).

$$W_{10}O_{32}^{4-} \xrightarrow{h\nu} [W_{10}O_{32}^{4-}]^* \rightarrow wO \tag{4.25}$$

$$wO + H_2O \rightarrow W_{10}O_{32}^{5-} + HO^\bullet + H^+ \tag{4.26}$$

$$H_2O_2 + W_{10}O_{32}^{5-} \rightarrow W_{10}O_{32}^{4-} + HO^\bullet + OH^- \tag{4.27}$$

$$HO^\bullet + Org. \rightarrow\rightarrow CO_2 + H_2O + Inorg. \tag{4.28}$$

$$O_2 + W_{10}O_{32}^{5-} \rightarrow W_{10}O_{32}^{4-} \text{ (regeneration)} \tag{4.29}$$
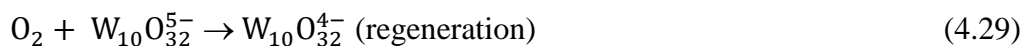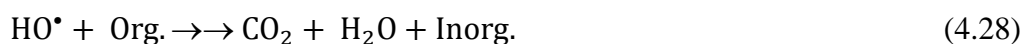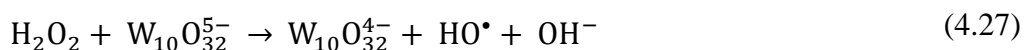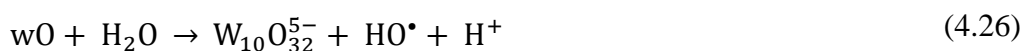
4.3.4 Polyoxometalates as photocatalysts for water remediation

One of the most striking characteristics of POMs is their ability to undergo stepwise multielectron redox reactions whilst their structure remains intact [64,70]. As a general rule, POMs participate in heterogeneous redox reactions in which oxygen is involved mainly as oxygen relays, whereas in homogeneous photocatalytic reactions almost exclusively as electron relays [82].

POMs also share very similar photochemical characteristics with semiconductor (SC) photocatalysts such as TiO_2 due to their combination of physical and chemical properties, *i.e.*, molecular and electronic versatility, reactivity and stability [54,65]. A few comparative studies on their photocatalytic behaviors have been conducted and POMs are considered the analogs of semiconductors [53,54]. Both classes of materials are constituted by d^0 transition-metals and oxide ion and exhibit similar electronic attributes including well defined HOMO-LUMO gaps (semiconductor ''band gaps''). The ''gaps'' inhibit the recombination of electrons (e^-) and holes (h^+) that are generated on the surface of the photocatalysts by the irradiation with light energy higher than the band gaps. The electrons and holes thus formed are capable of initiating chemical reactions due to the formation of $HO^\bullet$ radicals derived from the reaction of holes with water and with OH^- groups coming from water.

As far as the photooxidation of organic compound is concerned, the photocatalytic behavior of POMs is similar to that of SC photocatalysis [53] since both give rise to powerful oxidation reagents ($HO^\bullet$ radicals and POMs excited state) able to oxidize and mineralize a great variety of organic pollutants, going through overall similar intermediates [50,56]. The excited states of both POMs and SCs are able to oxidize H_2O to form $HO^\bullet$ radicals which are the main and most common oxidant in AOP technology. It is then not surprising that the pathways involved and the intermediates detected are very much the same, as earlier mentioned.

The overall reactions that take place in the photocatalytic cycle of POMs are summarized below. This process is the same as earlier described for $W_{10}O_{32}{}^{4-}$ photocatalysis except that the SC notation is now used. The excitation of POMs at the O-MCT band (or HOMO to LUMO) results in electron (e^-) and hole (h^+) separation (reaction 4.30) (equivalent to POM excited state). From here a cascade of reactions occurs since the photoexcited state of POM is able to undergo multi-electron reduction without structural rearrangement, leading to the well-known "blue" reduced form. The photogenerated hole of the photoexcited POM reacts with water to form the highly reactive $HO^\bullet$ radicals (reaction 4.31). These radicals, as well as the excited state of POM, can react directly with the organic substrate leading to its mineralization (reactions 4.32 and 4.33).

$$POM \xrightarrow{h\nu} POM^* \approx POM \ (h^+ + \ e^-) \tag{4.30}$$

$$POM \ (h^+ + \ e^-) \ + \ H_2O \rightarrow POM \ (e^-) \ + \ HO^\bullet \ + \ H^+ \tag{4.31}$$

$$HO^\bullet + Org. \rightarrow oxidation\ products \rightarrow\rightarrow$$
$$\rightarrow\rightarrow CO_2 + \ H_3O + inorg.\ anions \tag{4.32}$$

$$POM \ (h^+ + \ e^-) + Org. \rightarrow POM \ (e^-) + \ Org.^+ \ \rightarrow\rightarrow$$
$$\rightarrow\rightarrow CO_2 + \ H_2O + inorg.\ anions \tag{4.33}$$

$$POM \ (e^-) + \ O_2 \rightarrow POM + \ O_2^{\bullet-} \tag{4.34}$$

$$O_2^{\bullet-} + \ H^+ \rightarrow HO_2^\bullet \quad (pKa = 4.88) \tag{4.35}$$

$$O_2^{\bullet-}/HO_2^\bullet + \ Org. \rightarrow oxidation\ products \tag{4.36}$$

$$POM \ (e^-) + \ O_2 \ \rightarrow POM \ (regeneration\ ) \tag{4.37}$$
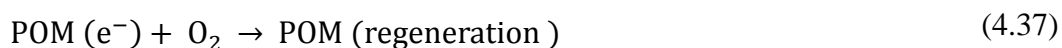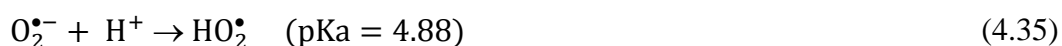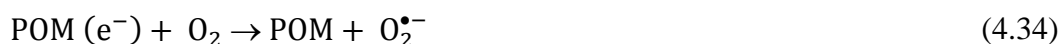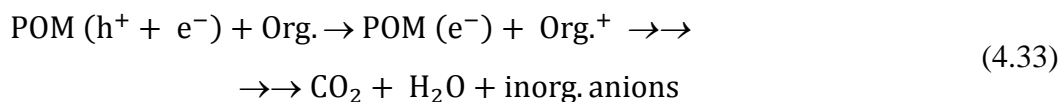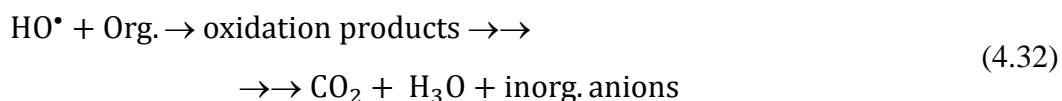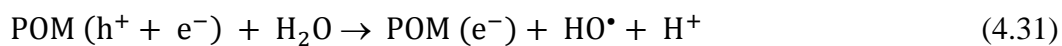
Oxygen, known to be an effective electron scavenger inhibiting the recombination of electrons and holes and producing $O_2^{\bullet-}/HO_2^\bullet$ radicals plays a double role in the process: i) it reacts with the reduced POM to generate reduced oxygenated species such as $O_2^{\bullet-}$ and $HO_2^\bullet$ (oxygen activation) (reactions 4.34 to 4.36) further reacting with the organic radicals formed giving rise to an autooxidation chain and ii) providing the re-oxidation of the reduced POM, POM (e^-) to its initial form thus closing the cycle (reaction 4.37).

4.3.4.1 Homogenous photocatalysis of organic pollutants by POMs

Several POMs, including $W_{10}O_{32}^{4-}$, were efficiently employed as homogeneous photocatalysts for the degradation of metals and organic pollutants in waters (chlorophenols, lindane, endosulfan, atrazine, dyes, chromium, copper, etc.) [52,56,57,104]. These interesting applications of decatungstate in the field of water decontamination, among other polyoxotungstates, have been systematically explored by Papaconstantinou and co-workers for organic compounds such as pesticides, phenol, chlorophenols, chloroacetic acids and dyes [50,52,77,97,105] . The results show that aqueous solutions containing the target pollutants upon degradation in the presence of POMs undergo effective mineralization to CO_2, H_2O and the corresponding inorganic anions. Moreover, the photolysis of aqueous solution of metal ions in the presence of

POMs and organic substrate leads to the oxidative degradation of the organic and the simultaneous reduction-precipitation of metals in elemental state. This process has been successful in the removal-recovery of metal ions including toxic metallic compounds as chromium and mercury [104]. Zhang *et al.* tested several POMs for the reduction of chromium (VI), a known carcinogenic pollutant. All POMs revealed to be effective to reduce Cr (VI) into Cr (III) though their activity were different from one another following the order: $H_3PW_{12}O_{40} \geq H_4SiW_{12}O_{40} > H_4GeW_{12}O_{40} > H_3PMo_{12}O_{40}$.

The degradation of diverse pesticides such as lindane [57], other organochlorine compounds [106], etc., by decatunsgate anion was also subject of study since these pollutants are often persistent and show toxicity. Atrazine degradation was also evaluated using TiO_2 and $W_{10}O_{32}^{4-}$ as photocatalysts [56], as already discussed in section 4.2.2.3. In all cases, the final degradation products were CO_2, H_2O and inorganic anions, with the exception of atrazine which is degraded into the non-toxic cyanuric acid in agreement with the results obtained with TiO_2. The irradiation of organochlorine compounds [106] in the presence of paratungstate A anion $W_7O_{24}^{6-}$ was also efficiency reaching the total mineralization.

Mylonas *et al.* examined the degradation of representative water pollutants such as chlorinated acetic acids [105] and *p*-cresol [95] in the presence of $W_{10}O_{32}^{4-}$ and other polyoxotungstates. All the compounds were completely degraded and mineralized. The hydroxyl radical formed by the reaction of the excited polyoxotungstate with H_2O was the main reactive species. These hydroxyl radicals, whose formation was confirmed by ESR detection and product analysis, may react by hydrogen abstraction and/or addition with organic substrates leading to their photodegradation. Texier and co-workers [98] reported a comparative study on the photocatalytic efficiency of $W_{10}O_{32}^{4-}$ and TiO_2 by means of solar photodegradation of phenols and pesticides (phenol, 4-chlorophenol, 2,4-dichlorophenol, bromoxynil, atrazine, imidachloprid and oxamyl) in aqueous solution. The authors found that TiO_2 was more effective in terms of rate of degradation and mineralization than $W_{10}O_{32}^{4-}$. However, when formulated pesticides were used, $W_{10}O_{32}^{4-}$ was as efficient as or more efficient than TiO_2. The catalysed degradation of the pesticides 2-mercaptobenzothiazole [96] and metsulfuron [107] in the presence of $W_{10}O_{32}^{4-}$ as photocatalyst was recently studied. In both cases an efficient degradation and mineralization was achieved, and a mechanistic scheme of degradation was proposed.

Although POMs, and decatungstate anion in particular, have been applied with success as UV-vis light homogeneous photocatalysts for the degradation of organic pollutants in water, they present as disadvantage high solubility in aqueous medium due to their strong Bronsted acid property that hinders their separation/recover from the reaction medium. As so, it is essential to immobilize POMs in a solid support in order to overcome this limitation.

4.3.4.2 Heterogenous photocatalysis of organic pollutants by POMs

Several research groups have put forward great efforts to develop novel solid catalysts able to enhance surface area and porosity of POMs and to decrease their solubility in water providing recyclable photocatalytic systems. The heterogenization represents a suitable means to tailor efficiency and selectivity of the photocatalytic processes through the control of the microscopic environment surrounding the photoactive POM. As a result, a new branch of heterogeneous photocatalysis by "solid POMs" [108] has emerged in recent years with the immobilization of POMs in several supporting materials using different techniques. Decatungstate anion, either as sodium ($Na_4W_{10}O_{32}$) or tetrabutylamonium salts (($nBu_4N)_4W_{10}O_{32}$), as well as other POMs anions of different nuclearities have been immobilized/impregnated in solid supports such as: NaY zeolite [109], silica [110-118], activated carbon [119,120], carbon fibers [121], amorphous or anatase TiO_2 [122,123], mesoporous molecular sieve MCM-41 [124,125] and anionic clays [126-128].

The final materials obtained by these heterogenization processes lead to an easy recovery and increased specific surface area of the supported POMs resulting in their increased catalytic reactivity by proving larger contact areas between the catalyst and the substrate. Okun *et al.* [110] reported the more efficient oxidation of sulfides and aldehydes in dark reactions by immobilization of POMs on cationic silica nanoparticles. Moreover, the surface effects of supports on the reaction pathways of POMs have also been recognized. The immobilization of POMs on an inactive silica surface greatly changed the distribution of products upon UV irradiation of 4-chlorophenol. These changes were ascribed to the introduction of a solid support surface that changed the surface chemistry and pathway of POM mediated reaction. In another study, sodium and tetrabutylamonium salts of decatunsgtate ($Na_4W_{10}O_{32}$ and $(n-Bu4N)_4W_{10}O_{32}$) have been entrapped in a silica matrix by sol gel technique [111,112] and its photocatalytic

activity has been examined towards photooxidation of 1- and 3-pentanol in organic solvent using tetrabutyl decatungstate [111], and on the photooxidation of glycerol in aqueous media using the sodium salt of decatungstate [112]. The authors observed the formation of $HO^\bullet$ radicals arising from the excited state of $Na_4W_{10}O_{32}$ and water. This finding was demonstrated by EPR spin-trapping using DMPO as spin trap. The hydroxyl radicals are very strong, unselective oxidants, able to degrade both the initial substrate and the reaction intermediates. This photocatalytic behavior is in line with previous findings of other groups, including the Papaconstantinou group, who attributed the reactivity of the polyotungstates anions toward phenol and 2-propanol in water to the formation of $HO^\bullet$ radical.

In addition to these applications, the photocatalytic activity of decatungstate anion (and other POMs) immobilized in solid supports towards the degradation of pesticides and other pollutants have also been tested [109,122,123,126,129-133]. For instance, Ozer *et al.* [109] reported a faster photodegradation of 1,2-dichlorobenzene under UV irradiation by loading POMs on NaY zeolite than in homogeneous POM solution. In 2000 the group of Guo *et al.* [129] reported the photocatalytic degradation of the organocholorine pesticides hexachlorocyclohexane (HCH) and pentachloroenitrobenzene (PCNB) by Keggin type POMs ($H_3PW_{12}O_{40}$ and $H_4SiW_{12}O_{40}$) impregnated in silica matrix via a sol-gel technique. The catalysts POMs/SiO_2 thus obtained are insoluble and readily separable porous materials with uniform micropores and high specific surface areas. The irradiation of HCH and PCNB in the near-UV region in the presence of the POMs/SiO_2 slurry allowed the total degradation (Langmuir-Hinshelwood first-order kinetics) and mineralization into CO_2 and HCl. Studies on the reaction mechanism indicate that photogeneration of hydroxyl radicals originating from neutralization of OH^- groups on the catalyst surface with positive photoholes is responsible for the oxidation of the organic substrates in aqueous solution. In 2001 the same group [130] reported the immobilization of $Na_4W_{10}O_{32}$ and (n-Bu4N)$_4W_{10}O_{32}$ inside a silica network via a sol-gel technique resulting in the $Na_4W_{10}O_{32}$-SiO_2 and (n-Bu4N)$_4W_{10}O_{32}$-SiO_2 composites. Their photocatalytic activity was tested by degrading the organophosphorus pesticide trichlorofon (TCF) under near-UV irradiation in aerated conditions. The highest photocatalytic activity was obtained with microporous $Na_4W_{10}O_{32}$-SiO_2 material. Total mineralization of aqueous TCF into CO_2, H_2O, and other inorganic ions (such as Cl^-, $H_2PO_4^-$, and H^+) over the $Na_4W_{10}O_{32}$

composite was achieved only under atmospheric pressure. Studies on the reaction mechanism indicate that OH$^{\bullet}$ radical attack is most likely responsible for the degradation and final mineralization of TCF. Besides, adsorption might also play a key role in heterogeneous photocatalyst chemistry and the rapid diffusion of the reactants into the micropores of the catalyst may attain high photoactivities so that the mineralization may be performed by direct oxidation via excited $W_{10}O_{32}^{4-}$.

In 2002 Yue *et al.* [131] examined the degradation of 4-chlorophenol with near-UV light by POMs immobilized in silica. Four types of POMs ($W_7O_{24}^{6-}$, $W_{10}O_{32}^{4-}$, $PW_{12}O_{40}^{3-}$, and $P_2W_{18}O_{62}^{6-}$) were immobilized into a silica matrix through the sol-gel hydrothermal technique. The obtained POM-in-SiO$_2$ solids catalysts were insoluble and readily separable microporous materials with a large surface area and a shape pore-size distribution. These solids present absorption bands in the region of 190-410 nm in UV-Vis diffuse reflectance spectra. During irradiation, 4-chlorophenol was first dechlorinated to form hydroquinone and p-benzoquinone, and then the intermediates further mineralized into to CO_2 and H_2O. The decatungstate based composite, $W_{10}O_{32}^{4-}$-SiO$_2$, exhibited the highest activity among all the POMs used, affording a complete mineralization of 4-chlorophenol after 60 min of irradiation. The homogeneous precursor $W_{10}O_{32}^{4-}$ was also found to be the most active catalyst between the polyoxotungstates studied, under the same reaction conditions, albeit in a lower yield compared with its heterogeneous analogue. The generation of hydroxyl radicals which were responsible for the initial oxidation and subsequent mineralization of 4-chorophenol to CO_2, H_2O, and HCl, was confirmed by ESR studies, which is in agreement with Papaconstantinou and co-workers findings.

Another example of microporous decatungstate application was reported for the photocatalytic degradation of hydroxyl butanedioic acid (malic acid) in the presence of POMs ($H_3PW_{12}O_{40}$, $H_4SiW_{12}O_{40}$ and $Na_4W_{10}O_{32}$) incorporated into the silica matrix also via a sol–gel technique [132]. Among the three polyoxotungstate–SiO$_2$ composites studied, $Na_4W_{10}O_{32}$–SiO$_2$ was found to be the most photocatalytically active material allowing the total degradation of an aqueous malic acid (100 mg L^{-1}) into several intermediates (i.e., oxalic, glyceric, tartaric, butenedioic, acetic, and formic acid) in only 90 min of irradiation. These intermediates were totally mineralized under the same conditions after successive irradiation of 90 or 60 min. The photocatalytic activity of the polyoxotungstate-SiO$_2$ composites was attributed to their unique structure and microporosity, so that the photodegradation reaction could be performed effectively on

the surface and in the micropores of the catalysts. Further studies showed that hydroxyl radicals were also involved in the overall mechanism, as observed in the case of 4-chlorophenol degradation. The entrapment of POMs in silica material seems to enhance the catalytic activity of POMs, as well as to contribute for their recycle and reuse.

POMs have also been immobilized in layered double hydroxides (LDH) by an intercalation process in which the catalytic activity of the POM is greatly increased since it presents meso or microporous structure. For example, the POM paratungstate A ion was intercalated in the precursor Mg_2Al-terephthalate LDH via anionic exchange reaction originating the final material $Mg_{12}Al_6(OH)_{36}(W_7O_{24})\cdot4H_2O$ [126]. The photocatalytic activity of this material was tested towards the irradiation of aqueous solution of trace organocholorine pesticide hexachlorocyclohexane (HCH) in the near UV. Under these conditions the total degradation and mineralization of HCH to CO_2 and HCl was achieved. The authors propose as the reaction field the interlayer of the LDH and that the photogenerated hydroxyl radicals are responsible for the degradation pathway. This immobilized material present as advantage the easy recover from the reaction system, which enable it to be reused during five catalytic cycles without significant loose of the catalytic activity.

LDH materials present excellent anionic exchange capacity which is of great interest to intercalate POMs of different sizes. Moreover, it is possible to synthesize LDH with micro and mesoporosity in which the ratio of surface hydrophobic-hydrophilic character improves the amount of substrates in the proximity of the POM, enhancing the catalytic activity. Consequently, this stimulates our interest to use LDH as solid supports for the intercalation of $W_{10}O_{32}^{4-}$ in order to test this material for the degradation of pesticides in water. Therefore, the next section is dedicated to layered double hydroxide materials and their use as solid supports for immobilization of POMs.

4.4 Layered double hydroxides

4.4.1 Composition and structure

Layered double hydroxides (LDHs), also known as hydrotalcite (HT)-like compounds, were discovered around 1842 in Sweden. However, it was only in 1915 that Manasse [134] published the exact formula of the natural mineral hydrotalcite $[Mg_6Al_2(OH)_{16}]CO_3.4H_2O$. The interest in these compounds has grown since then and

intense investigation has been carried in recent years mainly due to the excellent LDH anionic exchange capacity, which makes them unique as far as inorganic materials are concerned, and leads to their application in various different fields.

The basic structure of LDHs is based on brucite, $[Mg(OH)_2]$, and consists of stacked positively charged sheets formed through $M(OH)_6$ edge-sharing octahedra equilibrated by the presence of interlayer anions in order to maintain overall charge neutrality [135-137]. Electrostatic interactions and hydrogen bonding occur between the hydroxyl groups of the host sheets (brucite-like layer) and the interlayer anions. LDHs may be represented by the general formula (4.38):

$$[M^{II}_{(1-x)} M^{III}_x (OH)_2]^{x+} [(A^{n-})_{x/n}.mH_2O] \qquad (4.38)$$

where M^{II} and M^{III} usually represent divalent and trivalent metallic cations, x is the molar ratio and A^{n-} is the interlayer anion of valence n. The idealized structure of LDH and a typical octahedral unit are shown in Figure 4-8.

The central positions of octahedral $M(OH)_6$ are occupied by the cations which can be Mg^{2+}, Co^{2+}, Cu^{2+}, Ni^{2+}, Zn^{2+}, Al^{3+}, Cr^{3+}, Ga^{3+}, Fe^{3+}, etc. The cations are usually incorporated as combinations of divalent M^{II} and trivalent metal ions M^{III}. A wide range of binary combinations of M^{II} and M^{III} incorporated in LDH is possible. The trivalent metal ratio (or molar ratio) x is given by the expression (4.39) and usually ranges from 0.10 to 0.33, while the divalent *vs* trivalent ratio is given by R ($= M^{II}/M^{III}$).

$$x = M^{III+}/M^{II+}+M^{III+} \qquad (4.39)$$

The preparation of LDH with $x > 0.33$ seems to be limited by the electrostatic interactions between the metals. R and x vary in inverse way, this is, higher R values lead to smaller x ratios and to a decrease of the layer charge density (c.d.).
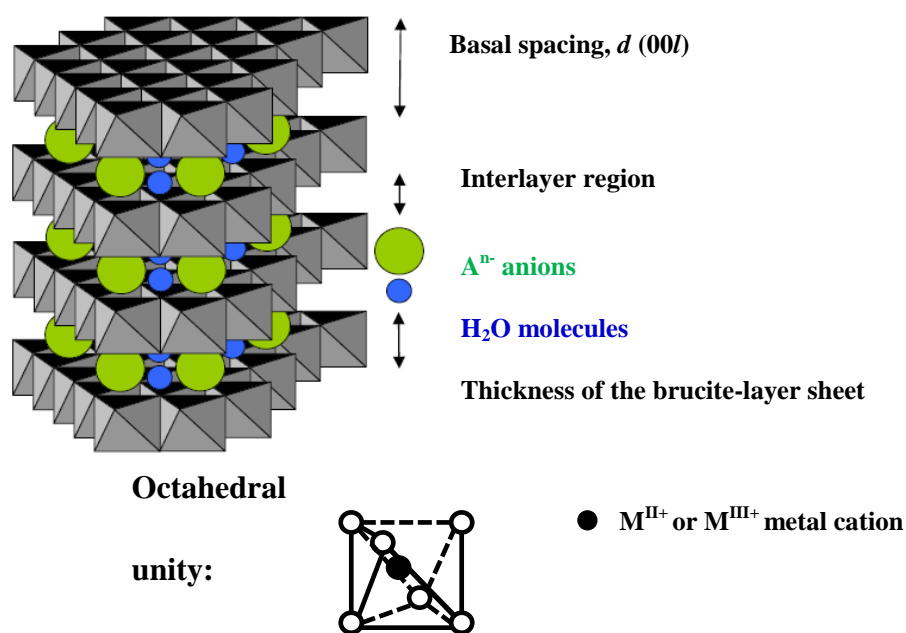
Figure 4-8 Illustration of the idealized structure of LDH [137].

The interlayer domain, given by the chemical composition $[(A^{n-})_{x/n}.mH_2O]$, is composed of interlayer anions A^{n-}, water molecules and sometimes other neutral or charged moieties [135]. *A priori*, no limitation exists for the type of anion to be intercalated in the LDH structure and a large variety of anions has been intercalated [138]:

a) *inorganic anions*: halide ions (F^-, Cl^-, Br^- and I^-), small oxo anions (CO_3^{2-}, NO_3^-, ClO_4^-, SO_4^{2-}, $S_2O_3^{2-}$ and CrO_4^{2-}, etc.), inorganic coordination compounds ($NiCl_4^{2-}$, $CoCl_4^{2-}$, $Fe(CN)_6^{3-}$ and $Fe(CN)_6^{4-}$), etc.

b) *organic anions*: adipate, oxalate, succinate, benzoate, phthalate, terephthalate, alkyl sulfonates, alkyl sulfates, phthalocyanines, polymers, etc.

c) *polyoxometalates:* $[Mo_7O_24]^{6-}$, $[SiV_3W_9O_{40}]^{7-}$, $[W_{10}O_{32}]^{4-}$, $[V_{10}O_{28}]^{6-}$, $[H_2W_{12}O_{40}]^{6-}$, $[BVW_{11}O_{40}]^{7-}$, $[SiW_{11}O_{39}]^{8-}$, etc.

The amount of the anions in the interlayer region is directly related to the charge density of the hydroxide layers which can be controlled by the M^{II+}/M^{III+} ratio, whereas their arrangement depends on the interlayer packing related to the layer charge density as well as the anion size and the presence of water molecules. Additional parameters

such as the preparation route and the synthesis temperature may also influence the interlayer arrangement, especially in the case of intercalated organic molecules [139].

The *anionic exchange capacity* of LDHs, A.E.C., [140,141] is dependent on x and for an ideal composition of $M^{II}_{1-x} M^{III}_x (OH)_2A.0.66H_2O$ is defined by equation (4.40):

$$A.E.C. = \frac{x.10^5}{F.W} \quad (cmol/kg) \qquad (4.40)$$

where F.W. is the formula weight which supposes a full occupancy (2/3) of the interlayer crystallographic sites for the water molecules, 0.66 H_2O/Metal. The formula weight is given by F.W. = $(M_{MII} + 46) + x(M_{MIII} + M_A - M_{MII})$.Usually, the A.E.C. values are lower than calculated by structural formula due to carbonate contamination.

The brucite-like sheets can be stacked with two layers per unit cell in hexagonal symmetry (manasseite), with three layers per unit cell in rhombohedral symmetry (hydrotalcite) or in less symmetrical arrangements [136,137]. In general, mainly LDHs of rhombohedral symmetry have been found. M^{II} (Mg^{2+}, Fe^{2+}, Co^{2+}, etc.) and M^{III} (Al^{3+}, Cr^{3+}, Fe^{3+}, etc.) ions that have ionic radii similar to that of Mg^{2+} can be accommodated in the holes of the close-packed configuration of OH groups in the brucite-like sheets to form LDHs.

The *basal spacing* of a LDH, *d*, is given by the distance from the center of one layer to that in the adjacent layer, *i.e*., is given by the total thickness of the brucite-like sheet and the interlayer region, as observed in Figure 4-8. It is obvious that the basal spacing is much greater than that in the brucite-like layer (assumed to be *co* = 0.4766 nm $\cong$ 0.48 nm) because of the absence of any interlayer anions and water in the latter.

The LDH basal spacing shows some correlation with the composition of the layers, although clearly the size of the anion and the extent of hydration will also have a major influence on it [142]. The *d* decreases with the increase of layer *c.d.* due to the enhanced electrostatic attraction between hydroxide layers and interlayer anions. The gallery height in LDHs, *l*, is normally estimated by subtracting the thickness of the brucite-like layers from the basal spacing *d* given by the X-ray diffraction data [143] (expression 4.41):

$$l \text{ anion (nm)} = d \text{ basal - 0.48} \hspace{4cm} (4.41)$$

where l anion includes the van der Waals radii of appropriate external atoms of the anion.

A large class of LDH materials with versatile physical and chemical properties can be obtained by changing the nature of the metal cations, the molar ratios of M^{II}/M^{III} and the types of interlayer anions. The stability of the LDH, given by its solubility in water, is important for some applications and should be taken in consideration. The stability of LDHs has been assessed from pH titration following the increased order for divalent: $Mg^{2+} < Mn^{2+} < Co^{2+} \approx Ni^{2+} < Zn^{2+}$ and trivalent cations $Al^{3+} < Fe^{3+}$ [144].

4.4.2 Synthesis

LDHs cover a broad class of materials that are very easy to synthesize on both the laboratory and industrial scales [142], even though not always as pure phases. The particle size structure, morphology, crystallinity and orientation of the LDH can be tailored according to the synthetic method employed, thus broadening the field of LDH applications.

LDHs may be synthesized with a wide series of compositions, and a large number of materials with a variety of M^{II}/M^{III} cation combinations having different anions in the interlayer can be obtained. Several synthetic techniques have been successfully employed in the synthesis of LDHs [145-147]. A brief description of some of the most common methods used for the synthesis of LDHs is described here. More information on the subject can be found in specialized books and published reviews on LDHs.

Co-precipitation at constant pH

This is the most widely method used to prepare LDHs and allows the production in laboratory of large quantities of material containing a variety of layer cations and interlayer anions [142,148,149]. Figure 4-9 shows the experimental set up of such a process that has been used in this research work. The method consists in the simultaneous precipitation of a mixture of M^{II} and MI^{III} metal cation salts by the addition of a basic solution (normally NaOH) at constant pH in which the counter anions of the metal salts become the interlayer anions. The constant pH value to be used

is dependent on the nature of the metal cations (Zn^{2+}, Mg^{2+}, etc.) and leads to the co-precipitation of the two metallic salts within the hydroxide layers. The pH of the co-precipitation has a crucial effect on the chemical, structural and textural properties of the LDH. Therefore, constant pH is recommended to ensure the attainment of LDHs with high chemical homogeneity and good crystallinity [149]. This method allows the preparation of a large number of LDHs with anions such as Cl^-, CO_3^{2-}, NO_3^-, which can further be used for anionic exchange, impregnation, etc. LDHs containing large anions such as dodecyl sulfate (DDS) [150] and terephthalate [151] in the interlayer have also been prepared by direct co-precipitation as precursors for anionic exchange reactions (an example is the intercalation of POMs in LDH).
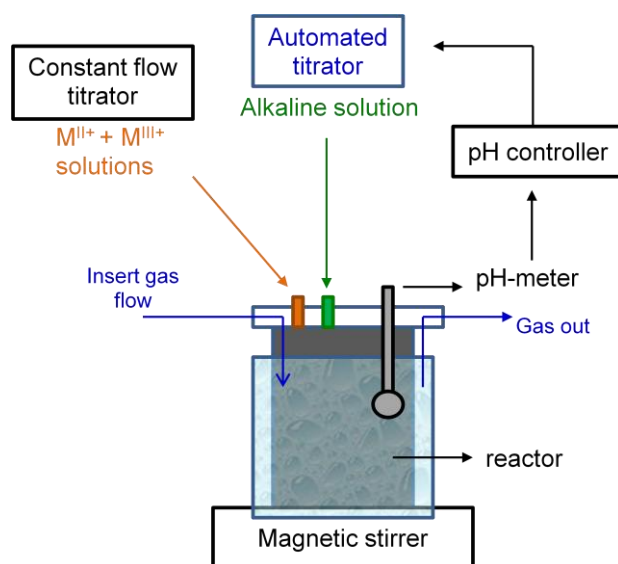
Figure 4-9 Experimental co-precipitation step-up process.

For the intercalation of other anions apart from the counter anions, the desired anions are initially introduced into the reacting flask in a large excess (an excess between 5 and 10 times over the M^{III} content is commonly used). After complete addition of the metallic salts the precipitate is aged in the mother solution for periods from a few hours to several days, and the LDH is then recovered by four dispersion and centrifugation cycles in deionized and decarbonated water.

The mechanism of the co-precipitation method relies upon the condensation of hexaaqua complexes in solution in order to form the brucite-like layers with a distribution of both metallic cations and solvated interlayer anions [148]. In addition to pH control, to obtain well crystallized LDH phases, some of other experimental

parameters should be controlled and optimized. They are the concentration of both metallic salts, concentration of alkaline solution, addition rate of reactants, the aging time and temperature of the precipitate.

Anionic exchange

As the name indicates, this method is based on the anion exchange properties of LDHs. A large variety of anionic species can be incorporated into the interlayer region of the LDH using this method, allowing the host lattice to be completely changed, together with modification of the chemical, optical, electronic and magnetic properties [138,140].

The anionic exchange depends mainly on the electrostatic interactions between positively charged sheets and the exchanging anions. This method is useful when the co-precipitation method is inapplicable, such as when the anions or the metal cations (divalent or trivalent) are unstable in alkaline solution, or when the direct reaction between metal ions and guest anions is more favorable. The anion exchange reaction can be described by the following equilibrium given by reaction (4.42):

$$LDH.A^{n-} + X^{y-} \Leftrightarrow LDH.(X)_{n/y}^{y-} + A^{n-} \qquad (4.42)$$
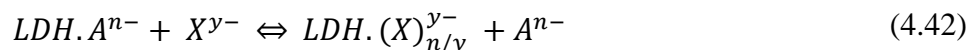
where X^{y-} represents the anion to be exchanged and intercalated in the LDH.

Based on the mass action law, an excess of incoming anions (X^{y-}) will favor the exchange reaction of outcoming anions (A^{n-}) to generate the fully exchanged phase LDH.(X^{y-})$_{n/y}$. The equilibrium constant increases when the radius of the bare anion decreases. Consequently, exchange is favored for ingoing anions with a high charge density. Anion exchange properties of LDH depend on LDH affinity towards outcoming and incoming anions. By comparing the equilibrium constant of exchange reactions between monovalent anions and divalent anions, the following order of anion selectivity was proposed by Miyata [152]:

$$OH^- > F^- > Cl^- > Br^- > NO_3^- > I^- \text{ and } CO_3^{2-} > SO_4^{2-}$$

These results suggest, for example, that NO_3^- anions are easily displaced by OH^- anions of higher affinity towards the metal hydroxide layers. Based on these observations, LDH containing chloride and nitrate are often used as precursors for anion

exchange reactions. Additionally, the results also confirm the strong affinity of carbonate anions (CO_3^{2-}) which is the reason why the synthesis of LDH must be prepared under a CO_2-free atmosphere. The exchange process may be limited by the expansion of the interlayer space to accommodate large size anions. In this case, spaced LDH precursors intercalated with lauryl sulfate, p-toluenesufonate, dodecyl sulphate, terephthalate, 2,5-dihydroxy-1,4- benzendisulfonate, 1,5-naphthalenedisulfonate anions can be used [150], as reported for the preparation of LDHs containing oxometalate anions [153].

Several parameters have to be taken into consideration when performing an anionic exchange reaction. One of those parameters is pH, as indicated above. The pH determines the stability of the hydroxide layer and the properties of the incoming anions. Higher pH values (10.0-12.0) favor the intercalation of carbonate anions while lower pH values (4.5-6.0) lead to the liberation of the initial anion as the conjugate acid and incorporation of a less basic anion from the reaction system [149]. However, pH values smaller than 4.0 can lead to the dissolution of the LDH hydroxide layer. A suitable solvent may also favor the anion-exchange processes. It was found that ethanol/water mixture as solvent can effectively reduce the dissolution of LDH host during the intercalation of $[Mo_7O_{24}]^{6-}$ into Mg_RAl-LDH ($1.27 \leq R \leq 3.0$) [154]. A study made by O'Hare *et al.* [155] also established that the mixed ethanol/water solvent may improve the crystallinity and decrease the production of $Al(OH)_3$ as an undesired product during the exchange reaction involving all isomers of both pyridinecarboxylate and toluate in $[LiAl_2(OH)_6]Cl \cdot H_2O$ [155] .

Rehydration using the structural memory effect

The reconstruction of the LDH phase from calcined LDH derivatives is an alternative method for the preparation of hybrid LDH [156]. It has also been widely used for the incorporation of bulky anions such as polyoxometalates [157,158]. The calcination temperature and the composition of the hydroxide layers are the key factors influencing the reconstruction process [159]. However, it is still difficult to avoid the presence of carbonate anions due to their high affinity towards the mixed oxide [160] and the production of some amorphous phases due to incomplete reconstruction.

Colloidal crystal templating

The development of nanostructured LDH materials with improved surface area, porosity, low density and good permeability is of great significance for several applications. Having this in mind, a new strategy for the preparation of macroporous materials using a colloidal crystal templating method has been established [161-163]. The synthesis of macroporous materials with three-dimensional periodicals are currently of great interest for a wide range of applications related to their porosity that exploit high surface area structures such as in catalysis, filtration, molecular sieving and chemical/biosensors. A typical strategy to prepare three-dimensional ordered macroporous structures is to employ a colloidal crystal (opal) as a sacrificial template. So-called ''inverse opals'' are formed by infiltrating the interstitial voids of the opal with the desired precursor solution which after fluid-solid transformation and subsequent removal of the opal arrays form macroporous inorganic structures. Géraud *et al.* [164] have reported a general method to prepare three-dimensional ordered macroporous (3-DOM) LDH replicas by co-precipitation of divalent and trivalent metal cations in the interstices of PS colloidal crystals, followed by successive infiltrations, and subsequent removal of PS template through dissolution in an organic solvent. The Mg/Al-LDH with CO_3^{2-} anions was first prepared by this method [163]. Subsequently, this method was extended to produce various 3-DOM LDH materials with tunable layer compositions and intercalated guest anions. This synthesis method has also been employed under the framework of this thesis.

Other methods such as sol-gel synthesis using ethanol and acetone solutions [165] and a fast nucleation process followed by a separate aging step at elevated temperatures [166] have also been reported.

4.4.3 Characterization

Given that synthetic LDHs often do not possess high crystallinity various analytical techniques have been developed to characterize their structures [149]. Routine analytical techniques include powder X-Ray diffraction (PXRD), Fourier transformed infrared spectroscopy (FTIR), thermogravimetry (TG), differential scanning calorimetry (DSC), differential thermal analysis (DTA), and techniques for the

determination of the morphology and size such as scanning electron microscopy (SEM) and transmission electron microscopy (TEM). Other techniques may also be employed.

4.4.3.1 Powder X-Ray Diffraction

X-ray powder diffraction (PXRD) is one of the most powerful techniques used to investigate the composition, purity and structural orientation of a material [149]. The X-ray radiation that is directed towards the material is either reflected or diffracted at different angles. The interaction of the X-rays with the crystal lattice results in the formation of secondary diffracted beams. The relationship between diffracted X-rays and the interplanar spacing (Figure 4-10) is given by Bragg´s law (equation 4.43):

$$n\,\lambda = 2\,d_{hkl}\,\sin\theta \tag{4.43}$$

where n is the diffraction order, λ is wavelength of the X-ray beam, d is the basal (or interplanar) spacing, θ is the diffraction angle and hkl are the diffraction or Miller indices of the plane where a, b and c are the axes.
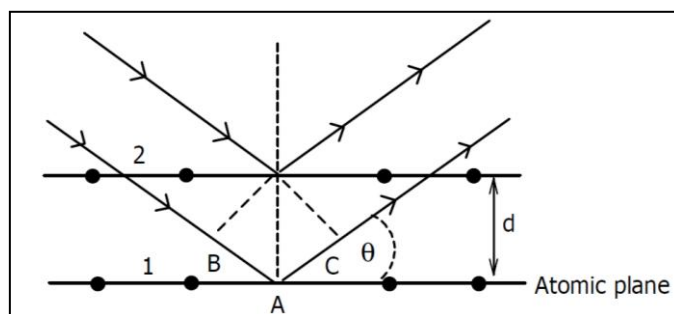
Figure 4-10 Diffraction of X-rays on crystal lattice according to Bragg.

PXRD data are recorded as the plot of intensity *vs* the diffraction angle 2θ giving the "fingerprint" of the crystal structure. PXRD can be used to study both the purity and crystallinity of the LDH and intercalated LDH. The diffraction peaks of the LDH are usually refined in R-3m space group in rhombohedral symmetry. The d is expected to decrease with increasing layer charge density and vice-versa as result of the enhanced electrostatic attraction between hydroxide layers and interlayer anions. The phase purity of the material is determined by the sharpness and/or the broadness of the diffraction peaks. The sharper reflections correspond to the crystalline phase while the broader reflections correspond to the amorphous phase. The d-spacing of a LDH material

depends on the size and orientation of the intercalated anion when n is the stacking sequence of the brucite-like layers [167].

4.4.3.2 Fourier Transformed Infrared Spectroscopy

Fourier Transformed Infrared Spectroscopy (FTIR) is a valuable technique used for the characterization of LDHs involving the vibrations in the octahedral lattice, the hydroxyl groups and the interlayer anions. It is also employed to follow the alteration of the vibrational bands after intercalation and/or thermal treatment. This method can be used to identify the presence of the charge-balancing anion in the interlayer, the type of bonds formed by the anions and their orientations. For example, the absorption at 3500–3600cm^{-1} in the IR spectra of all LDHs is attributed to the H-bonding stretching vibrations of the OH group in the brucite-like layer [136,149]. The bending vibration of the interlayer water occurs at 1600-1650cm^{-1} giving a characteristic peak rarely overlapped by others. With this technique, samples may be studied directly as solids but due to the intense absorptions in crystals KBr pellet are more commonly used in FTIR.

4.4.3.3 Thermogravimetry

Thermogravimetry (TG) is used to measure the changes in sample weight of LDHs (or other materials) as a function of increasing temperature [149]. This technique has been widely used to study the thermal stability of LDH and of LDH intercalated materials [168] since the thermal decomposition products are interesting as catalysts. The properties of the material (such as thermal stability, decomposition and composition) are measured under specific atmospheric conditions while the sample is subjected to a controlled temperature program [154]. LDH may contain different numbers of water molecules and an increase in the temperature causes water to be released in the form of vapour. In addition, various other decomposition steps may occur. The temperatures at which these steps occur are given by TG [169]. LDH decompose in three stages [167]:

1- Dehydroxylation - loss of interlayer water up to 300 ºC

2- Dehydroxylation of brucite-like layers in the range 300-500 ºC,

3- Loss of interlayer anion. The temperature at which the interlayer anion is lost depends on the nature of the intercalated anion.

The decomposition of LDH results in the formation of thermally stable mixed oxides that are mostly used in catalysis [170]. The amount of the intercalated anion can be estimated from the TG data.

4.4.3.4 Other techniques

Other techniques often used include scanning and transmission electron microscopy (SEM and TEM), differential scanning calorimetry (DSC), differential thermal analysis (DTA), X-ray fluorescence spectroscopy (XRF), measurement of zeta potential and size of particles, and N_2 isotherms [149]. DSC, like TG, is also used to assess the chemical and physical properties of a material corresponding to the temperature changes. It is used to detect the phase transitions and melting points of materials. XRF is employed for trace element analysis and is also used for the determination of the divalent to trivalent cation ratios. SEM and TEM give images of textural and crystal morphologies of LDHs and intercalated LDHs. The shape and size of the particles are clearly dependent on the synthesis method. SEM is used to study the surface topography of LDH intercalates giving information of the particle porosity, morphology and phase composition of the material. The theoretical surface area (S_{theo}) of one LDH monolayer can be calculated taking in account its structural property and composition as depicted by equation (4.44):

$$S_{theo} = a^2 \sqrt{3} \ 10^{-18} \ N/(F.W.) \qquad (4.44)$$

a is the cell parameter (nm), N is the Avogrado number and F.W. is the formula weight relative to the unit formula (g mol^{-1}) as previously given. Anionic clays generally display N_2 isotherm characteristic corresponding to mesoporous or nearly non-porous materials. Typical values of specific surface area of LDH measured by BET range from 20 to 85 m^2 g^{-1} [149]. For example, MgAl-LDH containing anions such as chloride, nitrate and carbonate present surface areas less than 100 m^2 g^{-1}. One approach to enhance the specific surface area consists in performing the synthesis in a mixture of water/alcohol. In contrast, specific surface area of LDH is decreased when hydrothermal crystallization occurs.

4.4.4 Applications

LDH materials have relatively weak interlayer bonding and as a consequence exhibit excellent properties involving interlayer expansion. Several organic and inorganic molecules can be introduced in the interlayer by anionic exchange [140,141] giving rise to materials with desirable physical and chemical properties, designed to fulfill specific requirements. These features lead to high versatility, easily tailored properties and low cost, among other properties, and make LDHs promising materials for a large number of practical applications. Some of the most important applications of LDHs include catalysis, medicine, pharmaceutics (drug delivery), photochemistry (luminescence), electrochemistry (biosensors), polymer industries and in environmental remediation (removal of metal and organic pollutants, adsorbents, etc.) [136,137,171-173]. LDHs have been employed as catalysts in a wide variety of reactions such as condensation of ketones and aldehydes, polymerization of alkene oxides, synthesis of methanol, etc. [173].

The application of LDHs for environmental remediation started to arouse interest nearly 20 years ago. Several contaminants can be removed from waters and industrial effluents by catalytic remediation, photocatalysis, anion exchange and adsorption using LDHs [171,174]. Among the environmental contaminants studied are pesticides, heavy metals and toxic organic chemicals. LDHs have displayed efficient photoactivity towards degradation of pollutants such as phenol, *p*-cresol and dyes [175-178]. LDHs have also been revealed to be effective as visible light photocatalyst for water splitting [179]. $ZnCr-CO_3$ LDH was examined as photocatalyst for the degradation of rhodamine dyes and 4-chloro 2-nitrophenol compounds [180] using visible light. The material was shown to be photoactive in the photodegradation process of these pollutants. The formation of reactive species (hydroxyl radical, singlet oxygen and superoxide anion) and their participation on the mechanism of degradation was tested by using quenchers.

As mentioned in section 4.2 and, although the POM photocatalysts are efficiently employed for the degradation of pesticides, they present as a drawback the difficult separation of the catalyst from the reaction media. Therefore, LDH has been employed as a solid support for the immobilization/intercalation of photocatalysts creating insoluble materials with higher specific areas compared with the pure catalyst. The heterogeneity of POMs is of primordial importance for several applications,

particularly as catalysts and photocatalysts for environmental remediation. The intercalation of POMs in LDH and its applications is the subject of discussion in the next sections.

4.4.5 Polyoxometalate complexes in layered double hydroxides

The development of easily recoverable and recyclable POM-based catalysts is important for their development for heterogeneous catalysis, either to be applied as photocatalyst for degradation of organic compounds or as catalysts in organic reactions. The high stability and, in particular, the negative electric charge of POMs are very important features in the intercalation with LDH. The intercalation of POMs in the galleries of the LDH layers is mainly based on the electrostatic interactions between the intercalated complexes and the positively charged layers of the LDH [127]. Moreover, the possibility to incorporate POMs with different sizes in the interlayer will modulate the reactivity of the POM-pillared compounds. The interlayer POMs are sufficiently large to create gallery heights close to 0.9-2.0 nm. Such dimensions provide sufficient room to allow physical and chemical processes to occur at the interior active sites [181]. In addition, this provides a way of immobilizing the catalytic POMs in order to control their losses in a polar solvent like water. At the same time, their specific surface areas are improved by formation of the pillared compounds [127,181].

4.4.5.1 Synthesis

Although POMs have been intercalated in LDHs with success for use in several fields, particularly in catalysis, it is not easy to synthesize them in high crystalline and pure form since LDHs hosts are basic, whereas POMs are more stable under acidic conditions. Thus, hydrolysis reactions of the LDHs or POMs may partially occur and can result in products that are poorly ordered, X-ray amorphous, or that contain multicrystalline phases inter layered by different anions [127,181,182].

The most widespread and effective method to incorporate POMs in LDH layers is by an anionic exchange reaction [127,183] which provides a pathway for phase separation between the catalyst and the substrate. As so, the resultant catalyst is trapped in a heterogeneous and restricted environment. Direct methods such as co-precipitation are not suitable for the preparation of these systems due to LDH ability to incorporate or precipitate metal cations. For the anionic exchange to occur it is necessary to have a

tight control of the solution pH [181,184]. As earlier mentioned, LDH are stable at more basic pH (around 8 or above) while most of the POMs require acid conditions. Therefore, in order for the anionic exchange to be successful the pH of the solution should be such so that a equilibrium between the hydroxyl layer and the anion to be intercalated is attained. The properties such as the basicity and charge density of the precursors have effects on the crystallinity and the orientations of the products, which finally ensure the maximum interactions between OH groups on the host sheets and the interlayer guest POM anions.

Since 1988, several groups such as those of Pinnavaia [185-187] and Drezdzon [188] have reported the intercalation of POMs in LDH. Given that polyotungstates are considered more stable than polyoxovanadates or polyoxomolybdates, the majority of the research has been conducted on the intercalation of polytungstate compounds. The synthesis of POM-LDH complexes was first reported by Pannavaia *et al.* [185] in 1988 and involved the intercalation of $[V_{10}O_{28}]^{6-}$ in LDH by anionic exchange with precursors of Zn_2Al-Cl, Zn_2Cr-Cl and Ni_3Al-Cl (Cl represents chloride as the interlayer anion). The authors observed that a pH of 4.5 was required to achieve a complete exchange of chloride by $[V_{10}O_{28}]^{6-}$. At higher pH the intercalation of carbonate may occur preventing the complete exchange reaction. Since then many new POM-LDH materials have been synthesized, mostly by anionic exchange, always with careful control of the pH and using LDH precursors with small oxo anions such as Cl^-, NO_3^{2-}, SO_4^{2-}, etc., [127]. Table 4-5 lists some examples of POMs intercalated with different nuclearities (polyotungstates, polyoxovanadates and polyoxomolybdates).

When the POMs to be intercalated are bulky, a high gallery height of the LDH is necessary. Therefore, a new procedure of the anionic exchange method was developed by using LDH precursors intercalated with large organic anions such as terephthalate (TA) or DDS [186]. The introduction of the DDS or TA molecules allows the LDH interlayer gallery to expand, facilitating the diffusion of the POM and its easy introduction in the interlayer by anionic exchange. This new procedure minimizes the hydrolysis reactions. The high crystallinity of the precursor is very important for the subsequent synthesis of the POM-LDH given that the crystallinity of the final material is intrinsically related with that of the precursor. Guo *et al.* [181] reported the intercalation of a series of robust POMs (Preyssler anion $[NaP_5W_{30}O_{110}]^{14-}$, Paratungstate A anion $[W_7O_{24}]^{6-}$, monosubstituted Dawson anion $[P_2W_{17}O_{61}Mn(H_2O)]^{8-}$ and the monosubstituted or lacunary Keggin anions ($[SiW_{11}O_{39}Mn(H_2O)]^{6-}$,

$[SiW_{11}O_{39}Ni(H_2O)]^{6-}$ and $[SiW_{11}O_{39}]^{8-}$) into LDH by anionic exchange using as precursors Mg_2Al, Zn_3Cr, Zn_2Al-LDHs with TA, DDS and nitrite anions, respectively. These precursors were prepared by co-precipitation and presented good crystallinity with basal spacing d_{001} of 1.43 (Mg_2Al-TA), 0.89 (Zn_2Al-NO_3^-) and 2.79 nm (Zn_3Cr-DS). Although the pH of the anionic exchange reaction was taking in consideration, the obtained POMs presented low crystallinity and gallery heights in the range 0.76 to 1.70 nm.

Table 4-5 POMs of different nuclearities intercalated in LDH materials and respective references.

Intercalated POM	LDH-POM Formula	Reference
$[V_{10}O_{28}]^{-6}$	$MgAl$-$V_{10}O_{28}$	[185]
	$ZnAl$-$V_{10}O_{28}$	[182]
$[V_4O_{12}]^{4-}$	$ZnAl$-V_4O_{12}	[182]
$[Mo_7O_{24}]^{6-}$	$MgAl$-Mo_7O_{24}	[188]
$[W_7O_{24}]^{6-}$	$MgAl$-W_7O_{24}	[126]
α-$[H_2W_{12}O_{40}]^{6-}$	$ZnAl$-H_2W_{12}	[189]
$[SiW_{11}O_{39}]^{8}$	$MgAl$-$SiW_{11}O_{39}$	[189]
α-$[SiW_{11}O_{39}]^{8-}$	$ZnAl$-$SiW_{11}O_{39}$	[187]
α-$[SiV_3W_9O_{37}]^{n-}$	$ZnAl$-$SiV_3W_9O_{37}$	[187]
$[NaP_5W_{30}O_{110}]^{14-}$	$ZnAl$-$NaP_5W_{30}O_{110}$	[185,181]
α-$[P_2W_{18}O_{62}]^{6-}$	$Mg(Zn)Al$- $P_2W_{18}O_{62}$	[185,189]
α-$[P_2W_{17}O_{61}]^{10-}$	$Mg(Zn)Al$- $P_2W_{17}O_{61}$	[185,189]
$[P_4W_{30}Zn_4(H_2O)_2O_{112}]^{16-}$	$Mg(Zn)Al$-$P_4W_{30}Zn_4(H_2O)_2O_{112}$	[185,189]

4.4.5.2 Structural characterization

The main techniques used for the characterization of the "pillared" POM-LDH structure and of POM structure in the gallery of the LDH are PXRD and FTIR spectroscopy [182]. These techniques give essential information of the effective intercalation of POMs as well as their orientation inside the LDH layers. However, complementary techniques are also used to give information on the textural and thermal properties of the POMs-LDH. The layered structure of the POM-LDH resembles to that

of brucite, $(Mg(OH)_2)$. The divalent metal cations M^{II} in the layers are partially replaced by trivalent cations M^{III} forming the double hydroxides. The intercalated POMs are linked with the positively charged layer of the host (LDH) by electrostatic interactions and hydrogen bonding formed through the water molecules of the interlayer of the hydroxyl group in the layers, in order to maintain the electrical neutrality of the system. The gallery height l of the POM-LDH is calculated by subtracting the thickness of the host layer (assumed to be equal to the brucite layer $\cong 0.48$ nm) from the basal spacing (d_{001}) calculated by the respective X-PRD data. It is important to note that the size of the intercalated POM anions is responsible for the gallery height (interlayer spacing) of the POM-LDH. Table 4-6 lists the basal spacing values (d_{001}) experimentally obtained and the calculated gallery height of some POM-LDH materials reported in literature.

Table 4-6 Basal spacing values (d_{001}) and respective calculated gallery height of some POM-LDH systems.

POM	d_{001} (nm)	Gallery height (nm)	Ref.
$[V_{10}O_{28}]^{6-}$	1.22	0.75	[185]
$[Mo_7O_{24}]^{6-}$	1.44	0.97	[188]
$[H_2W_{12}O_{40}]^{6-}$	1.48	1.01	[189]
$[SiW_{11}O_{39}]^{8-}$	1.45	0.98	[189]
$[NaP_5W_{30}O_{110}]^{14-}$ (Preyssler anion)	2.17 or 1.71	1.70 or 1.24	[189]

From the analysis of the d_{001} it is possible to infer that the intercalation of POM anions of smaller size (small d_{001}) such as $[V_{10}O_{28}]^{6-}$ lead to smaller gallery heights, while POMs of larger size such as the Preyssler type lead to higher d_{001} values. The study performed by Guo *et al.* [181] on the intercalation of Keggin, Paratungstate A, Dawson and Preyssler POMs in Mg_2Al, Zn_3CrL and Zn_2Al-LDHs revealed interesting results. The interlayer Dawson and Preyssler anions exhibited the highest d_{001} values among the POMs listed in Table 4-6. Furthermore, these systems presented two different d_{001} values. The authors conclude that these differences of the d_{001} values were directly related to the different orientations that the anions can have inside the interlayer space. The interlayer Paratungstate A and Keggin anions show gallery heights in

agreement with the length of C_2 axis orientation of the corresponding POM cluster anion, which favors hydrogen bonding interactions with the hydroxyl groups of the layer. For the interlayer Dawson anion, the gallery height is in agreement with the short dimension of the cluster anion. The intercalated anion is most likely oriented with the pseudo C_2 axis orthogonal or parallel to the brucite-like layer, explaing therefore the two d_{001} values obtained. However, for the interlayer Preyssler anion, one of the largest known POMs, the two d_{001} values were related with the type of LDH precursor used, Mg_2Al-TA or Zn_2Al-NO_3. The interlayer of the Preyssler anion is orientated with its C_5 axis parallel to the brucite-layer when the precursor Mg_2Al-TA is used while it shows a orientation of it C_5 axis perpendicular to the brucite-layer when the precursor is Zn_2Al-NO_3 (2.17 nm).

4.4.5.3 POM-LDH as photocatalysts for degradation of organic pollutants

POM-LDH materials have been employed mainly as catalysts and photocatalysts due to their excellent acid and redox properties. The application of POM-LDH in heterogeneous photocatalysis for the degradation of organic pollutants in water has been carried out by some researchers, although so far the main application of these systems is as catalysts for organic synthesis. Some examples of heterogeneous photocatalysis are given though others have already been mentioned in the last part of the POMs section.

Guo and co-workers [181] reported the synthesis of several robust POMs intercalated in LDH (Paratungstate A anion $W_7O_{24}^{6-}$; $SiW_{11}O_{39}Z(H_2O)^{6-}$ ($Z = Cu^{2+}$, Co^{2+}, Ni^{2+}); $P_2W_{18}O_{62}^{6-}$, Preyssler anion $NaP_5W_{30}O_{110}^{14-}$, $P_2W_{17}O_6Mn(H_2O)^{8-}$) and tested their photocatalytic activity towards the degradation of the organochlorine pesticide hexachlorocyclohexane (HCH) in water. HCH is an important target as it is persistent in environment. The POM-LDH systems were prepared by anion exchange reaction of the synthetic LDH precursor $Mg_4Al_2(OH)_{12}TA.H_2O$, $Zn_3Cr(OH)_8DDS.2H_2O$ or $Zn_2Al(OH)_6NO_3.H_2O$, with pH control. The authors found that the POM-LDH materials prepared have gallery heights in the range 0.70 to 1.7 nm, different surface area and particle sizes of 20-150 nm. These sizes allow the POM-LDH to be considered as supermolecular layered nanometer materials. All these systems exhibit photocatalytic activity towards the degradation of HCH. After 4h of irradiation in near UV region HCH was converted into CO_2 and HCl with conversions ranging from 30 to 80%,

depending on the POM-LDH system used. Moreover, HCB can be totally mineralized by controlling the reactions conditions. The variation on the percentage of HCH conversion resulted from the different surface areas of the POM-LDH systems tested (larger particle size or higher crystallinity usually leads to a lower surface area) and also on the amount of interior active sites (the bonds of W-O-W) that exist in each intercalated POM. All the POM-LDH systems could be separated and reused after simple treatment.

It has already been stated that POMs can be considered as analogues of the semiconductor TiO_2. Therefore, it is expected that its photochemical mechanism of degradation will be similar to TiO_2 with formation of well-defined HOMO-LUMO gaps (band gaps). The gaps inhibit the recombination of electrons (e^-) and holes (h^+) that are generated by the irradiation of the surface with light energy greater than the band gaps. These formed species, e^- and h^+, will then initiate chemical reactions leading to the formation of $HO^\bullet$ through the reaction of holes and water molecules or OH^- groups. Other reactive species formed such as superoxide radical anion may also participate in the degradation of the pollutants, and together with $HO^\bullet$ lead to the degradation and mineralization of these molecules.

Taking this in consideration Guo *et al*. [181] proposed the following reaction mechanism for the photocatalytic degradation of aqueous hexachlorocyclohexane (HCH) on the POM-HDL intercalate: as a heterogeneous photocatalyst, the POM in the interlayer has the double aptitudes of adsorption of the reactants on the catalyst´s surface and absorption of the photon with energy greater than its band gap. When the POM-LDH is irradiated with suitable light energy, POMs in the interlayers are excited to their charge-transfer excited state (POM-LDH)*. The interlayer space provides the reaction place and easier accesses to the POMs active sites and shorter diffusion pathways. The excitation of the POM-LDH at the O-MCT band can be presented using the semiconductor notation as (reaction 4.42), with generation of reactive holes (h^+) and electrons (e^-).

$$POM - LDH \xrightarrow{h\nu} (POM - LDH)^* \approx POM - LDH\,(h^+ + e^-) \tag{4.42}$$

$$POM - LDH\,(h^+ + e^-) + H_2O \rightarrow POM\,(e^-) + HO^\bullet + H^+ \tag{4.43}$$

$$HO^\bullet + HCB \rightarrow \text{oxidation products} \rightarrow\rightarrow \tag{4.44}$$

$$\rightarrow\rightarrow CO_2 + H_3O + \text{inorg. anions}$$

$$POM - LDH\ (e^-) + O_2 \rightarrow POM + O_2^{\bullet -} \tag{4.45}$$

$$O_2^{\bullet -}/HO_2^{\bullet} + HCB \rightarrow \text{oxidation products} \tag{4.46}$$
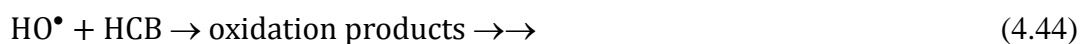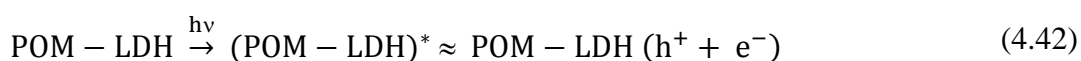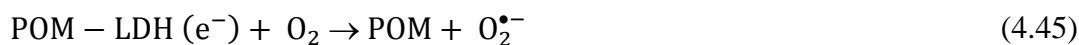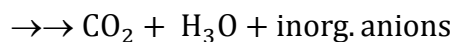
POM-LDH (e^- + h^+) has a more powerful redox ability by forming electron-hole pairs and their recombination is inhibited by the "gap" of the POM. At the same time the HCH molecules diffuse into the interlayer space and are photoactivated by the (POM-LDH)*. The electron and holes formed can cause reduction and oxidation, respectively. The photo-holes (h^+) can react with water molecules or with hydroxyl groups coming from the LDH sheets generating the highly reactive HO$^{\bullet}$ radicals (reaction 4.43). The electrons can react with the oxygen present in air to form superoxide anions (reaction 4.45). The HO$^{\bullet}$ radicals formed, which are strong and unselective oxidant species, are the main species responsible for the degradation and mineralization of the pesticide HCB into CO_2, water and inorganic molecules (reaction 4.44). The superoxide anion can also react with HCB molecules to form oxidation products (reaction 4.46). The final product molecules desorb from the POM active sites and escape from the interlayer space through diffusion. A schematic model for the overall process is depicted in Figure 4-11.
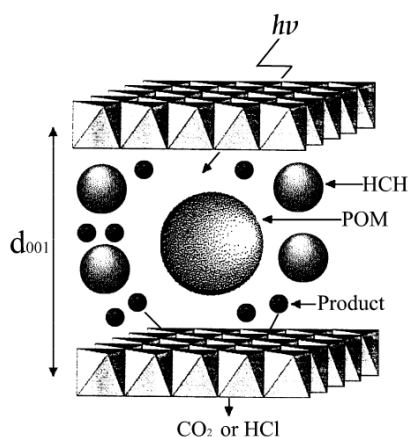
Figure 4-11 Model of the photocatalytic degradation of HCH on the POM-LDHs proposed by Guo *et al.* [181]. Interlayer water and oxygen molecules were omitted by the authors in the proposed model.

The same group of Guo *et al.* in 2002 [190] prepared Zn/Al/W(Mn) mixed oxides by calcination of the POM precursors $Zn_2Al(OH)_6SiW_{11}O_{39}]_{0.12}.0.2H_2O$

(abbreviated as ZnAl-SiW$_{11}$) and Zn$_2$Al(OH)$_6$[SiW$_{11}$O$_{39}$Mn$_{(H2O)}$]$_{0.16}$.0.3H$_2$O (abbreviated as ZnAl-SiW$_{11}$Mn) intercalated in LDHs at 600-700 ºC and also tested them in the photodegradation of HCH. These compounds present different absorption bands (O-MCT bands) ranging from 200 to 400 nm depending on the system. It was observed that the mixed oxides thus obtained exhibited higher photocatalytic activity to degrade aqueous HCH pesticide when compared with the POM-LDH precursors. Their photocatalytic activity was correlated with the absorption bands, surface physicochemical properties and with porous structure. The *as*-synthesized mixed oxides, which had as predominant phase a ZnWO4 inverse spinel structure, exhibited relatively high BET surface areas and large sizes. The ZnAl-SiW$_{11}$Mn metal oxide presented the highest photocatalytic activity due to its mesoporous structure that allowed the reaction to take place inside the pores, increasing the host-guest interaction. These photocatalytic materials were also easy to separate from the reaction and are reusable.

These results obtained in this study seem to show that the photocatalytic activity of the POMs intercalated in LDH is dependent on:

• absorption band region: in general, lower band gaps (higher O-MCT band) result in higher photocatalytic activity since the transition from the ground state to the excited state is easier.

• surface physicochemical properties and porous structures: the small particle size near the nanometer range of the POM-LDH compounds is essential to enhance its photochemical activity because the distance that the formed photoinduced holes and electrons have to diffuse before reaching the interface decreases. Hence, the holes and electrons can be captured by the electrolyte in aqueous solution such as OH$^-$ groups, and then photogenerate HO$^{\bullet}$ via neutralization of OH$^-$ groups on the surface of the POM-LDH with the positive holes. The electrophilic HO$^{\bullet}$ radicals thus obtained are responsible for the total oxidation of the organic substrates in aqueous solutions.

The photochemical properties presented by the decatungstate anion and its potential application as AOP process for the degradation of pollutants led us to study its effective application for the photocatalytic degradation of the pesticide NAD. However, the high solubility of decatungstate requires its immobilization in a solid support. LDH materials were chosen with this purpose since its anionic exchange capacity allows tailoring the textural properties of the porous structure enhancing therefore the photocatalytic activity of decatungstate by creating LDH-POM materials with higher surface and insoluble in water.

4.5 References

[1] R. Andreozzi, V. Caprio, A. Insola, R. Marotta, Advanced oxidation processes (AOP) for water purification. *Catal. Today*, **1999**, 53, 51-59.

[2] O. Legrini, E. Oliveros, A. M. Braun, Photochemical processes for water treatment. *Chem. Rev.*, **1993**, 93, 671-698.

[3] P. M. Poyatos, M. M. Muñio, M. C. Almecija, J. C. Torres, E. Hontoria, F. Osorio, Advanced oxidation processes for wastewater treatment: state of the art. *Water Air Soil Pollut.*, **2010**, 205, 187-204.

[4] S. J. Masten, S. H. R. Davies, The use of ozonation to degrade organic contaminants in wastewaters. *Environ. Sci. Technol.*, **1994**, 28, 180A-185A.

[5] D. Chen, M. Sivakumar, A. K. Ray, Heterogeneous photocatalysis in environmental remediation. *Dev. Chem. Eng. Mineral Process*, **2000**, 8, 505-550.

[6] M. Romero, J. Blanco, B. Sánchez, A. Vidal, S. Malato, A. I. Cardona, E. Garcia, Solar photocatalytic degradation of water and air pollutants. Challenges and perspectives. *Sol. Energy*, **1999**, 66, 169-182.

[7] D. Ljubas, Solar photocatalysis - a possible step in drinking water treatment. *Energy*, **2005**, 30, 1699-1710.

[8] W. H. Glaze, J. W. Kang, D. H. Chapin, The chemistry of water treatment processes involving ozone, hydrogen peroxide and UV-radiation. *Ozone Sci. Eng.*, **1987**, 9, 335-352.

[9] L. M. Dorfman, G. E. Adams, *Reactivity of the Hydroxyl Radical*, National Bureau of Standards, Report No. NSRDS-NBS-46, **1973**.

[10] P. Saritha, D. S. S. Raj, C. Aparna, P. N. V. Laxmi, V. Himabindu, Y. Anjaneyulu, Degradative oxidation of 2,4,6-trichlorophenol using advanced oxidation processes - a comparative study. *Water Air Soil Pollut.*, **2009**, 200,169-179.

[11] M. Pelaeza, N. T. Nolan, S. C. Pillai, M. K. Seery, P. Falaras, A. G. Kontos, P. S. M. Dunlop, J. W. J. Hamilton, J. A. Byrne, K. O'Shea, M. H. Entezari, D. D. Dionysiou, A review

on the visible light active titanium dioxide photocatalysts for environmental applications. *Appl. Catal. B: Environ.*, **2012**, 125, 331-349.

[12] U. I. Gaya, A. H. Abdullah, Heterogeneous photocatalytic degradation of organic contaminants over titanium dioxide: A review of fundamentals, progress and problems. *J. Photochem. Photobiol. C: Photochem. Rev.*, **2008**, 9, 1-12.

[13] M. N. Chong, B. Jin, C. W. K. Chow, C. Saint, Recent developments in photocatalytic water treatment technology: a review. *Water Res.*, **2010**, 44, 2997-3027.

[14] D. Zhang, G. Li. J. C. Yu, Inorganic materials for photocatalytic water disinfection. *J. Mater. Chem.*, **2010**, 20, 4529-4536.

[15] S Guittoneau J. P. Duguet, C. Bonnel, M. Dore, Oxidation of parachloronitrobenzene in dilute aqueous solution by O_3+UV and H_2O_2+UV: a comparative study. *Ozone Sci. Eng.*, **1990**, 12, 73-94.

[16] Y. Qu., X. Duan, Progress, challenge and perspective of heterogeneous photocatalysts. *Chem. Soc. Rev.*, **2013**, 42, 2568-2580.

[17] J. M. Herrmann, Photocatalysis fundamentals revisited to avoid several misconceptions. *Appl. Catal. B: Environ.*, **2010**, 99, 461-468.

[18] N. Serpone, E. Pelizzetti, *Photocatalysis, Fundamentals and Applications*, Wiley, New York, **1989**.

[19] J. M. Herrmann, Heterogeneous photocatalysis: state of the art and present applications. *Top. Catal.*, **2005**, 34, 49-65.

[20] L. Muszkat, L. Bir, L. Feigelson, Solar photocatalytic mineralization of pesticides in polluted waters. *J. Photochem. Photobiol. A: Chem.*, **1995**, 87, 85-88.

[21] D. Ravelli, D. Dondi, M. Fagnonia, A. Albini, Photocatalysis. A multi-faceted concept for green chemistry. *Chem. Soc. Rev.*, **2009**, 38, 1999-2011.

[22] D. A. Keane, K. G. McGuigan, P. F. Ibáñez, M. I. Polo-López, J. A. Byrne, P. S. M. Dunlop, K. O'Shea, D. D. Dionysiou, S. C. Pillai, Solar photocatalysis for water disinfection: materials and reactor design. *Catal. Sci. Technol.*, **2014**, 4, 1211-1226.

[23] S. Malato, J. Blanco, C. Richter, B. Braun, M. I. Maldonado, Enhancement of the rate of solar photocatalytic mineralization of organic pollutants by inorganic oxidizing species. *Appl. Catal. B: Environ.*, **1998**, 17, 347-356.

[24] S. Tamimi, Q. N. Barka, A. Assabbane, Y. Ait-Ichou, Methomyl degradation in aqueous solutions by Fenton's reagent and the photo-Fenton system. *Sep. Purif. Technol.*, **2008**, 6, 103-108.

[25] R. F. P. Nogueira, A. G. Trovo, M. R. A. da Silva, Fundaments and environmental applications of Fenton and photo-Fenton processes. *Química Nova*, **2007**, 30, 400-408.

[26] J. J. Pignatello, E. Oliveros, A. MacKay, Advanced oxidation processes for organic contaminant destruction based on the Fenton reaction and related chemistry. *Crit. Rev. Environ. Sci. Technol.*, **2006**, 36, 1-84.

[27] E. Brillas, I. Sires, M. A. Oturan, Electro-Fenton process and related electrochemical technologies based on Fenton's reaction chemistry. *Chem. Rev.*, **2009**, 109, 6570-6631.

[28] V. Kavitha, K. Palanivelu, The role of ferrous ion in Fenton and photo-Fenton processes for the degradation of phenol. *Chemosphere*, **2004**, 55, 1235-1243.

[29] V. Kavitha, K. Palanivelu, Degradation of nitrophenols by Fenton and photo-Fenton processes. *J. Photochem. Photobiol. A: Chem.*, **2005**, 170, 83-95.

[30] A. N. Soon, B. H. Hameed, Heterogeneous catalytic treatment of synthetic dyes in aqueous media using Fenton and photo-assisted Fenton process. *Desalination*, **2011**, 269, 1-16.

[31] A. Mills, S. Le Hunte, An overview of semiconductor photocatalysis. *J. Photochem. Photobiol. A: Chem.*, **1997**, 108, 1-35.

[32] M. R. Hoffmann, S. T. Martin, W. Choi, D. W. Bahnemann, Environmental applications of semiconductor photocatalysis. *Chem. Rev.*, **1995**, 95, 69-96.

[33] M. A. Fox, M. I. Dulay, Heterogeneous photocatalysis. *Chem. Rev.*, **1993**, 93, 341-357.

[34] A. Kudo, Y. Miseki, Heterogeneous photocatalyst materials for water splitting. *Chem. Soc. Rev.*, **2009**, 38, 253-278.

[35] N. Serpone, E. Pelizzetti, M. Grätzel, Photosensitization of semiconductors with transition metal complexes - a route to the photoassisted cleavage of water. *Coord. Chem. Rev.*, **1985**, 64, 225-245.

[36] G. K. Mor, O. K. Varghese, M. Paulose, K. Shankar, C. A. Grimes, A review on highly ordered, vertically oriented TiO_2 nanotube arrays: Fabrication, material properties, and solar energy applications. *Sol. Ener. Mat. Sol. Cells*, **2006**, 90, 2011-2075.

[37] J. Gamage, Z. Zhang, Applications of photocatalytic disinfection. *Int. J. Photoenergy*, **2010**, 2010, 1-11.

[38] I. K. Konstantinou, Triantafyllos A. Albanis, Review. Photocatalytic transformation of pesticides in aqueous titanium dioxide suspensions using artificial and solar light: intermediates and degradation pathways. *App. Catal. B: Environ.*, **2003**, 42, 319-335.

[39] E. Pelizzetti, V. Maurino, C. Minero, O. Zerbinati, E. Borgarello, Photocatalytic degradation of bentazon by TiO_2 particles. *Chemosphere*, **1989**, 18, 1437-1445.

[40] K. D. Zoh, T. S. Kim, J. G. Kim, K. H. Choi, Degradation of parathion and the reduction of acute toxicity in TiO_2 photocatalysis. *Water Sci. Tech.*, **2005**, 52, 45-52.

[41] D. S. Bhatkhande, V. G. Pangarkar, A. A. C. M Beenackers, Photocatalytic degradation for environmental applications - a review. *J. Chem. Technol. Biotechnol.*, **2001**, 77, 102-116.

[42] A. Di Paola, E. García-López, G. Marcìa, L. Palmisano, A survey of photocatalytic materials for environmental remediation. *J. Hazard. Mater.*, **2012**, 211-212, 3-29.

[43] G. Palmisano, V. Augugliaro, M. Pagliarob, L. Palmisano, Photocatalysis: a promising route for 21st century organic chemistry. *Chem. Commun.*, **2007**, 3425-3437.

[44] S. Pehkonen, R. Siefert, S. Webb, M. R. Hoffmann, Photoreduction of iron oxyhydroxides in the presence of important atmospheric organic compounds. *Environ. Sci. Technol.*, **1993**, 27, 2056-20629.

[45] E. R. Carraway, A. J. Hoffman, M. R. Hoffmann, Photocatalytic oxidation of organic acids on quantum-sized semiconductor colloids. *Environ. Sci. Technol.*, **1994**, 28, 786-793.

[46] N. T. Nolan, M. K. Seery, S. C. Pillai, Spectroscopic investigation of the anatase-to-rutile transformation of sol-gel-synthesized TiO_2 photocatalysts. *J. Phys. Chem. C*, **2009**, 113, 16151-16157.

[47] K. Fujihara, T. Ohno, M. Matsumura, Splitting of water by electrochemical combination of two photocatalytic reactions on TiO_2 particles. *J. Chem. Soc., Faraday Trans.*, **1998**, 94, **3705-3709.**

[48] W. Choi, A. Termin, M. R. Hoffmann, The role of metal ion dopants in quantum-sized TiO_2: correlation between photoreactivity and charge carrier recombination dynamics. *J. Phys. Chem. B*, **1994**, 98, 13669-13679.

[49] C. H. Wu, Comparison of azo dye degradation efficiency using UV/single semiconductor and UV/coupled semiconductor systems. *Chemosphere*, **2004**, **57**, 601-608.

[50] E. Gkika, P. Kormali, S. Antonaraki, D. Dimoticali, E. Papaconstantinou, A. Hiskia, Polyoxometallates as effective photocatalysts in water purification from pesticides. *Int. J. Photoenergy*, **2004**, 6, 227-231.

[51] A. Hiskia, E. Androulaki, A. Mylonas, A. Troupis, E. Papaconstantinou, *Photocatalytic decontamination by polyoxometalates*. In: Polyoxometalate Chemistry, Eds. M. T. Pope, A. Müller, pp 417-424, Kluwer Academic Publishers, **2001**.

[52] A. Mylonas, E. Papaconstantinou, On the mechanism of photocatalytic degradation of chlorinated phenols to CO_2 and HCl by polyoxometalates. *J. Photochem. Photobiol. A: Chem.*, **1996**, 94, 77-82.

[53] P. Kormali, A. Troupis, Triantis, T., Hiskia, A., E. Papaconstantinou, Photocatalysis by polyoxometallates and TiO_2: a comparative study. *Catal. Today*, **2007**, 124, 149-155.

[54] A. Hiskia, A. Mylonas, E. Papaconstantinou, Comparison of the photoredox properties of polyoxometalates and semiconducting particles. *Chem. Soc. Rev.*, **2001**, 30, 62-69.

[55] E. Pelizzetti, V. Maurino, C. Minero, V. Carlin, M. L. Tosato, E. Pramauro, O. Zerbinati, Photocatalytic degradation of atrazine and other s-triazine herbicides. *Environ. Sci. Technol.*, **1990**, 24, 1559-1565.

[56] I. Texier, J. Ouazzani, J. Delaire, C. Giannotti, Study of the Mechanisms of the photodegradation of atrazine in the presence of two photocatalysts: TiO_2 and $Na_4W_{10}O_{32}$. *Tetrahedron*, **1999**, 55, 3401-3412.

[57] S. Antonaraki, T. M. Triantis, E. Papaconstantinou, A. Hiskia, Photocatalytic degradation of lindane by polyoxometalates: intermediates and mechanistic aspects. *Catal. Today*, **2010**, 151, 119-124.

[58] J. J. Berzelius, The preparation of phosphomolybdate ion $[PMo_{12}O_{40}]^{3-}$. *Ann. Phys. Chem.*, **1826**, 82, 369-392.

[59] L. Pauling, The molecular structure of the tungstosilicates and related compounds. *J. Am. Chem. Soc.*, **1929**, 51, 2868-2880.

[60] J. F. Keggin, The structure and formula of 12-phosphotungstic acid. *Proc. R. Soc. Lond. A*, **1934**, 144, 75-100.

[61] J. S. Anderson, Constitution of the poly-acids. *Nature*, **1937**, 140, 850-850.

[62] H. T. Evans, The crystal structures of ammonium and potassium molybdotellurates. *J. Am. Chem. Soc.*, **1948**, 70, 1291-1292.

[63] I. Lindqvist, A crystal structure investigation of the paramolybdate ion. *Arkiv. Kemi*, **1950**, 2, 325-341.

[64] M. T. Pope, A. Müller, Polyoxometalate chemistry: an old field with new dimensions in several disciplines. *Angew. Chem., Int. Ed. Engl.*, **1991**, 30, 34-48.

[65] C. L. Hill, Introduction: polyoxometalates-multicomponent molecular vehicles to probe fundamental issues and practical problems. *Chem. Rev.*, **1998,** 98, 1-2.

[66] R. M. Ammam, Polyoxometalates: formation, structures, principal properties, main deposition methods and application in sensing. *J. Mater. Chem. A*, **2013**, 1, 6291-6312.

[67] D. L. Long, E. Burkholder, L. Cronin, Polyoxometalate clusters, nanostructures and materials: From self assembly to designer materials and devices. *Chem. Soc. Rev.*, **2007**, 36, 105-121.

[68] Y.-F. Song, R. Tsunashima, Recent advances on polyoxometalate-based molecular and composite materials. *Chem. Soc. Rev.*, **2012**, 41, 7384-7402.

[69] D. Fan, J. Hao, Q. Wei, Assembly of polyoxometalate-based composite materials. *J. Inorg. Organomet. Polym.*, **2012**, 22, 301-306.

[70] M. T. Pope, *Heteropoly and Isopoly Oxometalates*. In: Polyoxometalate Molecular Science, Eds J. J. Borrás-Almenar, E. Coronado, A. Müller, M. Pope, Kluwer Academic Publishers, Springer-Verlag, Dordrecht, **2003**.

[71] C. R. Deltcheff, M. Fournier, R. Franck, R. Thouvenot, Vibrational investigations of polyoxometalates. 2. Evidence for anion-anion interactions in molybdenum (VI) and tungsten (VI) compounds related to the Keggin structure. *Inorg. Chem.*, **1983**, 22, 207-216.

[72] Y. P. Jeannin, The nomenclature of polyoxometalates: how to connect a name and a structure. *Chem. Rev.*, **1998**, 98, 51-76.

[73] D. E. Katsoulis, A survey of applications of polyoxometalates. *Chem. Rev.*, **1998**, 98, 359-387.

[74] M. Sadakane, E. Steckhan, Electrochemical properties of polyoxometalates as electrocatalysts. *Chem. Rev.*, **1998**, 98, 219-237.

[75] J. T. Rhule, C. L. Hill, D. A. Judd, R. F. Schinazi, Polyoxometalates in medicine. *Chem. Rev.*, **1998**, 98, 327-358.

[76] C.L. Hill, C. M. Prosser-McCartha, Homogeneous catalysis by transition metal oxygen anion clusters. *Coord. Chem. Rev.*, **1995**, 143, 407-455.

[77] A. Hiskia, E. Androulaki, A. Mylonas, S. Boyatzis, D. Dimoticali, C. Minero, E. Pelizzetti, E. Papaconstantinou, Photocatalytic mineralization of chlorinated organic pollutants in water by polyoxometallates. Determination of intermediates and final degradation products. *Res. Chem. Intermed.*, **2000**, 26, 235-251.

[78] J. J. Stracke, R. G. Finke, Electrocatalytic water oxidation beginning with the cobalt polyoxometalate $[Co_4(H_2O)_2(PW_9O_{34})2]^{10-}$: identification of heterogeneous CoOx as the dominant catalyst. *J. Am. Chem. Soc.*, **2011**, 133, 14872-14875.

[79] Y. Sasaki, T. Yamase, Y. Ohashi, Y. Sasada, Structural retention of decatungstates upon photoreduction. *Bull. Chem. Soc. Jpn.*, **1987**, 60, 4285-4290.

[80] A. J. Bridgeman, G. Cavigliasso, Structure and bonding in $[W_{10}O_{32}]^{n-}$ isopolyanions, *J. Phys. Chem. A*, **2002**, 106, 6114-6120.

[81] T. Yamase, N. Takabayashi, M. Kaji, Solution photochemistry of tetrakis (tetrabutylammonium) decatungstate (VI) and catalytic hydrogen evolution from alcohols. *J. Chem. Soc., Dalton Trans.*, **1984**, 793-799.

[82] R. F. Renneke, M. Pasquali, C. L. Hill, Polyoxometalate systems for the catalytic selective production of non thermodynamic alkenes from alkanes. Nature of excited-state deactivation processes and control of subsequent thermal processes in polyoxometalate photoredox chemistry. *J. Am. Chem. Soc.*, **1990**, 112, 6585-6594.

[83] Y. Nosaka, T. Takei, N. Fujii, Photinduced reduction of $W_{10}O_{32}^{4-}$ by organic compounds in aqueous solution. *J. Photochem. Photobiol. A: Chem.*, **1995**, 92, 173-179.

[84] D. C. Duncan, T. L. Netzerl, C. Hill, Early-time dynamics and reactivity of polyoxometalate excited states. Identification of a short-lived LMCT excited state and a reactive long-lived charge-transfer intermediate following picoseconds flash excitation of $[W_{10}O_{32}]^{4-}$ in acetonitrile. *Inorg. Chem.*, **1995**, 34, 4640-4646.

[85] D. C. Duncan, M. A. Fox, Early events in decatungstate photocatalyzed oxidations: a nanosecond laser transient absorbance reinvestigation. *Phys. Chem. A*, **1998**, 102, 4559-4567.

[86] I. Texier, J. A. Delaire, C. Giannotti, Reactivity of the charge transfer excited state of sodium decatungstate at the nanosecond time scale. *Phys. Chem. Chem. Phys.*, **2000**, 2, 1205-1212.

[87] A. Chemseddine, C. Sanchez, J. Livage, J. P. Launay, M. Fournieric, Electrochemical and photochemical reduction of decatungstate: a reinvestigation. *Inorg. Chem.*, **1984**, 23, 2609-2613.

[88] D. Ravelli, D. Dondi, M. Fagnoni, A. Albinia, A. Bagno, Electronic and EPR spectra of the species involved in $[W_{10}O_{32}]^{4-}$ photocatalysis. A relativistic DFT investigation. *Phys. Chem. Chem. Phys.*, **2013**, 15, 2890-2896.

[89] M. D. Tzirakis, I. N. Lykakis, M. Orfanopoulos, Decatungstate as an efficient photocatalyst in organic chemistry. *Chem. Soc. Rev.*, **2009**, 38, 2609-2621.

[90] C. Tanielian, Decatungstate photocatalysis. *Coord. Chem. Rev.*, **1998**, 178-180, 1165-1181.

[91] C. Tanielian, I. N. Lykakis, R. Seghrouchni, F. Cougnon, M. Orfanopoulos, Mechanism of decatungstate photocatalyzed oxygenation of aromatic alcohols: Part I. Continuous photolysis and laser flash photolysis studies. *J. Mol. Catal. A*, **2007**, 262, 170-175.

[92] C. Giannotti, C. Richter, Photocatalysed oxidation of cyclohexane by $W_{10}O_{32}{}^{4-}$ irradiation with natural sunlight. *Int. J. Photoenergy*, **1999**, 1, 1-5.

[93] I. N. Lykakis, C. Tanielian, R. Seghrouchni, M. Orfanopoulos, Mechanism of decatungstate photocatalyzed oxygenation of aromatic alcohols: Part II. Kinetic isotope effect studies. *J. Mol. Catal. A*, **2007**, 262, 176-184.

[94] C. Tanielian, R. Seghrouchni, C. Schweitzer, Decatungstate photocatalyzed electron-transfer reactions of alkenes. Interception of the geminate radical ion pair by oxygen. *J. Phys. Chem. A*, **2003**, 107, 1102-1111.

[95] I. N. Lykakis, E. Evgenidou, M. Orfanopoulos, Photo-catalysis and polyoxo-anion decatungstate in organic chemistry: a manifold concept for green chemistry. *Curr. Org. Chem.*, **2012**, 16, 2400-2414.

[96] A. Allaoui, M. A. Amlouki, P. Wong-Wah-Chung, Homogeneous photodegradation study of 2-mercaptobenzothiazole photocatalysed by sodium decatungstate salts: Kinetics and mechanistic pathways. *J. Photochem. Photobiol. A: Chem.*, **2010**, 212, 153-160.

[97] A. Mylonas, E. Papaconstantinou, Photocatalytic degradation of p-cresol by polyoxotugstates. Mechanistic implications. *Polyhedron*, **1996**, 15, 3211-3217.

[98] I. Texier, C. Giannotti, S. Malato, C. Richter, J. Delaire, Solar photodegradation of pesticides in water by sodium decatungstate. *Catal. Today*, **1999**, 54, 297-307.

[99] C. Tanielian, K. Duffy, A. Jones, Kinetic and mechanistic aspects of photocatalysis by polyoxotungstates: a laser flash photolysis, pulse radiolysis and continuous photolysis study. *J. Phys. Chem. B*, **1997**, 101, 4276-4282.

[100] I. Texier, J. F. Delouis, J. A. Delaire, C. Giannotti, P. Plaza, M. M. Martin, Dynamics of the first excited state of the decatungstate anion studied by subpicosecond laser spectroscopy. *Chem. Phys. Lett.*, **1999**, 3111, 139-145.

[101] A. Hiskia, E. Papaconstantinou, Photocatalytic oxidation of organic compounds by polyoxometalates of molybdenum and tungsten. Catalyst regeneration by dioxygen. *Inorg. Chem.*, **1992**, 31, 163-167.

[102] A. Mylonas, A. Hiskia, E. Androulaki, D. Dimotikali, E. Papaconstantinou, New aspect of the mechanism of photocatalytic oxidation of organic compounds by polyoxometalates in aqueous solutions. The selective photooxidation of 2-propan-2-ol to propanone: the role of the OH radicals. *Phys. Chem. Chem. Phys.*, **1999**, 1, 437-440.

[103] A. Molinari, R. Argazzi, A. Maldotti, Photocatalysis with $Na_4W_{10}O_{32}$ in water system: formation and reactivity of HO• radicals. *J. Mol. Catal. A: Chem.*, **2013**, 372, 23-28.

[104] G. Zhang, Y. Xu, Polyoxometalate-mediated reduction of dichromate under UV irradiation. *Inorg. Chem. Comm.*, **2005**, 8, 520-523.

[105] A. Mylonas, A. Hiskia, E. Papaconstantinou, Contribution to water purification using polyoxometalates. Aromatic derivatives, chloroacetic acids, *J. Mol. Catal. A*, **1996**, 114, 191-200.

[106] C. Hu, B. Yue, T. Yamase, Photoassisted dehalogenation of organochlorine compounds by paratungstate A in aqueous solutions. *Appl. Catal. A*, **2000**, 194-195, 99-107.

[107] S. Rafqah, P. Wong-Wah Chung, C. Forano, M. Sarakha, Photocatalytic degradation of metsulfuron methyl in aqueous solution by decatungstate anions. *J. Photochem. Photobiol. A: Chem.*, **2008,**199, 297-302.

[108] Y. Guo, C. Hu, Heterogeneous photocatalysis by solid polyoxometalates. *J. Mol. Catal. A: Chem.*, **2007**, 262, 136-148.

[109] R. R. Ozer, J. L. Ferry, Photocatalytic oxidation of aqueous 1,2- dichlorobenzene by polyoxometalates supported on the NaY zeolite. *J. Phys. Chem. B*, **2002**, 106, 4336-4342.

[110] N. Okun, T. Anderson, C. Hill, $[(Fe^{III}(OH_2)_2)_3(A-\alpha-PW_9O_{34})_2]^{9-}$ on cationic silica nanoparticles, a new type of material and efficient heterogeneous catalyst for aerobic oxidations. *J. Am. Chem. Soc.*, **2003**, 125, 3194-3195.

[111] A. Molinari, A. Bratovcic, G. Magnacca, A. Maldotti, Matrix effects on the photocatalytic oxidation of alcohols by $[nBu_4N]_4W_{10}O_{32}$ incorporated into sol-gel silica. *Dalton Trans.*, **2010**, 39, 7826-7833.

[112] A. Molinari, A. Maldotti, A. Bratovcic, G. Magnacca, Photocatalytic properties of sodium decatungstate supported on sol-gel silica in the oxidation of glycerol. *Catal. Today*, **2013**, 206, 46-52.

[113] L. Ni, J. Ni, Y. Lu, P. Yang, Y. Cao, Photooxygenation of hydrocarbons over efficient and reusable decatungstate heterogenized on hydrophobically-modified mesoporous silica. *Chem. Commun.*, **2009**, 2171-2173.

[114] C. Rocchiccioli-Deltcheff, M. Amirouche, G. Herve, M. Fournier, M. Che, J. M. Tatibouet, Structure and catalytic properties of silica supported polyoxomolybdates: II. Thermal

behavior of unsupported and silica-supported 12-molybdosilicic acid catalysts from IR and catalytic reactivity studies. *J. Catal.*, **1990**, 126, 591-599.

[115] H. Choi, Y. Chang, Y. Kwon, O. Han, Incorporation of decavanadate ions into silica gels and mesostructured silica walls. *Chem. Mater.*, **2003**, 15, 3261-3267.

[116] L. Li, C. Liu, A. Geng, C. Jiang, Y. Guo, C. Hu, Preparation, characterization and photocatalytic applications of amine-functionalized mesoporous silica impregnated with transition-metal-monosubstituted polyoxometalates. *Mater. Res. Bull.*, **2006**, 41, 319-332.

[117] B. J. S. Johnson, A. Stein, Surface modification of mesoporous, macroporous, and amorphous silica with catalytically active polyoxometalate clusters. *Inorg. Chem.*, **2001**, 40, 801-808.

[118] A. Molinari, R. Amadelli, A. Mazzacani, G. Sartori, A. Maldotti, Tetralkylammonium and sodium decatungstate heterogenized on silica: effects of the nature of cations on the photocatalytic oxidation of organic substrates. *Langmuir*, **2002**, 18, 5400-5405.

[119] Y. Izumi, K. Urabe, Catalysis of heteropoly acids entrapped in activated carbon. *Chem. Lett.*, **1981**, 63-666.

[120] S. Fujibayashi, K. Nakayama, Y. Nishiyama, Y. Ishii, Oxidation of phenols and hydroquinones by dioxygen catalyzed by mixed addenda heteropolyoxometalate on active carbon (NPV_6Mo_6). *Chem. Lett.*, **1994**, 1345-1348.

[121] R. Gall, C. Hill, J. Walker, Carbon powder and fiber-supported polyoxometalate catalytic materials. Preparation, characterization, and catalytic oxidation of dialkyl sulfide as mustard (HD) analogues. *Chem. Mater.* **1996**, 8, 2523-2527.

[122] Y. Yang, Y. Guo, C. Hu, Y.Wang, E. Wang, Preparation of surface modifications of mesoporous titania with monosubstituted Keggin units and their catalytic performance for organochlorine pesticide and dyes under UV irradiation. *Appl. Catal. A: Gen.*, **2004**, 273, 201-210.

[123] L. Li, Q-y. Wu, Y-h. Guo, C.-w. Hu, Nanosize and bimodal porous polyoxotungstate–anatase TiO_2 composites: preparation and photocatalytic degradation of organophosphorus pesticide using visible-light excitation. *Microp. Mesop. Mat.*, **2005**, 87, 1-9.

[124] I. V. Kozhevnikov, A. Sinnema, R. J. J. Jansen, K. Pamin, H. van Bekkum, New acid catalyst comprising heteropoly acid on a mesoporous molecular-sieve MCM-41. *Catal. Lett.*, **1995**, 30, 241-252.

[125] A. Maldotti, A. Molinari, G. Varani, M. Lenarda, L.Storaro, F. Bigi, R. Maggi, A. Mazzacani, G. Sartori, Immobilization of (n-$Bu_4N)_4W_{10}O_{32}$ on mesoporous MCM-41 and amorphous silica for photocatalytic oxidation of cycloalkanes with molecular oxygen. *J. Catal.*, **2002**, 209, 210-216.

[126] Y. Guo, D. Li, C. Hu, Y. Wang, E. Wang, Y. Zhou, S. Feng, Photocatalytic degradation of aqueous organocholorine pesticide on the layered double hydroxide pillared by Paratungstate A ion, $Mg_{12}Al_6(OH)_{36}(W_7O_{24})\cdot 4H_2O$. *Appl. Catal. B: Environ.*, **2001**, 30, 337-349.

[127] C. Hu, Q. He, Y. Zhang, E. Wang, T. Okura, M. Misono, Synthesis, stability and oxidative activity of polyoxometalates pillared anionic clays $ZnAl-SiW_{11}$ and $ZnAl-SiW_{11}Z$. *Catal. Today*, **1996**, 30, 141-146.

[128] C. Hu, Q. He, Y. Zhang, Y. Liu, Y. Zhang, T. Tang, J. Zhang, E. Wang, Synthesis of new types of polyoxometalate pillared anionic clays: ^{31}P and ^{27}Al MAS NMR study of the orientation of intercalated $PW_{11}VO_{40}^{4-}$. *Chem. Commun.*, **1996**, 2, 121-122.

[129] Y. Guo, Y. Wang, C. Hu, Y. Wang, E. Wang, Y. Zhou, S. Feng, Microporous Polyoxometalates $POMs/SiO_2$: Synthesis and photocatalytic degradation of aqueous organocholorine pesticides. *Chem. Mater.*, **2000**, 12, 3501-3508.

[130] Y. Guo, C. Hu, X. Wang, Y. Wang, E. Wang, Microporous decatungstates: synthesis and photochemical behavior. *Chem. Mater.*, **2001**, 13, 4058-4064.

[131] B. Yue, Y. Zhou, J. Xu, Z. Wu, X. Zhang, Y. Zou, S. Jin, Photocatalytic degradation of aqueous 4-chlorophenol by silica-immobilized polyoxometalates. *Environ. Sci. Technol.*, **2002**, 36, 1325-1329.

[132] Y. Guo, C. Hu, S. Jiang, C. Guo, Y. Yang, E. Wang, Heterogeneous photodegradation of aqueous hydroxy butanedioic acid by microporous polyoxometalates. *Appl. Catal. B: Environ.*, **2002**, 36, 9-17.

[133] M. D. Tzirakis, I. N. Lykakis, G. D. Panagiotou, K. Bourikas, A. Lycourghiotis, C. Kordulis, Decatungstate catalyst supported on silica and γ -alumina: Efficient photocatalytic oxidation of benzyl alcohols. *J. Catal.*, **2007**, 252,178-189.

[134] E. Manasse, Idrotalcite e piroaurite. *Atti. Soc. Toscana Sci. Nat., Proc. Verb.*, **1915**, 24, 92-105.

[135] S. P. Newman, W. Jones, Synthesis, characterization and applications of layered double hydroxides containing organic guests. *New J. Chem.*, **1998**, 22, 105-115.

[136] P. Nalawade, B. Aware, V. J. Kadam, R. S. Hirlekar, Layered double hydroxides: a review. *J. Sci. Ind. Res.*, **2009**, 68, 267-272.

[137] K-H. Goh, T-T. Lim, Z. Dong, Application of layered double hydroxides for removal of oxyanions: a review. *Water Res.*, **2008**, 42, 1343-1368.

[138] A. I. Khan, D. O´Hare, Intercalation chemistry of layered double hydroxides: recent developments and applications. *J. Mater. Chem.*, **2002**, 12, 3191-3198.

[139] B. M. Choudary, B. Kavita, N. S. Chowdari, B. Sreedhar, M. L. Kantam, Layered double hydroxides containing chiral organic guests: synthesis, characterization and application for asymmetric C–C bond-forming reactions. *Catal. Lett.*, **2002**, 78, 373-377.

[140] M. R. Kang, H. M. Lim, S. Chun Lee, S.-Ho Lee, K. J. Kim, Layered double hydroxide and its anion exchange capacity. *Azo Mat. J. Mat.*, **2005**, 1, 1-13.

[141] M. Meyn, K. Beneke, G. Lagaly, Anion-exchange reactions of layered double hydroxides. *Inorg. Chem.*, **1990**, 29, 5201-5207.

[142] F. Cavani, F. Trifirò, A. Vaccari, Hydrotalcite-type anionic clays: preparation, properties and applications. *Catal. Today*, **1991**, 11, 173-301.

[143] S. Carlino, M. J. Hudson, Thermal intercalation of layered double hydroxides: capric acid into an Mg-Al LDH. *J. Mater. Chem.*, **1995**, 5, 1433-1442.

[144] J. W. Boclair, P. S. Braterman, Layered double hydroxide stability. 1. Relative stabilities of layered double hydroxides and their simple counterparts. C*hem. Mater.*, **1999**, 11, 298-302.

[145] J. He, M. Wei, B. Li, Y. Kang, D. G. Evans, X. Duan, Preparation of layered double hydroxides. *Struct. Bond.*, **2005**, 119, 89-119.

[146] Y. Kuang, L. Zhao, S. Zhang, F. Zhang, M. Dong, S. Xu, Morphologies, preparations and applications of layered double hydroxide micro-/nanostructures. *Materials*, **2010**, 3, 5220-5235.

[147] M. R. Weir, R. A. Kydd, Synthesis of metatungstate pillared layered double hydroxides with variable layer composition. Effect of Mg:Al ratio on the microporous structure. *Microp. Mesop. Mater.*, **1998**, 20, 339-347.

[148] E. L. Crepaldi, P. C. Pavan, J. B. Valim, Comparative study of the coprecipitation methods for the preparation of layered double hydroxides. *J. Braz. Chem. Soc.*, **2000**, 11, 64-70.

[149] A. De Roy, C. Forano, J. P. Besse, *Layered Double Hydroxides: Present and Future*, Ed. V. Rives, Nova Science Publishers, Inc., New York, **2001**.

[150] A. Clearfield, M. Kieke, J. Kwan, J. L. Colon, R.-C. Wang, Intercalation of dodecyl sulfate into layered double hydroxides. *J. Inclusion Phenom. Mol. Recognit. Chem.*, **1991**, 1, 361-378.

[151] V. Prevot, C. Forano, J. P. Besse, F. Abraham, Synthesis and thermal and chemical behaviors of tartrate and succinate intercalated Zn_3Al and Zn_2Cr layered double hydroxides. *Inorg. Chem.,* **1998**, 37, 4293-4301.

[152] S. Miyata, Anion-exchange properties of hydrotalcite-like compounds. *Clays Clay Miner.*, **1983**, 31, 305-311.

[153] V. Rives, M. A. Ulibarri, Layered double hydroxides (LDH) intercalated with metal coordination compounds and oxometalates. *Coord. Chem. Rev.*, **1999**, 181, 61-120.

[154] T. Hibino, A. Tsunashima, Synthesis of paramolybdate intercalates of hydrotalcite-like compounds by ion exchange in ethanol/water. *Chem. Mater.*, **1997**, 9, 2082-2089.

[155] L. X. Lei, R. P. Vijayan, D. O'Hare, Preferential anion exchange intercalation of pyridinecarboxylate and toluate isomers in the layered double hydroxide $[LiAl_2(OH)_6]Cl \cdot H_2O$. *J. Mater. Chem.*, **2001**, 11, 3276-3280.

[156] T. Sato, A. Okuwaki, Intercalation of benzenecarboxylate ions into the interlayer of hydrotalcite. *Solid State Ionics*, **1991**, 45, 43-48.

[157] E. Kooli, C. Depège, A. Ennqadi, A. De Roy, J. P. Besse, Rehydration of Zn-Al layered double hydroxides. *Clays Clays Miner.*, **1997**, 45, 92-98.

[158] E. Narita, P. Kaviratna, T. J. Pinnavaia, Synthesis of heteropolyoxometalate pillared layered double hydroxides via calcined zinc-aluminium oxide precursors. *Chem. Lett.*, **1991**, 805-808.

[159] T. Sato, H. Fujita, T. Endo, M. Shimada, A. Tsunashima, Synthesis of hydrotalcite-like compounds and their physico-chemical properties. *React. Solids*, **1988**, 5, 219-228.

[160] W. Kagunya, M. Chibwe and W. Jones, Synthesis and structural characterization of LDH-organic intercalates. *Mol. Cryst. Liq. Cryst.*, **1994**, 244, 155-160.

[161] R. C. Schroden, A. Stein, *3D ordered macroporous materials.* In: Colloids and Colloid Assemblies, Ed. F. Caruso. Wiley-VCH, pp. 465-493, **2004**.

[162] A. Stein, B. E. Wilson, S. G. Rudisill, Design and functionality of colloidal-crystal templated materials. *Chem. Soc. Rev.*, **2013**, 42, 2763-2803.

[163] E. Géraud, V. Prévot, F. Leroux, Synthesis and characterization of macroporous MgAl LDH using polystyrene spheres as template. *J. Phys. Chem. Solids*, **2006**, 67, 903-908.

[164] E. Géraud, S. Rafqah, M. Sarakha, C. Forano, V. Prevot, F. Leroux, Three dimensionally ordered macroporous layered double hydroxides: preparation by templated impregnation/coprecipitation and pattern stability upon calcination. *Chem. Mater.*, **2008**, 20, 1116-1125.

[165] M. A. Aramendia, V. Borau, C. Jimenez, J. M. Marinas, J. R. Ruiz, F. J. Urbano, Comparative study of Mg/M(III) (M=Al, Ga, In) layered double hydroxides obtained by coprecipitation and the sol-gel method. *J. Solid State Chem.*, **2002**, 168, 156-161.

[166] Y. Zhao, F. Li, R. Zhang, D. G. Evans, X. Duan, Preparation of layered double hydroxide materials using a method with separate nucleation and aging steps. *Chem. Mater.*, **2000**, 14, 4286-4291.

[167] G. R. Williams, D. O´Hare, Towards understanding, control and application of layered hydroxide chemistry. *J. Mater. Chem.*, **2006**, 16, 3065-3074.

[168] M. E. Charles, *Composition analysis by thermogravimetry*. American Society for testing and materials, pp. 291, Baltimore, **1988**.

[169] A. Van der Pol, B. L. Mojet, E. Van der Ven, E. De Boer, Ordering of intercalated water and carbonated anions in hydrotalcite. An NMR study. *J. Phys. Chem.*, **1994**, 98, 4050-4054.

[170] W. T. Reichle, Anionic clay minerals. *Chemtech*, **1986**, 58-63.

[171] Y. H. Chuang, Y. M. Tzou, M. K. Wang, C. H. Liu, P. N. Chiang, Removal of 2-chlorophenol from aqueous solution by Mg/Al layered double hydroxide (LDH) and modified LDH. *Ind. Eng. Chem. Res.*, **2008**, 47, 3813-3819.

[172] C. Del Hoyo, Layered double hydroxides and human health: an overview. *Appl. Clay Sci.*, **2007**, 36, 103-121.

[173] F. Zhang, Xu Xiang, F. Li, X. Duan, Layered double hydroxides as catalytic materials: recent development. *Catal. Surv. Asia*, **2008**, 12, 253-265.

[174] J. Inacio, C. Taviot-Guého, C. Forano, J. P. Besse, Adsorption of MCPA pesticides by MgAl-layered double hydroxide. *Appl. Clay. Sci.*, **2001**, 18, 255-264.

[175] J. S. Valente, F. Tzompantzi, J. Prince, J. G. H. Cortez, R. Gomez, Adsorption and photocatalytic degradation of phenol and 2,4-dichlorophenoxiacetic acid by Mg-Zn-Al layered double hydroxides. *Appl. Cat. B: Environ.*, **2009**, 90, 330-338.

[176] E. M. Seftel, E. Popovici, M. Mertens, K. De Witte, G. Van Tendeloo, P. Cool, E. F. Vansant, Zn-Al layered double hydroxides: synthesis, characterization and photocatalytic activity. *Microp. Mesop. Mat.*, **2008**, 113, 296-304.

[177] A. Patzkó, R. Kun, V. Hornok, I. Dékány, T. Engelhardt, N. Schall, ZnAl-layer double hydroxides as photocatalysts for oxidation of phenol in aqueous solution. *Colloids Surf., A*, **2005**, 265, 64-72.

[178] F. Tzompantzi, A. Mantilla, F. Bañuelos, J. L. Fernández, R. Gómez, Improved photocatalytic degradation of phenolic compounds with ZnAl mixed oxides obtained from LDH materials. *Top. Catal.*, **2011**, 54, 257-263.

[179] C. G. Silva, Y. Bouizi, V. Fornés, H. Garcıa, Layered double hydroxides as highly efficient photocatalysts for visible light oxygen generation from water. *J. Am. Chem. Soc.*, **2009**, 131, 13833-13839.

[180] L. Mohapatra, K. M. Parida, Zn-Cr layered double hydroxide: visible light responsive photocatalyst for photocatalytic degradation of organic pollutants. *Sep. Purif. Technol.*, **2012**, 91, 73-80.

[181] Y. Guo, D. Li, C. Hu, Y. Wang, E. Wang, Layered double hydroxide pillared by tungsten polyoxometalates. Synthesis and photocatalytic activity. *Inter. J. Inorg. Mater.*, **2001,** 3, 347-355.

[182] C. Barriga, W. Jones, P. Malet, V. Rives, M. A. Ulibarri, Synthesis and characterization of polyoxovanadate-pillared Zn-Al layered double hydroxides: an X-ray absorption and diffraction study. *Inorg. Chem.*, **1998**, 37, 1812-1820.

[183] H. Nijs, M. De Bock, E. F. Vansant, Comparative study of the synthesis and properties of polyoxometalate pillared layered double hydroxides (POM-LDHs). *J. Porous Mater.*, **1999**, 6, 101-110.

[184] Mark R. Weir, Jocelyn Moore, Ronald A. Kydd, Effects of pH and Mg:Ga ratio on the synthesis of gallium-containing layered double hydroxides and their polyoxometalate anion exchanged products. *Chem. Mater.*, **1997**, 9, 1686-1690.

[185] T. Kwon, G. A. Tsigdinos, T. J. Pinnavaia, Pillaring of layered double hydroxides (LDH´s) by polyoxometalate anions. *J. Am. Chem. Soc.*, **1988**, 110, 3653-3654.

[186] E. A. Garner, S. K. Yun, T. J. Pannavaia, Layered double hydroxides pillared by macropolyoxometalates. *Appl. Clay Sci.*, **1998**, 13, 479-494.

[187] E. Narita, P. D. Kaviratna, T. J. Pinnavaia, Synthesis of heteropolyoxometalate pillared layered double hydroxides via calcined zinc-aluminium oxide precursors. *Chem. Lett.*, **1991**, 805-808.

[188] M. A. Drezdzon, Synthesis of isopolymetalate-pillared hydrotalcite via organic-anion-pillared precursors. *Inorg. Chem.*, **1988**, 27, 4628-4632.

[189] E. D. Dimotakis, T. J. Pinnavaia, New route to layered double hydroxides intercalated by organic anions: precursors to polyoxometalate-pillared derivatives. *Inorg. Chem.*, **1990**, 29, 2393-2394.

[190] Y. Guo, D. Li, C. Hu, E. Wang, Y. Zou, H. Ding, S. Feng, Preparation and photocatalytic behavior of Zn/Al/W(Mn) mixed oxides via polyoxometalates intercalated layered double hydroxides. *Microp. Mesop. Mater.*, **2002**, 56, 153-162.

# Homogeneous photocatalysed degradation of 2-(1-naphthyl) acetamide by decatungstate anion in aqueous solution

5.1 Introduction

In this Chapter the results are given concerning the photocatalytic degradation of 2-(1-napthyl) acetamide (NAD) in the presence of the polyoxometalate decatungstate anion $W_{10}O_{32}^{4-}$ in aqueous solution under UV and simulated solar light irradiation. One of the aims of this study was to examine the efficiency of the photocatalyst on NAD degradation and to see if mineralization takes place. Thus, the disappearance kinetics, the initial rate constants and quantum yields as function of oxygen concentration were all determined and the total organic carbon (TOC) was measured. A comparison was also made between NAD degradation in presence of $W_{10}O_{32}^{4-}$ and of the semiconductor TiO_2. The last part of the chapter is dedicated to the identification of the primary photoproducts formed during the photocatalytic degradation in order to establish the degradation mechanism and compare it with the products of NAD obtained under direct photolysis.

5.2 Synthesis and characterization of the catalyst sodium decatungstate

The catalyst sodium decatungstate, $Na_4W_{10}O_{32}.7H_2O$ (from now on designated in its anionic form as decatungstate anion or $W_{10}O_{32}^{4-}$) has been synthesized according to the literature procedure [1] (details in Chapter 8) and characterized by UV-vis and Infrared spectroscopies. Figure 5-1 illustrates the UV-vis absorption spectrum of an aqueous solution of sodium decatungstate (3.0×10^{-4} mol L^{-1}) at its natural pH (around 5.0).
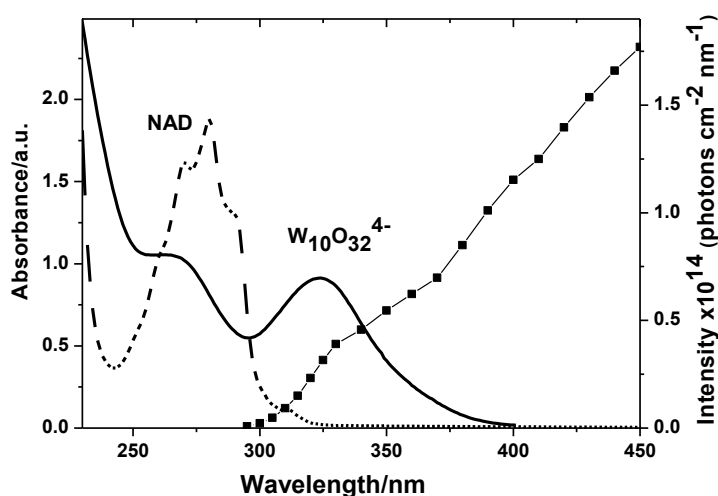
Figure 5-1 UV-vis absorption spectra of $W_{10}O_{32}^{4-}$ (3.0×10^{-4} mol L^{-1}) (solid line) and of NAD (3.0×10^{-4} mol L^{-1}) (dotted line) in aqueous solution; emission spectrum of solar light (-■-).

The UV-vis spectrum presents two absorption bands with maximum wavelengths at 267 and 323 nm, which are in agreement with literature data [2,3]. The first band is attributed to $H_2W_{12}O_{40}^{6-}$ which is in equilibrium with the band at 323 nm corresponding to $W_{10}O_{32}^{4-}$. Since the metal ions in the oxidized POMs have a d^0 electronic configuration, the only absorption band that occurs in the UV range of the electronic spectra is due to the oxygen-to-metal (O→M) ligand-to-metal charge transfer (LMCT) [4]. The recorded Fourier Transform InfraRed (FTIR) spectrum of $W_{10}O_{32}^{4-}$ exhibits several vibrational bands with various positions and intensities (Figure 5-2). The strong, broad band centered around 3500 cm^{-1} and the peak around 1600 cm^{-1} is attributed to the O–H stretching vibrations and to the bending modes of water molecules. The characteristic vibrational bands of decatungstate anion are observed at 957 (ν(W=Ot), corresponding to the elongation of W-O bond), 890 and 805 cm^{-1} (deformation of W-Ob-W). These bands are in agreement with literature data [1].
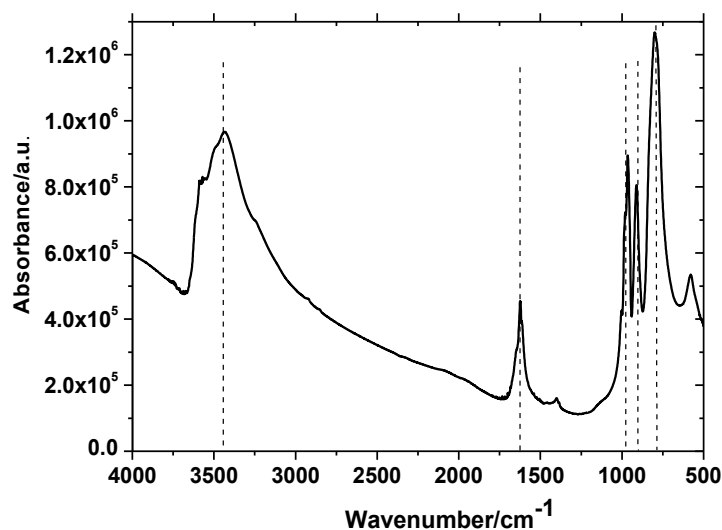
Figure 5-2 FTIR spectrum of the catalyst $Na_4W_{10}O_{32}.7H_2O$.

5.3 Photodegradation of NAD in presence and absence of decatungstate anion irradiated with simulated solar light

As discussed in Chapter 2B, despite the small overlap of NAD absorption band with the emission spectrum of solar light (Figure 5-1), it is possible to state that NAD is susceptible to degradation under environmental conditions. Therefore, simulated solar light (Suntest system) was used as light source to irradiate an aqueous NAD solution

$(3.0 \times 10^{-4}$ mol $L^{-1})$. The kinetics of its transformation (Figure 5-3) shows that NAD is effectively degraded under these conditions: 51 % of disappearance in 8 h. However, as can be seen in Figure 5-1, the decatungstate anion presents a higher overlap than NAD with the emission spectrum of solar light within the range 290-400 nm, which allows it to be used as a photocatalyst for water decontamination. Hence, the effect of the catalyst $W_{10}O_{32}^{4-}$ $(3.0 \times 10^{-4}$ mol $L^{-1})$ on NAD $(3.0 \times 10^{-4}$ mol $L^{-1})$ degradation was assessed using the Suntest system. The results (Figure 5-3), provide evidence of the photocatalytic activity of $W_{10}O_{32}^{4-}$ in NAD degradation: 89 % disappearance is seen after 8 h of irradiation. However, in this case both NAD and $W_{10}O_{32}^{4-}$ contribute to the degradation since they absorb at $\lambda > 290$ nm, although the $W_{10}O_{32}^{4-}$ band overlaps the solar emission spectrum to a much greater extent. These results confirm, once more, the efficient use of $W_{10}O_{32}^{4-}$ as catalyst for the degradation of organic pollutants under solar irradiation, in agreement with existing literature studies [5-7].
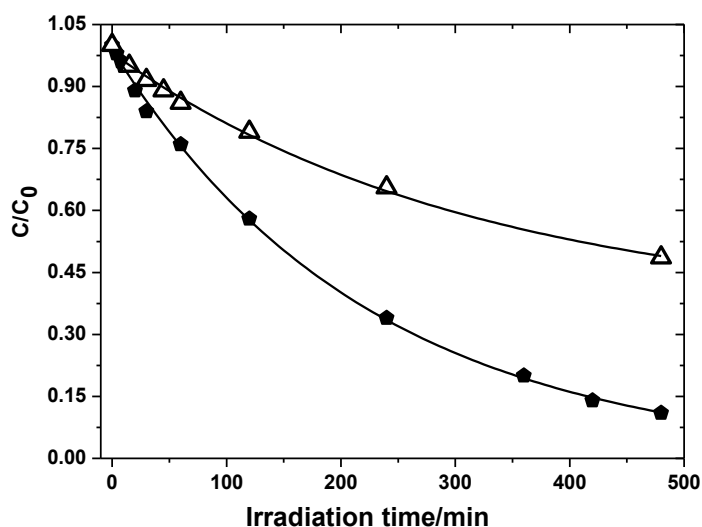
Figure 5-3 Kinetics of NAD $(3.0 \times 10^{-4}$ mol $L^{-1})$ degradation in aerated aqueous solution under irradiation using the Suntest in: (⬠) presence and (△) absence of $W_{10}O_{32}^{4-}$ $(3.0 \times 10^{-4}$ mol $L^{-1})$ at pH 5.1, obtained by HPLC-DAD $(\lambda_{det} = 280$ nm).

Given that the main goal of this work was to study the degradation of NAD promoted by the catalyst $W_{10}O_{32}^{4-}$, further studies were performed using an irradiation system at 365 nm. Under these conditions, the direct photolysis of NAD is avoided and only $W_{10}O_{32}^{4-}$ will be responsible for NAD disappearance, thus allowing assessment of the efficiency of the catalyst on the degradation process.

5.4 Direct and photocatalysed degradation of NAD by decatungstate anion under irradiation at 365 nm

The direct irradiation of aerated aqueous NAD solutions (3.0×10^{-4} mol L^{-1}) in absence of $W_{10}O_{32}^{4-}$ at 365 nm was evaluated in order to determine the efficiency of the photocatalyst (Figure 5-4). Under these conditions, high stability of the pesticide is observed after 22 hours of irradiation (5 % of degradation). Since NAD does not absorb at 365 nm, this small disappearance can be explained by the presence of the incompletely filtered rays at 313 nm on the irradiation system at 365 nm, as referred to in Chapter 8.

5.4.1 Effect of oxygen concentration

The photocatalytic degradation of aqueous NAD solutions (3.0×10^{-4} mol L^{-1}) in the presence of the polyoxometalate $W_{10}O_{32}^{4-}$ (3.0×10^{-4} mol L^{-1}) under illumination at 365 nm was studied as function of oxygen concentration: aerated, de-aerated and oxygenated (Figure 5-4). The initial rate constants, half-lives and quantum yields of NAD transformation in the presence of $W_{10}O_{32}^{4-}$ were also determined at this wavelength (Table 5-1).
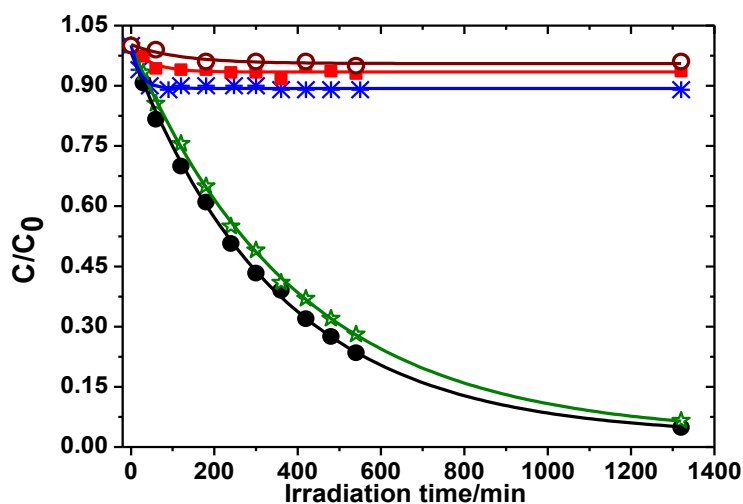
Figure 5-4 Evolution of NAD (3.0×10^{-4} mol L^{-1}) disappearance in aqueous solution: i) in absence of $W_{10}O_{32}^{4-}$ and under direct irradiation at 365 nm (○); ii) in presence of $W_{10}O_{32}^{4-}$ (3.0×10^{-4} mol L^{-1}) under irradiation at 365 nm in de-aerated (■), aerated (●) and oxygenated (☆) conditions; and iii) in presence of $W_{10}O_{32}^{4-}$ (3.0×10^{-4} mol L^{-1}) and 2-propanol (1.0 mol L^{-1}) under aerated conditions (✳).

The kinetic profile presented in Figure 5-4 provides evidence for the significant role that oxygen plays in NAD photocatalysed degradation. The degradation rate follows the order: aerated $\cong$ > oxygenated > de-aerated.

Under aerated conditions, 95 % of NAD disappeared after 22 h of irradiation with an estimated first order rate constant of 3.2×10^{-3} min^{-1}. This indicates that the catalyst $W_{10}O_{32}^{4-}$ enhanced NAD degradation by a factor of 19 when compared with direct NAD degradation. Furthermore, the addition of oxygen to the solution did not increase the photocatalytic activity of $W_{10}O_{32}^{4-}$, as can be seen in Figure 5-4. In fact, the quantum yields, half-lives and rate constants given in Table 5-1 indicate that degradation is faster by a factor of 1.4 in aerated conditions when compared with oxygenated conditions. This means that the oxygen concentration existing in solution was enough for the regeneration of the initial form $W_{10}O_{32}^{4-}$, leading to the continuous degradation of NAD through the photocatalytic cycle. The presence of oxygen is vital to reoxidize the reduced form $W_{10}O_{32}^{5-}$ to its initial form $W_{10}O_{32}^{4-}$, closing the photocatalytic cycle [6]. The oxygen consumption in this step leads to the formation of superoxide anion which can further participate in the degradation process leading on protonation to hydroperoxyl species [6].

Table 5-1 Initial rate constants (k), half-lives ($t_{1/2}$) and quantum yields (ϕ) of NAD (3.0×10^{-4} mol L^{-1}) degradation in aqueous solution in presence of the catalyst $W_{10}O_{32}^{4-}$ (3.0×10^{-4} mol L^{-1}) irradiated with monochromatic light at 365 nm, under different oxygen concentrations [8].

Conditions	[O_2] (mol L^{-1}) (20 ºC)	k (min^{-1})	$t_{1/2}$ (h)	ϕ NAD
Aerated	2.9×10^{-4}	3.2×10^{-3}	3.6	1.9×10^{-3}
Oxygenated	1.39×10^{-3}	2.3×10^{-3}	5.0	1.3×10^{-3}
De-aerated	$< 10^{-5}$	-	-	8.4×10^{-4}

In de-aerated conditions (Figure 5-4) and in the earliest times of irradiation, a small degradation of NAD is observed, after which the degradation is almost completely inhibited (94 % after 22 h). This small decrease may be due to the presence of some residual oxygen left in solution and also of $W_{10}O_{32}^{4-}$ availability present in initial times. After that a plateau is reached since the formed excited species of decatunsgate, wO [9],

decays to form the one electron reduced species $W_{10}O_{32}^{5-}$ which accumulates in the course of the reaction since there is no oxygen to oxidize this latter species to the initial $W_{10}O_{32}^{4-}$ leading to the opening of the cycle. Moreover, the formation of a blue color was observed after the earliest times of irradiation, which persisted till the end of the irradiation, consistent with the formation of the reduced species $W_{10}O_{32}^{5-}$ that presents a maximum absorption at 780 nm [10]. When this solution is left exposed to air, the blue color disappears, with oxygen playing an important role on regenerating the reduced species $W_{10}O_{32}^{5-}$ to the starting form of the catalyst, $W_{10}O_{32}^{-4}$, with parallel production of superoxide anion [6].
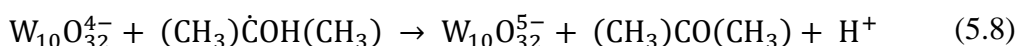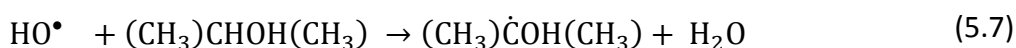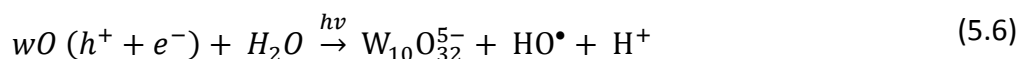
5.4.2 Effect of 2-propanol

In order to ascertain the reactive species involved in NAD photocatalysed degradation pathway, the irradiation of aqueous aerated solution of NAD (3.0×10^{-4} mol L^{-1}) containing $W_{10}O_{32}^{4-}$ (3.0×10^{-4} mol L^{-1}) was carried out in the presence of 2-propanol (1.0 mol L^{-1}) (known to be an electron donor) at 365 nm (see Figure 5-4). Under these conditions, in the first 60 minutes of irradiation 11 % of NAD disappeared after which a complete inhibition of degradation was observed till 22 h of irradiation. This initial decrease of NAD concentration was accompanied by the formation of a blue color typical of the one electron reduced species $W_{10}O_{32}^{5-}$, whose yield is known to increase in presence of 2-propanol [7]. Once the irradiation was stopped and the solution was left open to air, the generation of the initial form $W_{10}O_{32}^{4-}$ occurred with consequent disappearance of the blue color. Within these first 60 minutes, NAD disappearance may be explained by the competition between 2-propanol and the available $W_{10}O_{32}^{4-}$ to form the reactive species wO responsible for NAD transformation. After this time, the inhibition of NAD degradation in presence of 2-propanol may be explained by the efficient trapping of the formed reactive excited species wO by the alcohol. This suggests the involvement of hydrogen atom abstraction (HA) by the excited state of $W_{10}O_{32}^{4-}$, wO, (estimated oxidation potential ≤ 2.23 V *vs* NHE [9]) to 2-propanol, leading to the formation and accumulation of the reduced form $W_{10}O_{32}^{5-}$ evidenced by the blue coloration. The classical reaction of the excited species wO with 2-propanol via HA is proposed in reactions (5.1) to (5.4):

$$wO + (CH_3)CHOH(CH_3) \xrightarrow{h\nu} W_{10}O_{32}^{5-} + (CH_3)\dot{C}OH(CH_3) + H^+ \qquad (5.1)$$

$$(CH_3)\dot{C}OH(CH_3) + O_2 \rightarrow (CH_3)CO(CH_3) + HO_2^\bullet \qquad (5.2)$$

$$W_{10}O_{32}^{5-} + O_2 + H^+ \rightarrow W_{10}O_{32}^{4-} + HO_2^\bullet \qquad (5.3)$$

$$2HO_2^\bullet \rightarrow H_2O_2 + O_2 \qquad (5.4)$$
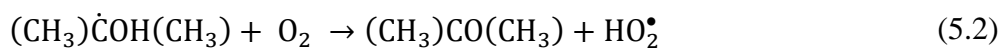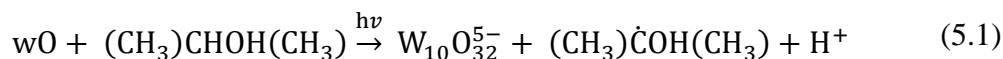
The overall photocatalytic oxidation of 2-propanol in the presence of oxygen and $W_{10}O_{32}^{4-}$ is given by reaction (5.5), in which the alcohol is transformed in acetone and hydrogen peroxide:

$$(CH_3)CHOH(CH_3) + O_2 + W_{10}O_{32}^{4-} \xrightarrow{hv} (CH_3)CO(CH_3) + H_2O_2 \quad (5.5)$$
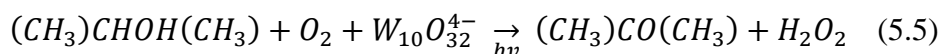
The results obtained with 2-propanol are in agreement with literature mechanistic studies which show that in photosensitized oxidations of organic substrates by $W_{10}O_{32}^{4-}$, in presence of oxygen, either HA or electron transfer (ET) or even both mechanisms may occur [11-14]. Nevertheless, some authors suggested that the reactive species wO also reacts with organic substrates in aqueous solution by indirect H abstraction via OH radicals. These OH radicals may be formed through the reaction of wO with water molecules (oxidative trapping holes) [15,16] since the excited state potential of the decatungstate is more positive than the one-electron oxidation of water [16] (reaction 5.6). The OH radicals thus formed react with organic substrates via mainly α-C H abstraction (reaction 5.7). The formed highly reducing hydroxyl alkyl radical $(CH_3)\dot{C}OH(CH_3)$ further reacts with the polyoxometalate (reaction 5.8). In absence of strong oxidant agents (such as oxygen), electron accumulate on the polyoxometalate driving the redox potential to more negative values until an oxidant in solution is able to act as electron acceptor and close the photocatalytic cycle.

$$wO\ (h^+ + e^-) + H_2O \xrightarrow{hv} W_{10}O_{32}^{5-} + HO^\bullet + H^+ \qquad (5.6)$$

$$HO^\bullet + (CH_3)CHOH(CH_3) \rightarrow (CH_3)\dot{C}OH(CH_3) + H_2O \qquad (5.7)$$

$$W_{10}O_{32}^{4-} + (CH_3)\dot{C}OH(CH_3) \rightarrow W_{10}O_{32}^{5-} + (CH_3)CO(CH_3) + H^+ \qquad (5.8)$$

Even though there are some experimental results that support the formation of these OH radicals, this possibility is still a matter of debate and no consensus exists on the subject.

5.5 Comparison of photocatalytic degradation of NAD by decatungstate anion and by TiO$_2$

Since $W_{10}O_{32}{}^{4-}$ photochemistry is considered as having many similarities with the semiconductor oxide TiO$_2$, aerated aqueous NAD solutions (3.0×10^{-4} mol L^{-1}) were irradiated at 365 nm using TiO$_2$ as catalyst (1.0 g L^{-1}). The reaction was followed by HPLC and the kinetics presented in Figure 5-5 shows that NAD degradation is more efficient in presence of $W_{10}O_{32}{}^{4-}$ (95 % after 22 h) than in presence of TiO$_2$ (63 % after 22 h). Nevertheless, it is possible to notice that at the initial times NAD degradation is much faster in presence of TiO$_2$ than with $W_{10}O_{32}{}^{4-}$. In presence of $W_{10}O_{32}{}^{4-}$ the kinetics fit a first order rate perfectly well, while with TiO$_2$ a bi-exponential fit is required. It is necessary to keep in mind that $W_{10}O_{32}{}^{4-}$ induces the photocatalysed degradation of NAD in homogeneous media whereas TiO$_2$ in heterogeneous media. TiO$_2$ produces the very reactive OH radicals in solution [17], known to be more strongly oxidizing than the excited state of $W_{10}O_{32}{}^{4-}$. Therefore, it is possible that these OH radicals may be responsible for the rapid initial degradation of NAD. However, for longer irradiation times the reaction slows down and a less efficient degradation of NAD is observed as compared with $W_{10}O_{32}{}^{4-}$. Although no adsorption of NAD (3.0×10^{-4} mol L^{-1}) in TiO$_2$ (1.0 g L^{-1}) suspensions was observed during 24 h, it is possible that the intermediates formed during irradiation may adsorb on TiO$_2$ surface, thereby decreasing the degradation process.
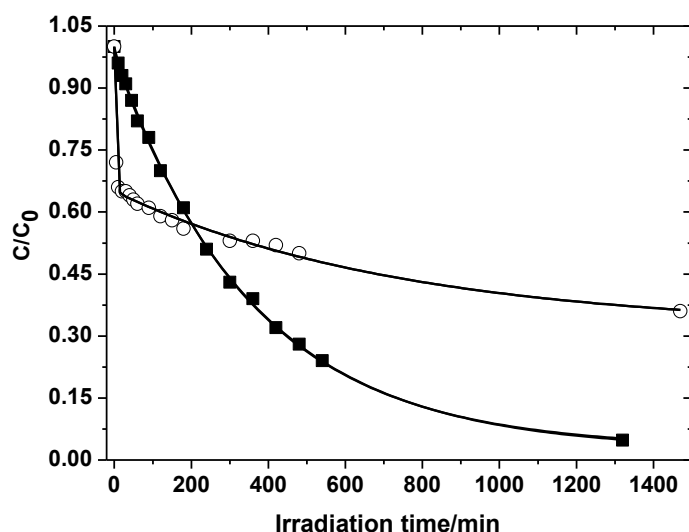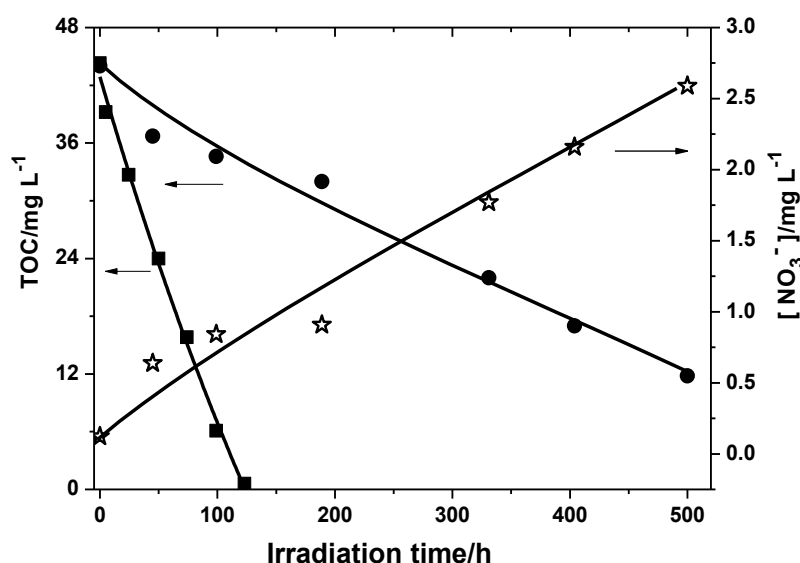

Figure 5-5 Evolution of NAD (3.0×10^{-4} mol L^{-1}) disappearance under irradiation at 365 nm: (■) in the presence of $W_{10}O_{32}{}^{4-}$ (3.0×10^{-4} mol L^{-1}) and (○) in the presence of TiO$_2$ (1.0 g L^{-1}).

5.6 Mineralization

The mineralization of NAD (3.0×10^{-4} mol L^{-1}) has been determined by total organic carbon (TOC) measurements as function of irradiation time in aerated solutions in presence of $W_{10}O_{32}^{4-}$ (3.0×10^{-4} mol L^{-1}) as well as in presence of TiO_2 (1.0 g L^{-1}) under 365 nm light, in order to compare the efficiency of the two catalysts. The results shown in Figure 5-6 demonstrate that TiO_2 leads to a faster and more efficient mineralization than $W_{10}O_{32}^{4-}$: NAD is 100 % mineralized after 123 h in presence of TiO_2 while it takes 500 h of irradiation in presence of $W_{10}O_{32}^{4-}$ to achieve 73 % of mineralization.

A comparison between Figure 5-5 and Figure 5-6 reveals that the degradation of NAD in presence of $W_{10}O_{32}^{4-}$ takes place much faster than the mineralization. Almost 100 % of NAD degradation is achieved after 22 hours of irradiation while for complete mineralization more than 600 hours are necessary. This seems to point out that the intermediate species formed during the course of NAD degradation are difficult to be further oxidized, leading to a mineralization on a longer time scale.

Figure 5-6 Evolution of TOC for aerated aqueous NAD solution (3.0×10^{-4} mol L^{-1}) irradiated at 365 nm: (●) in the presence of $W_{10}O_{32}^{4-}$ (3.0×10^{-4} mol L^{-1}) and (■) in the presence of TiO_2 (1.0 g L^{-1}). Formation of nitrates (☆) upon irradiation of aqueous NAD solution (3.0×10^{-4} mol L^{-1}) in presence of $W_{10}O_{32}^{4-}$ (3.0×10^{-4} mol L^{-1}) at 365 nm.

The formation of inorganic anions such as nitrates, nitrites and ammonium was also evaluated in the presence of $W_{10}O_{32}^{4-}$ under the same experimental conditions by ionic chromatography. The concentration of nitrites during the course of reaction presents values at trace levels < 6.0 µg L^{-1} and ammonium presents concentrations < 0.5 mg L^{-1}. Nitrates, on the other hand, have a more important contribution, and a correlation can be made between the decrease of TOC and the formation of nitrates (NO_3^-), as shown in Figure 5-6. After 500 h of irradiation, 73 % of NAD is mineralized with a concentration of nitrates equal to 2.59 mg L^{-1}, very similar, within the experimental errors, to the expected value calculated from the NAD concentration (2.68 mg L^{-1}). These results are in agreement with the mineralization of NAD in presence of $W_{10}O_{32}^{4-}$.

5.7 Photoproduct identification

Aerated aqueous NAD solutions irradiated at 365 nm in presence of $W_{10}O_{32}^{4-}$ were analyzed by HPLC-DAD to detect degradation products (Figure 5-7). This analysis was done in different elution conditions than those used in Chapter 2B to identify NAD products under direct irradiation. As such, all the retention times are different. In this case, NAD was eluted at 10.85 min. Several photoproducts have been observed and the main ones have been identified by LC-ESI-MS/MS with electrospray ionization in positive (ES^+) and negative modes (ES^-) after 10, 30 and 50 % conversion. Thirteen main products were identified by the molecular ion ($[M+H]^+$ or $[M-H]^-$) and mass fragments ions, with lower retention times than that of NAD indicating the formation of more polar photoproducts (Table 5-2). The exception was the product eluted at 11.38 min which corresponds to 1-naphthylacetic acid (1-NAA), in agreement with previously results given in Chapter 2B concerning the direct degradation of NAD.

NAD fragmentation pattern has already been discussed in Chapter 2B, as well as the identification of the product 1-NAA. Therefore, although no discussion is made here, the fragmentation and the proposed structures are given in Table 5-2.
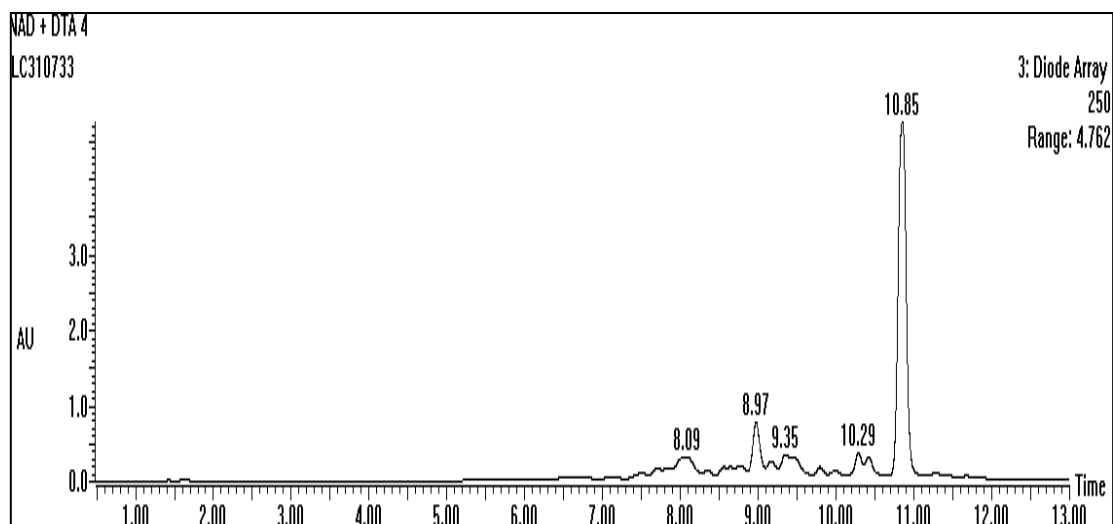
Figure 5-7 HPLC-DAD chromatogram of aerated aqueous irradiated NAD (3.0×10^{-4} mol L^{-1}) solution in the presence of $W_{10}O_{32}{}^{4-}$ (3.0×10^{-4} mol L^{-1}) irradiated at 365 nm (λ_{det} = 250 nm).

Table 5-2 Retention time (t_{ret}), main fragments, UV data and proposed structure of the main photoproducts obtained by LC-MS/MS. UV absorption data were obtained by LC-DAD.

t_{ret} (min)	Main fragments m/z (% abundance)	λ_{max} (nm)	Proposed chemical structure
10.9	[M+H$^+$] = 186 (15 %), 169 (10 %), 141 (100 %)	280	
11.3	-	280	
10.3	[M+H]$^+$ = 202 (100 %), 185 (50 %), 157 (15 %), 143 (10 %)	290	
9.4	[M+H]$^+$ = 202 (100 %), 184 (30 %), 156 (20 %)	280	and/or
8.8	[M+H]$^+$ = 216 (40 %), 199 (30 %), 171 (60 %), 143 (100 %)	240, 330	* and/r

Table 5-2 (Continuation) Retention time (t_{ret}), main fragments (m/z), UV data and proposed structure of the main photoproducts obtained by LC-MS/MS. UV absorption data was obtained by LC-DAD ([*] most stable structure; a - shoulder).

t_{ret} (min)	Main fragments m/z (% abundance)	λ_{max} (nm)	Proposed chemical structure
7.8	$[M+H]^+ = 218$ (25 %), 201 (30 %), 173 (50 %), 155 (100%)	248, 290	
8.1	$[M+H]^+ = 218$ (15 %), 201 (35 %), 173 (50 %), 155 (100 %)	252, 290	and/or
6.6	$[M+H]^+ = 218$ (5.0 %), 201 (20 %), 173 (30 %), 155 (100 %)	290	
8.6	$[M+H]^+ = 218$ (5.0 %), 200 (20 %), 182 (100 %), 154 (20 %)	231, 280[a], 300	and/or
9.0	$[M+H]^+ = 218$ (15.0 %), 200 (40 %), 182 (100 %), 154 (30%)	252, 285[a]	
7.4	$[M+H]^+ = 218$ (10 %), 200 (20 %), 172 (100 %), 155 (35 %)	260	
6.8	$[M+H]^+ = 232$ (50 %), 214 (15 %), 200 (100 %), 172 (75 %), 155 (50 %)	265, 320	and/or
9.5	$[M+H]^+ = 232$ (50 %), 216 (20 %), 200 (100 %), 172 (10 %), 155 (8.0 %)	275, 340	[*]
7.12	$[M+H]^+ = 234$ (10 %), 216 (100 %), 188 (35 %), 171 (60 %), 157 (10 %)	234	and/or
6.0	$[M+H]^+ = 234$ (10 %), 216 (100 %), 198 (55 %), 170 (10 %), 153 (10%)	232, 300[a]	[*]

Characterization of hydroxylated products

Two products with retention times of 10.3 and 9.4 min were detected from the early stages of the irradiation. These products with m/z ratio equal to 202 ($[M+H]^+$) have different fragmentation and correspond to mono-hydroxylated forms of NAD. The hydroxylation of the aromatic ring to give the mono-substituted products can occur at either one of the two aromatic rings of NAD, taking in account the fragmentation results. The product at 10.3 min presents as main fragmentation m/z = 185, 157 and 143, corresponding to the loss of NH_3^+, acetamide group ($CO-NH_3^+$) and $CH_2-CO-NH_3^+$ group, respectively. The other product observed at 9.4 min presents as main fragmentation m/z = 184 and 156. The fragment ions indicate the loss of a water molecule and of $CO-H_2O$, respectively. Such hydroxylated compounds are one of the major products found in photodegradation studies of naphthalene and naphthalene derivatives in solution, either under direct or sensitized degradation [18-22].

Characterization of di-hydroxylated products

Several photoproducts with molecular ion peak at m/z = 218 ($[M+H]^+$) were detected with retention times 7.8, 8.1, 6.6, 8.6, 9.0 and 7.4 min. The diverse fragments suggest the formation of various isomers of di-hydroxylated products, either in one or in both aromatic rings. Three isomers with times 7.8, 8.6 and 6.6 min have main fragments at 201, 173 and 155 corresponding to the loss of NH_3^+, $CO-NH_3^+$ and $H_2O-CO-NH_3^+$, respectively. The product eluted at 7.4 min has fragments at 200, 172 and 155 which is attributed to the loss of H_2O molecule, H_2O-CO and $H_2O-CO-NH_3^+$, respectively. Two other isomers with retention times at 8.6 and 9.0 min present fragment ions at 200, 182 and 154, which are ascribed to the loss of one H_2O molecule, two H_2O molecules and $2H_2O-CO$ group. Di-hydroxylated products have also been found when exposing naphthalene and its derivative to light [23].

Characterization of tri-hydroxylated products

Two products with molecular ion peak m/z = 234 ($[M+H]^+$) and retention time of 7.12 and 6.0 min have been detected. The product at 6.0 min presents as main fragments ions 216, 198, 170 and 153 which correspond to the loss of one H_2O molecule, two H_2O molecule, $2H_2O-CO$ and $2H_2O-CO-NH_3^+$ groups. The main fragments of the product at 7.12 min are 216, 188 and 171 and 157. These are attributed

to the loss of H_2O, H_2O-CO, H_2O-CO-NH_3^+ and H_2O-CH_2-CO-NH_3^+, respectively. The presence of these fragments is in good accordance with tri-hydroxylated derivatives of NAD. Although several authors have suggested the hypothesis of the formation of the tri-hydroxy compounds in the mechanism of naphthalene degradation [23], they have not been clearly identified in these studies.

Characterization of naphthoquinone product

A photoproduct with retention time of 8.8 min was assigned to NAD naphthoquinone. The molecular anion with m/z = 216 ([M+H]$^+$) presents fragments at 199, 171 and 143. These indicate the loss of NH_3, CO-NH_3^+ and also CO-CO-NH_3 groups, respectively, which is in agreement with the proposed structure. Furthermore, these results were also corroborated by the LC-ESI-MS analysis in negative mode ([M-H]$^-$ = 214). Two structures are proposed in Table 5-2; however, the most stable should correspond to having the carbonyl groups in the 1,4 position of the free aromatic ring since at 1,2 position the quinone will be unstable and likely to lead to opening of the ring. Naphthoquinones have been evidenced in literature as one of naphthalene degradation products [18,21-24].

Characterization of hydroxy-naphthoquinone products

Two products with molecular ion peak [M+H]$^+$ = 232 and retention times of 6.8 and 9.5 min were detected and identified as the hydroxy-naphthoquinone derivatives. The main fragments of the product at 6.8 min are 214, 200, 172 and 155. These are attributed to the loss of H_2O molecule, H_2O-CH_2, H_2O-CH_2-CO and H_2O-CH_2-CO-NH_3^+. The product eluted at 9.5 min has as fragmentation pattern 216, 200, 172 and 155. These corresponds to the loss of one oxygen (216) and two oxygen atoms (200), O_2-CO and O_2-$CONH_3^+$. Such hydroxyl-naphthoquinone derivatives have been identified as products in some naphthalene degradation studies [18,21,24].
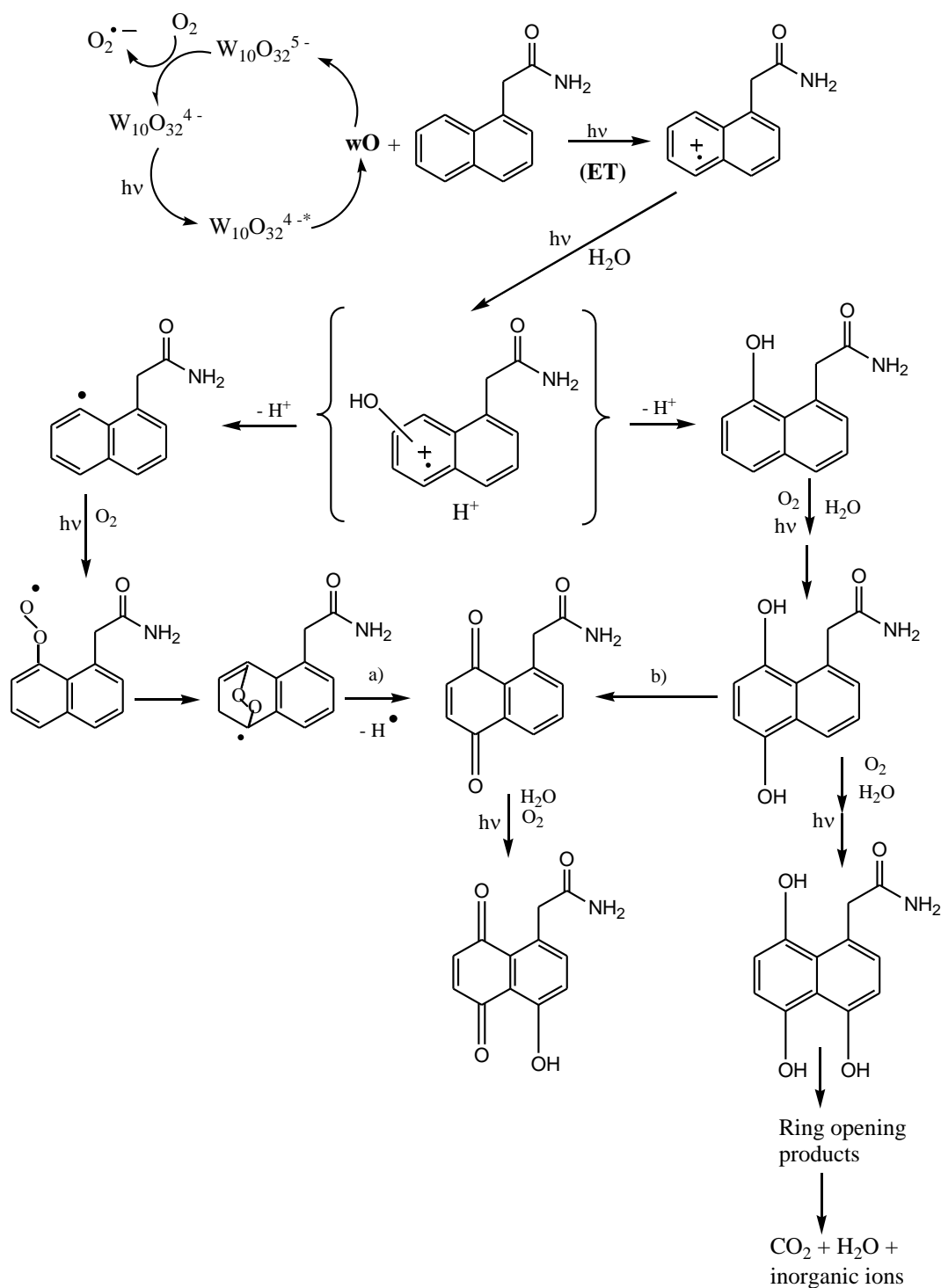
5.8 Proposed mechanism

Based on the above and previous results, a mechanism of NAD degradation photocatalysed by $W_{10}O_{32}^{4-}$ is proposed in Scheme 5-1. The absorption of light by the decatungstate ground state $W_{10}O_{32}^{4-}$ leads to an oxygen to metal charge transfer excited state $W_{10}O_{32}^{4-*}$ [9] that decays in few picoseconds in both aerated and de-aerated

solutions to a very reactive non-emissive transient species wO [9,25] . This species will react with NAD leading to the formation of NAD radical cation and to the reduced form of the decatungstate anion ($W_{10}O_{32}^{5-}$) [10,26]. In the presence of oxygen, $W_{10}O_{32}^{5-}$ is oxidized to its initial form, $W_{10}O_{32}^{4-}$, closing in this way the catalytic cycle. The oxygen consumption is accompanied by its reductive activation to form the superoxide anion which ultimately can also lead to the formation of peroxy products.

According to the photoproducts identified by LC-ESI-MS, the first step of the photodegradation corresponds to an electron transfer (ET) process involving the reactive species wO and the aromatic ring of NAD, with consequent formation of NAD radical cation species and decatungstate reduced species. The reaction of NAD radical cation with water leads to the hydroxylation of the aromatic ring. Two mono-hydroxylated products were identified as primary products. Such hydroxylated products have been previously been seen in naphthalene and naphthalene derivative degradation [18-22]. The consequent reaction of the mono-hydroxylated products with oxygen leads to the formation of the di- and tri-hydroxylated NAD products.

The proposed naphthoquinone derivative may arise from two different pathways. One possibility is by hydrogen abstraction of the di-hydroxylated NAD product (step b). Since the exact positions of the OH groups on the aromatic ring are not known, the drawn structures correspond to the most stable one in 1,4-position. The second possibility starts with the deprotonation of the formed NAD radical, followed by oxygenation process, leading to the formation of an unstable endoperoxide at positions 1,4, which dissociates in the presence of light into the 1,4-naphthoquinone derivative (step a). The hydroxylation of this naphthoquinone derivative leads to the 1,4-hydroxyl-1,4-naphthoquinone. The hydroxyl-1,4-naphthoquinone derivative would be expected to have greater stability than the parent 1,2-naphthoquinone as the hydroxyl group would stabilize the quinone due to intermolecular hydrogen bonding between the hydroxyl group and the oxygen on carbon 1.

Scheme 5-1 Proposed degradation mechanism for NAD in presence of decatungstate anion ($W_{10}O_{32}{}^{4-}$) under irradiation at 365 nm.

For prolonged photolysis times, it is expected that the irradiation of the tri-hydroxylated products leads to the opening of the aromatic ring, with formation of various aliphatic derivatives, which, in turn, can undergo oxidation and decarboxylation steps with the formation of CO_2 as final product. The opening of the ring has been

reported in several studies concerning the degradation of naphthalene and its derivatives, either by direct or photocatalysed degradation [21-24].

A comparison between the products of NAD degradation identified under direct (Chapter 2B) and photocatalysed ($W_{10}O_{32}^{4-}$) excitation reveals some similarities but also some differences, suggesting different mechanisms of degradation for the two cases. The hydroxylated (mono- and di-) as well as the naphthoquinone products were identified in both situations whereas the furanone and coumarine compounds were just found under NAD direct irradiation. In contrast, tri-hydroxylation and hydroxyl-naphthoquinone products were only identified in the photocatalysed degradation of NAD in the presence of $W_{10}O_{32}^{4-}$. The formation of these tri-hydroxylated products may be favored by the proximity of the catalyst, which ultimately will lead to the ring opening and to the mineralization process, which does not occur under direct degradation.

5.9 Conclusions

The homogenous photocatalytic degradation of NAD in water in the presence of the polyoxometalate decatungstate anion $W_{10}O_{32}^{4-}$ under UV irradiation has proved to be very efficient. The effect of oxygen concentration in this photocatalysed degradationindicates a faster degradation of NAD in aerated conditions, in which oxygen plays an important role on the regeneration of the catalyst in order to favor the photocatalytic cycle. In addition, mineralization studies show that NAD is indeed mineralized to CO_2, H_2O and nitrates as inorganic anions. The identification of NAD primary products was also assessed, in which a degradation mechanistic scheme was proposed. The primary step of NAD degradation corresponds to an electron transfer process, as evidenced by degradation studies performed in the presence of 2-propanol. Electron transfer occurs between the reactive species of excited decatungstate and the aromatic ring of NAD, with consequent formation of NAD radical cation species and decatungstate reduced species. As a result, hydroxylation and oxidation products were identified and no reactivity of NAD amide side chain was observed.

5.10 References

[1] R. F. Renneke, M. I. Pasqual, C. L. Hill, Polyoxometalate systems for the catalytic selective production of non thermodynamic alkenes form alkanes. Nature of excited state deactivation

processes and control of subsequent thermal processes in polyoxometalate photoredox chemistry. *J. Am. Chem. Soc.*, **1990,** 112, 6585-6594.

[2] I. Texier, C. Giannotti, S. Malato, C. Richter, J. Delaire, Solar photodegradation of pesticides in water by sodium decatungstate. *Catal. Today*, **1999**, 54, 297-307.

[3] Y. Nosaka, T. Takei, N. Fujii, Photoinduced reduction of $W_{10}O_{32}^{4-}$ by organic compounds in aqueous solution. *J. Photochem. Photobiol. A: Chem.*, **1995**, 92, 173-179.

[4] T. Yamase, Photoredox chemistry of polyoxometalates as a photocatalyst. *Catal. Surv. Asia*, **2003**, 7, 203-217.

 [5] M. D. Tzirakis, I. N. Lykakis, M. Orfanopoulos, Decatungstate as an efficient photocatalyst in organic chemistry. *Chem. Soc. Rev.*, **2009**, 38, 2609-2621.

[6] C. Tanielian, Decatungstate photocatalysis, *Coord. Chem. Rev.*, **1998**, 178-180, 1165-1181.

[7] A. Allaoui, M. A. Amlouki, P. Wong-Wah-Chung, Homogeneous photodegradation study of 2-mercaptobenzothiazole photocatalysed by sodium decatungstate salts: Kinetics and mechanistic pathways. *J. Photochem. Photobiol. A: Chem.*, **2010**, 212, 153-160.

[8] M. Montalti, A. Credi, L. Prodi, M.T. Gandolfi, *Handbook of Photochemistry*, third edition, Taylor & Francis Group, Florida, **2006**.

[9] D. C. Duncan, M. A. Fox, Early events in decatungstate photocatalyzed oxidations: a nanosecond laser transient absorbance reinvestigation. *Phys. Chem. A*, **1998**, 102, 4559-4567.

[10] D. Ravelli, D. Dondi, M. Fagnoni, A. Albini, A. Bagno, Electronic and EPR spectra of the species involved in $[W_{10}O_{32}]^{4-}$ photocatalysis. A relativistic DFT investigation. *Phys.Chem. Chem. Phys.*, **2013**, 15, 2890-2896.

[11] C. Tanielian, R. Seghrouchni, C. Schweitzer, Decatungstate photocatalyzed electron-transfer reactions of alkenes. Interception of the geminate radical ion pair by oxygen. *J. Phys. Chem. A*, **2003**, 107, 1102-1111.

[12] C. Tanielian, I. N. Lykakis, R. Seghrouchni, F. Cougnon, M. Orfanopoulos, Mechanism of decatungstate photocatalyzed oxygenation of aromatic alcohols: Part I. Continuous photolysis and laser flash photolysis studies. *J. Mol. Catal. Part A,* **2007**, 262, 170-175.

[13] C. Giannotti, C. Richter, Photocatalysed oxidation of cyclohexane by $W_{10}O_{32}^{4-}$ irradiation with natural sunlight. *Inter. J. Photoenergy*, **1999**, 1, 1-5.

[14] I. N. Lykakis, C. Tanielian, R. Seghrouchni, M. Orfanopoulos, Mechanism of decatungstate photocatalyzed oxygenation of aromatic alcohols: Part II. Kinetic isotope effect studies. *J. Mol. Catal. A*, **2007**, 262,176-184.

[15] A. Mylonas, A. Hiskia, E. Androulaki, D. Dimotikali, E. Papaconstantinou, New aspect of the mechanism of photocatalytic oxidation of organic compounds by polyoxometalates in aqueous solutions. The selective photooxidation of 2-propan-2-ol to propanone: the role of the OH radicals. *Phys. Chem. Chem. Phys.*, **1999**, 1, 437-440.

[16] A. Molinaria, R. Argazzib, A Maldotti, Photocatalysis with $Na_4W_{10}O_{32}$ in water system: Formation and reactivity of OH• radicals. *J. Mol. Catalysis A: Chem.*, **2013**, 372, 23-28.

[17] U. I. Gaya, A. H. Abdullah, Heterogeneous photocatalytic degradation of organic contaminants over titanium dioxide: a review of fundamentals, progress and problems. *J. Photochem. Photobiol. C: Photochem. Rev.*, **2008**, 9, 1-12.

[18] B. J. McConkey, L. M. Hewitt, D. G. Dixon, B. M. Greenberg, Natural sunlight induced photooxidation of naphthalene in aqueous solution. *Water, Air, Soil Pollut.*, **2002**, 136, 347-359.

[19] M. J. Climent, M. A. Miranda, Photodegradation of dichlorprop and 2-naphthoxyacetic acid in water. Combined GC-MS and GC-FTIR study. *J. Agric. Food Chem.*, **1997**, 45, 1916-1919.

[20] M. J. Garcia-Martinez, L. Canoira, G. Blazquez, I. Da Riva, R. Alcantara, J. F. Llamas, Continuous photodegradation of naphthalene in water catalyzed by TiO_2 supported on glass Raschig rings. *Chem. Eng. J.*, **2005**, 110, 123-128.

[21] A. Lair, C. Ferronato, J. -M. Chovelon, J. -M. Herrmann, Naphthalene degradation in water by heterogeneous photocatalysis: an investigation of the influence of inorganic anions. *J. Photochem. Photobiol. A: Chem.*, **2008**, 193, 193-203.

[22] L. Hykrdová, J. Jirkovský, G. Mailhot, M. Bolte, Fe(III) photoinduced and Q-TiO_2 photocatalysed degradation of naphthalene: comparison of kinetics and proposal of mechanism. *J. Photochem. Photobiol. A: Chem.*, **2002**, 151, 181-193.

[23] E. Pramauro, A. B. Prevot, M. Vincenti, R. Gamberini, Photocatalytic degradation of naphthalene in aqueous TiO_2 dispersions: effect of nonionic surfactants. *Chemosphere,* **1998**, 36, 1523-1542.

[24] D. Vialaton, C. Richard, D. Baglio, A. Paya-Perez, Mechanism of the photochemical transformation of naphthalene in water. *J. Photochem. Photobiol. A: Chem.*, **1999**, 123, 15-19.

[25] T. Kothe, R. Martschke, H. Fischer, Photoreactions of the decatungstate anion $W_{10}O_{32}^{4-}$ with organic substrates in solution studied by EPR and kinetic absorption spectroscopy: an example for the persistent radical effect. *J. Chem. Soc., Perkin Trans. 2*, **1998**, 503-508.

[26] A. Chemseddine, C. Sanchez, J. Livage, J. P. Launay, M. Fournieric, Electrochemical and photochemical reduction of decatungstate: a reinvestigation. *Inorg. Chem.*, **1984**, 23, 2609-2613.

Chapter 6

**Heterogeneous photocatalysed degradation of
2-(1-naphthyl) acetamide by decatungstate anion
immobilized in layered double hydroxides**

6.1 Introduction

As discussed in Chapter 5, the decatungstate anion $W_{10}O_{32}{}^{4-}$ has proved to be an efficient catalyst for NAD degradation in homogeneous solution. However, for environmental applications it is necessary to immobilize it due to its high solubility in water. The aim of this Chapter, therefore, was to prepare new catalytic materials through the intercalation of $W_{10}O_{32}{}^{4-}$ into a solid support and test its photocatalytic activity towards NAD degradation. Although several types of solid supports have been described in literature, layered double hydroxide (LDH) materials were chosen since they are easy to synthesize and to recover from the reaction medium, have high surface area, are catalytically inert and, above all, present good anion exchange and expansion properties, which make them promising matrices for the immobilization of anionic compounds such as polyoxometalates.

Several synthetical approaches were undertaken to prepare the catalytic material in order to tune its properties: synthesis of classical Mg_2Al-DDS LDH by co-precipitation method at constant pH, synthesis of three dimensionally ordered macroporous solid 3-DOM-Mg_2Al-DDS LDH by template impregnation/coprecipitation and synthesis of aerogels of LDH SC-Mg_2Al-DDS prepared by fast co-precipitation followed by supercritical drying (SC) with CO_2. Such aerogels display high surface areas and enhanced adsorption behavior when compared to the macroporous solid. The catalyst $W_{10}O_{32}{}^{4-}$ was then incorporated into the above synthesized LDH precursors by an anionic exchange reaction yielding the final photocatalytic materials with the following nomenclature: classical Mg_2Al-$W_{10}O_{32}{}^{4-}$ LDH, 3-DOM-Mg_2Al-$W_{10}O_{32}{}^{4-}$ LDH and SC-Mg_2Al-$W_{10}O_{32}{}^{4-}$ LDH. The photocatalytic efficiency of these heterogeneous materials towards NAD degradation was assessed, as well as the recovery/reuse efficacy and mineralization process. The products formed under homogeneous (Chapter 5) and heterogeneous degradation is compared, and a mechanism for NAD heterogeneous degradation is proposed.

6.2 Synthesis and characterization of the Mg_2Al-DDS LDH precursors. Intercalation of decatungstate anion into LDHs by anionic exchange reaction

A series of LDH precursors with different textural properties (surface area, porous size) containing in the interlayer the anion dodecyl sulfate (DDS) were synthesized by different methods. Mg/Al cations were chosen to constitute the brucite

layer while DDS was chosen as the interlayer anion since this gives an increased basal spacing [1,2] and acts a spacer which will facilitate the insertion of the polyoxometalate $W_{10}O_{32}{}^{4-}$ in between the layers. DDS was then replaced by the catalyst $W_{10}O_{32}{}^{4-}$ through an anionic exchange reaction, always using the same procedure, yielding the final $W_{10}O_{32}{}^{4-}$-LDH materials.

6.2.1 Synthesis and characterization of the catalyst $Mg_2Al-W_{10}O_{32}{}^{4-}$ LDH prepared by classical co-precipitation method at constant pH

The precursor MgAl-DDS LDH with ratio Mg/Al = 2 was synthesized by the classical co-precipitation method [3] with magnesium and aluminium nitrate salts in an aqueous solution of DDS at constant pH. This constant pH gives rise to LDHs with high chemical homogeneity and good crystallinity, as indicated by the X-ray powder diffraction (PXRD) analysis given in Figure 6-1a. The intercalation of $W_{10}O_{32}{}^{4-}$ by anionic exchange reaction in the *as*-prepared $Mg_2Al-DDS$ LDH precursor yields the final $Mg_2Al-W_{10}O_{32}{}^{4-}$ LDH material, herein abbreviated as classical Mg_2Al-W_{10} LDH. The exchange of DDS anion by $W_{10}O_{32}{}^{4-}$ was confirmed by the EDS spectra (Figure 6-1c and 6-1d), which shows the complete replacement of the sulfur peak (2.35 keV) by the tungstate peaks (8.4 and 9.65 keV). The performed chemical analysis indicates that LDH precipitates at a higher Mg/Al ratio, nearer 3 rather than theoretical 2, as indicated in Table 6-1. Moreover, the slightly lower amount of W than expected into the materials (W/Al = 2.0 instead of 2.5), can be explained by the formation of amorphous magnesium and aluminium simple hydroxides. According to the chemical composition, it appears that 78 % of materials in mass correspond to $W_{10}O_{32}{}^{4-}$ species.

Table 6-1 Chemical composition (obtained by EDS) and cell parameters for the LDH materials prepared by classical co-precipitation method.

Sample	Mg/Al	S/Al	W/Al	d (nm)	a (nm)
Classical $Mg_2Al-DDS$	2.7	1.1	-	2.47	0.303
Classical Mg_2Al-W_{10}	3.0	-	2.0	1.03	0.303

The PXRD pattern (Figure 6-1a) of the prepared LDH (DDS and W_{10}) reveals typical lines of LDH structure. The sharper reflections given by the powder X-ray

diffraction pattern of classical Mg_2Al-DDS LDH correspond to crystalline phase while the broader reflections of the Mg_2Al-W_{10} LDH correspond to an amorphous phase. The Mg_2Al-DDS LDH presents characteristic $00l$ reflections at low angles (d = 2.47 nm) and the 012 and 110 lines respectively at 35.2° and 61.2° on X-ray refractogram. The exchange of DDS by decatunsgate anion is supported by the shift of the $00l$ diffraction lines to higher theta values due to the contraction of the interlayer galleries of Mg_2Al-W_{10} LDH (d = 0.95 nm).
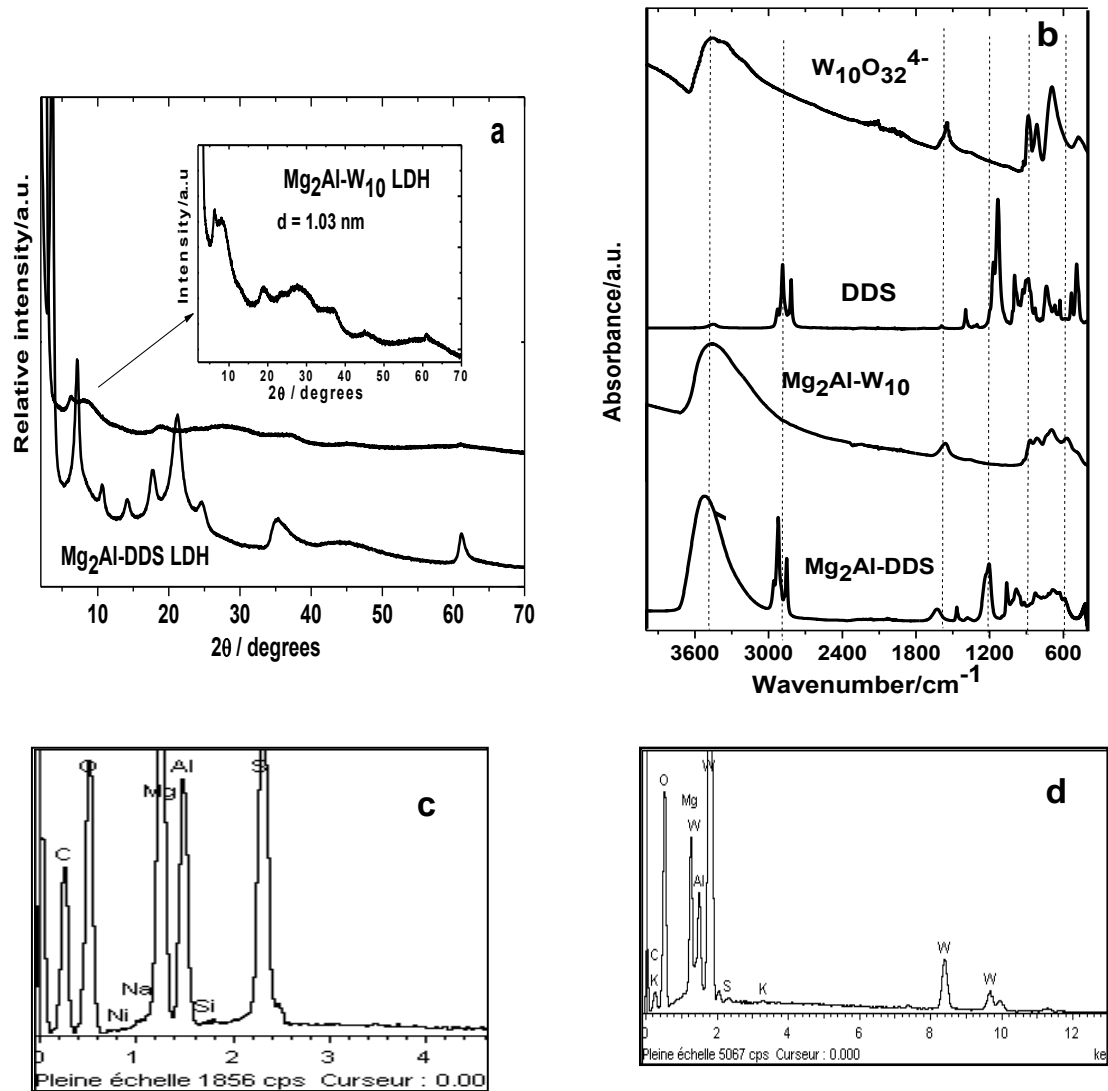

Figure 6-1 a) PXRD patterns of classical LDH Mg_2Al-DDS and Mg_2Al-W_{10} b) FTIR spectra of $W_{10}O_{32}{}^{4-}$, DDS and classical LDHs Mg_2Al-DDS and Mg_2Al-W_{10}. EDS spectrum of c) classical Mg_2Al-DDS LDH and d) classical Mg_2Al-W_{10} LDH.

The Infra-Red (FTIR) spectra of pure DDS and $W_{10}O_{32}{}^{4-}$ anions, and of the *as-*prepared classical LDH Mg_2Al-DDS and Mg_2Al-W_{10}, is depicted in Figure 6-1b. The FTIR spectrum of DDS (Figure 6-1b) shows the typical bands of the sulfonate group

together with the C-H stretching and bending modes. The C-H vibration bands are centered at 2957, 2924, 2852 cm^{-1} (C-H stretch), 1468 cm^{-1} (CH bend) and in the region of 1080-810 cm^{-1}. The sulfonate groups are distinguished by the bands at 1250 and 1220 cm^{-1} ($v SO_4$). The FTIR spectra of the *as*-prepared classical Mg_2Al-DDS and Mg_2Al-W_{10} exhibits characteristic bands of LDH, in particular those at 3460, 1620 and 648 cm^{-1}. The broad band around 3460 cm^{-1} is attributed to the stretching vibration of OH groups in the brucite-like layers and of the interlayer water molecules [4]. The medium intensity band recorded at 1620 cm^{-1} (δH_2O) corresponds to the bending mode of these interlayer water molecules [5] while the band at 648 cm^{-1} is due to the O-M-O vibrations in the brucite-like layers [6,7]. The FTIR spectrum clearly indicates the loss of the vibration bands characteristic of the DDS anion after the exchange reaction and its replacement by the vW-O and vO-W-O stretching and bending modes of the decatunsgtate species at 977 and 905 cm^{-1}, while the LDH lattice vibration at 648 cm^{-1} is maintained. SEM images of Mg_2Al-DDS and Mg_2Al-W_{10} classical LDH (Figure 6-2) indicate aggregates of particles.
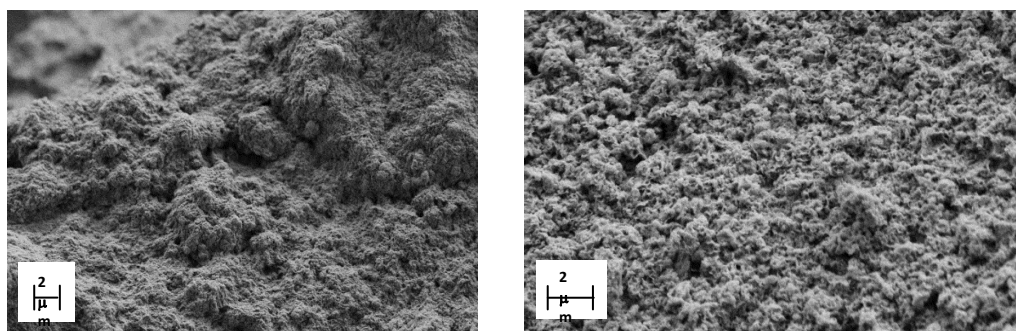

Figure 6-2 SEM images of: Mg_2Al-DDS LDH (left) and Mg_2Al-W_{10} LDH (right) prepared by the classical co-precipitation method.

6.2.2 Synthesis and characterization of the catalyst 3-DOM-Mg_2Al-$W_{10}O_{32}^{4-}$ LDH prepared by colloidal crystal templating impregnation

To overcome some limitations of LDH materials when prepared by conventional co-precipitation (poor diffusion and accessibility to active sites), macroporous LDH materials with higher surface and open structure have been synthesized.

Three dimensionally ordered macroporous layered double hydroxides (3-DOM LDH) have been synthesized by the well-known 'inverse opals method' using sacrificial polystyrene (PS) colloidal crystal as template [8,9], followed by successive

impregnations of divalent and trivalent metal salts (Mg/Al = 2) and NaOH into the voids [10,11], to ensure the confined co-precipitation. Macroporous Mg_2Al-DDS replica is subsequently obtained by removing the PS template by calcination of the composite and reconstruction of the LDH structure in DDS aqueous solution. As previously underline, the enlarged basal spacing of the DDS intercalated 3-DOM-Mg_2Al favors the intercalation of voluminous and reactive decatungstate anions by anion exchange, yielding the final material 3-DOM-Mg_2Al-$W_{10}O_{32}^{4-}$ LDH, herein abbreviated as 3-DOM-Mg_2Al-W_{10} LDH. The global scheme of the synthesis is depicted in Figure 6-3.
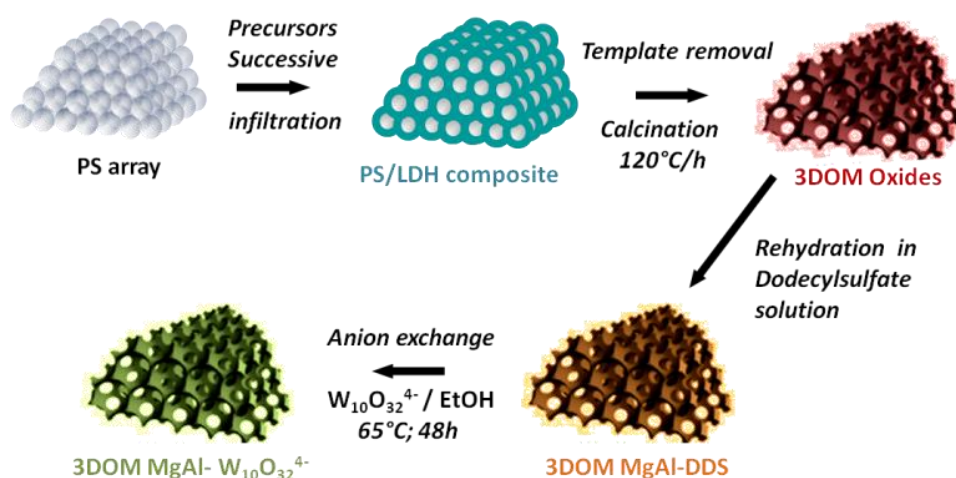

Figure 6-3 Schematic representation of the synthesis of 3-DOM-Mg_2Al-W_{10} LDH.

The characterization of the material by PXRD and FTIR analysis is given in Figure 6-4a and Figure 6-4b, respectively. The Mg_2Al LDH formation after successive impregnations of the PS crystal is evidenced by the presence of the {003} and {006} diffraction lines (11.5 and 23.4°) typical of a carbonate intercalated Mg_2Al matrix, even if these diffraction lines are partially masked by the large contribution of semi-crystalline PS centred at 20°. The ability of Mg-Al oxide solid solutions to recover the lamellar structure of LDH with DDS anions intercalated is indicated by the characteristic 00l reflections at low angles (d = 2.49 nm) and the 012 and 110 lines respectively at 36.1° and 61.3° on X-ray diagram. Finally, the success of the anion exchange reaction with decatungstate (Figure 6-4a(d)) is seen by the expected shift of the 00l diffraction lines to higher theta values due to the contraction of the interlayer galleries of 3-DOM-Mg_2Al-W_{10} LDH (d = 0.95 nm). The powder X-ray diffraction

patterns of 3-DOM-Mg_2Al-W_{10} LDH (Figure 6-4a) reveals typical lines of LDH structure and low crystallinity, as well described in literature for polyoxometalate anions intercalation into LDH precursors [7].

The FTIR spectra of the prepared LDH catalysts 3-DOM-Mg_2Al-DDS and 3-DOM-Mg_2Al-W_{10} and of $W_{10}O_{32}^{4-}$ are illustrated in Figure 6-4b whereas the spectrum of the pure DDS anion was already given in Figure 6-1.
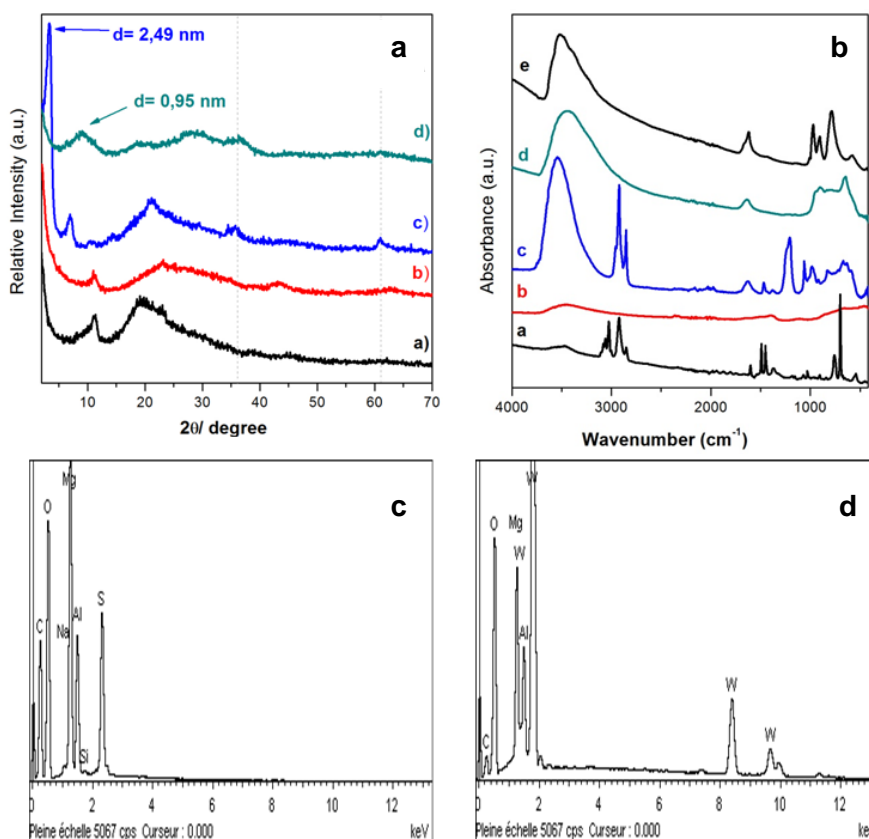
Figure 6-4 a) Powder XRD patterns and b) FTIR spectra of: *a)* PS-LDH composite *b)* 3-DOM oxides *c)* 3-DOM Mg_2Al-DDS *d)* 3-DOM-Mg_2Al-W_{10} and *e)* $W_{10}O_{32}^{4-}$. EDS spectrum of c) 3-DOM-Mg_2Al-DDS LDH and d) 3-DOM-Mg_2Al-W_{10} LDH.

The FTIR spectrum of the PS-LDH composite (*a*) presents characteristic bands (CH, CH_2 vibrational bands at 2900-3100 cm^{-1}, 1450-1600 cm^{-1}, 700 cm^{-1}, 750 cm^{-1}, and sulfate at 1450 cm^{-1}). After calcination (*b*), the PS bands have completely disappeared from the FTIR spectrum, evidencing the complete removal of the polymeric template upon calcination while the mixed oxide formation leads to a somewhat amorphous diffraction pattern (*b*). The FTIR spectra of 3-DOM-Mg_2Al-DDS and 3-DOM-Mg_2Al-W_{10} exhibits the same LDH characteristic bands as when prepared by the

classical method (section 6.2.1). The replacement of the DDS characteristic vibration bands by those of decatunsgtate species is clearly evidenced in the FTIR spectra, while the LDH lattice vibration at 648 cm^{-1} is maintained (*d*). This successful anionic exchange process is clearly shown on the EDS spectra (Figure 6-4c and Figure 6-4d) by the complete replacement of the sulfur peak (2.35 keV) by tungstate peaks (8.4 and 9.65 keV). The chemical analysis (Table 6-2) also indicates that in our conditions LDH precipitates in a higher Mg/Al ratio, nearer 3 rather than 2. Moreover, the slightly lower amount of W than expected (W/Al = 2.0 instead of 2.5) into the materials, can be explained by the formation of amorphous magnesium and aluminium simple hydroxides. According to the chemical composition, it appears that 71 % of materials in mass correspond to $W_{10}O_{32}^{4-}$ species.

Table 6-2 Chemical composition (obtained by EDS*)* and cell parameters for the 3-DOM-Mg_2Al LDH.

Sample	Mg/Al	S/Al	W/Al	d (nm)	a (nm)
3-DOM-Mg_2Al-DDS	3.4	1.0	-	2.49	0.303
3-DOM-Mg_2Al-W_{10}	3.3	-	2.0	0.95	0.303

SEM images of the different steps of the synthesis are gathered in Figure 6-5 and show typical macroporous structure. LDH-PS composite image clearly indicates that the order of the PS array is maintained during the different processes of infiltration, precipitation and drying. After the subsequent treatments of calcination and dehydration, a macroporous inorganic replica of the colloidal array is obtained. The average diameter of the voids was 35 % smaller than that of the original PS beads (600 ± 10 nm) due to shrinkage of the structure during template removal, as previously reported [8]. It is noteworthy that the macroporosity is maintained for 3-DOM-Mg_2Al-DDS and 3-DOM-Mg_2Al-W_{10} (Figure 6-5c and 6-5d) even if the ordered macroporosity is present to a lower extent. It should also be noted that the wall morphology changes during the rehydration process. While for the macroporous mixed oxides, smooth walls with well-defined interconnected windows are observed (inset Figure 6-5b), the rehydration phenomenon induces the formation of small interconnected plate-like

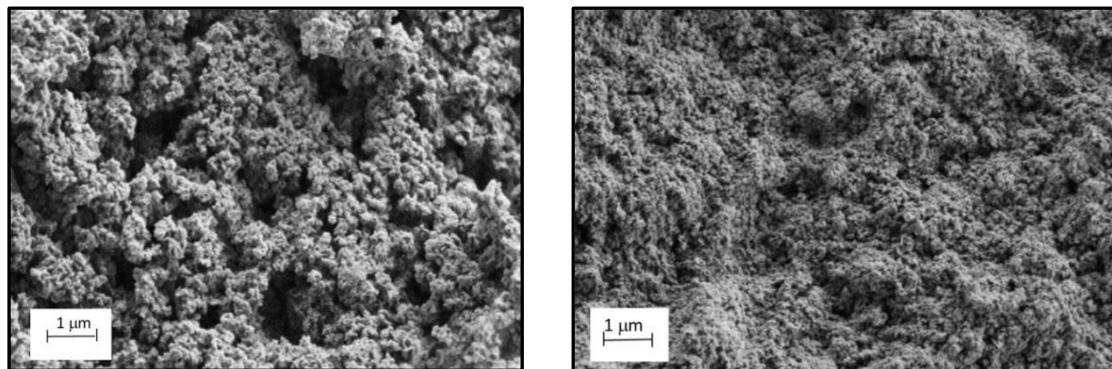particles, unmodified during the anion exchange reaction with decatungstate (inset Figure 6-5c and 6-5d).
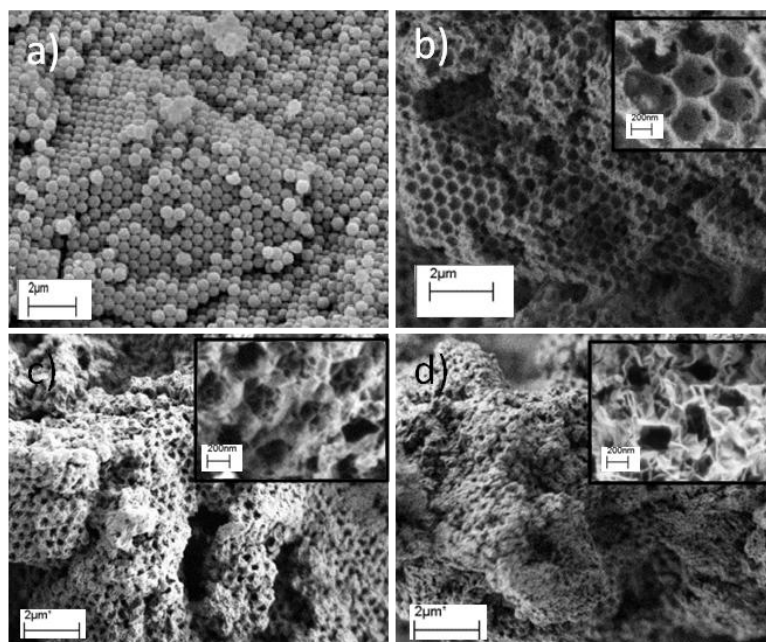
Figure 6-5 SEM images of: a) colloidal crystal after successive impregnations. b) 3-DOM oxides obtained after calcination at 400 °C. c) 3-DOM-Mg$_2$Al-DDS and d) 3-DOM-Mg$_2$Al-W$_{10}$.

6.2.3 Synthesis and characterization of the catalyst SC-Mg$_2$Al-W$_{10}$O$_{32}$$^{4-}$ LDH prepared by fast co-precipitation followed by supercritical drying with CO$_2$
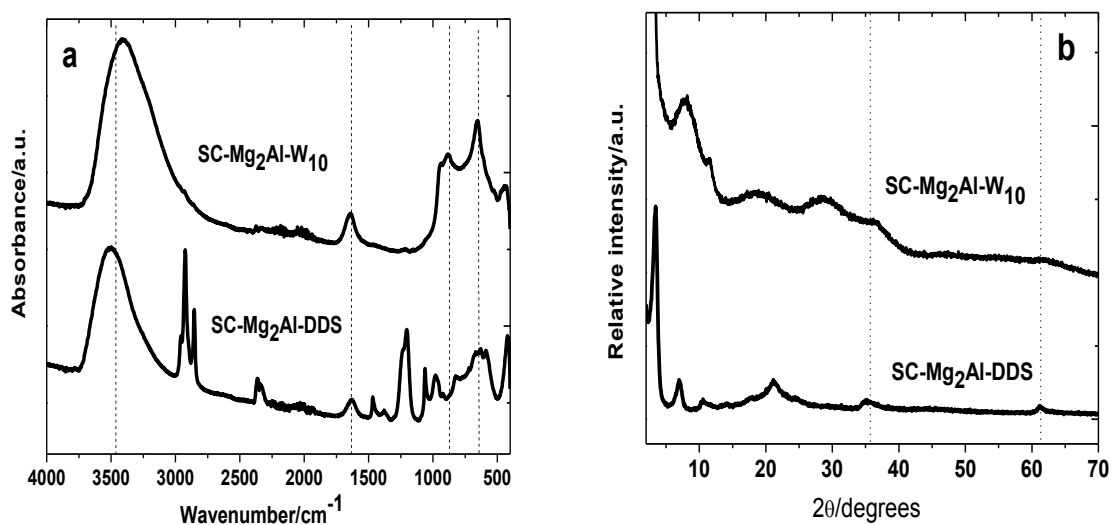
Mg$_2$Al LDH precursor intercalated with DDS was synthesized by a fast co-precipitation method under a nitrogen atmosphere followed by supercritical (SC) drying with CO$_2$ [12]. The LDH nanoparticles were first prepared by a fast co-precipitation at constant pH. The aquagel obtained was carefully washed with deionized water, which was further replaced by ethanol. The alcogel *as*-prepared was then placed in an autoclave and subjected to the SC drying CO$_2$ process during 6 h above the CO$_2$ critical point (31.1 ºC, 73.8 bar). In contrast with the classical co-precipitation method, the subsequent SC drying in CO$_2$ allows one to obtain LDH open framework nanoparticles with no aggregation. The use of SC CO$_2$ as the reaction media has many advantages arising from the fact that CO$_2$ is inexpensive, environmentally benign, non-inflammable, non-toxic, can be regenerated easily by a cyclic system and has a relatively low critical temperature Tc (304.2 K) and a moderate critical pressure Pc (7.4 MPa).

Once again, and as explained in section 6.2.1 and 6.2.2, the intercalation of $W_{10}O_{32}{}^{4-}$ in the obtained aerogel SC-Mg$_2$Al-DDS LDH was achieved by anionic exchange reaction. SEM images of these LDH materials illustrated in Figure 6-6 reveal that SC LDH presents aggregates of nanoparticles as spheres.

Figure 6-6 SEM images of SC-Mg$_2$Al-DDS LDH (left) and of SC-Mg$_2$Al-W$_{10}$ LDH (right).

FTIR and powder X-ray analysis of SC-Mg$_2$Al-DDS LDH and SC-Mg$_2$Al-W$_{10}$ LDH are given in Figure 6-7.

Figure 6-7 a) FTIR spectra and b) PXRD patterns of SC-Mg$_2$Al-DDS and SC-Mg$_2$Al-W$_{10}$ LDHs.

The FTIR spectra of SC-Mg$_2$Al-DDS and SC-Mg$_2$Al-W$_{10}$ LDH (Figure 6-7a) exhibit characteristic LDH bands, as elucidated in section 6.2.1. Additionally, the efficient exchange of DDS by decatungste anion was achieved, as shown by the vibrational bands of by decatungste anion. The PXRD pattern of SC-Mg$_2$Al-DSS and SC-Mg$_2$Al-W$_{10}$ LDHs (Figure 6-7b) exhibits the characteristic reflections of LDH
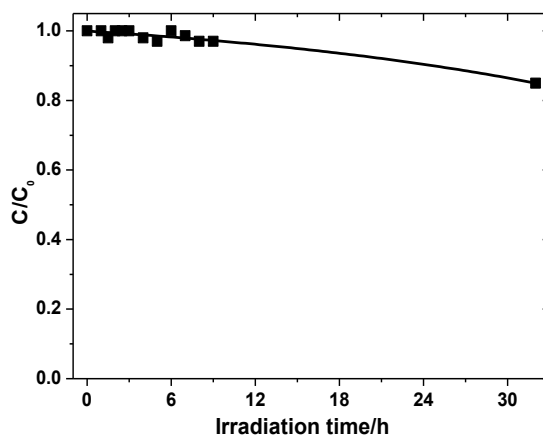
materials. The PXRD pattern of SC-Mg$_2$Al-DDS LDH presents characteristic 00l reflections at 3.5° (d = 2.50 nm) and the 012 and 110 lines respectively at 35.1° and 61°. The intercalation of decatungsate anion is indicated by the shift of the 00l diffraction lines to higher theta values (7.7°) due to the contraction of the interlayer galleries of SC-Mg$_2$Al-W$_{10}$ LDH (d = 1.14 nm). As previously underlined decatungstate intercalation induces a net decrease of LDH cristallinity [7].

6.3 Heterogeneous degradation of NAD photocatalysed by W$_{10}$O$_{32}$$^{4-}$ intercalated in different LDHs

In order to evaluate the influence of the surface properties of the LDHs catalytic system *as*-prepared by classical, macroporous and aerogel methods, the photocatalytic capacity of these materials towards NAD degradation was investigated with UV light at 365 nm. Under these conditions, the incident light was specifically absorbed by the photocatalyst since NAD does not absorb at this wavelength.

6.3.1 Photocatalytic degradation in the presence of classical Mg$_2$Al-W$_{10}$O$_{32}$$^{4-}$ LDH

A photocatalytic degradation of NAD (3.0×10^{-4} mol L^{-1}) in the presence of the classical Mg$_2$Al-W$_{10}$ LDH under 365 nm irradiation was performed. The kinetic result presented in Figure 6-8 shows that only 15 % of degradation was achieved after 32 h. This may be related with the morphology of the LDH material, with difficulties in light penetration in the layers due to the agglomerated particles.

Figure 6-8 Heterogeneous degradation of aerated aqueous NAD solution (3.0×10^{-4} mol L^{-1}) in the presence of classical Mg$_2$Al-W$_{10}$ LDH under irradiation at 365 nm.

6.3.2 Photocatalytic degradation in the presence of 3-DOM-Mg$_2$Al-W$_{10}$O$_{32}$$^{4-}$ LDH and SC-Mg$_2$Al-W$_{10}$O$_{32}$$^{4-}$ LDH

The catalytic activity of W$_{10}$O$_{32}$$^{4-}$ intercalated (heterogeneous catalysis) on the synthesized macroporous 3-DOM-Mg$_2$Al-W$_{10}$ LDH and on the aerogel SC-Mg$_2$Al-W$_{10}$ LDH was investigated towards the photodegradation of NAD (3.0×10^{-4} mol L^{-1}) under irradiation with 365 nm UV light. Parameters such as catalyst amount and pH of the solution were optimized in order to obtain a better rate for NAD degradation. The effect of oxygen concentration on NAD degradation was also studied by bubbling oxygen and nitrogen prior to irradiation and during the entire irradiation time. However, although the results with these gases were reproducible, they were inconclusive since the solution becomes cloudy, which was not observed when air was bubbled in the system. By bubbling air, degradation occurs and is the same as when the suspension is irradiated in aerated condition. It is possible that the flow or the pressure used for bubbling oxygen and nitrogen influences in some way the dispersion of the particles and even the LDH matrix. Once the best conditions were achieved, the degradation kinetics and mineralization of NAD in the presence of these two photocatalysts was studied by HPLC-DAD and by measuring the total organic carbon (TOC). An additional important parameter in a heterogeneous system is the ability of a catalyst to be recycled and reused, which was also assessed for these systems. Furthermore, under these conditions, some of the products of NAD heterogeneous degradation were identified using LC-MS/MS with electrospray ionization.

6.3.2.1 Amount of catalyst

The amount of the catalysts 3-DOM-Mg$_2$Al-W$_{10}$ and SC-Mg$_2$Al-W$_{10}$ LDH used for NAD degradation was optimized in order to avoid an unnecessary excess of catalyst as well as to guarantee an efficient absorption of photons [13], with consequent influence on the initial rates of the reactions.

The amount of the solid catalyst 3-DOM-Mg$_2$Al-W$_{10}$ LDH suspended in 10 mL of NAD aqueous solution (3.0×10^{-4} mol L^{-1}) was varied between 0.15 to 5.0 mg. These solutions were irradiated at 365 nm during 17 h, in aerated conditions at pH of the solution (6.6). As observed in Figure 6-9a, the amount of the catalyst 3-DOM-Mg$_2$Al-W$_{10}$ LDH that gives the best rate of degradation is 0.6 mg in 10 mL of solution (60 mg L^{-1}).

With the catalyst SC-Mg$_2$Al-W$_{10}$ LDH, the optimization started with the suspension of 0.5 mL of the aerogel SC-Mg$_2$Al-W$_{10}$ LDH in 10 mL of NAD aqueous solution (3.0×10^{-4} mol L^{-1}) and varied to 10 μL. These solutions were irradiated at 365 nm during 10 h, under aerated conditions at natural pH of the solution (7.5). As observed in Figure 6-9b, the best amount of the catalyst is 0.025 mL (in 10 mL of total solution).

In both cases, higher quantities than the optimal amount found for the catalyst lead to a screening effect which reduces the light reaching the catalyst, leading to an inefficient absorption of photons and a decrease in the reactivity. Thus, it was concluded that higher dose of catalyst was not required in view of aggregation as well as reduced irradiation due to light scattering. Such an effect is usually observed in heterogeneous photocatalytic systems [14].
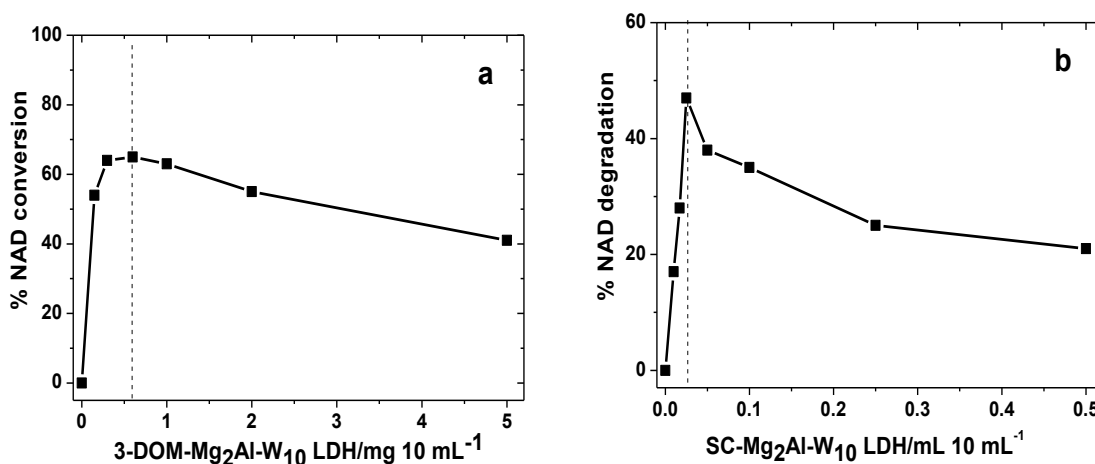
Figure 6-9 Effect of the amount of photocatalyst a) 3-DOM-Mg$_2$Al-W$_{10}$ LDH (mg per 10 mL^{-1} solution). b) SC-Mg$_2$Al-W$_{10}$ LDH (mL per 10 mL^{-1} solution), suspended on aerated aqueous NAD solution (3.0×10^{-4} mol L^{-1}) under irradiation at 365 nm.

6.3.2.2 Effect of pH

The pH of the solution is a very important factor that influences the stability and photoactivity of the W$_{10}$O$_{32}$$^{4-}$ and of the LDH materials [7]. Thus, the role of pH on the photocatalytic degradation of NAD in the presence of the solid catalysts 3-DOM-Mg$_2$Al-W$_{10}$ LDH (Figure 6-10a) and of aerogel SC-Mg$_2$Al-W$_{10}$ LDH (Figure 6-10b) catalysts was studied.

Solutions of the catalyst 3-DOM-Mg$_2$Al-W$_{10}$ LDH (0.6 mg) and of the aerogel SC-Mg$_2$Al-W$_{10}$ LDH (0.025 mL) were suspended in 10 mL of NAD aqueous solution (3.0×10^{-4} mol L^{-1}) with pH varying between 3.3 and 7.5 (adjusted with some HClO$_4$ drops) and irradiated at 365 nm under constant stirring. As depicted in Figure 6-10, the rate of NAD degradation is faster under acidic conditions for both photocatalysts. At acidic pH, the LDH structure was destroyed with consequent release of W$_{10}$O$_{32}$$^{4-}$ to the solution, promoting a faster degradation similar to the one obtained in homogeneous phase. The loss of the LDH structure was confirmed by recording the UV-vis spectra of the solution (maximum absorption band around 324 nm). Therefore, the optimal pH conditions chosen for the catalysts SC-Mg$_2$Al-W$_{10}$ and 3-DOM-Mg$_2$Al-W$_{10}$ LDH was the natural pH of the solution, 7.5 and 6.6, respectively.
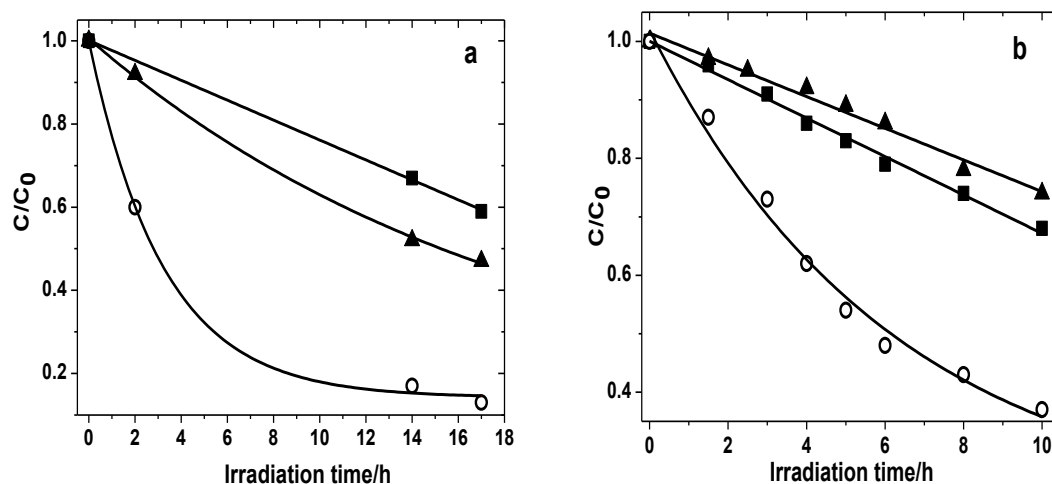
Figure 6-10 Effect of pH on NAD (3.0×10^{-4} mol L^{-1}) degradation under irradiation at 365 nm in the presence of the catalysts: a) 6 3-DOM-Mg$_2$Al-W$_{10}$ LDH (0.6 mg 10 mL^{-1}; ○ pH 3.3; ▲pH 5.6; ■ pH solution 6.6. b) SC-Mg$_2$Al-W$_{10}$ LDH (0.025 mL 10 mL^{-1}; ○ pH 3.6; ▲pH 5.6; ■ pH solution 7.5).

6.3.2.3 Kinetics of degradation in the presence of the catalysts 3-DOM-Mg$_2$Al-W$_{10}$O$_{32}$$^{4-}$ and SC-Mg$_2$Al- W$_{10}$O$_{32}$$^{4-}$ LDH

Once the optimal conditions of the catalysts 3-DOM-Mg$_2$Al-W$_{10}$ (pH 6.6; 0.6 mg 10 mL^{-1}; aerated) and SC-Mg$_2$Al-W$_{10}$ LDHs (pH 7.5; 0.025 mL 10 mL^{-1}; aerated) were achieved, the photocatalytic degradation of NAD (3.0×10^{-4} mol L^{-1}) suspended in these two LDH systems was carried out at 365 nm, with constant stirring. The kinetics of disappearance of NAD was followed by HPLC-DAD (Figure 6-11). Under these

conditions, very similar kinetics was obtained for NAD degradation in the presence of both LDH catalysts, with 75 % of degradation within 50 hours irradiation. The kinetics of degradation followed a two-step kinetic process: a rapid process that permits 50 % conversion followed by a slower one for higher conversions. This is in agreement with the Langmuir-Hinshelwood model that is used to describe the relationship between the photocatalytic degradation rate and the initial concentration of the catalyst in heterogeneous processes [13]. Under initial conditions of photocatalytic procedure (t=0, $C=C_0$), the degradation rate constant k follows first order kinetics, expressed by - ln $C/C_0 = k \times t$. The k value will be the slope of the curve ln C/C_0 *vs* time and the half-life ($t_{1/2}$) is given by ln 2/k. The pseudo first order rate constant for the rapid process were estimated to be 0.13 h^{-1} ($t_{1/2}$ = 5.5 h) and 0.099 h^{-1} ($t_{1/2}$ = 7.0 h) for 3-DOM-Mg$_2$Al-W$_{10}$ LDH and SC-Mg$_2$Al-W$_{10}$ LDH, respectively. The results were reproducible as far as temperature, light intensity and a constant stirring were perfectly controlled during the irradiation. It is necessary to point out that in absence of $W_{10}O_{32}^{4-}$ (abbreviated as W_{10}) less than 5.0 % of NAD was degraded under irradiation at 365 nm, as already discussed in Chapter 5A. Moreover, adsorption studies of NAD in the two heterogeneous systems SC and 3-DOM were carried out in the dark for more than 24 h and no adsorption was observed.
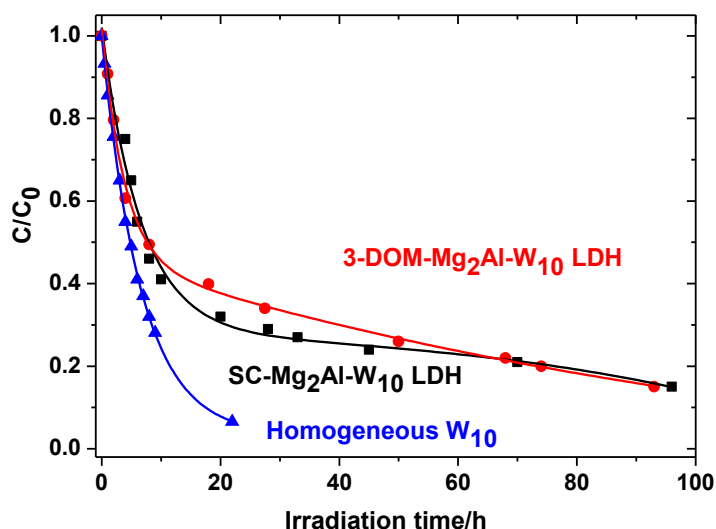
**Figure 6-11** Heterogeneous degradation of aqueous NAD (3.0×10^{-4} mol L^{-1}) in the presence of SC-Mg$_2$Al-W$_{10}$ LDH (0.025 mL 10 mL^{-1}; pH 7.5) and 3-DOM Mg$_2$Al-W$_{10}$ LDH (0.6 mg10 mL^{-1}; pH 6.6) *vs* NAD homogeneous degradation in the presence of $W_{10}O_{32}^{4-}$ (abbreviated as W_{10}) under 365 nm irradiation followed by HPLC-DAD (λ_{det} = 280 nm).

Furthermore, the comparison of NAD photocatalytic degradation in homogeneous (W_{10}) and heterogeneous media (SC-Mg_2Al-W_{10} and 3-DOM Mg_2Al-W_{10} LDH systems) reinforces the catalytic efficiency of the decatungstate anion even when immobilized (Figure 6-11).

6.3.2.4 Recovery and recycling of the photocatalyst

A very important parameter concerning the use of a catalyst is its reusability and stability [14]. Thus, the photocatalysts 3-DOM-Mg_2Al-W_{10} and SC-Mg_2Al-W_{10} LDHs were re-used for several cycles using the optimal conditions previously obtained (amount and pH) in order to examine its reuse and stability during NAD degradation process. The recovery consisted on collecting each catalyst by centrifuge the solution that remains after the first irradiation, washing it three times with water in order to remove possible particles, centrifuging it again to remove the water and recover the catalyst for its re-use on degradation of NAD fresh solution (3.0×10^{-4} mol L^{-1}). This process of wash and recover was repeated for several cycles of degradation at 365 nm irradiation. As shown in Figure 6-12a, the irradiation of NAD (3.0×10^{-4} mol L^{-1}) in the presence of the 3-DOM-Mg_2Al-W_{10} LDH (0.6 mg 10 mL^{-1}; pH 6.6; aerated) lead to 60 % of NAD conversion after 17 h of irradiation at 365 nm. The catalyst efficiency on NAD degradation over four cycles was maintained without any loss of photocatalytic activity. Moreover, no leaching of the decatungstate anion from the solid support was observed in any cycle, as verified by UV-vis absorption and FTIR measurements.
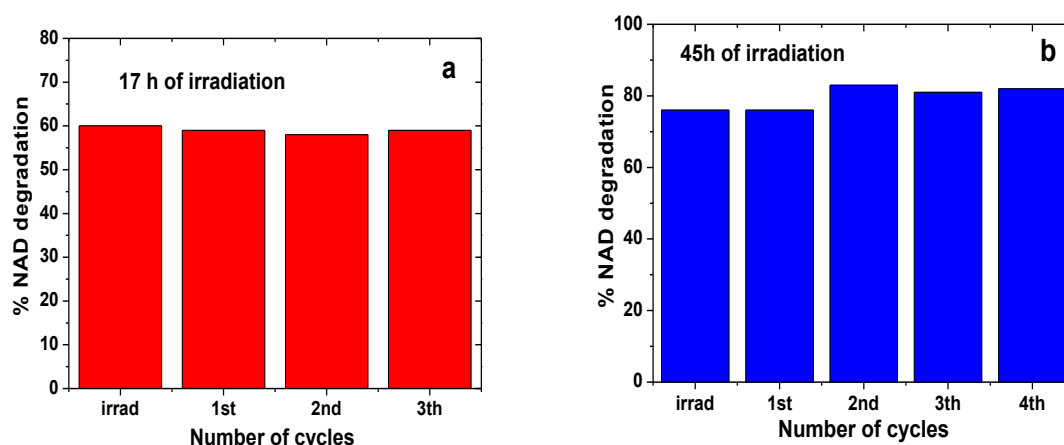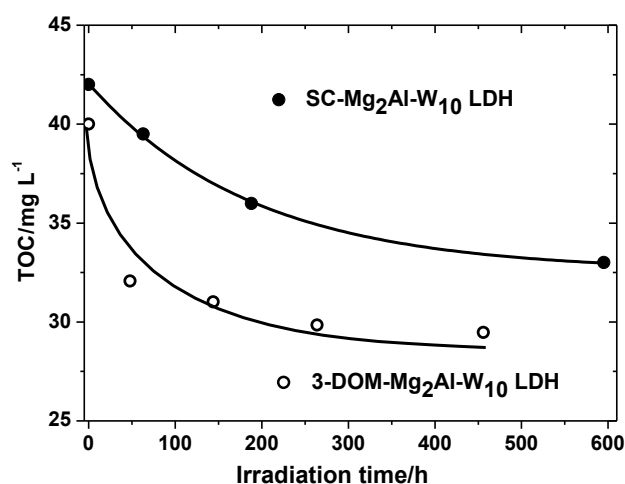

Figure 6-12 Efficiency of the reuse of the catalysts a) 3-DOM-Mg_2Al-W_{10} LDH and of b) SC-Mg_2Al-W_{10} LDH, upon irradiation with NAD (3.0×10^{-4} mol L^{-1}) at 365 nm.

The same procedure was employed for the reuse of the catalyst SC-Mg_2Al-W_{10} LDH on NAD degradation. Therefore, NAD (3.0×10^{-4} mol L^{-1}) was irradiated at 365 nm in the presence of the SC-Mg_2Al-W_{10} LDH (0.025 mL10 mL^{-1}; pH 7.5; aerated) for five cycles, each with the duration of 45 h (Figure 6-12b). Under these conditions, more than 80 % of NAD degradation was achieved in each cycle, highlighting the high efficiency of catalyst activity even after being recovered and reuse for five cycles. Once again no leaching of the decatungstate anion from the solid support was observed in any cycle. These results indicate that the catalysts 3-DOM-Mg_2Al-W_{10} and SC-Mg_2Al-W_{10} LDH are very stable and efficient during the degradation process making it a promising heterogeneous catalyst for water treatment.

6.3.2.5 Mineralization

The mineralization of NAD (3.0×10^{-4} mol L^{-1}) in the presence of the catalysts SC-Mg_2Al-W_{10} LDH and 3-DOM-Mg_2Al-W_{10} under the previously optimized conditions was determined by measuring the total organic carbon (TOC) as a function of irradiation time in aerated solutions (Figure 6-13). The results show that NAD is in fact mineralized in the presence of both LDHs materials, with 25 and 21 % of organic carbonic abatement reached after roughly 600 and 400 h of irradiation in presence of SC-Mg_2Al-W_{10} LDH and 3-DOM-Mg_2Al-W_{10} LDH, respectively. No lag period was observed in either mineralization studies, indicating that the prepared photocatalysts are able to lead to the degradation of organic compounds and also to their mineralization.

Figure 6-13 Evolution of TOC for aerated aqueous NAD solution (3.0×10^{-4} mol L^{-1}) irradiated at 365 nm in the presence of the catalysts 3-DOM-Mg_2Al-W_{10} LDH and SC-Mg_2Al-W_{10} LDH.

The results also provide evidence for the more efficient mineralization of NAD in presence of 3-DOM-Mg$_2$Al-W$_{10}$ LDH than of SC-Mg$_2$Al-W$_{10}$ LDH. This can be explained by the good permeability and higher porosity of the macroporous open structure leading to a more efficient light penetration and better accessibility to the active site of the material when compared to the aerogel. As usual, NAD mineralization process is much slower than the photodegradation due to the formation of intermediates compounds that may be adsorbed in the interlayer, slowing down the process.

6.3.2.6 Photoproduct identification

The heterogeneous degradation of aerated aqueous NAD solutions (3.0×10^{-4} mol L^{-1}) irradiated at 365 nm in presence of both catalysts 3-DOM-Mg$_2$Al-W$_{10}$ and SC-Mg$_2$Al-W$_{10}$ LDH was analyzed by LC-ESI-MS/MS with electrospray ionization in positive mode (ES$^+$) after 20 % conversion (Figure 6-14). Several photoproducts (Table 6-3) have been identified by the molecular ion [M+H]$^+$ (and mass fragments ions). In our elution conditions, NAD presents a retention time of 24 min and all the products were eluted before NAD. The product of NAD hydrolysis, 1-naphthylacetic acid (1-NAA), identified by the injection of the commercial product, was the only one eluted with a retention time higher than NAD, with 24.7 min. This product was also observed in NAD direct and homogeneous degradation. These products of NAD degradation were compared with the identified under homogeneous degradation (Chapter 5).

Several mono-, di- and one tri-hydroxylated products, as well as a naphthoquinone NAD product were identified in the presence of the catalyst 3-DOM-Mg$_2$Al-W$_{10}$ LDH whereas in the presence of SC-Mg$_2$Al-W$_{10}$ LDH only mono- and di-hydroxylated products were identified. These products are the same as those identified in homogeneous conditions, except that in latter case more tri-hydroxylated products were formed. This may be explained by the proximity of NAD and decatungstate anion molecules in homogeneous conditions. In heterogeneous conditions, NAD is expected to be part of the interlayer region of the LDH and the position in which decatunsgtate anion is intercalated on SC-Mg$_2$Al-W$_{10}$ LDH and 3-DOM-Mg$_2$Al-W$_{10}$ LDH materials may influence the rate of NAD degradation, as well as the morphology of the LDH materials itself. The lower amount of identified products in the presence of SC-Mg$_2$Al-W$_{10}$ LDH in the primary steps of degradation may be due to the formation of

intermediates which are adsorbed on the interlay and more difficult to degrade, leading to a longer mineralization time scale.
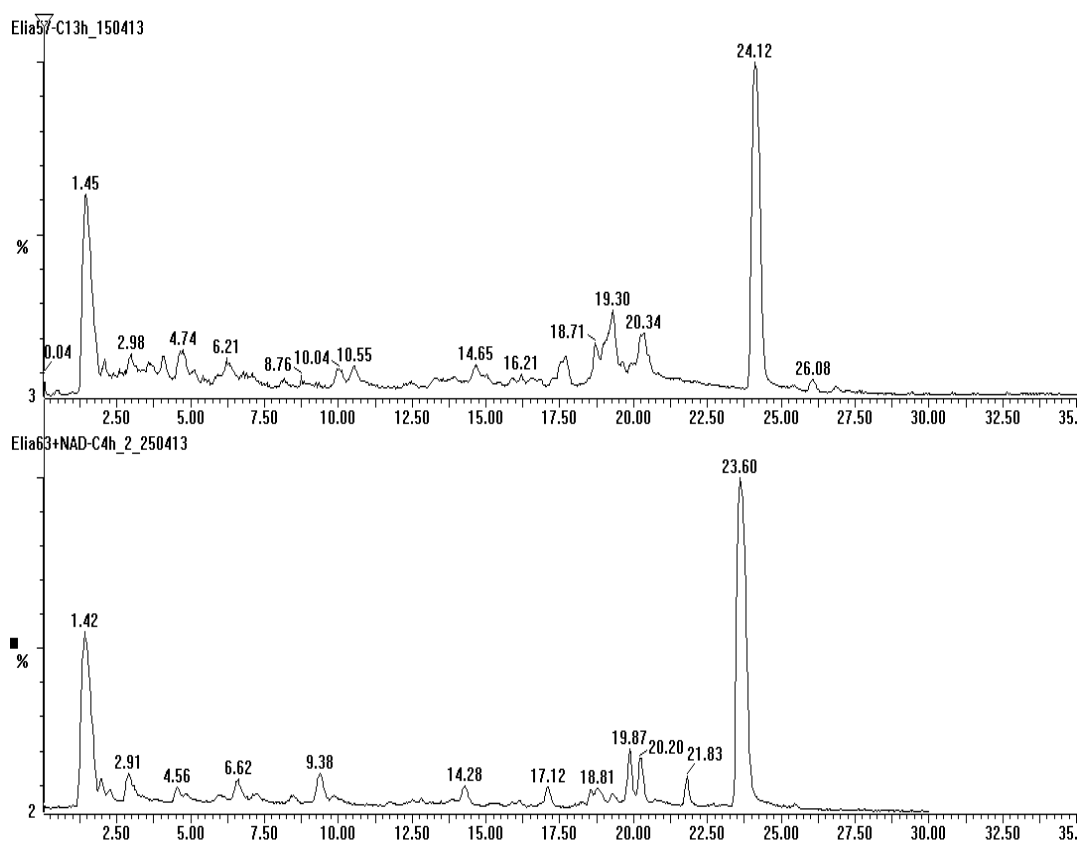
Figure 6-14 TIC chromatogram (ES$^+$) of NAD aerated aqueous solution (3.0×10^{-4} mol L^{-1}) irradiated at 365 nm in the presence of: 3-DOM-Mg$_2$Al-W$_{10}$O$_{32}$$^{4-}$ LDH (top figure) and SC-Mg$_2$Al-W$_{10}$ LDH (bottom figure).

Table 6-3 Retention time (t_{ret}), molecular ion peak [M+H]$^+$ and proposed structure of the main photoproducts obtained for NAD heterogeneous degradation (* most stable structure).

3-DOM-Mg$_2$Al-W$_{10}$ LDH			SC-Mg$_2$Al-W$_{10}$ LDH		
t_{ret} (min)	[M+H]$^+$	Proposed structure	t_{ret} (min)	[M+H]$^+$	Proposed structure
16.8	234			Not detected	

Table 6-3 (Continuation) Retention time (t_{ret}), molecular ion peak $[M+H]^+$ and proposed structure of the main photoproducts for NAD heterogeneous degradation (*most stable structure).

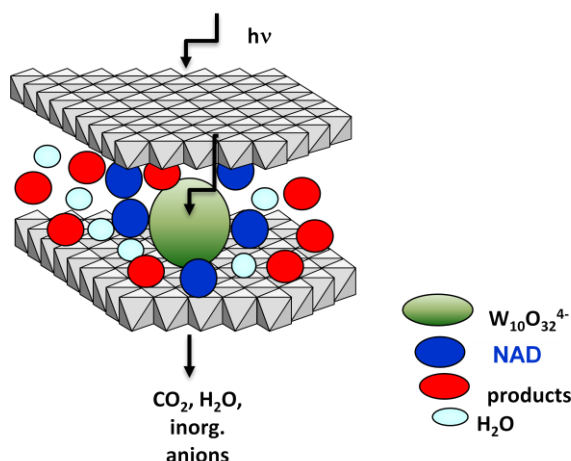| 3-DOM-Mg$_2$Al-W$_{10}$ LDH			SC-Mg$_2$Al-W$_{10}$ LDH		
t_{ret} (min)	$[M+H]^+$	Proposed structure	t_{ret} (min)	$[M+H]^+$	Proposed structure
10.0 6.21	202		4.59 6.58 12.7 19.8	202	
10.5 16.5 17.4 18.7 19.9 20.2 20.6	218		9.37 9.86 11.7 12.6 14.3 15.3 18.3 18.8	218	
20.4	216				Not detected

6.3.2.7 Proposed mechanism

A mechanism for NAD degradation in heterogeneous conditions in the presence of the catalysts $3\text{-DOM-Mg}_2\text{Al-W}_{10}$ and $\text{SC-Mg}_2\text{Al-W}_{10}$ LDH is proposed (Scheme 6-1). It is believed that the photocatalytic reaction of NAD with the catalyst occurs in the interlayer space, *i.e.*, in the solid interface in contact with solution. Upon absorption of light, the photons penetrate the sheets of the system $3\text{-DOM-Mg}_2\text{Al-W}_{10}$ (or $\text{SC-Mg}_2\text{Al-W}_{10}$ LDH). The interlayer catalyst $W_{10} (=W_{10}O_{32}^{4-})$ is photonic activated by exciting $3\text{-DOM-Mg}_2\text{Al-W}_{10}$ LDH (or $\text{SC-Mg}_2\text{Al-W}_{10}$ LDH) with light energy higher than the band gap of $W_{10}O_{32}^{4-}$. The formed charge transfer excited state $W_{10}O_{32}^{4-*}$ decays very rapidly to a longer-lived extremely reactive and non-emissive transient designated as wO [15], as already explained in Chapter 4. It is therefore this species $(wO\text{-LDH})^*$ that will be further involved in the degradation process. At the same time NAD molecules diffuses into the layer space and are photoactivated by the $(wO\text{-LDH})^*$ and then degraded into inorganic product molecules (CO_2 and inorganic anions). The interlayer catalyst $W_{10}O_{32}^{4-}$ in heterogeneous degradation has therefore the double function of absorption of light with $E > E_{band\ gap}$ and adsorption of the reactant´s on the catalyst surface.

To simplify the proposed mechanism, the initial photocatalytic material (3-DOM or SC LDH) is designated as $W_{10}O_{32}^{4-}$-LDH and its excited state as $(wO\text{-LDH})^*$. Therefore, the excitation of the $W_{10}O_{32}^{4-}$-LDH at the O-MCT band can be presented by equation (6.1) using the semiconductor notation as:

$$W_{10}O_{32}^{4-}\text{-LDH} + \ h\nu \rightarrow \ (wO\text{-LDH})^* \approx wO\text{-LDH} \ (e^-_{(CB)} + h^+_{(VB)}) \qquad (6.1)$$

where e^- causes reductions and h^+ oxidations. wO-LDH ($e^- + h^+$) has more powerful redox ability by forming electron-hole pairs and their recombination is inhibited by the "gap" of the decatungstate. Taking in consideration the identified products, it is most probable that the electron e^- will initiate the degradation process by reacting with molecular oxygen producing superoxide anion. The holes h^+ species may also react with NAD to form NAD radical cation. Both the superoxide anion and the radical cation can give rise to the products through hydroxylation and oxidation steps. It is possible to assume that these radicals will be responsible for NAD degradation and mineralization, and that in the end the products (CO_2 and inorganic anions) will escape from the interlayer space through diffusion.

Scheme 6-1 Illustration of NAD heterogeneous degradation process.

6.4 Conclusions

The synthesis of several *as*-prepared LHD-$W_{10}O_{32}^{4-}$ materials has been carried out and their activity as heterogeneous photocatalysts for pollutant treatment in water was tested towards NAD irradiation at 365 nm.

The synthesis of the $W_{10}O_{32}^{4-}$-LHD materials was carried out by three different procedures: classical co-precipitation at constant pH, fast co-precipitation followed by supercritical drying (SC) with CO_2 and template impregnation/coprecipitation of three dimensionally ordered macroporous (3-DOM). The intercalation of the catalyst $W_{10}O_{32}^{4-}$ on the *as*-prepared LDH precursors was successfully accomplished through anion exchange reaction, yielding the following materials: classical Mg_2Al-$W_{10}O_{32}^{4-}$ LDH; SC-Mg_2Al-$W_{10}O_{32}^{4-}$ LDH and 3-DOM-Mg_2Al-$W_{10}O_{32}^{4-}$ LDH.

These synthesized materials present structures with different morphologies in terms of size and porosity (agglomerated particles, macroporous open structure, aggregates as spheres, respectively) which directly affect the rate of NAD degradation.

Higher degradation rates was obtained with macroporous structure (3-DOM-Mg_2Al-$W_{10}O_{32}^{4-}$ LDH) which can be explained by the textural properties of the material, since the porous facilitate light penetration in the structure, with consequent activation of the photocatalyst.

Mineralization studies of NAD in the presence of 3-DOM- $W_{10}O_{32}^{4-}$ and SC-$W_{10}O_{32}^{4-}$ LDH show an effective transformation into CO_2, H_2O and anions. The recovery and reuse of these two catalysts was also investigated. Their activity was very efficient and stable during at least four cycles of irradiation, with no leaching of the

material to the reaction medium. Finally, the products of NAD formed in the presence of these same catalysts were evaluated. Once again, the formation of hydroxylation and oxidation products was observed, but with some differences concerning the homogeneous degradation. It is believed that the photocatalytic reaction of NAD with these types of catalysts occurs in the interlayer region of the LDH. The mechanism of degradation involves the catalyst activation by absorption of light, followed by the formation of the extremely reactive and non-emissive transient designated as wO which ultimately leads to the formation of hydroxylation and oxidation products.

6.5 References

[1] H. Zhao, K. L. Nagy, Dodecyl sulfate-hydrotalcite nanocomposites for trapping chlorinated organic pollutants in water. *J. Colloid Interface Sci.*, **2004**, 274, 613-624.

[2] A. Clearfield, M. Kieke, J. Kwan, J. L. Colon, R. -C. Wang, Intercalation of dodecyl sulfate into layered double hydroxides. *J. Inclusion Phenom. Mol. Recognit. Chem.*, **1991**, 1, 361-378.

[3] F. Cavani, F. Trifirò, A. Vaccari, Hydrotalcite-type anionic clays: preparation, properties and applications. *Catal. Today*, **1991**, 11, 173-301.

[4] X. Cheng, X. Huang, X. Wang, D. Sun, Influence of calcination on the adsorptive removal of phosphate by Zn–Al layered double hydroxides from excess sludge liquor. *J. Hazard. Mater.*, **2010**, 177, 516-523.

[5] Y. Feng, D. Li, Y. Wang, D. G. Evans, X. Duan, Synthesis and characterization of a UV absorbent-intercalated Zn-Al layered double hydroxide. *Polym. Degrad. Stab.*, **2006**, 91, 789-794.

[6] G. G. Arizaga, J. E. Gardolinski, W. H. Schreiner, F. Wypych, Intercalation of an oxalatooxoniobate complex into layered double hydroxide and layered zinc hydroxide nitrate. *J. Colloid Interface Sci.*, **2009**, 330, 352-358.

[7] V. Rives, *Layered Double Hydroxides: Present and Future*. New Science, New York, **2001.**

[8] R. C. Schroden, A. Stein, *3D ordered macroporous materials.* In: Colloids and Colloid Assemblies, ed. F. Caruso. Wiley-VCH, pp. 465-493, **2004**.

[9] A. Stein, B. E. Wilson, S. G. Rudisill, Design and functionality of colloidal-crystal templated materials. *Chem. Soc. Rev.*, **2013**, 42, 2763-2803.

[10] E. Géraud, V. Prévot, F. Leroux, Synthesis and characterization of macroporous MgAl LDH using polystyrene spheres as template. *J. Phys. Chem. Solids*, **2006**, 67, 903-908.

[11] E. Géraud, S. Rafqah, M. Sarakha, C. Forano, V. Prevot, F. Leroux, Three dimensionally ordered macroporous layered double hydroxides: preparation by template

impregnation/coprecipitation and pattern stability upon calcination. *Chem. Mater.,* **2008**, 20, 1116-1125.

[12] S. Touati, H. Mansouri, A. Bengueddach, A. de Roy, C. Forano, V. Prevot, Nanostructured layered double hydroxide aerogels with enhanced adsorption properties. *Chem. Commun.*, **2012**, 48, 7197-7199.

[13] J.-M. Herrmann, Heterogeneous photocatalysis: state of the art and present applications. *Top. Catal.*, **2005**, 34, 49-65.

[14] S. Rafqah, P. Wong-Wah-Chung, S. Nelieu, J. Einhorn, M. Sarakha, Phototransformation of triclosan in the presence of TiO_2 in aqueous suspension: mechanistic approach. *Appl. Catal. B Environ.*, **2006**, 66, 119-125.

[15] D. C. Duncan, M. A. Fox, Early events in decatungstate photocatalyzed oxidations: a nanosecond laser transient absorbance reinvestigation. *J. Phys. Chem. A,* **1998**, 102, 4559-4567.

Part 3

General conclusions

and experimental part

Chapter 7

General conclusions and perspectives

7.1 General conclusions and perspectives

The research work developed within this thesis has aimed to obtain a better understanding of the degradation processes that could occur under environmental conditions of the two plant regulating compounds, 2-(1-naphthyl) acetamide (NAD) and 2-naphthoxyacetic acid (2-NOA), and also to develop a catalytic material that might be used for the elimination of these type of pollutants from waters. In order to ascertain which pathways were involved in the degradation process, photophysical studies were carried out for both compounds and the following conclusions can be made. NAD and 2-NOA excited states are dependent on solvent polarity and have different behavior in water and organic solvents. Furthermore, both compounds present fluorescence and phosphorescence. The main deactivation pathways for NAD and 2-NOA excited states are the non-radiative processes of internal conversion and intersystem crossing. The quenching of NAD and 2-NOA triplet excited state leads to singlet oxygen formation. This species seems to be involved in the mechanism of degradation but as a minor pathway. Laser flash photolysis studies also show that both compounds give rise to the formation of the reactive species hydrated electron and radical cation through a photoionization process. The reaction of hydrated electron with oxygen produces the reactive species superoxide anion, which has been demonstrated to be involved in degradation mechanisms of NAD and 2-NOA. The major influences that the substituent groups in NAD and 2-NOA have on the photophysical properties are a decrease of the fluorescence and triplet lifetimes and an increase of the energy of the triplet state, when compared to the naphthalene molecule.

The photochemical degradation studies performed in NAD and 2-NOA in water under UV excitation and using simulated solar light lead to the degradation of these compounds with formation of several products. For NAD, hydroxylation and oxidation products were identified, which arise from the reactivity of the aromatic ring and not of the amide group. For NAD and 2-NOA, the photoinization process with consequent formation of superoxide anion radical seems to be one of the major degradation pathways in aerated conditions. Additionally to this pathway, 2-NOA degradation mechanism also involves a photo-Fries rearrangement, as well as the participation of singlet oxygen (experimentally demonstrated by using Rose Bengal as singlet oxygen

sensitizer), although as a minor route. 2-Naphthol was identified as one of the major primary products of 2-NOA degradation.

Toxicity studies of NAD and its products reveal that the formed primary products are more toxic than the parent compound. This is of great concern since it can cause adverse effects for both human health and the environment. Therefore, the development of methods that allow the stabilization of formulations of this compound towards photodegradation is essential for obtaining more efficient application of the active ingredient with enhanced safety. As a consequence, the degradation of NAD inclusion complexes with β-cyclodextrin (β-CD) was studied by irradiation with UV and simulated solar light. The results show a stabilizing effect of β-CD on NAD degradation. This suggests that β-CD may be used as potential additive for NAD formulations since it is nontoxic and biodegradable under environmental conditions. Thus, this can be regarded as a more sustainable, economic and rational use of the plant growth regulator.

Photocatalysis presents as advantages over direct 254 nm irradiation the possibility of using solar light as energy source and the fact that the pollutants can be mineralized and not just transformed into other products that can be more toxic than the parent compounds. This arouses our interest in studying the photocatalytic degradation of NAD in presence of the polyoxometalate decatungstate anion given that its absorption spectrum overlaps in some extension solar light spectrum.

Therefore, the photocatalytic degradation and mineralization of NAD in the presence of decatungstate anion under irradiation at 365 nm was studied. The results show an efficient degradation and mineralization of NAD under these conditions. A dependence of NAD degradation rate with oxygen concentration was also observed. This is due to the fact that oxygen is necessary to regenerate the catalyst in order to favor the photocatalytic cycle. The products formed under catalyzed degradation have some differences with those identified under direct irradiation of NAD. This suggests the involvement of different mechanisms of degradation.

One major drawback of homogeneous photocatalysis is that the reaction occurs in one phase, thus preventing the separation of the catalyst from the solution. Consequently, an alternative has to be found in order to be possible to use this catalyst in the environment. The alternative comes through immobilization of the catalyst

decatungstate anion into layered double hydroxides (LDH). The choice of these materials was proved to be wise since very good results were obtained when the heterogeneous degradation of NAD was carried out in their presence, either concerning degradation or mineralization processes. Another important parameter assessed in this heterogeneous photocatalysed degradation of NAD was the recovery and reuse of the catalyst. This is very important for environmental purposes and for financial reasons. The recovery and reuse experiments gave excellent results, in which the catalysts were used for several cycles of degradation, always maintaining the photocatalytic activity and stability.

The results obtained for NAD heterogeneous photocatalysed degradation highlight the influence of morphology and nanostructuration of LDH-decatungstate materials on the photocatalytic activity. Taking this in consideration, the *as*-prepared macroporous and supercritical LDH materials intercalated with decatungstate anion can be considered promising catalysts for pollutant water treatment.

Some future perspectives

- Optimize experimental conditions of the prepared photocatalyst (pH, amount decatungstate, Mg/Al ratio, etc.)
- Validate the performance of this system using solar light and natural waters
- Validate the performance of this new photocatalyst using natural waters spiked with organic pollutants like NAD or 2-NOA by determining degradation kinetics and testing potential reuse
- Widen the use of such photocatalyst to eliminate emerging and refractant (to WWTP treatments) pollutants, such as pharmaceuticals.

Chapter 8

Materials and methods

8.1 Introduction

In this Chapter are described the reagents, solvents, equipment, experimental procedures and analytical methods employed within this research work. The synthesis and characterization of the catalyst sodium decatungstate and the solid supports LDHs are also reported in the last part of this Chapter.

8.2 Reagents and solvents

Reagents

2-(1-Naphthyl) acetamide, Pestanal

2-Napththoxyacetic acid, Pestanal

1-Naphthylacetic acetic acid, Pestanal

Naphthalene, Riedel-de Haën

2-Naphthol, Merck

Benzophenone, Sigma Aldrich

Perinaphthenone (or Phenalenone), Sigma Aldrich

Biphenyl, Sigma Aldrich

Rose Bengal, Fluka

Sodium azide, Fluka

1,10-Phenantroline, Sigma Aldrich

β-Cyclodextrin, Sigma Aldrich

Dodecyl sulphate sodium salt, Sigma Aldrich

Titanium dioxide Degussa (P25), Riedel-de Haën

Sodium chloride, Sigma Aldrich

Potassium chloride, Sigma Aldrich

Potassium iodide, Merck

Potassium bromide, May & Baker

Potassium thiocyanate, Riedel-de-Haën

Triethylamine, Sigma Aldrich

4-Hydroxyphenylacetic acid, Sigma Aldrich

Peroxidase, from Horseradish, Sigma Aldrich

Hydrogen peroxide, Fluka

Sodium phosphate dibasic dihydrate, Fluka

Sodium dihydrogen phosphate monobasic, Aldrich

Sodium decatungstate (synthesized)

Sodium tungstate dihydrate, Sigma Aldrich

Aluminum nitrate monohydrate, Agros Organics

Magnesium nitrate hexahydrate, Agros Organics

Magnesium chloride hexahydrate, Sigma Aldrich

Aluminum chloride hexahydrate, Fischer Scientific

Polystyrene beads (provided by Doctor Vanessa Prevot)

Solvents

Methanol, Sigma Aldrich

Ethanol, Sigma Aldrich

Acetonitrile, Merck

Ethylene glycol, Sigma Aldrich

Chloroform, Panreac

1,4-Dioxane, Panreac

Deuterated water, Sigma Aldrich

2-Propanol, Prolabo

Sodium hydroxide, Merck

Acetic acid, Sigma Aldrich

Formic acid, Sigma Aldrich

Perchloric acid, Sigma Aldrich

Cyclohexane, Merck

Hydrochloric acid, Merck

Methylcyclohexane, Merck

8.3 Preparation of solutions

- Stock solutions

Aqueous stock solutions of NAD and 2-NOA (1.0×10^{-3} mol L^{-1} and 3.0×10^{-4} mol L^{-1}) were prepared by dissolving the solid with constant stirring in ultra pure water obtained by a Millipore system (18.2 M Ω cm^{-1}). These solutions were kept in the dark and were stable for a large period of time. Diluted and fresh work solutions were prepared from these stock solutions whenever was necessary. Aqueous $W_{10}O_{32}^{4-}$ solutions (3.0×10^{-4} mol L^{-1}) were prepared freshly due to their instability. For mixtures of (NAD or 2-NOA + $W_{10}O_{32}^{4-}$), a certain amount of the solid $W_{10}O_{32}^{4-}$ was dissolved

in 2-NOA or NAD aqueous stock solutions prior to irradiation. NAD and 2-NOA solutions in organic solvents were prepared daily before use by dissolving the respective solid with constant stirring.

- *Solutions of NAD and 2-NOA in the presence of quenchers*

Fluorescence quenching studies were performed in water by adding different concentrations (range 10^{-4}-10^{-2} mol L^{-1}) of aqueous KBr, KI, KCl, KSCN, NaN$_3$ solutions, and in acetonitrile using triethylamine solution in the same solvent, to NAD (1.0×10^{-5} mol L^{-1}) and 2-NOA solutions at a constant concentration (2.0×10^{-5} mol L^{-1}).

- *Aqueous solutions of NAD and 2-NOA in presence of β-Cyclodextrin (β-CD)*

Aqueous NAD working solution (1.0×10^{-5} mol L^{-1}) (solution 1) was prepared from the stock solution. Another solution composed of β-CD (1.0×10^{-2} mol L^{-1}) + NAD (1.0×10^{-5} mol L^{-1}) (solution 2) in water was prepared by dissolving a few mg of β-CD solid in NAD working solution 1. These solutions were then used for absorbance and fluorescence measurements. Aliquots of solution 1 and 2 were mixed in order to obtain solutions with constant NAD concentration and varying β-CD concentrations in the range 5.0×10^{-4} - 8.0×10^{-3} mol L^{-1}. These solutions were stirred during 1 h prior to absorbance/fluorescence measurements in order to incorporate NAD on the β-CD. For degradation studies, different amounts (mg) of the solid β-CD was dissolved in NAD stock solution (3.0×10^{-4} mol L^{-1}) with constant stirring in order to obtain the final solutions of NAD with constant concentration (3.0×10^{-4} mol L^{-1}) in presence of β-CD with concentrations of 1.0×10^{-3}, 5.0×10^{-3} and 1.0×10^{-2} mol L^{-1}.

- *Phosphate buffer solution (0.2 mol L^{-1}):*

40.5 mL of a sodium phosphate dibasic dihydrate aqueous solution (0.2 mol L^{-1}) was added to 9.5 mL of a sodium dihydrogen phosphate monobasic solution (0.2 mol L^{-1}) in a 50 mL flask. The pH of the final solution was around 7.4.

The pH of the solutions was measured by using a pH meter JENWAY 3310 with a combined electrode Ag/AgCl of type Orion 90102 at 20 º C. The precision was of 0.1 unit. The pH of the solutions was adjusted by using HClO$_4$ and NaOH. The ionic strength of the solutions was not controlled.

The water used as eluent in HPLC was adjusted with formic acid (pH 3.5) and acetic acid (2.0 %), for NAD and 2-NOA determination, respectively.
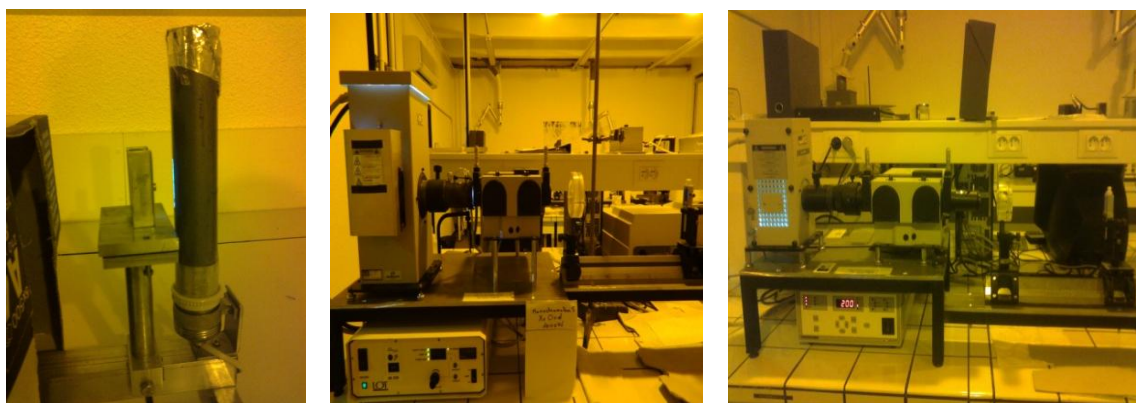
8.4 De-aerating and oxygen saturation of solutions

To obtain de-aerated or oxygenated solutions, argon (or nitrogen) and oxygen was bubbled during 20 minutes for volumes between 2-5 mL, respectively, prior to analysis. For the measurement of the quantum yields of photodegradation, the cell was then closed with a septum with parafilm around in order to avoid entrance of air. For the photophysical measurements, proper closed cells were used. For irradiations with volumes greater than 10 mL, the deoxygenation or oxygenation of the solution was carried out for 30 minutes prior to irradiation and during the entire course of irradiation using the previously referred gas.

8.5 Irradiation systems

8.5.1 Irradiation with monochromatic light at different wavelengths: determination of the photon flux and quantum yields

Irradiations with monochromatic light at 254 nm were performed with a low pressure mercury lamp (Philips TUV 6 W) delivering a parallel beam. For irradiations at 300 and 310 nm a system equipped with a LOT Oriel grating monochromator and a xenon short arc lamp (1000 W) were used while for irradiations at 313 and 365 nm a system equipped with a LOT Oriel grating monochromator and a mercury lamp (200 W) were used. Figure 8-1 gives an image of all the systems. A quartz cell with 1 cm optic path length was used for these irradiations. The intensity of light (or the photonic flux) I_0 emitted for each one of the wavelength was evaluated by chemical actinometry using potassium ferrioxalate [1].

Figure 8-1 Irradiation monochromatic systems: 254 nm (left), 300 and 310 nm (centre) and at 313 and 365 nm (right).

The light intensity or photonic flux, I_0, was determined by the potassium ferrrioxalate ($K_3Fe(C_2O_4)_3$) method [1] which is based on the photochemical reactivity of potassium ferriooxalate in acid solution. Under irradiation, Fe^{3+} is reduced to Fe^{2+} (reaction 8.1) and the oxalate anion is oxidized to CO_2 (reaction 8.2 and 8.3):

$$Fe^{3+}[(C_2O_4)_3]^{3-} \xrightarrow{\ h\nu\ } [Fe^{2+}(C_2O_4)_2]^{2-} + C_2O_4^{\bullet -} \qquad (8.1)$$

$$Fe^{3+}[(C_2O_4)_3]^{3-} + C_2O_4^{\bullet -} \longrightarrow [Fe^{3+}(C_2O_4)_3]^{2-} + C_2O_4^{2-} \qquad (8.2)$$

$$Fe^{3+}[(C_2O_4)_3]^{2-} \longrightarrow [Fe^{2+}(C_2O_4)_2]^{2-} + 2CO_2 \qquad (8.3)$$

Fe^{2+} can then be measured at 510 nm by the formation of a red complex with 1,10-phenanthroline. The molar absorption coefficient of this complex at 510 nm, ε_{510}, is 1.118×10^4 L mol^{-1} cm^{-1}. The experiment consists of irradiating a certain volume of potassium ferriooxalate solution (0.006 mol L^{-1}) for a certain time t (in seconds) and then transferring 2 mL of this solution (V_{irrad}) to a 5.0 mL volumetric flask, to which is added 1.0 mL of acetate buffer, 0.5 mL of 1,10-phenanthroline (0.1 % by mass) and filled up with water. The solution is mixed for a few seconds and kept in dark for 1 h to allow the formation of the complex. A blank solution was also prepared in the same conditions, except that in this case the potassium ferriooxalate solution was not irradiated. The measurement of the absorbance at 510 nm of the sample subtracted to the reference was then performed in a quartz cell with an optical path equal to *l*. The photonic flux I_0 (photons cm^{-2} s^{-1}) is therefore calculated by the following equation (8.4):

$$I_0 = \frac{6.023 \times 10^{20}\ V_{total}\ l_{irrad}\ D_{510}}{V_{irrad}\ l_{510}\ \varepsilon_{510}\ \phi_{Fe2+}\ t\ (1-10^{D0})} \qquad (8.4)$$

where:

V_{total} is the total volume of solution (5.0 mL), l_{irrad} is the optical path of the quartz cell (1.0 cm), V_{irrad} is the volume of potassium ferriooxalate irradiated (2.0 mL), l_{510} is the optical path of the quartz cell (1.0 cm), ε_{510} is the molar absorption coefficient for the complex ferriooxalate and 1,10-phenanthroline at 510 nm (1.118×10^4 L mol^{-1} cm^{-1}), D_{510} is difference given by the absorbance of sample and of the blank solution, D_0 is the absorbance of the ferriooxalate solution at the excitation wavelength (254, 300, 310 and 365 nm) and $\phi_{Fe^{2+}}$ = 1.25 (at 254 nm); 1.24 (at 300 nm); 1.23 (at 310 nm) and 1.21 (at 365 nm).

Once the photonic flux is known, it is possible to calculate the quantum yield (ϕ) of transformation. This parameter, given in equation (8.5), is representative of the efficiency of a photochemical process.

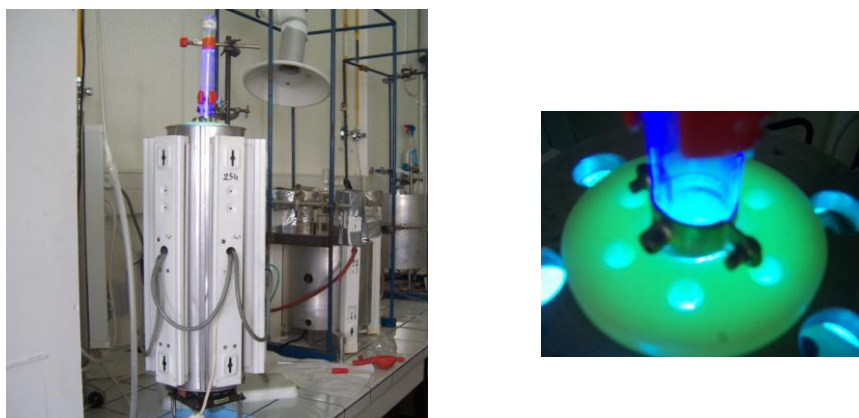$$\phi = l \times \frac{6.023 \times 10^{20} \ \dfrac{\Delta C}{\Delta t}}{I_0 \ (1 - 10^{-Abs})} \tag{8.5}$$

where:

l is the optical path length of the irradiation cell (1.0 cm), I_0 is the photon flux (photons $s^{-1} \ cm^{-2}$) determined by eq. (8.4), Abs is the initial fraction of light absorbed by the solution containing the organic compound and $\Delta C / \Delta t$ (mol $L^{-1} \ s^{-1}$) is the slope of the plot of the variation of the concentration *vs* time of irradiation (s).

For the calculation of quantum yields some attention is necessary since the irradiation times have to be chosen in order to not exceed 10-15 % disappearance of transformation of the initial product. If this condition is not fulfilled, the degradation intermediates of initial product could interfere with the measures of the primary conversion. The quantum yields were obtained with a standard error of around 10 %.

8.5.2 Irradiation with UV light at 254 nm

For analytical and kinetic purposes, the irradiation of aqueous solutions of the pesticides NAD and 2-NOA were performed in a cylindrical quartz reactor (50 mL) using up to six germicidal lamp (Mazda TG 15 W) emitting at 254 nm equipped with a ventilator system (Figure 8-2).

Figure 8-2 Irradiation system at 254 nm with 6 germicidal lamps (Mazda TG 15 W).

This allows the determination of the initial rate constants (k) and the half-lives times ($t_{1/2}$). The solution was put in a quartz reactor which was placed in the centre of the irradiation system, together with a ventilation system. This device is not appropriate for the calculation of the quantum yields since the optical path is not well defined and it is not possible to calculate the percentage of light absorbed.

8.5.3 Irradiation with UV light at 365 nm

For analytical and kinetic purposes, the irradiations of NAD, 2-NOA, (2-NOA or NAD+$W_{10}O_{32}^{4-}$) and (NAD+$W_{10}O_{32}^{4-}$-LDH) at 365 nm were carried out in an elliptical stainless steel cylinder, where three high pressure mercury lamps (black lamp, Mazda MAW 125 W) were symmetrically installed in the down part of the cylinder (Figure 8-3). These lamps, also called Wood lamps, emit selectively at 365 nm (97 % of the emission), although two incompletely filtered rays at 313 nm (2 %) and 334 nm (1 %) were also present. A cooling system was also used with temperature set at 20 °C. Solutions were stirred during irradiation and, when necessary, oxygen or argon was bubble during the entire irradiation to assure the oxygenated and de-aerated conditions.

Figure 8-3 Irradiation system at 365 nm with 3 wood lamps.

8.5.4 Irradiation with simulated solar light

In order to mimic the environmental conditions of solar irradiation, aqueous solutions of NAD and 2-NOA (3.0×10^{-4} mol L^{-1}) in the absence and presence of the catalyst $W_{10}O_{32}^{4-}$ (3.0×10^{-4} mol L^{-1}), and of NAD in the presence of β-CD (different concentrations) were irradiated with the simulated solar light system (Suntest - model CPS, Atlas) as shown in Figure 8-4. The system is equipped with a xenon lamp and

with different filters in order to simulate solar irradiation. The global emission intensity ($470\ \text{W m}^{-2}$) was controlled by a potentiometer and a cooling system was also used to maintain the temperature constant (16 ºC). A quartz cell of 1.0 cm of path length was used for the experiments. This system was used only a few times and not on a regular basis during our studies since our compounds do not absorb much at these wavelengths, leading to longer irradiation times.

Figure 8-4 Suntest system (CPS model) used within the work.

8.6 Analytical methods

8.6.1 Spectroscopic methods

8.6.1.1 UV-visible absorption

The UV-vis absorption spectra measurements were acquired either on a Cary 3 double-beam UV-Vis (Varian) or on a Shimadzu UV-2010 double-beam spectrometer with a 1 cm quartz cuvette over the range 200-800 nm. The molar absorption (extinction) coefficient, ε, of NAD and 2-NOA in water and in organic solvents was obtained with six solutions of different concentrations. The slope of the plot of the absorption (at the maximum wavelength of absorption) *vs* the concentration values gave ε values with correlation > 0.999.

8.6.1.2 Fluorescence

Corrected steady state fluorescence emission and excitation spectra were acquired on a Horiba-Jobin-Yvon SPEX Fluorolog 3-2.2 spectrofluorometer equipped with a 300 W xenon lamp using a 1 cm quartz cuvette. Excitation wavelengths were recorded at the absorption maxima of the respective compounds. Slits of 1.0 mm were used for emission and excitation measurements. Fluorescence spectra were corrected for the wavelength response of the system. Fluorescence quantum yields were determined

by comparison with standards of known quantum yield. The emission quantum yields of these reference compounds should be independent of the excitation wavelength, so the standards can be used in their full absorption range. In practice, the quantum yield was determined by comparison of the integrated area under the emission spectra of optically matched solutions of the samples ($\int I (\lambda)^S d\lambda$) and that of the reference ($\int I (\lambda)^R d\lambda$) compound. The absorption and emission range of the samples (S) and reference (R) compound should match as such as possible. The absorbance values should be kept as lower as possible to avoid inner filter effects [2]. In these conditions, using the same excitation wavelength, the unknown fluorescence quantum yield is calculated using the equation (8.6):

$$\phi_F^S = \frac{\int I(\lambda)^S d\lambda}{I(\lambda)^R d\lambda} \frac{n_S^2}{n_R^2} \frac{Abs_R}{Abs_S} \phi_F^R = \phi_F^R \frac{I_S A_R n_S^2}{I_R A_S n_R^2} \frac{f_S}{f_R} \tag{8.6}$$

and
$$f_S = \frac{I_{N2}^S}{I_{O2}^S} \qquad f_S = \frac{I_{N2}^R}{I_{O2}^R}$$

where ϕ_F represents the fluorescence quantum yield, I is the integrated area under the respective fluorescence spectra, A is the respective absorbance, n is the refractive index of the solvents used and f represents the de-aerating factor, which is given by the ratio of the integrated area under the respective fluorescence spectra in absence and presence of oxygen, for the sample and for the reference. The subscripts S and R refer to the sample and reference, respectively.

NAD and 2-NOA fluorescence quantum yields were measured in different solvents by using naphthalene in ethanol as standard ($\phi_F = 0.21$) [2]. Samples and reference were bubbled for 20 minutes with nitrogen prior to the measure due to the influence of oxygen. Sample and reference absorbances (below 0.1) were matched at the excitation wavelength.

The energy of singlet state (E_S) was determined at the point crossing of the normalized absorption and fluorescence emission spectra.

For fluorescence quenching, Stern-Volmer plots were constructed from relative integrated fluorescence emission intensities and the Stern-Volmer quenching coefficient, K_{SV} (L mol^{-1}), was obtained by linear regression using the expression (8.7):

$$\frac{I_0}{I} = 1 + K_{SV}[Q] \tag{8.7}$$

where I_0 and I are the fluorescence intensities in absence and presence of the quencher Q, respectively, and [Q] is the concentration of the quencher (in mol L^{-1}). K_{SV} is also defined as ($=\tau_F \times k_q$), being τ_F the fluorescence lifetime of the compound in absence of Q and k_q the quenching rate constant (L mol^{-1} s^{-1}).

- Assessment of H$_2$O$_2$ formation

The determination of H$_2$O$_2$ was performed by using the Lazrus method [3]. This method is based on the reduction of H$_2$O$_2$ in presence of 4-hydroxyphenylacetic acid (4-HPC) catalysed by peroxidase. This reaction leads to the formation of 4-HPC dimer which is easy detected by fluorescence spectroscopy ($\lambda_{ex/em}$ = 320/400 nm). A solution containing 1 mL of phosphate buffer (pH 7.4), 1 mL of 4-HAP solution and 100 μL of NAD or 2-NOA sample (non irradiated and irradiated at 254 nm) was put in a fluorescence cuvette with 1 cm optical path. This solution was stirred manually and kept in dark during 1 h prior to measurement of fluorescence.

- Toxicity measurements

These measurements were kindly performed by Pascal Wong-Wah-Chung and Cyril le Fur at the group of Professor Polonca Trebše (University of Nova Gorica, Slovenia). The toxicity of aqueous NAD solution ([NAD]$_0$ = 3.0×10^{-4} mol L^{-1}, pH around 7.0) irradiated at 254 nm was evaluated using luminescence marine bacterium *Vibrio Fischeri*, with a LUMIStox test, as described in literature [4]. The comparison was performed by using a non irradiated solution. The bacterium was incubated for a period of 30 min after which the luminescence was measured. After 30 min of exposure of the bacteria with and without NAD sample, the luminescence of bacteria was again measured as the % of inhibition (% I), leading to the total toxicity, % I$_T$.

The toxicity due to the photoproducts was calculated according to equations (8.8) and (8.9):

$$\%I\,(NAD)_t = \frac{\%I(NAD)_{t=0} \times [NAD]_t}{[NAD]_{t=0}} \tag{8.8}$$

where % I(NAD)$_{t=0}$ = 73 % and [NAD]$_t$ is NAD concentration at different irradiation time. Therefore, the % I owing to the formation of products is given by equation (8.9):

$$\%\,I\,(products)_t = \%\,I_T\,\frac{\%\,I(NAD)_{t=0}\times[NAD]_t}{[NAD]_{t=0}}$$

(8.9)

8.6.1.3 Phosphorescence

Phosphorescence measurements were made in glasses at 77 K (in order to avoid the quenching by the molecular oxygen dissolved in those solutions) using the Horiba-Jobin-Yvon Fluorolog 3-2.2 spectrometer equipped with a 1934 D phosphorimeter unit and a 150 W pulsed xenon lamp. The phosphorescence spectra were corrected for the wavelength response of the system.

Excitation of NAD and 2-NOA solution was done at the maximum absorption wavelength. Slits of 4.0 mm were used for excitation and emission measurements. The emission and excitation spectra were recorded as well as decay studies in order to determine the lifetimes of phosphorescence.

The phosphorescence emission spectra from optically matched solutions at the excitation wavelength of the samples and reference compound (benzophenone in ethanol ($\phi_P = 0.74$) [2] were collected and the phosphorescence quantum yields were determined using the following equation (8.10):

$$\phi_P^S = \phi_P^R\,\frac{I_S\,A_R\,n_S^2}{I_R\,A_S\,n_R^2}$$

(8.10)

where ϕ_P represents the phosphorescence quantum yield, I is the integrated area under the respective phosphorescence spectra, A is the respective absorbance, n is the refractive index of the solvents used and the subscripts S and R refer to the sample and reference, respectively.

8.6.1.4 Mass spectrometry

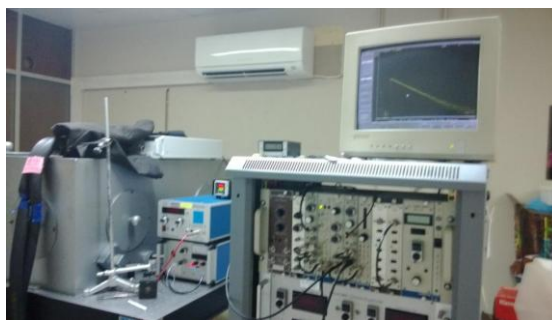Since the photoproducts were obtained at very low concentrations, a pre-concentration step on a solid phase extraction (SPE) cartridges Oasis HLB 3cc (Waters) was performed on NAD and 2-NOA samples prior to LC-MS and LC-MS/MS analysis. The solid phase was first washed with methanol and then conditioned with water. Finally, the sample was eluted with methanol and evaporated to obtain a solution concentrated by a factor of 50.

LC-MS and LC-MS/MS studies were then carried out with a Waters HPLC system (Alliance 2695) coupled to a Q-TOF mass spectrometer equipped with a pneumatically assisted electro spray ionization source (ESI). The HPLC system was also coupled with a Waters 996 diode array detector. Chromatographic separation was achieved by using an elution program from 95 % water (with 0.2 % formic acid) and 5 % methanol to 5 % water (with 0.2 % formic acid) and 95 % methanol after 15 min; the isocratic conditions obtained were maintained during 10 min. The flow rate was 0.2 mL min^{-1}, the injected volume was 3.0 µL and a Phenomenex column (Kinetex MS C18, 3.5 µm, 100 mm × 2.1 mm) was used. The electro spray source parameters were in positive mode: capillary voltage 3000 V (2100 V in negative mode), cone voltage 35 V, extraction cone voltage 2 V, desolvation temperature 250 °C, source temperature 100 °C, ion energy 2 V and collision energy 10 eV (7 eV in negative mode).

8.6.2 Time resolved methods

8.6.2.1 Time correlated single photon counting

Fluorescence lifetimes, τ_F, of NAD and 2-NOA were measured using a home built time correlated single photon counting (TCSPC) apparatus (University of Coimbra), with a Horiba-JI-IBH NanoLed (282 nm) as excitation source, a Jovin-Yvon excitation and emission monochromators, a Philips XP2020Q photomultiplier, and Caberra instruments TAC and MCA (Figure 8-5). Alternate measurements (1000 counts per cycle) of the pulse profile were performed until 5×10^4 counts at the maximum were reached. Measurements were performed in de-aerated samples at maximum excitation and emission wavelength. The fluorescence decays were analysed using the modulating functions method of Striker with automatic correction for the photomultiplier "wavelength shift" [5] using the SAND program.

Figure 8-5 TCSPC apparatus employed in this work.

8.6.2.2 Nanosecond laser flash photolysis

8.6.2.2.1 Transient absorption spectra, triplet extinction coefficient and triplet quantum yields

Transient absorption experiments were carried out on a nanosecond laser flash photolysis spectrometer from Applied Photophysics (LKS 60). Excitation was achieved by using the fourth harmonic (266 nm) and/or the third harmonic (355 nm) of a Quanta Ray GCR130-1 Nd:YAG laser (pulse width ~ 5 ns) which was used in a right angle geometry with the respect to the monitoring beam. Transient spectra were obtained by monitoring the optical density change (ΔOD) at intervals of 5-10 nm over the range 260-800 nm and averaging at least 10 decays at each wavelength. Solutions with absorbencies around 0.2 were bubbled with nitrogen and oxygen prior to the analysis during 20 minutes in a proper quartz cell (3 mL volume), in order to study the effect of oxygen in the transient state. The transient absorbance at preselected wavelengths was monitored by a detection system consisting in a pulsed xenon lamp (150 W), monochromator and a IP28 photomultiplier Housing (Applying Photophysics). The signal from the photomultiplier was digitized by a programmable digital oscilloscope TDS 30528 (Tektronix) and the signal was analyzed with a 32-bit RISC-processor kinetic spectrometer. First order kinetics was observed for the decays of the lower triplet state. Special care was taken in order to have low laser energy to avoid multiphoton and triplet-triplet annihilation effects.

Triplet lifetimes, τ_T, were calculated from kinetic analysis of the transient decays. The rate constants for oxygen quenching of the triplet state $k^T_{O_2}$ were determined by measuring the decay of the triplet-triplet absorption at the absorption maximum for NAD and 2-NOA in each solvent in the presence and absence of air.

The triplet molar extinction coefficient, ε_T, was determined by the energy transfer method [6] using benzophenone in acetonitrile as triplet energy donor ($\varepsilon_{520\ nm}$ = 6500 L mol^{-1} cm^{-1}; ϕ_T = 1.0) [2]. All solutions were de-aerated with argon for approximately 20 minutes and sealed prior to measurement. The excitation wavelength was of 355 nm. The molar triplet-triplet absorption coefficients [7] were then determined from the equation (8.11):

$$\frac{\varepsilon^D_{TT}}{\varepsilon^A_{TT}} = \frac{\Delta OD^D}{\Delta OD^A} \qquad\qquad (8.11)$$

where ε^D_{TT} and ε^A_{TT} are the triplet molar absorption coefficients of donor and acceptor, respectively, ΔOD^D is the maximum absorbance from the transient triplet-triplet absorption spectra of the donor in the absence of acceptor; ΔODA^A is the maximum absorbance of the acceptor triplet when the acceptor and donor are present. When the acceptor decay rate constant (k_3) is not negligible, a correction is necessary to calculate the ΔOD^A (equation 8.12):

$$\Delta OD^A_{obs} = \Delta OD^A \exp\left[\frac{-\ln\left(\frac{k_2}{k_3}\right)}{k_2/k_3 - 1}\right] \tag{8.12}$$

where k_2 is the decay rate constant of the donor in the presence of the acceptor and ΔOD^A_{obs} is the maximum obtained in the triplet-singlet difference spectra of the acceptor in the presence of the donor.

The triplet quantum yields, ϕ_T, were obtained by the comparative actinometry method using naphthalene in methylcyclohexane as reference ($\varepsilon = 13200$ L mol^{-1} cm^{-1}; $\phi_T = 0.75$) [2]. Optically matched samples of NAD and 2-NOA and of the reference naphthalene with absorbance around 0.2 in the excitation wavelength were irradiated with the 266 nm laser in the nitrogen-saturated solvent. The quantum yield of triplet formation is giving according to equation (8.13), where S and R refers to the sample and reference, respectively.

$$\phi^S_T = \frac{\varepsilon^R_T}{\varepsilon^S_T} \frac{\Delta OD^S_T}{\Delta OD^R_T} \frac{n^2_S}{n^2_R} \phi^R_T \tag{8.13}$$

8.6.2.2.2 Singlet oxygen measurements

Singlet oxygen quantum yield, ϕ_Δ, was detected by monitoring room temperature phosphorescence centred at 1270 nm using a Hamamatsu R5509-42 photomultiplier, cooled at 193 K in a liquid nitrogen chamber, following laser excitation of aerated NAD and 2-NOA solutions in different solvents at 266 nm, with an Applied Photophysics flash kinetic spectrometer. Signal averaging was performed to improve the signal to noise ratio. The relative yield of singlet oxygen formation was determined by comparison of the slopes of the laser energy dependence plots of the phosphorescence emission at 1270 nm obtained for the sample in the different solvents and for the

standard. For high values of energy the variation of the phosphorescence intensity with the laser intensity is no longer linear. Thus, the linear zone was used to evaluate the ϕ_Δ. Biphenyl in cyclohexane ($\phi_\Delta = 0.73$) [8] with excitation at 266 nm was used as reference. Studies were carried out in optically matched solutions in the solvents mentioned before. Hence, the singlet oxygen quantum yield sensitized by NAD and/or 2-NOA, was calculated from the equation (8.14):

$$\phi_\Delta^S = \frac{I^S}{I^R} \frac{Abs^R}{Abs^S} \frac{n_S^2}{n_R^2} \phi_\Delta^R \tag{8.14}$$

where I is the intensity of the phosphorescence decay measured at 1270 nm, Abs is the absorbance of the solutions at 266 nm, n is the refractive index for each solvent, ϕ_Δ is the singlet oxygen quantum yield and S and R represent sample and reference, respectively. Additionally, photosensitization experiments were also carried out for NAD using phenalenone in chloroform ($\phi_\Delta = 0.98 \pm 0.15$, $\lambda_{ex} = 355$ nm) [9] with absorbencies varying between 0.2-0.3 at 355 nm excitation. Solutions of phenalenone in chloroform (3.0×10^{-5} mol L^{-1}) were excited at 355 nm in absence and presence of NAD (1.0×10^{-4}- 1.0×10^{-2} mol L^{-1}) in order to evaluate the quenching constant of excited singlet oxygen.

8.6.3 Chromatographic methods

8.6.3.1 High performance liquid chromatography

High performance liquid chromatography (HPLC) was used to follow the kinetics of NAD and 2-NOA degradation, the formation of photoproducts and its quantification, when possible. Throughout this work, two HPLC systems with diode array detection were used:

- HPLC Alliance, equipped with a multi wavelength fluorescence detector (Waters 2475), a dual wavelength absorbance detector (2478 Waters) and a separation module ((Waters 2695) with a C18 Phenomex column (Kinetex 2.6 μ, 100 x 2.10 mm)

- HPLC Waters 540 equipped with a Waters 996 photodiode array detector and a reverse phase Nucleodur column C18 column (250 mm x 4.6 mm, 5 μ).

NAD was eluted by using as mobile phase a mixture of acidified water (pH 3.5 formic acid) and methanol (60/40 v/v), whereas for 2-NOA kinetics was used a mixture of acidified water (2.0 % acetic acid) and methanol (45/55 v/v). For both pesticides, the flow rate was set at 1.0 mL min^{-1} and 20 µL of solution was injected. Each sample was injected three times in order to determine the standard deviation, which was not higher than 5.0 %. The detection wavelength was set at 280 and 270 nm, for NAD and 2-NOA, respectively. The evolution of photoproducts was followed at different wavelength then 280 or 270 nm whenever necessary. For a better chromatographic separation of NAD products, the following gradient program was used: 95 % water (with 0.2 % formic acid) and 5 % methanol to 5.0 % water (with 0.2 % formic acid) and 95 % methanol after 15 min; the isocratic conditions obtained were maintained during 10 min. The flow rate was 0.2 mL min^{-1}, the injected volume was 3.0 µL and a Phenomenex column (Kinetex MS C18, 3.5 µm, 100 mm × 2.1 mm) was used. Calibration curves were previously constructed in order to quantify the amount of NAD and 2-NOA present in each analysed sample. The same procedure was applied for 2-naphthol quantification.

8.6.3.2 Ionic liquid chromatography

Ionic liquid chromatography was used to measure the evolution of the anions nitrate, nitrate and ammonia concentration as a function of irradiation time, upon mineralization of NAD in presence of sodium decatungstate. For the anions, a Dionex DX320 column, with a AS11+AG11 pre-column were used while for ammonia a Dionex ICS1500 column with a CS16+CG16 pre-column was employed, with 1.0 mL min^{-1} flow. The elution for anions was accomplished by using a gradient with KOH and for ammonia cation a 50/50 mixture of water and methylsulfonic acid was used.

8.6.4 Determination of the total organic carbon

For the determination of the total organic carbon (TOC) an analyzer Shimadzu TOC 5050A equipped with an automatic sample injector (Figure 8-6) was used in order to evaluate the total mineralization of the pollutants NAD. TOC was measured for the following studies:

- homogeneous degradation of NAD in presence of sodium decatungstate and in presence of TiO$_2$,

- and heterogeneous degradation of NAD immobilized on the *as*-prepared macroporous and aerogel Mg$_2$Al-layered double hydroxides (see section 8.7.2).

Taking in account the initial amount of carbon existent in NAD and 2-NOA solutions, proper calibration curves were drawn for the measurement of the total carbon (TC) and inorganic carbon (IC). The TOC values are then given by:

$$TOC = TC - IC \qquad (mg\ L^{-1})$$

The TC corresponds to the total amount of carbon present in the solution while the IC represents the carbon in the form of carbonates and bicarbonates. Each sample was analyzed three times and the final values are given by the average.

Figure 8-6 Total organic carbon analyser 5050A (Shimadzu) used in this work.

8.6.4.1 Measure of total carbon

The carbon present in the pesticide solution analysed is transformed in a tube by combustion in the presence of an oxidation catalyser (platinum) that ensures the total conversion of the solution constituents into carbon dioxide (CO_2). The detection of the CO_2 formed its performed in a cell NIDR (Non Dispersive Infra-Red Gas). A calibration curve is performed in the range of concentrations expected allowing the quantification of the TC in the solution. The detection of CO_2 formed is made inside the NIDR cell.

8.6.4.2 Measure of the inorganic carbon

The inorganic carbon present in the solution is transformed into CO_2 after reaction with phosphoric acid (25 %) and it is detected in the NIDR cell. The

concentration of IC is determined as for TC, using a calibration curve in the expected range.

8.7 Synthesis and characterization of the catalysts and measurement of the photocatalytic activity

8.7.1 Synthesis of the catalyst sodium decatungstate

Sodium decatungstate, $Na_4W_{10}O_{32}.7H_2O$, was synthesized according to the method described in literature [10]. To a boiling solution containing $Na_2WO_4 \cdot 2H_2O$ (66 g) in distilled water (400 mL) was added 400 mL of a boiling aqueous HCl solution (1.0 mol L^{-1}). The resulting solution was allowed to boil for a few seconds and rapidly cooled to 30 °C in dry a dry ice/methanol bath with constant stirring. Solid NaCl was then added to near saturation, and the mixture was cooled further to 0 °C. The formed precipitate was collected and dried on a fritted funnel. The use of non-metallic spatula is recommended to avoid the formation of a blue colour. This precipitate was suspended in hot acetonitrile (200 mL) and filtered. The filtrate was placed in a freezer overnight. In order to obtain the solid with high purity, several recrystalization steps in acetonitrile were carried out. Large pale lime crystalline rectangular blocks of $Na_4W_{10}O_{32}$ were collected and dried on a fritted funnel. The obtained sodium decatungstate (purity 85-92 %), was characterized by UV-visible spectra and by FTIR. The absorption spectrum of $Na_4W_{10}O_{32}$ in acetonitrile consisted of well-defined maximum at 323 nm assigned to an O→WCT transition. In water, this maximum absorption wavelength shifts to 324 nm with (ε = 13 600 L mol^{-1} cm^{-1}). Several bands were detected in FTIR (KBr, cm^{-1}): 958 (W=Ot,); 895 and 806 (W–Ob–W) [11].

8.7.2 Synthesis of layered double hydroxides intercalated with decatungstate anion

8.7.2.1 Classical synthesis of $Mg_2Al-W_{10}O_{32}^{4-}$ LDH

The synthesis of the precursor MgAl-DDS LDH with Mg/Al ratio = 2 was carried out by means of the classical co-precipitation method [13], which consists of the co-precipitation of metallic salts with a concentrated alkaline solution at constant pH.

It was prepared by simultaneously adding, dropwise, mixed aqueous solution of salts ($Mg(NO_3)_2.6H_2O$ and $Al(NO_3)_3.9H_2O$ - 1.0 mol L^{-1}) and an aqueous solution of 1.0

mol L^{-1} NaOH into a reactor that contained 100 mL of double-distilled water (DDW) in which sodium dodecyl sulfate (DDS) has been dispersed (molar excess of two compared to Al). The two solutions were exposed to constant stirring by means of a magnetic stirrer to ensure the homogeneity of the reaction medium, purged with N$_2$ gas in order to avoid the contamination with carbonate anion and the suspension pH was maintained at pH 9.5. After complete addition of the metal salt solution the slurry was aged during 24 h, centrifuged at 4500 rpm for 5 min, washed by three dispersion/centrifugation cycles in double deionised water DDW, washed two times with ethanol and again with DDW for three dispersion/centrifugation cycles, and finally air-dried, originating the precursor Mg$_2$Al-DDS LDH. Figure 8-7 illustrates the experimental set up of this method.

The intercalation of W$_{10}$O$_{32}$$^{4-}$ on the *as*-prepared Mg$_2$Al-DDS LDH precursor was performed by anionic exchange reaction [13]. This consisted of suspending decatungstate anion (0.5 mol) in 100 mL of ethanol solution containing the desired LDH precursor (1.0 mol) to be exchanged, under nitrogen atmosphere at 65 ºC during two days. The obtained suspension was centrifuged, washed with four water cycles, and the collected compound was allowed to dry in the oven at 3 ºC for a few hours originating the final MgAl-W$_{10}$O$_{32}$$^{4-}$ LDH.

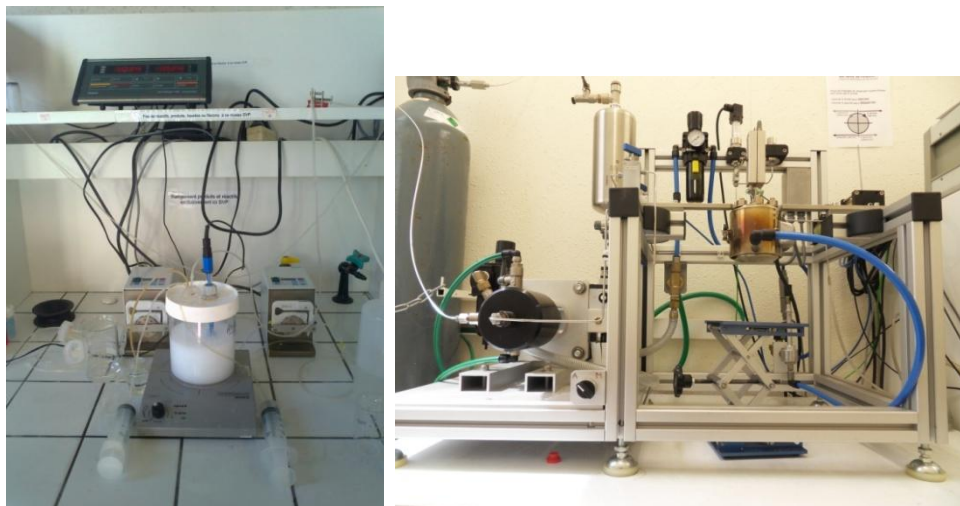**Figure 8-7** Illustration of the co-precipitation at constant pH set up employed in this thesis.

8.7.2.2 Synthesis of the three dimensionally ordered macroporous 3-DOM-Mg$_2$Al-W$_{10}$O$_{32}$$^{4-}$LDH

Monodisperse polystyrene (PS) beads (610 ± 10 nm) were synthesized by "emulsifier-free" emulsion polymerization of styrene [14] and were kindly provided by Doctor Vanessa Prevot (ICCF). The PS beads were submitted to a centrifugation step

(1200 rpm for 14 h) to produce a close packed colloidal array. Then, 3-DOM Mg_2Al was prepared by confined co-precipitation following an inverse opal method [15,16] as previously reported [17,18]. Typically, closed-packed arrays of polystyrene spheres (~1.0 g) were infiltrated by 6 mL of precursors aqueous solution ($MgCl_2$, $AlCl_3$ 1.0 mol L^{-1}, Mg/Al = 2). After 24 h, the infiltrated solid was filtered, dried at room temperature overnight and further soaked in a 6 mL of NaOH aqueous solution (2.0 mol L^{-1}) for 24 h to achieve the co-precipitation. The PS-LDH composite *as*-obtained was subsequently calcined at 400 °C to remove the polymeric template (3-DOM oxides) and immediately immersed into 50 mL of 0.1 mol L^{-1} DDS aqueous solutions for 4 h under nitrogen atmosphere and stirring. After washing and centrifugation, the 3-DOM-Mg_2Al-DDS LDH precursor was obtained. The intercalation of $W_{10}O_{32}^{4-}$ on the *as*-prepared 3-DOM-Mg_2Al-DDS LDH precursor was performed by anionic exchange reaction [13], as already explained in the previous synthesis. The final catalyst 3-DOM-Mg_2Al-$W_{10}O_{32}^{4-}$ LDH was thus obtained.

8.7.2.3 Synthesis of SC-Mg_2Al-$W_{10}O_{32}^{4-}$ LDH prepared by fast co-precipitation followed by supercritical drying with CO_2

The synthesis of Mg_2Al-DDS LDH nanoparticles was performed by fast co-precipitation followed by supercritical (SC) drying with CO_2. The fast co-precipitation process consisted in adding 10 mL of a metal salt solution ($MgCl_2$ 0.66 mol L^{-1} and $AlCl_3$ 0.33 mol L^{-1}) into 100 mL of water simultaneously with 10 mL of NaOH (2.0 mol L^{-1}) and DDS solution under vigorous stirring, which were let to react during 15 min with a final pH fixed at 10.0. The aquagel thus obtained was centrifuged, washed with deionized water for several times, the water is further replaced by ethanol giving rise to the alcogel Mg_2Al-DDS LDH. The alcogel *as*-prepared is then placed in an autoclave and subjected to the SC CO_2 drying process during 6 h above the CO_2 critical point (Tc = 304.2 K, Pc = 7.4 MPa). The experimental set up used for the fast co-precipitation and SC dry with CO_2 is shown in Figure 8-8. The intercalation of $W_{10}O_{32}^{4-}$ in the *as*-prepared SC-Mg_2Al-DDS LDH precursor gives rise to the final aerogel SC-Mg_2Al-$W_{10}O_{32}^{4-}$ LDH.

Figure 8-8 Illustration of the fast co-precipitation apparatus (left) and of the SC CO_2 drying equipment (right).

8.7.3 Techniques used for characterization of the catalysts

8.7.3.1 Powder X-ray diffraction

Powder X-ray diffraction (PXRD) patterns were recorded on a X'Pert Pro Philips diffractometer with a diffracted beam graphite monochromator using a Cu Kα (λ = 1.54 Å) radiation source in the 2θ range of 5-70° with a step of 0.013° and a counting time per step of 20 s.

8.7.3.2 Fourier transformed infrared spectroscopy

Attenuated Total Reflectance (ATR) Fourier Transform infrared (FT-IR) spectra were measured in the range 500-4000 cm^{-1} on a FTIR Nicolet 5700 spectrometer (Thermo Electron Corporation) equipped with a Smart Orbit accessory. Solid samples were also analysed in transmission mode, in which samples were prepared as pellets by adding 2.0 mg of the respective sample into 200 mg of KBr. The results are given in absorbance *vs* wavenumber in the region 500 to 4000 cm^{-1}. The resolution is of 2 cm^{-1} with 10-15 scans.

8.7.3.3 Scan electron microscopy

Scanning electron microscopy (SEM) characteristics of the samples were imaged by a Zeiss supra 55 FEG-VP operating at 3 keV combined with an energy dispersive X-

ray (EDX) analyzer. Specimens were mounted on conductive carbon adhesive tabs and imaged after gold sputter coating to make them conductive.

8.7.4 Photocatalytic activity measurements

The photocatalytic activitiy of $W_{10}O_{32}^{4-}$ intercalated into the *as*-prepared classical, 3-DOM and SC-Mg$_2$Al-LDH was tested towards the degradation at 365 nm of NAD in aqueous solution (3.0×10^{-4} mol L^{-1}). Prior to the irradiation experiments, the catalyst was photoactivated in order to remove any trace concentration of adsorbed organic compound on the catalyst. For this purpose, aqueous suspensions of the catalyst were ultrasonificated for 2 min and stirred during 30 min in the dark. The suspension was then photoactivated by irradiation at 365 nm during 2 h with constant stirring. Following this step, fresh NAD solution (3.0×10^{-4} mol L^{-1}) was added to this suspension in order to obtain a final volume of solution of 10 mL. This solution (LDH catalyst+NAD) was stirred during 30 min in the dark to promote the homogeneous distribution of the suspension. The last step consisted of introducing this mixed suspension into the reactor, a water-jacketed Pyrex tube (diameter = 1.8 cm), which was centered on the irradiation apparatus, and start the irradiation at 365 nm, always with constant stirring. The irradiation step up has already been described in section 8.5.3, Figure 8-3. This procedure was also applied for optimization of the variables that may affect the rate of degradation: amount of the catalyst, pH of solution (addition of HClO$_4$) and oxygen concentration (by bubbling oxygen, air or nitrogen during the course of reaction). For the evolution of NAD degradation kinetics, samples at zero min and at certain irradiated times were taken, centrifuged and the liquid was injected into the HPLC-DAD (λ_{det} = 280 nm).

8.7.5 Recover and reuse of the catalyst

The recovery of the LDH catalysts consists of collecting each irradiated suspension once the irradiation is stopped. For suspensions of (NAD+3-DOM-Mg$_2$Al-W$_{10}$ LDH) the reaction was stopped at 17 h (60 % NAD degradation) while for (NAD+SC-Mg$_2$Al-W$_{10}$ LDH) suspensions the irradiation was stopped at 45 h (80 % NAD degradation). These remaining solutions were centrifuged, washed three times with water in order to remove possible particles, centrifuged again to remove the water and the remained catalysts were recovered for the next degradation reaction, which

consisted in adding the desired NAD fresh solution (3.0×10^{-4} mol L^{-1}) and letting it stir during 30 min in the dark prior to start a new irradiation cycle at 365 nm, always under constant stirring. This process of wash and recover was repeated for several cycles of degradation.

8.8 References

[1] J. G. Calvert, J. N. Pitts, *Chapter 7 - Experimental Methods in Photochemistry*. In: Photochemistry, pp. 786, John Wiley& Sons, Inc, New York, **1966**.

[2] M. Montalti, A. Credi, L. Prodi, M. T. Gandolfi, *Handbook of Photochemistry*, third edition, Taylor & Francis Group, Florida, **2006**.

[3] G. L. Kok, K. Thompson, A. L. Lazrus, Derivatization technique for the determination of peroxides in precipitation. *Anal. Chem.*, **1986**, 58, 1195-1194.

[4] R. Žabar, D. Dolenc, T. Jerman, M. Franko, P. Trebše, Photolytic and photocatalytic degradation of 6-chloronicotinic acid. *Chemosphere*, **2011**, 85, 861-868.

[5] G. Stricker, V. Subramaniam, C. A. M. Seidel, A. Volkmer, Photochromicity and fluorescence lifetimes of green fluorescent protein. *J. Phys Chem. B*, **1999**, 103, 8612-8617.

[6] R. Bensasson, E. J. Land, Triplet-triplet extinction coefficients via energy transfer. *Trans. Faraday Soc.*, **1971**, 67, 1904-1915.

[7] B. Amand, R. Bensasson, Determination of triplet quantum yields by laser flash absorption spectroscopy. *Chem. Phys. Letters*, **1975**, 34, 44-48.

[8] M. Kristiansen, R. D. Scurlock, K. Long Lu, P. R. Ogilby, Charge-transfer state and singlet oxygen ($^1\Delta_g$ O$_2$) production in photoexcited organic molecule-molecular oxygen complexes. *J. Phys. Chem.*, **1991**, 95, 5190-5197.

[9] R. Schmidt, C. Tanielian, R. Dunsbach, C. Wolff, Phenalenone, a universal reference compound for the determination of quantum yields of singlet oxygen sensitization. *J. Photochem. Photobiol. A: Chem.*, **1994**, 79, 11-17.

[10] R. F. Renneke, M. I. Pasqual, C. L. Hill, Polyoxometalate systems for the catalytic selective production of non thermodynamic alkenes form alkanes. Nature of excited-state deactivation processes and control of subsequent thermal processes in polyoxometalate photoredox chemistry. *J. Am. Chem. Soc.*, **1990**, 112, 6585-6594.

[11] A. Chemseddine, C. Sanchez, J. Livage, J. P. Launay, M. Fournier, Electrochemical and photochemical reduction of decatungstate: a reinvestigation. *Inorg. Chem.*, **1984**, 23, 2609-2613.

[12] C. Taviot-Gueho, V. Prevot, C. Forano, *Layered Double Hydroxides.* In: Handbook of Clays Science. Ed. F. Bergaya, 2nd Edition, Elsevier, **2013**.

[13] M. Meyn, K. Beneke, G. Lagaly, Anion-exchange reactions of layered double hydroxides. *Inorg. Chem.*, **1990**, 29, 5201-5207.

[14] K. Furusawa, W. Norde, J. Lyklema, A method for preparing surfactant-free polystyrene latices of high surface charge. *Kolloid-Z. u. Z. Polymere*, **1972**, 250, 908-909.

[15] R. C. Schroden, A. Stein, *3D ordered macroporous materials.* In: Colloids and Colloid Assemblies. Ed. F. Caruso, pp. 465-493, Wiley-VCH, **2004**.

[16] A. Stein, B. E. Wilson, S. G. Rudisill, Design and functionality of colloidal-crystal-templated materials. *Chem. Soc. Rev.*, **2013**, 42, 2763-2803.

[17] E. Geraud, S. Rafqah, M. Sarakha, C. Forano, V. Prevot, F. Leroux, Three dimensionally ordered macroporous layered double hydroxides: preparation by templated impregnation/coprecipitation and pattern stability upon calcination. *Chem. Mater.*, **2008**, 20, 1116-1125.

[18] E. Geraud, V. Prevot, J. Ghanbaja, F. Leroux, Macroscopically ordered hydrotalcite-type materials using self-assembled colloidal crystal template. *Chem. Mater.*, **2006**, 18, 238-240.